



저작자표시-비영리-변경금지 2.0 대한민국

이용자는 아래의 조건을 따르는 경우에 한하여 자유롭게

- 이 저작물을 복제, 배포, 전송, 전시, 공연 및 방송할 수 있습니다.

다음과 같은 조건을 따라야 합니다:



저작자표시. 귀하는 원저작자를 표시하여야 합니다.



비영리. 귀하는 이 저작물을 영리 목적으로 이용할 수 없습니다.



변경금지. 귀하는 이 저작물을 개작, 변형 또는 가공할 수 없습니다.

- 귀하는, 이 저작물의 재이용이나 배포의 경우, 이 저작물에 적용된 이용허락조건을 명확하게 나타내어야 합니다.
- 저작권자로부터 별도의 허가를 받으면 이러한 조건들은 적용되지 않습니다.

저작권법에 따른 이용자의 권리는 위의 내용에 의하여 영향을 받지 않습니다.

이것은 [이용허락규약\(Legal Code\)](#)을 이해하기 쉽게 요약한 것입니다.

[Disclaimer](#)

공학박사학위논문

**A Study on Optimal Design for Gas-to-Liquid Process by
Utilizing Micro-channel Fischer-Tropsch Reactor**

마이크로채널 피셔-트롭쉬 반응기를 활용한 Gas-to-Liquid
공정의 최적 설계에 관한 연구

2015년 12월

서울대학교 대학원

화학생물공학부

박 성 호

Abstract

A Study on Optimal Design for Gas-to-Liquid Process by Utilizing Micro-channel Fischer- Tropsch Reactor

Seongho Park

School of Chemical & Biological Engineering

The Graduate School of Seoul National University

For several decades, a gas-to-liquid (GTL) process has been identified as a promising technology for converting abundant natural gas (NG) to clean synthetic fuel. Throughout the GTL process, NG is firstly converted to synthesis gas, mainly composed of hydrogen and carbon monoxide by a syngas reforming process. Syngas is then chemically converted into the liquid fuel by Fischer-Tropsch (FT) reaction process, wherein several carbon atoms in the syngas are oligomerized to form a long chain hydrocarbon product. This hydrocarbon product is also known as FT synfuel, and it contains many hydrocarbon species of carbon number ranging from 1 (methane) to more than 30 (FT wax). FT synfuel has high research octane number (RON) and cetane number (CN) and almost nitrogen and sulfur free. So it is taking a premium position in the fuel market.

FT synthesis reaction is known as a strongly exothermic reaction: A large amount of heat, ca. 165kJ per mol of converted CO is generated during the reaction. This heat must be removed to prevent runaway situation and achieve safe isothermal operation of the reactor. Various types of reactors, such as fixed bed, slurry bubble column, circulating fluidized bed, and fixed fluidized bed FT reactors, have been developed and applied to the GTL industries. In order to utilize the FT reaction in off-shore platform, however, more compact, but highly productive, FT reactor is essential.

Recently, the concept of micro channel FT reactor has evolved because it can effectively handle large amount of heat based on the high heat exchange surface area per unit volume. It was reported that the heat removal rate in the micro-channel reactor was around 15 times higher than that in a conventional fixed bed reactor. Moreover, micro-channel reactors are good for scale-up perspectives because the wax production can be easily increased by simply adding modularized reactors. It has been reported that the performance of the pilot scale micro-channel reactor was consistent with that of a single micro-channel reactor due to the achievement in isothermal operation.

This thesis has addressed the optimal design for GTL processes based on the micro-channel Fischer-Tropsch reactor technology: Modeling of the micro-channel FT reactor, optimization of the GTL process based on the developed reactor model, and dynamic simulation and optimal operating procedures for the micro-channel FT reaction system. The reactor models were validated against the real operation data.

A distributed parameter model for micro-channel FT reactor was developed by using a new method, in which all the process and cooling channels are decomposed

into a number of unit cells. Each neighboring process and cooling channel unit cells are coupled to set up material and energy balance equations, including heat-transfer equations for the entire reactor domain, which are then solved simultaneously. The model results were compared with the experimental data for a pilot-scale reactor described in the literature, and were found to be in good agreement. Several case studies were performed to see the effect of variables such as catalyst loading ratio, coolant flow rate, and channel layout on design of a cross-current type reactor with state-of-the-art Fischer–Tropsch catalyst.

The cell-coupling model was then modified to consider more realistic type of flow configurations and flow distribution effect. Cell domain was re-defined for each flow configuration, and the realistic flow distribution effect was incorporated into the model by using results obtained from computational fluid dynamics (CFD). Several case studies were conducted to see the effect of flow configurations, flow distribution, and catalyst loading zones. It was observed that the geometry of cross-co-current was found to give the best performance among the designs considered.

Optimal GTL process was suggested by conducting steady-state simulations where the developed micro-channel FT reactor model was implemented in the form of regressed artificial neural network (ANN) model. First, steady state model for a conventional GTL process was developed. Then, an optimization problem was formulated by defining objective function as the net profit. Design variables for this problem were the pressure and temperature of the FT reactor, split ratio for purge, and recycle flowrate to the FT reactor. Nelder-Mead algorithm was used to solve this derivative-free optimization problem. It can be said that by utilizing the reaction heat of the FT reactor, the reboiler duty for the CO₂ separation was

reduced, and the overall efficiency was increased. Optimal solution showed better economic performances over the base case design.

A dynamic model for the FT reactor was developed. A partial differential equation for the 3D cell-coupling model was formulated and solved to obtain time dependent temperature profile in the entire reactor domain. Several case studies were performed to analyze dynamic behavior of the micro-channel reactor. Separate dynamic simulations were also conducted to suggest optimal start-up and shut-down procedure for the FT reactor system. Several scenarios were generated to analyze the thermal and hydrodynamic behavior of the reactor. Optimal operating strategies for both start-up and shut-down of the reactor could be obtained.

This work could contribute to designing optimal GTL process, especially using a large-scale micro-channel Fischer-Tropsch reactor containing more than 1,000 process channels. The developed reactor model, steady-state model, and dynamic model could be utilized for designing and operation of the GTL system.

Keywords: Micro-channel reactor, Fischer-Tropsch, Reactor modeling, Gas-to-Liquid process, Process optimization, Dynamic simulation

Student ID: 2011-21036

Contents

Abstract	i
Contents.....	v
List of Figures	vii
List of Tables.....	x
CHAPTER 1 : Introduction.....	11
1.1. Research motivation.....	11
1.2. Research objectives.....	13
1.3. Outline of the thesis.....	14
CHAPTER 2 : Reactor model using cell-coupling method.....	15
2.1. Cross-current reactor model.....	15
2.1.1. Introduction	15
2.1.2. Model description.....	17
2.1.3. Model validation.....	27
2.1.4. Case studies	32
2.1.5. Conclusion.....	45
2.2. Improved reactor model	47
2.2.1. Introduction	47
2.2.2. Model construction.....	50
2.2.3. Model validation.....	60
2.2.4. Case studies	69
2.2.5. Conclusion.....	90

CHAPTER 3 : Optimization for GTL process	91
3.1. Introduction	91
3.2. Model description.....	92
3.2.1. Steady-state process model.....	92
3.2.2. Micro-channel reactor model	99
3.3. Optimization for the steady-state model	103
3.3.1. Cost model.....	103
3.3.2. Problem formulation.....	108
3.4. Results and discussion.....	112
3.5. Conclusion.....	115
CHAPTER 4 : Dynamic simulation for microchannel Fischer-Tropsch reactor ...	116
4.1. Introduction	116
4.2. Dynamic modeling for 3D reactor	118
4.2.1. Model description.....	118
4.2.2. Results and anlysis	120
4.3. Optimal operating strategies for FT reactor	125
4.3.1. Model description.....	125
4.3.2. Start-up	129
4.3.3. Shut-down	134
4.4. Conclusion.....	141
CHAPTER 5 : Concluding Remarks.....	142
5.1. Conclusions	142
5.2. Future works.....	144
Nomenclature	145

Literature cited	150
Abstract in Korean (요약).....	157

List of Figures

Figure 2-1. Conceptual diagrams of cross-current heat-exchange reactor, and channel decomposition and cell-coupling method.	19
Figure 2-2. Algorithm for computing material balance, energy balance, and heat transfer in model domain.....	21
Figure 2-3. Comparison of plots of literature experimental data (Deshmukh et al., 2010) (a) and the model estimations (b).....	28
Figure 2-4. Comparison between the model estimation and the experimental data of the conversion and selectivity	30
Figure 2-5. Results for base-case model simulation.....	34
Figure 2-6. Heat generation profiles for different catalyst loading ratio: 0.2(a), 0.7(b), and 1.0(c).	36
Figure 2-7. Heat generation and heat removal rate at various reaction temperature and catalyst loading ratio.....	38
Figure 2-8. Heat generation profile for the different catalyst loading at divided zones: Catalyst loading ratio of 0.2 and 0.7 for the 50% length of the channel, respectively. Same scale of color bar as in the Figure 2-5 was used.	41
Figure 2-9. Sensitivities of maximum temperature of process channels to coolant flow rate for different catalyst loading ratio.....	42
Figure 2-10. Sensitivities of maximum temperature difference and reactor volume	

to the process channel size	44
Figure 2-11. Flow configuration of multi-channel reactor: (a) Structure S1. Cross-counter-cross current with the same side; (b) Structure S2. Cross-co-cross current with the same side; (c) Structure S3. Cross-counter-cross with the different side; (d) Structure S4. Cross-co-cross current with the different side; (e) Structure S5. Fully cross-current	52
Figure 2-12. Conceptual diagram of a cell coupling model: (a) Cell domain construction for the entire reactor of cross-co-cross current with the same side scheme; (b) Flow path construction	54
Figure 2-13. Overall procedure for the computation of the integrated model.....	56
Figure 2-14. Flow distribution effect for the inlet/outlet of the channel and the channel plate inside the reactor: (a) Conceptual diagram representing the domain decomposition of the reactor geometry, ((b) and (d)) velocity profiles obtained from CFD simulation for the decomposed plates, and ((c) and (e)) the result of the data fitting with non-linear function.....	57
Figure 2-15. Comparison of the CO conversion between the measurement and the model estimation. The red line in the plot represents the trend line obtained from the regression.....	65
Figure 2-16. Temperature profile of the process channel for the cross-counter-cross current with the same side scheme	71
Figure 2-17. Result of the regression of the velocity profile for the inlet pipeline whose diameter is (a) 40 mm, (b) 50 mm, and (c) 60 mm.	79
Figure 2-18. Result of CFD simulation and data regression for the flow distribution of the coolant channel plate (a) without inlet guiding fin and (b) with inlet guiding	

fin.	81
Figure 2-19. Temperature profile for the case of (a) uniform distribution and (b) mal-distribution	84
Figure 2-20. Conceptual diagram of (a) partial-overlapping and (b) full-overlapping zone scheme	88
Figure 2-21. Temperature profile for the case of (a) partial-overlapping and (b) full-overlapping zone scheme	89
Figure 3-1. Process flow diagram for overall GTL process	94
Figure 3-2. Structure of the artificial neural network for the micro-channel FT reactor	101
Figure 3-3. Results for the artificial neural network model: (a) Training set and (b) test set	102
Figure 3-4. Concept of Nelder-Mead algorithm: (a) Reflection and expansion, (b) Contraction, (c) Shrink	111
Figure 3-5. CAPEX and OPEX for reference process and optimal process.....	113
Figure 4-1. Changes of the temperature profile with time (Scenario 1). The color bar of the same scale (230°C - 240°C) was used for all the subplots.	122
Figure 4-2. Changes of the temperature profile with time (Scenario 2).....	124
Figure 4-3. Process flow diagram for the dynamic simulation.....	127
Figure 4-4. Comparison between two extreme cases: Scenario 1 and 9.	132
Figure 4-5. Results of the case studies: Scenario 1 through 9.....	133
Figure 4-6. Result of dynamic simulation for three shut-down scenarios: Scenario 1, 3, and 8	137
Figure 4-7. Phase envelope	140

List of Tables

Table 2-1. Reaction Schemes and Kinetic Parameters for Fischer–Tropsch Catalyst Reported in Literature (Deshmukh et al., 2011).....	25
Table 2-2. Reaction conditions for the operation of multichannel Fischer Tropsch reactor.....	31
Table 2-3. Comparison of Sizes of Existing Computational Fluid Dynamic (CFD) ^a and Cell-Coupling Models	46
Table 2-4. Operating conditions ^a for the kinetic experiment.....	63
Table 2-5. Kinetic parameters ^a for Fischer–Tropsch catalyst used in this article....	66
Table 2-6. Comparison of CO conversion between model estimation and the data reported in literature (Deshmukh et al., 2011 ¹¹)	68
Table 2-7. Result of simulation for the five different flow configurations.....	74
Table 3-1. Stream table for the GTL process.....	97
Table 3-2. Results for the economic evaluation for the optimal design; (a) CAPEX and OPEX for the process equipment and (b) Other cost and earning.....	106
Table 3-3. Overall economic evaluation for reference process and optimal process	114
Table 4-1. Size of the process equipments	128
Table 4-2. Description for start-up scenarios	130
Table 4-3. Description for shut-down scenarios.....	136

CHAPTER 1 : Introduction

1.1. Research motivation

Gas-to-liquid (GTL) processes have been identified as promising processes for converting abundant natural gas (NG) to a clean synthetic fuel. The NG is first converted to syngas, which consists mainly of carbon monoxide (CO) and hydrogen, through a reforming process, and then the synthetic liquid fuel is chemically synthesized via a Fischer–Tropsch (FT) reaction. FT synfuel is almost sulfur and nitrogen free, and is therefore considered to be a clean energy fuel.

FT synthesis is known as a strongly exothermic reaction: A large amount of heat, ca. 165kJ per mol of converted CO is generated during the reaction. This heat must be removed to prevent runaway situation and achieve safe isothermal operation of the reactor. In that sense, micro-channel FT reactors are spotlighted as an alternative reactors because its heat removal performance is much better than that of conventional reactors such as fixed bed reactor or slurry-bubble reactor. The micro-channel reactors are also known to be good for scale-up perspectives due to its compactness and ease of manufacturing by modularization.

Although many researchers studied FT reaction performances in the micro-channel environment experimentally, few studies on the design of the micro-channel Fischer-Tropsch reactor can be found from the literature. In order to design a robust and reliable micro-channel reactor, the effect of design variables such as channel layout, reactant inlet temperature, coolant flow rate, catalyst loading ratio, flow configuration, and flow distribution on the reactor performances should be rigorously analyzed. In that perspectives, computational fluid dynamics (CFD) has

been widely used for such detailed evaluation of reaction systems. However, when many process and coolant channels are involved, for large-scale reactors, CFD is highly computationally intensive and time consuming. CFD therefore may not be able to handle all the channels; the problem is unrealistically large, because it deals with rigorous physics such as flow patterns over the entire domain, the shear stress and viscous effects of the flowing entity, and material and energy balances, rather than using simple empirical equations. The current research trend in FT reaction design in a CFD environment is towards reduction of the problem size and analysis of the effects of key variables in the newly defined reduced domain.

When dealing with the design problem of micro-channel reactors, where typically more than 1,000 channels are involved, more efficient way of modeling and solving approach should be considered so that we can practically conduct the design work such as sensitivity analysis, optimization, and dynamic simulations. The reactor model should be simplified in order to reduce the heavy computational load, without losing much physical rigors that are of main concern in the preliminary design of micro-channel FT reactor.

To find an optimal structure and operating conditions for GTL process is an important issue for economic process design. To be more specific, development of more efficient process by analyzing overall heat and mass flow, and design of better process alternatives by changing several important design variables play an important role in process optimization for entire GTL process. Such optimization problem, particularly for a GTL process with the micro-channel FT reactor, is hardly found from the literature.

Development of a dynamic model for the micro-channel FT reactor is essential part for safe operation of the GTL process. FT reaction is considered to be one of

the most exothermic reaction, so the dynamic behavior of the reaction system should be rigorously analyzed for safety. When the reaction heat is improperly controlled, abnormal situation such as thermal runaway takes place. Such undesirable situation is more likely to occur in transient state, for example, start-up and shut-down period of the reactor. It is therefore necessary to find the optimal, robust, and reliable operating procedure for the process safety.

1.2. Research objectives

The objective of this thesis is to suggest an optimal design for GTL process based on the micro-channel Fischer-Tropsch reactor. When a micro-channel reactor is to be scaled-up, more than 1,000 channels are involved, which makes it hard to handle such a large number of channels in conventional CFD environment. In order to solve that problem, a novel micro-channel FT reactor model was developed by using channel decomposition and cell coupling method. The model was validated against the pilot reactor operation data. An improved model that could handle variations in channel configuration and flow distribution. GTL process is known to be one of the most energy-intensive process. Improved versions of the process should be suggested for ensuring economic feasibility. For this purpose, an optimization problem for the GTL process was formulated and solved. A steady state model was developed with implementation of the aforementioned reactor model. Heat from the reformer's outlet stream and FT reactor's outlet stream was utilized to generate excess steam, and to provide required energy for CO₂ separation, respectively. For the safe operation of the FT reaction system, a dynamic model for the FT reactor was developed. Optimal start-up and shut-down procedure for the FT reactor was suggested to prevent thermal runaway or wax

clogging.

1.3. Outline of the thesis

The thesis is organized as follows. Chapter 1 provides motivation and objectives of this study. Chapter 2 describes the micro-channel FT reactor model using channel decomposition and cell coupling method. It includes validation with data from a pilot scale FT reactor. Furthermore, in this chapter, an improved model for the FT reactor which takes flow configuration and distribution effect into account is suggested. In chapter 3, an optimal structure and operating condition for the overall GTL process with the micro-channel FT reactor is suggested. The formulation of the optimization problem is stated, and the solution to that problem is analyzed. Chapter 4 describes the dynamic model for the micro-channel reactor. It also includes the optimal operating strategies for the FT reactor. Chapter 5 presents the conclusion and an outline for the future works.

CHAPTER 2 : Reactor model using cell-coupling method¹

2.1. Cross-current reactor model

2.1.1. Introduction

Gas-to-liquid (GTL) processes have been identified as promising processes for converting abundant natural gas (NG) to a clean synthetic fuel¹⁻⁶. The NG is first converted to syngas, which consists mainly of carbon monoxide (CO) and hydrogen, through a reforming process, and then the synthetic liquid fuel is chemically synthesized via a Fischer–Tropsch (FT) reaction. FT synfuel is almost sulfur and nitrogen free, and is therefore considered to be a clean energy fuel.

Recently, the GTL-FPSO (floating, production, storage, and offloading) process has been considered as an alternative process for exploiting NG from stranded gas reserves or for using associated gases in conventional oil fields^{7,8}. The design of compact, but highly productive, FT reactors will play a central role in the commercialization of GTL-FPSO. The large amount of heat generated during the FT reaction, ca. 165 kJ/mol, must be removed to achieve isothermal operation of the reactor and prevent runaway situations. Novel microchannel heat-exchange FT reactors have received much attention because of their high heat-transfer efficiencies and high production rates per unit volume of reactor^{2, 9-11}. A microchannel FT reactor was studied by Chin et al., using a novel engineered catalyst¹⁰, which improved mass- and heat-transfers and enabled safe operation of

¹ The partial part of this chapter is taken from the author's published paper.

the reactor without increasing undesired methane formation. Cao et al. evaluated the FT reaction performance of a supported cobalt catalyst in a microchannel catalytic reactor². Heat was effectively removed, enabling the reaction to be performed at a high gas hourly space velocity (GHSV).

Many variables such as channel layout, reactant inlet temperature, coolant flow rate, catalyst loading ratio, and space velocity are involved in multichannel FT reactor design. For successful reactor design, the effect of each important variable should be estimated and analyzed in the design step, and computational fluid dynamics (CFD) is widely used for detailed evaluation of reaction systems¹²⁻¹⁸. However, when many process and coolant channels are involved, for large-scale reactors, CFD is highly computationally intensive and time consuming. CFD therefore may not be able to handle all the channels; the problem is unrealistically large, because it deals with rigorous physics such as flow patterns over the entire domain, the shear stress and viscous effects of the flowing entity, and material and energy balances, rather than using simple empirical equations. The current research trend in FT reaction design in a CFD environment is towards reduction of the problem size and analysis of the effects of key variables in the newly defined reduced domain^{12, 19}.

A quick check of the effect of some variable changes is essential for decision making in the preliminary design phase. Sensitivity analyses of the channel layout such as channel width and height, gaps between channels, and wall thickness should be conducted to determine the feasible range of the channel size before the detailed design phase. The influences of some important variables such as reactant inlet temperature, coolant velocity, and feed composition on other related variables, e.g., heat generation, heat removal rate, reaction kinetics, and heat-transfer

coefficient, should be rapidly estimated throughout the entire channel.

In this study, a new method for modeling large-scale cross-current microchannel FT reactors using a channel decomposition and cell-coupling method was developed. External models such as the channel layout model, kinetic model, single-channel model, and empirical heat-transfer model were used to constitute an integrated multichannel distributed model. First, the method and algorithm for model construction were developed, and then the developed model was validated against literature data. Several case studies of the design of cross-current FT reactors with use of the state-of-the-art FT catalyst¹¹ were performed to determine design criteria, analyses, and strategies.

2.1.2. Model description

As will be described in the following sections, a distributed model for the cross-current FT reactor was developed to handle all the channels in the system. It is supported by four external models: a channel layout model that defines channel geometries, a kinetic model that provides kinetic information on the catalytic FT reaction, an empirical heat-transfer model that calculates the heat removal rate, and a single-channel model that evaluates the heat and mass balances for the reaction system in one dimension. Especially, in the channel layout model, structural information such as the number of both process and cooling channels, and the overall size of the reactor core is obtained by specifying the width, height, length, and wall thickness of the process and cooling channels, target wax production rate, space velocity of the reactant, and the catalyst loading amount.

Figure 2-1 shows a diagram of channel decomposition and cell coupling in the cross-current heat-exchange reactor. From the channel configuration, which was

predefined based on the channel layout model, all the process and cooling channels are decomposed in the i , j , and h directions. All the decomposed channel cells are then matched not only to the adjacent cells, but also to the distant cells that interact each other: A process cell located at an arbitrary position (j, i, h) is firstly coupled to every neighboring cells located at the position e.g., $(j, i \pm 1, h)$, $(j, i \pm 2, h)$, $(j, i, h \pm 1)$, $(j, i, h \pm 2)$, etc, to set up heat and material balance equations, which are then solved to obtain the solution. It is assumed that the heat transfer rate is in inverse relationship with the distance between each cell. The lower figure in Figure 2-1 illustrates this pairing concept over an arbitrary cell domain.

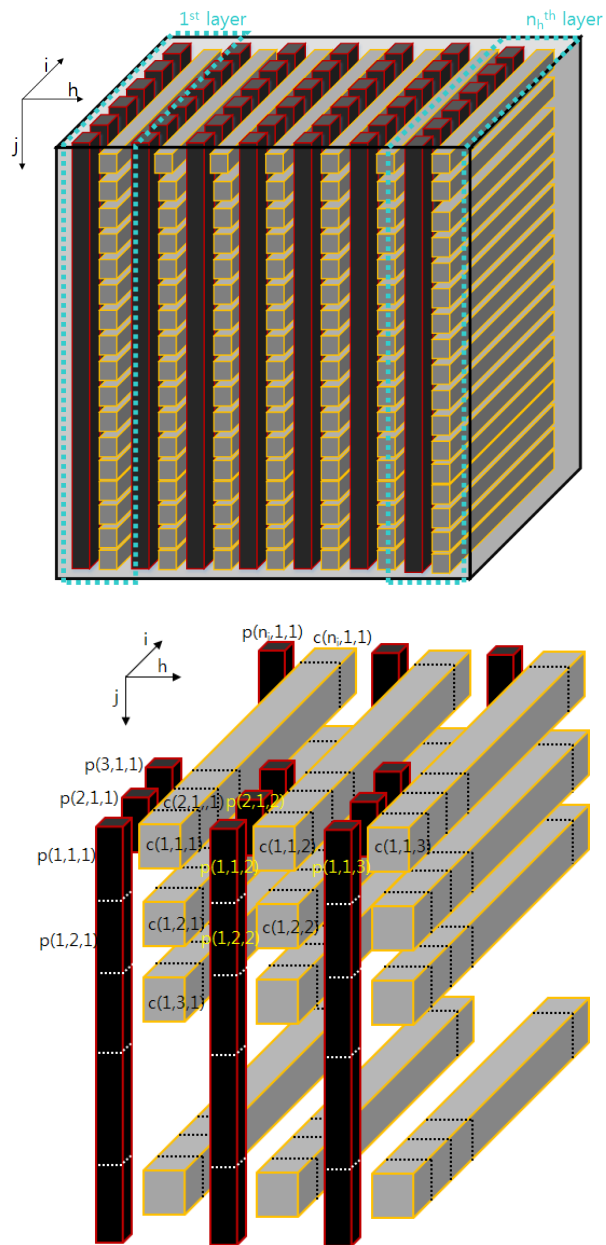


Figure 2-1. Conceptual diagrams of cross-current heat-exchange reactor, and channel decomposition and cell-coupling method.

Figure 2-2 shows the algorithm for computing the mass and energy balance and heat-transfer equations involved in the model. First, it decides the channel configurations over the entire reaction core, followed by the channel decomposition and cell-coupling procedure. It then runs the single channel reaction model, with the help of a predeveloped external kinetic model, to obtain initial values for all the decomposed cells. T_p , T_c , U , and Q in Figure 2-2 are $n_j \times n_i \times n_h$ matrices of the temperature of the process channel cells, temperature of the coolant channel cells, overall heat-transfer coefficient for every pair of matched cells, and amount of heat generated by the exothermic FT reaction in the process channel cells, respectively. U is evaluated using an empirical heat-transfer model:

$$U(j, i, h) = \left(\frac{1}{h_{\text{process}}(j, i, h)} + \frac{\Delta x}{k_{\text{channel}}} + \frac{1}{h_{\text{coolant}}(j, i, h)} \right)^{-1} \quad (2 - 1)$$

where $h_{\text{process}}(j, i, h)$ and $h_{\text{coolant}}(j, i, h)$ are the convective heat-transfer coefficients in a process channel cell and coolant channel cell, respectively, located at position (j, i, h) . In the conductive heat-transfer resistance term, Δx and k_{channel} represent the gap between two matched channel cells and the thermal conductivity of the reactor material, respectively.

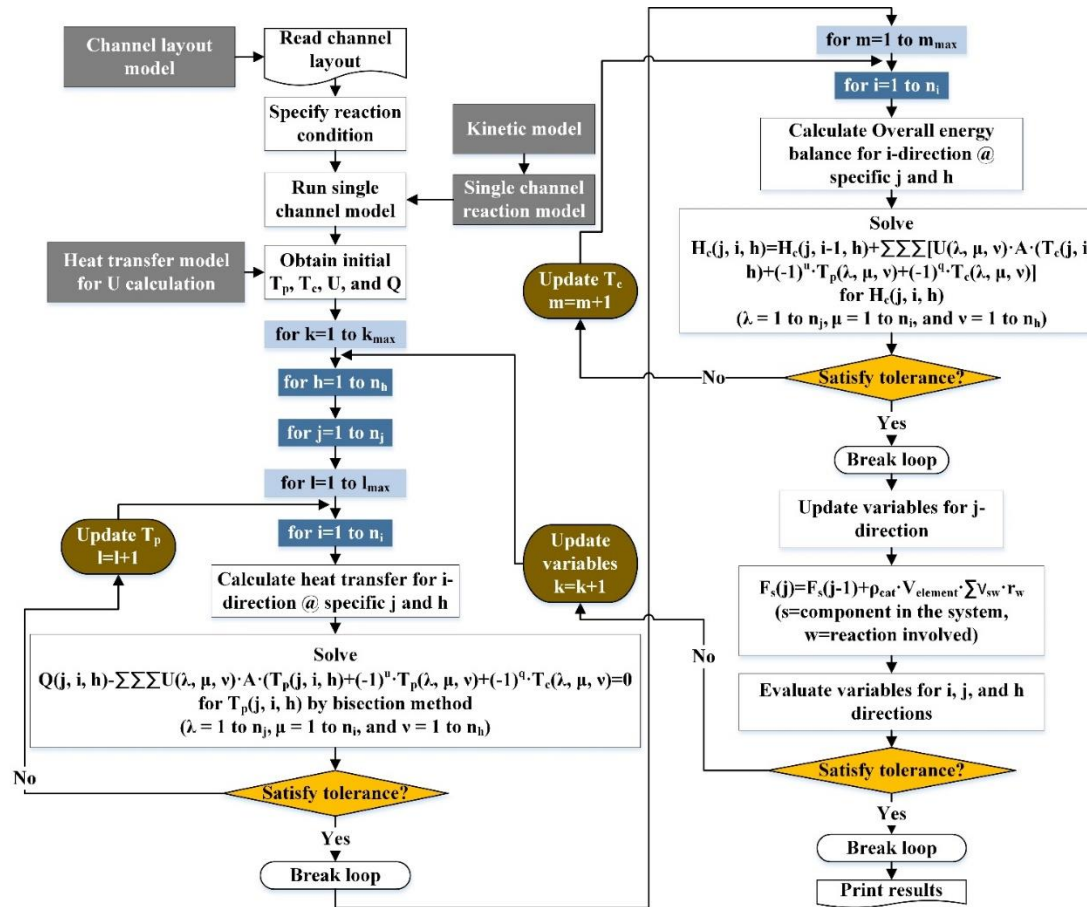


Figure 2-2. Algorithm for computing material balance, energy balance, and heat transfer in model domain.

After specifying the initial values, the model iteratively computes the heat transfer between cells (eq 2-2), and the overall energy balance (eq 2-3) along the i and j direction, respectively.

$$Q(j, i, h) - \sum_{\lambda} \sum_{\mu} \sum_{\nu} [U(\lambda, \mu, \nu) \cdot A \cdot (T_p(j, i, h) + (-1)^u \cdot T_p(\lambda, \mu, \nu) + (-1)^q \cdot T_c(\lambda, \mu, \nu))] = 0 \quad (2-2)$$

$$m_c \widehat{h}_c(j, i, h) = m_c \widehat{h}_c(j, i-1, h) + \sum_{\lambda} \sum_{\mu} \sum_{\nu} [U(\lambda, \mu, \nu) \cdot A \cdot (T_c(j, i, h) + (-1)^u \cdot T_p(\lambda, \mu, \nu) + (-1)^q \cdot T_c(\lambda, \mu, \nu))] \quad (2-3)$$

where the λ , μ , and ν in the sigma are evaluated from 1 to n_j , 1 to n_i , and 1 to n_h , except for j , i , and h , respectively. The u and q in the exponent of (-1) are used to decide the direction of the heat flow. The m_c and \widehat{h}_c are the coolant flow rate and specific enthalpy of the coolant, respectively. First, in the first loop with iteration variable i (Figure 2-2), the j th-vector component of T_p along the i -direction at a particular h is updated, using the bisection method, to solve eq 2-2. The model then evaluates the corresponding vectors of Q and U with a new T_p , and iteratively solves eq 2-2 with updated variables until the errors between the previous and present values are satisfactory within the tolerance. After finishing specification of the variables related to the process channels, i.e., T_p , Q , and U , the coolant channel temperature T_c is updated using the overall energy balance (eq 2-3). Eq 2-3 evaluates the enthalpy changes of the coolant along the i -direction and the heat flow into and out of the cell. In the second loop with iteration variable i (Figure 2-2), the model performs iterative calculations to update j th-vector component of T_c along the i -direction at a specific h until the errors are satisfactory within the

tolerance.

It then updates variables for j -direction using pseudo homogeneous 1-D reaction model (eq 2-4) which accounts for the net generation of all the chemical species in the system.

$$F_s(j, i, h) = F_s(j - 1, i, h) + \rho_{cat} \cdot V_{element} \cdot \sum_w \nu_{sw} \cdot r_w \quad (2 - 4)$$

where F_s , ρ_{cat} , $V_{element}$, and ν_{sw} are the molar flowrate of component s [mol/s], bulk catalyst packing density [gcat/m³], volume of unit element [m³], and stoichiometric coefficient of component s in reaction w , respectively. The reaction schemes considered in this study are presented in Table 2-1, so the $w = 1$ to 6. The same calculation is conducted for all other h s (the layer counting number for h -direction) to obtain the final versions of the variable matrices. The model iterates the computation until the error between the values in the present and previous step becomes negligible.

In summary, this cell decomposition model computes the heat and material balances for the process channel (j -direction), and the overall energy balance and heat transfer equation for the coolant channel (i -direction). It accounts for the heat flow for the j - and h -direction as well. Pseudo homogeneous 1-D reaction model can be applied because the reactions are taking place in the micro channel environment. Detailed computations such as flow viscous effect, heat dissipation along the construction material, and shear stress were not considered because they have negligible effect on the overall heat and mass balances. This simplification greatly reduces computational load without losing much physical rigors that are of main concern in the preliminary design of cross current micro channel FT reactor.

Table 2-1. Reaction Schemes and Kinetic Parameters for Fischer–Tropsch Catalyst
Reported in Literature (Deshmukh et al., 2011)

ID	Reaction	Reaction rate expression ^a
1	$3H_2 + CO \rightarrow H_2O + CH_4$	$r_{CH_4} = k_1 \exp(-E_1/RT) C_{H_2}$
2	$5H_2 + 2CO \rightarrow 2H_2O + C_2H_6$	$r_{C_2H_6} = k_2 \exp(-E_2/RT) C_{H_2}$
3	$7H_2 + 3CO \rightarrow 3H_2O + C_3H_8$	$r_{C_3H_8} = k_3 \exp(-E_3/RT) C_{H_2}$
4	$9H_2 + 4CO \rightarrow 4H_2O + C_4H_{10}$	$r_{C_4H_{10}} = k_4 \exp(-E_4/RT) C_{H_2}$
5	$H_2O + CO \rightarrow H_2 + CO_2$	$r_{CO_2} = k_5 \exp(-E_5/RT) C_{CO} C_{H_2O}$
6	$29H_2 + 14CO \rightarrow 14H_2O + C_{14}H_{30}$	$r_{C_{14}H_{30}} = \frac{k_6 \exp(-E_6/RT) C_{H_2} C_{CO}}{[1 + k_{ad} \exp(-E_{ad}/RT) C_{CO}]^2}$

(a) Reaction schemes and rate expressions

^aConcentrations in kmol/m³.

(b) Kinetic parameters

ID	k_i [rate in kmol/(kg-cat s)]	E_i (J/kmol)
1	2.509×10^9	1.30×10^8
2	3.469×10^7	1.25×10^8
3	1.480×10^7	1.20×10^8
4	1.264×10^7	1.20×10^8
5	2.470×10^7	1.20×10^8
6	3.165×10^4	8.0×10^7
	$k_{ad} = 63.5$	$E_{ad} = 8.0 \times 10^7$

2.1.3. Model validation

The model was validated using the experimental data reported by Deshmukh et al. for a pilot-scale FT reactor with 276 process channels, tested with a cobalt-based catalyst³. Two-phase boiling water was used as a coolant to maximize the heat removal rate. The process and cooling channels were oriented orthogonally to produce a cross-current flow scheme. Kinetic information for the catalyst are presented in Table 2-1; the data are taken from the literature¹¹. The cell-coupling model was constructed using these data.

The process channel, of width 3 mm and height 1 mm, was assumed to be packed with catalyst for 171 mm along the channel length. The size of the catalyst was 280 μ m and the pressure drop was 0.09 bar, which was calculated from Ergun equation. The widths, heights, and wall thicknesses of the cooling channels were all assumed to be 0.5 mm. A feed gas flow rate of 12 400 h⁻¹ GHSV was used. It was also assumed that the feed gas composition (H₂/CO molar ratio) was 2.0, the inlet pressure was 25 bar, the inlet coolant temperature was 210 °C, and the molar fraction of nitrogen in the feed gas was 16.5%.

Figure 2-3 shows a comparison of plots of the experimental data taken from the literature and the model results. The plots represent the temperature profiles in the process channels, and, as can be seen from the figure, the two contours are similar in both trend and values. The estimated results are in good agreement with the experimental data.

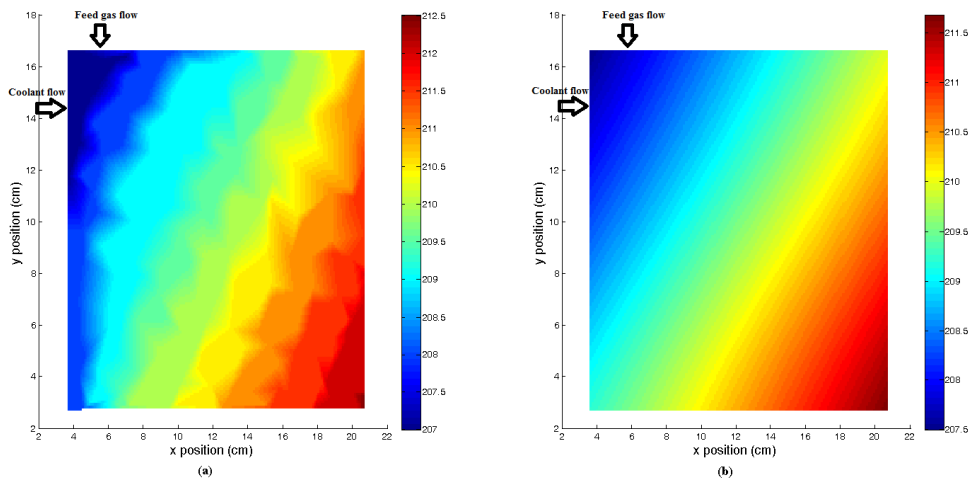


Figure 2-3. Comparison of plots of literature experimental data (Deshmukh et al., 2010) (a) and the model estimations (b).

The robustness of the model was also checked so that it can be applied for the various operating conditions. That is, the model estimation of the CO conversion and methane selectivity were compared with the experimental data taken from the literature¹¹, where the performance of the cross current FT reactor was tested at various reaction temperature (Figure 2-4). In the experiment, the contact time was adjusted to maintain CO conversion of ca. 0.7. Methane selectivity increased as the temperature increased, which is a common phenomenon in the FT reaction systems. The reactor consisted of 274 process channels whose width, height, and length are 0.95 mm, 6.35 mm, and 76.2 mm, respectively. The device was loaded with 66.5 grams of the catalyst with the bulk packing density of 1.054 g/mL. Detailed description of the operating conditions are in Table 2-2.

As can be seen from the figure, the model well predicts both conversion and selectivity for the wide operating range. They are very sensitive to the reaction conditions, so it can be concluded that the model is robust enough to evaluate the performance of the reactor design in terms of safety, operability, and production rate, as well as the temperature distribution over the entire domain.

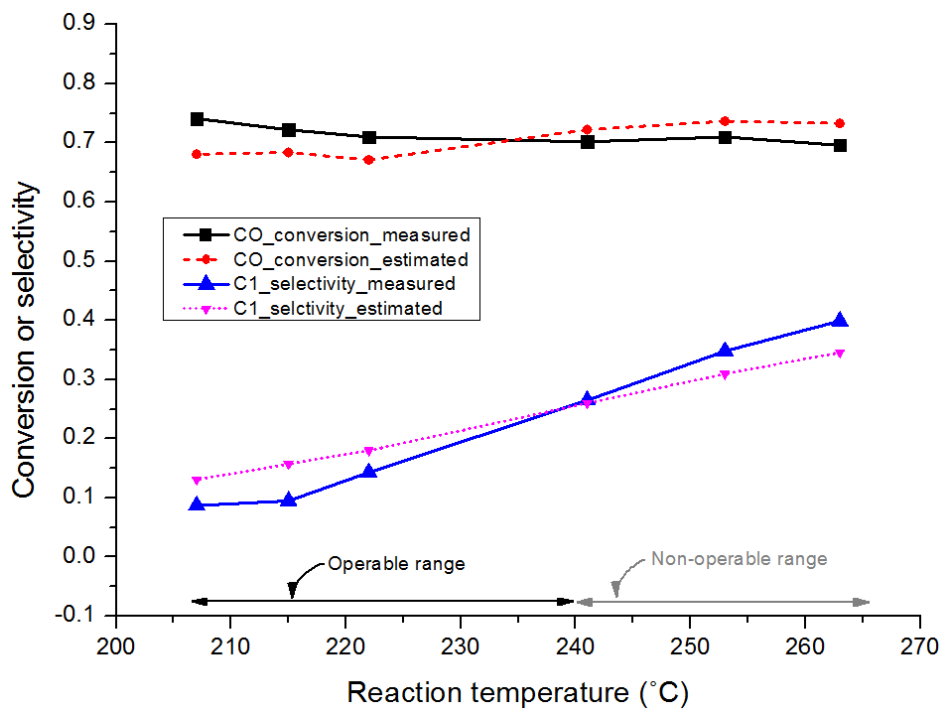


Figure 2-4. Comparison between the model estimation and the experimental data of the conversion and selectivity

Table 2-2. Reaction conditions for the operation of multichannel Fischer Tropsch reactor

Experimental number	Temperature (°C)	GHSV (mL/gcat-hr)
1	207	11,800
2	215	16,200
3	222	22,800
4	241	34,200
5	253	40,200
6	263	48,800

For all the cases, the pressure is 24.13 bar, volume ratio of H₂/CO is 2, volume percent of N₂ in the feed gas is 16.8%, catalyst packing density is 1.054 gcat/cm³.

2.1.4. Case studies

In this section, several case studies for the preliminary design of a FT reactor using the state-of-the-art FT catalyst¹¹ were carried out to clarify the influence of some variables on the design. First, a base-case model was developed, and the results are presented. Sensitivity analyses of the process catalyst loading ratio, coolant flow rate, and channel layout were then conducted to see how the model responded to variations in the design variables.

2.1.4.1. Base-case model

In this base-case study, it is assumed that the highly active cobalt catalyst is used for the low temperature FT reaction in the micro channel reactor. It is therefore a preliminary design study based on the kinetics for the catalyst.

A production rate of 1 barrel per day of FT wax was aimed at in this study. The process channel, of width 1 mm and height 3 mm, was assumed to be packed with the catalyst for 500 mm along the channel length. The widths, heights, and wall thicknesses of the cooling channels were assumed to be 2, 2, and 1 mm, respectively. A feed gas space velocity of 32 000 mL/gcat-hr was used. Assuming 70% CO conversion and 80% wax selectivity, a total of 1704 process channels and 3432 coolant channels with 24 layers was required to achieve the production rate.

The same catalyst in the previous section (model validation part), which follows the kinetics in Table 2-1 was used. Liquid oil was assumed to be used as the coolant, so the coolant phase did not change in the normal operating range. It was also assumed that the H₂/CO molar ratio in the feed was 2.0, and the molar fraction of nitrogen in the feed gas was 16.8 vol%. The reaction pressure and temperature were 24.13 bar and 230 °C respectively. The catalyst loading ratio, defined as the

ratio of the volume of the supported catalyst beads to the sum of the volumes of inert beads and supported catalyst bead, was 70%. The proposed cell-coupling algorithm was implemented in Matlab R2012a to solve the problem.

The simulation results are shown in Figure 2-5, where the temperature profile of the process channel cells are presented. First, for the i-direction, in which the coolant flows, the temperature increases as it takes up the reaction heat. Then the temperatures of the adjacent process channel cells also increase under the influence of the heated coolant cells. For the j-direction in which the reactant flows, however, the temperature decreases as the reaction proceeds: The reaction rate decreases because the syngas concentration decreases as it is consumed by FT synthesis. The decrease in reaction rate reduces the amount of heat generation, which results in the decrease in the process channel cell's temperature for the j-direction. Parabolic temperature profile is found for the h-direction in which the subassemblies of process and cooling channel plates are stacked up: For the vertical direction in the figure, the temperature at the center is higher than those at the two edges because the coolant channel cell at the center is influenced by more process channel cells than the other positions. It therefore absorbs more heat from the process cells, and the heated coolant cell gives that heat to the adjacent process cell resulting in acceleration of reaction heat generation.

A maximum temperature difference (ΔT_{\max}), defined as the difference between the maximum temperature value and the inlet temperature, was 2.55°C for this design. The increase in overall reaction temperature increased the catalyst activity. And as a result, the actual wax production rate of 1.15 barrel per day, which is 15% higher than the target production rate was achieved. The CPU time requirements of this model calculation was 943 s based on the Intel Core i5-2500 3.30GHz.

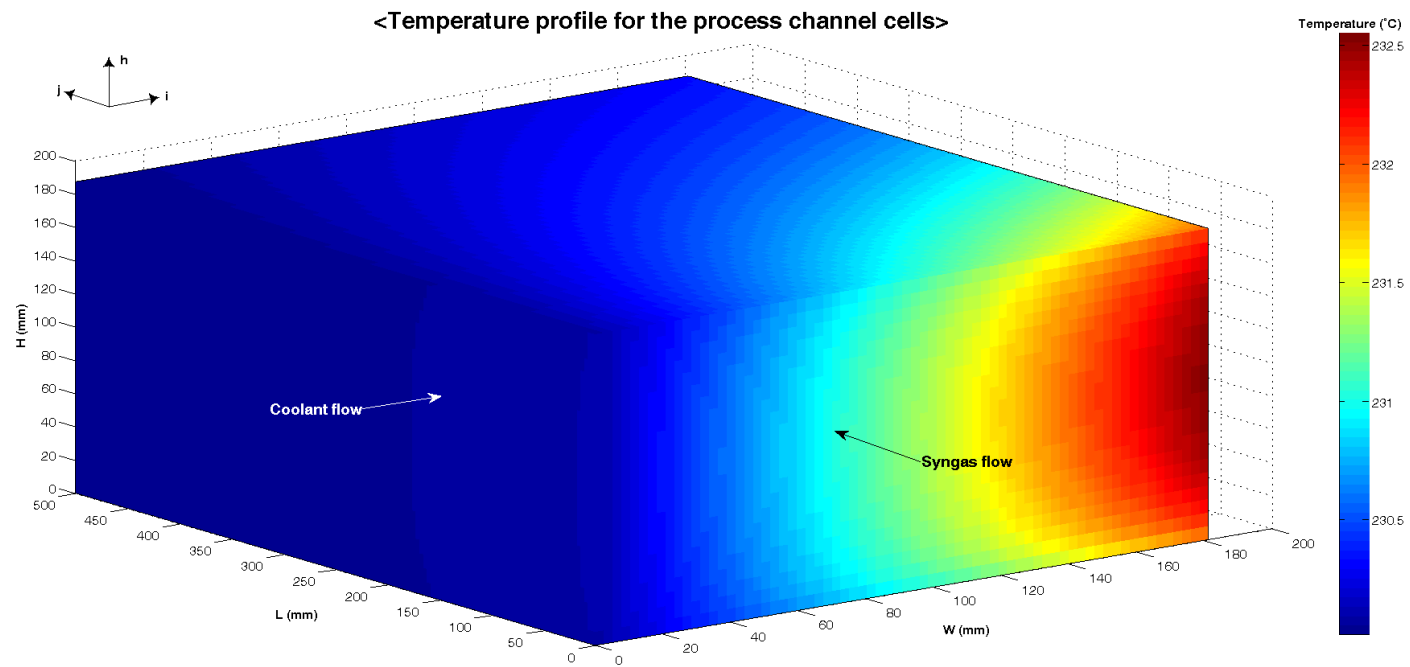


Figure 2-5. Results for base-case model simulation.

2.1.4.2. Sensitivity Analysis.

Sensitivity analyses were performed to determine the effects of three variables: the process catalyst loading ratio, coolant flow rate, and channel layout. Those are the main variables that we can control in the design phase.

First, the effects of model changes were examined by setting the catalyst loading ratio at 0.2, 0.7, or 1.0, with all the remaining operational variables fixed. And for the basis, the same wax production rate of 1 barrel per day was aimed for each case. The catalyst loading amount is controlled so as to control the heat generation, because it directly affects the quantity of the reaction heat per unit volume [kW/m^3]. So the loading ratio should be carefully controlled for a stable and isothermal operation of the reactor.

Figure 2-6 is a graphic representation of the results of the analysis. As can be seen from the figure, the amount of heat generation increases as the catalyst loading increases. So, the case with the low catalyst loading ratio is better design than the case with higher catalyst loading ratio in terms of the heat removal: More stable and safe operation is possible with low catalyst loading. When the loading ratio is 1, however, a large amount of heat is generated from the inlet of the process channels where the concentration of the syngas is the highest. Heat generation there should be carefully controlled to prevent undesired situation such as thermal runaway of the reactor, thermal degradation of the catalyst, or acceleration of the side reaction such as methane formation.

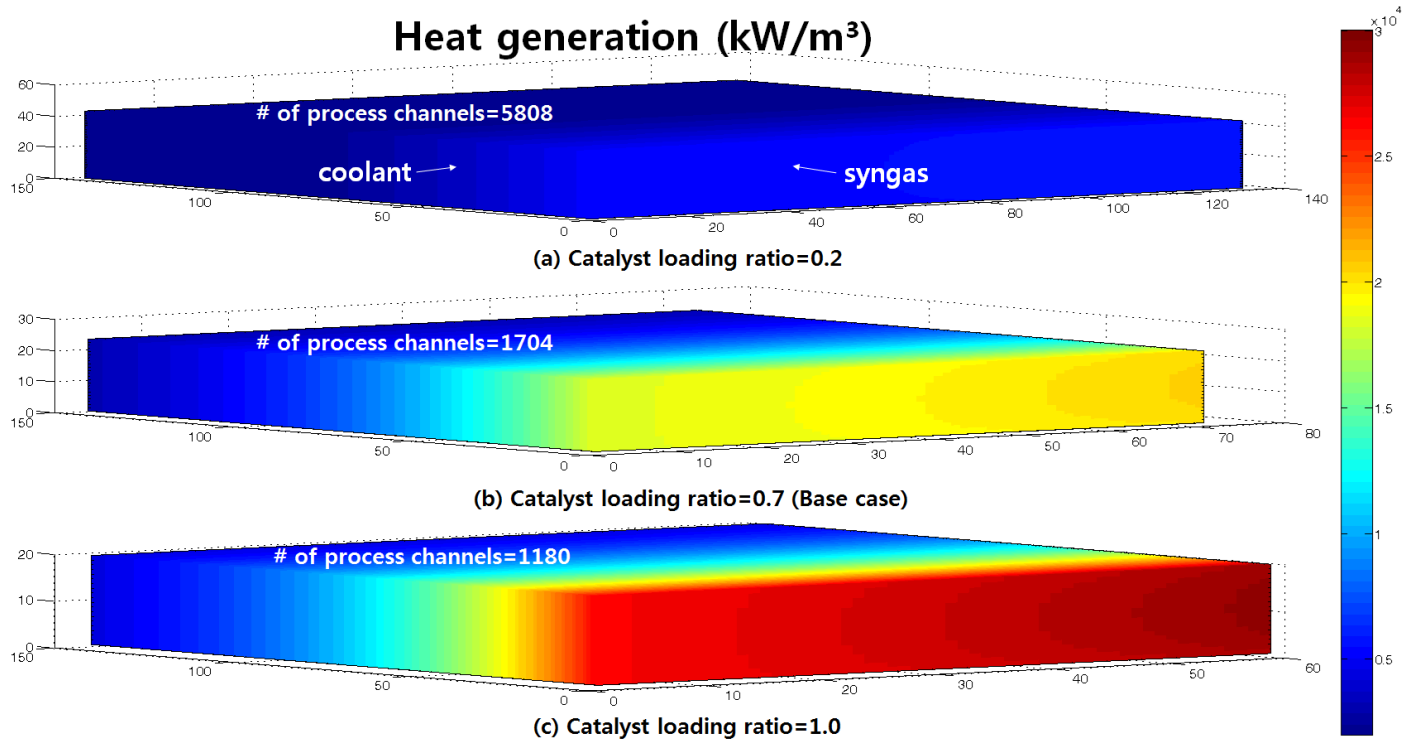


Figure 2-6. Heat generation profiles for different catalyst loading ratio: 0.2(a), 0.7(b), and 1.0(c).

Figure 2-7 is a comparison of the plot of heat generation and heat removal rate at the various operating conditions. First, the reaction heat increases exponentially with the temperature increase because of the activation energy term in reaction constants. The curve should be below the heat removal line for the feasible operation. As the catalyst loading ratio increases, the heat generation curve is moved in vertical direction, and at some point it is located at the upper side of the heat removal line. In that case, heat cannot be perfectly removed, resulting in thermal runaway of the reactor.

For the productivity, however, it is less effective to use low amount of catalyst. As presented in the Figure 2-6, more number of process channels are required to achieve the same amount wax production rate of 1 barrel per day. The productivity per unit volume was reduced as the catalyst loading amount decreased. So, there is a trade-off relationship between safety (heat generation) and economic efficiency (number of channels). (Note that if the reactor is operated at lower catalyst amount and thus smaller hot spot, one can operate the reactor at higher temperature to achieve higher productivity, as discussed by Guettel et al²⁰. But in this study, the operating temperature was fixed at 230°C for the comparison.)

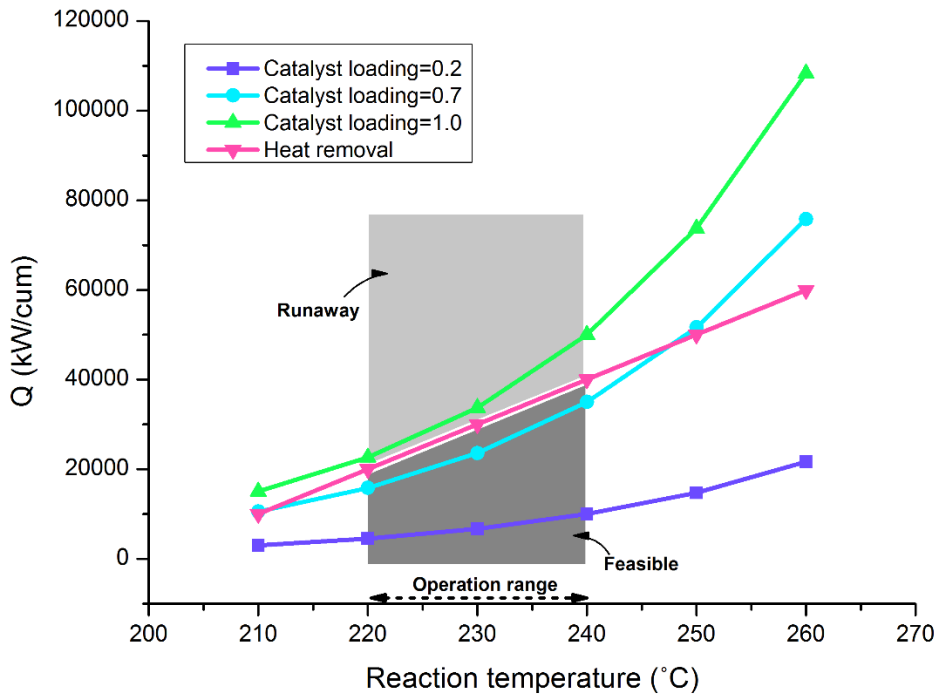


Figure 2-7. Heat generation and heat removal rate at various reaction temperature and catalyst loading ratio.

One way to achieve the high productivity, as well as satisfying the safety problem is to utilize different catalyst loading with zone division. When the high amount of heat generation is expected in the channel inlet, more diluted catalyst is loaded in the zone, after which the higher amount of catalyst is loaded to achieve high productivity. In other words, in the first part of the reaction zone filled with low amount of catalyst, the reaction proceeds to some extent with low heat generation. And in the next zone with high catalyst loading, high productivity can be accomplished without severe heat generation because some amount of reactants has been consumed in the earlier zone: The reaction can start with low concentration. Figure 2-8 illustrates this idea. For the first 50% of the process channel length, the catalyst was filled with the loading ratio of 0.2, and for the next 50%, loading ratio of 0.7. The number of process channels was reduced to 2555 (zone division) from 5808 (lumped loading ratio of 0.2), which means higher productivity is achieved. The maximum heat generation was also reduced to $1.39 \times 10^4 \text{ kJ/m}^3$ (zone division) from $2.05 \times 10^4 \text{ kJ/m}^3$ (lumped loading ratio of 0.7), which means more safe operation could be accomplished.

Next, an analysis of the coolant flow rate was performed. The model was run several times with various coolant flow rates to observe the changes in the results. Figure 2-9 shows the response of the maximum temperature in the process channels to the coolant flow rate for different catalyst loading ratio. First, if the coolant flow rate is increased, the maximum process temperature decreases due to the enhancement of the cooling capacity. The temperature decreases dramatically at the low flow rate region where the temperature difference between the process and the cooling channel is large, whereas it slowly decreases to converge to the inlet temperature of 230°C as the coolant flow rate is increased. The extent of change in

the slope becomes steeper for the high catalyst loading ratio, because the amount of heat generation increases as the catalyst loading amount is increased. The catalyst loading also affects to the minimum requirement of the coolant flow rate: For example, as in the Figure 2-9, if ΔT_{\max} is set to 5°C, then the minimum coolant flow rate requirement is 137 L/min and 439 L/min for the catalyst loading ratio of 0.2 and 0.7, respectively. The higher the catalyst loading, the more the coolant is required. So, for the feasible reactor design, the utility requirement should be checked to prevent thermal runaway. The developed model could decide the feasible range taking into account the interaction among all the process and cooling channel cells.

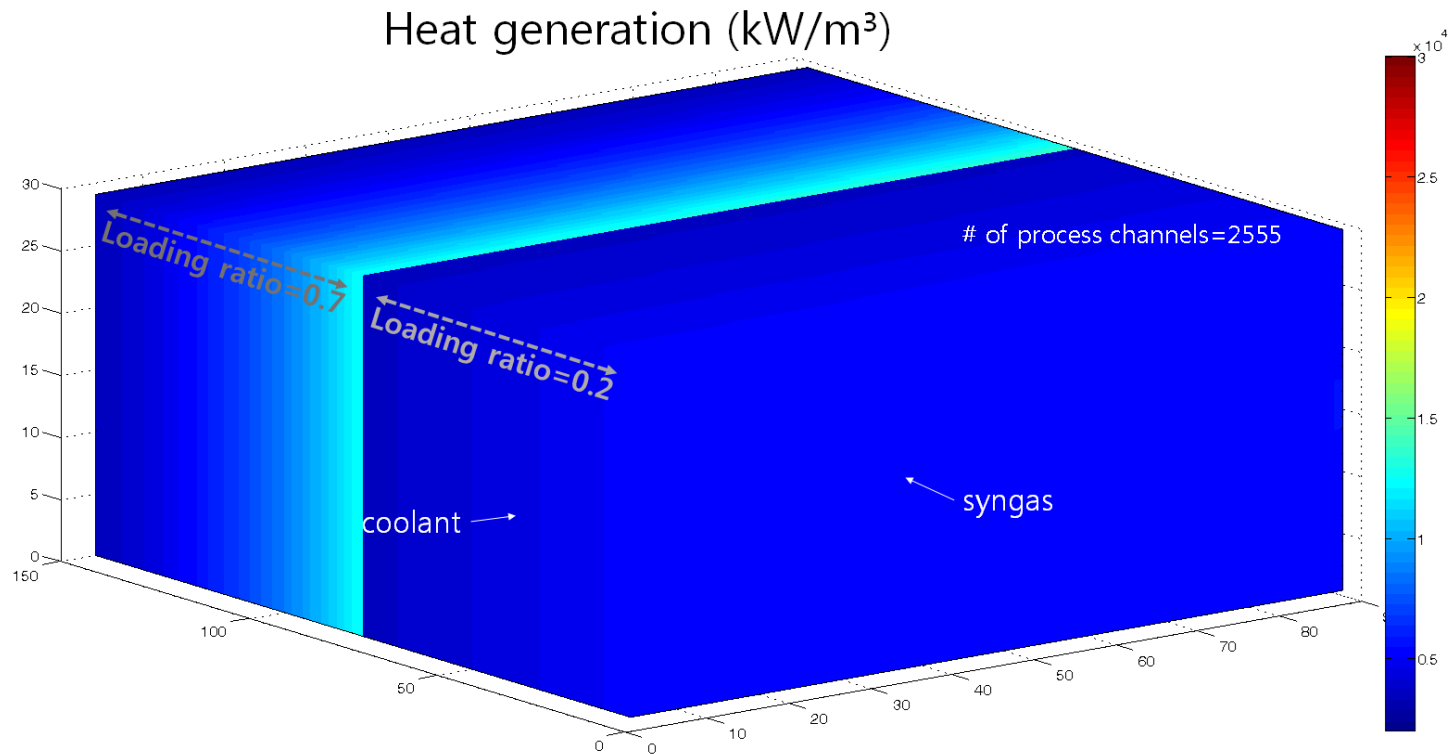


Figure 2-8. Heat generation profile for the different catalyst loading at divided zones: Catalyst loading ratio of 0.2 and 0.7 for the 50% length of the channel, respectively. Same scale of color bar as in the Figure 2-5 was used.

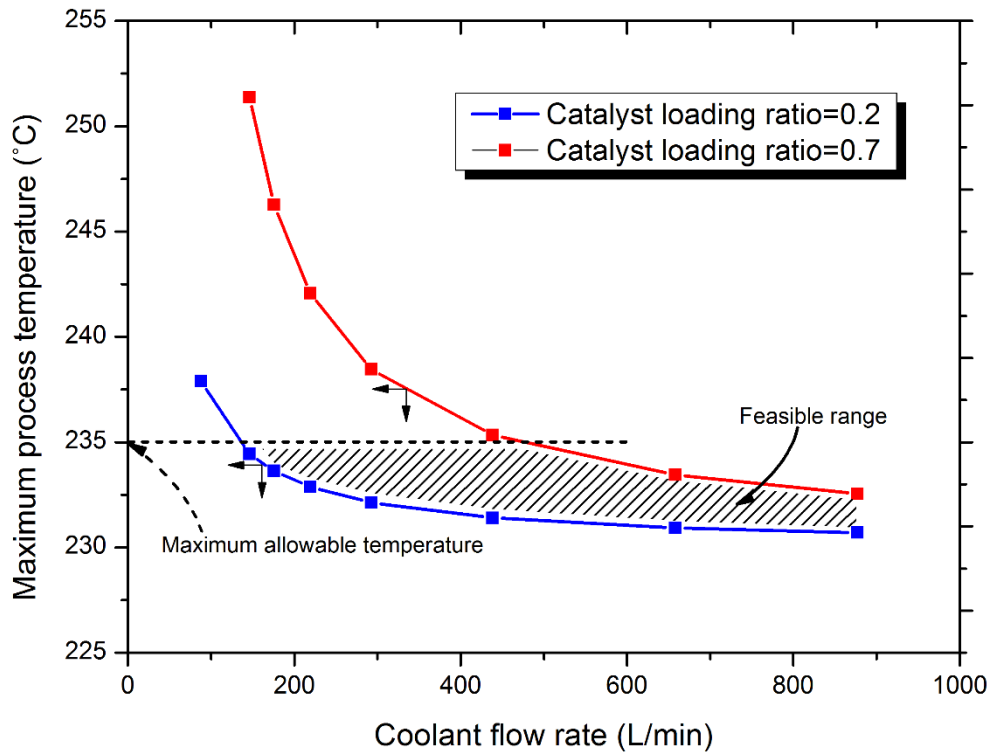


Figure 2-9. Sensitivities of maximum temperature of process channels to coolant flow rate for different catalyst loading ratio.

Finally, a sensitivity analysis was performed on the channel geometry. The characteristic length for heat removal, which is defined by the channel volume divided by the surface area responsible for heat removal, was changed from 0.75 mm to 1.97 mm by varying the width and height. Figure 2-10 shows the result of the analysis. First, as the channel size increases, ΔT_{\max} increases because of the reaction heat. The amount of heat generation increased due to the increase in the unit cell size. The figure illustrates that there is a limit on the characteristic length of 1.20 mm, above which ΔT_{\max} becomes larger than the predefined upper limit of 5°C. So, for the safe operation, it is better to use the channel with small size.

The coolant flow rate affects to the feasibility of the design. For example, the case with the characteristic length of 1.36 mm in Figure 2-10 does not satisfy ΔT_{\max} specification when the normal coolant flow rate (m_{c0}) is used. However, when the coolant flow rate is increased by 20%, it meets the specification. The design, or the operation becomes more dangerous when the flow rate is decreased.

Although ΔT_{\max} decreases when the small channel size is used, the volume of the reactor core becomes large because more number of channels are required to meet the production specification. Also, the core volume increases due to the increase in the free space, where the construction material such as process wall seam should be filled to divide the process channels. As can be seen from the figure, there is a limit on the channel size, below which the reactor volume becomes too large for the fabrication. So, the trade-off relationship between safety (ΔT_{\max}) and economic efficiency (reactor volume) should be considered when deciding the feasible and optimal channel geometry. The cell coupling model could easily determine the feasibility of the design by accounting for the interaction among the variables involved in the reactor design.

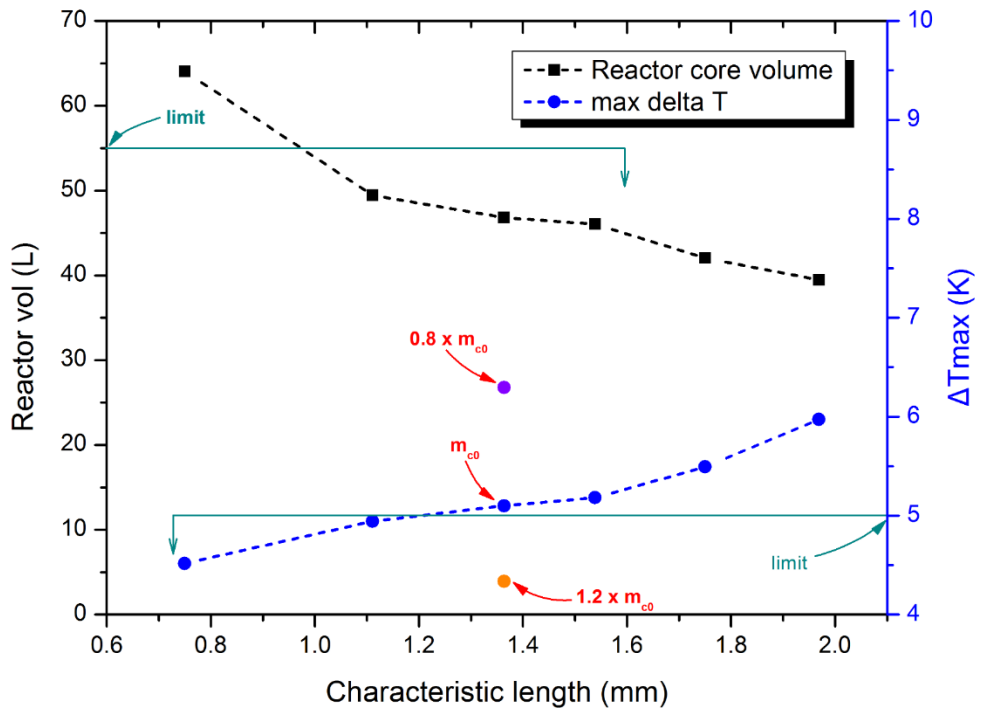


Figure 2-10. Sensitivities of maximum temperature difference and reactor volume to the process channel size

2.1.5. Conclusion

In this study, a new modeling method was developed for the design of a multichannel cross-current heat-exchange micro FT reactor. The model was constructed using the channel decomposition and cell-coupling approach, and was validated with literature data. A case study for design of a FT reactor with the state-of-the-art catalyst was also conducted, followed by sensitivity analyses of the main design variables.

Several external empirical models were incorporated into the integrated model. As a result, the design problem was significantly simplified, without losing physical validity, and the model was able to handle more channels, larger reactor volumes, and more complex reactions compared with existing models¹² (Table 2-3).

The model can be extensively used for preliminary FT reactor design, in which sensitivity analyses of many design variables, and a study of the correlation and causal relationships among variables should be carried out. It can be applied not only to FT reaction systems, but also to other endo- or exo-thermic reaction systems. The model can also be modified to handle more complex flow schemes, and co-current or counter-current architectures with cell rearrangement.

Table 2-3. Comparison of Sizes of Existing Computational Fluid Dynamic (CFD)^a and Cell-Coupling Models

	Existing CFD model ^a	Cell-coupling model
Number of process channels	40	5800 ^b
Number of cooling channels	40	7500 ^c
Number of layers	4	130 ^b
Reactor volume (mm³)	7.5×10^3	6.4×10^{7c}
Number of reactions involved	0	6 ^{b, c}

^aThe compared CFD model is based on the model reported in the reference (Arzamendi et al., 2010).

^bThe numbers correspond to the values used in section 3 of this article.

^cThe numbers correspond to the values used in section 4 of this article.

2.2. Improved reactor model[†]

2.2.1. Introduction

In recent years, gas-to-liquid (GTL) process has attracted considerable attention because it can produce a high quality, clean synthetic liquid product from abundant natural gas (NG) resources^{1, 22-24}. The process consists of two main sub processes. First, the NG is converted into the syngas, mainly composed of carbon monoxide (CO) and hydrogen by a reforming process. The syngas then flows into the Fischer-Tropsch (FT) process, where it is chemically synthesized into a liquid product, also known as a FT synfuel. FT synfuel has high research octane (RON) and cetane number (CN) and almost nitrogen and sulfur free. So it is taking a premium position in the fuel market²⁴⁻²⁶.

FT synthesis is known as an strongly exothermic reaction: A large amount of heat, ca. 165kJ per mol of converted CO is generated during the reaction²⁷⁻³⁰. This heat must be removed to prevent runaway situation and achieve safe isothermal operation of the reactor. Various types of reactors, such as fixed bed, slurry bubble column, circulating fluidized bed, and fixed fluidized bed FT reactors, have been developed and applied to the GTL industries^{31, 32}. Recently, the concept of micro channel FT reactor has evolved because it can effectively handle large amount of heat based on the high heat exchange surface area per unit volume. Cao et al. studied micro-channel reactor for screening several FT catalyst³³. The heat removal rate in the micro-channel reactor was around 15 times higher than that in a conventional fixed bed reactor. Moreover, a scale-up of micro-channel FT reactor was successfully performed by Deshmukh et al²⁷. It was shown that the

[†] The partial part of this chapter is taken from the author's publications.

performance of the pilot scale reactor was consistent with that of a single micro-channel reactor due to the achievement in isothermal operation.

Several design studies for the multi micro-channel reactor have been reported in literatures^{12, 13, 18, 34, 35}. Arzamendi et al. evaluated the effectiveness of the heat removal of micro-channel FT reactor by using computational fluid dynamics (CFD) tools¹². They clarified an important role of the buoyancy effects on the thermal performance of the reactor having cross-current channel structure. Uriz et al. also conducted CFD simulations for designing micro-channel ethanol steam reformer¹⁸. They changed the size of the square channels from 0.1 mm to 0.7 mm and it was shown that the reactor with high surface area-to-volume ratio could remove the heat more effectively. But only four channels were considered due to the complicated kinetic systems implemented onto the CFD environment.

Structural variables such as flow configuration, channel geometry inside the reactor, and the flow distribution play an important role in the reactor performances. For example, Deshmukh and Vlachos analyzed the effect of co-current and counter-current flow configurations on the operation of micro devices for hydrogen production using 2-D CFD model³⁶. The co-current configuration showed the better performance when using medium and low thermal conductivity materials, while the counter-current configuration showed a slightly superior performance in a rather narrow operating region of high space velocity and high thermal conductivity materials. Agrawal et al. investigated the effect of mal-distribution on the reaction and thermal performance of the multi-channel reactor composed of 85 channels³⁷. They simulated 2-D CFD model which accounts for the momentum, material, and energy balance equations simultaneously. Flow mal-distribution affected the reactor performances significantly, especially at high space velocity.

To the best of our knowledge, however, few attempts have been made to model a large scale reactor consisting of more than 1,000 channels. In most cases, the results obtained from simple- or small-scale model and the bench-scale experiment are extrapolated to design the pilot- or industrial-scale reactors due to the practical reason. When developing a large scale multi-channel reactor, many decision variables such as flow configuration, channel geometry, channel layout, flow distribution strategy, catalyst loading, and cooling capacity are involved. In that case, even CFD cannot be utilized for the analysis due to the heavy computational load. A new modeling approach is needed to clarify the interaction among each variable in the entire reactor domain. Especially, some structural variables related to the reactor's cooling capacity are of utmost importance because they directly affect the heat removal rate and safety. Therefore, the effects should be precisely analyzed for design of the large scale, highly exothermic FT reactor.

In the previous work³⁸, we reported the design methods and strategies for the large-scale multichannel FT reactor. A cell-coupling modeling approach was proposed to handle the design problem, where a number of process and coolant channels were oriented orthogonally to produce a cross-current flow scheme. Several case studies were carried out to clarify the effect of some variables such as the process catalyst loading ratio, coolant flow rate, and the size of the process channel. The analysis was performed only based on the cross current configuration, in order to precisely determine the influence of the variables on the *pre-defined* flow scheme.

In this study, we develop the cell-coupling model to handle various flow configurations, so that the design can be conducted at the higher (more conceptual) level. In other words, the improved model is extended to wider searching area:

Several, not only one, flow configurations are considered. This extension helps to determine the optimal flow configuration out of the whole design candidates, which cannot be achieved by using the previous model. We design and evaluate the micro channel FT reactor having more than 5,000 channels based on five representative flow configurations: Cross-counter-cross current with the same side (Fig. 2-11(a)), cross-co-cross current with the same side (Fig. 2-11(b)), cross-counter-cross with the different side (Fig. 2-11(c)), cross-co-cross with the different side (Fig. 2-11(d)), and fully cross current (Fig. 2-11(e)). The modelling approach was slightly modified to apply the cell-coupling model to the various configurations, which will be explained in the following section. The improved model was used to construct the entire 3D domain and set up the material and energy balance equations for the five flow schemes. Moreover, the results from flow simulation using CFD were incorporated into the model to examine the effect of the flow distribution on the temperature profile inside the reactor. Essentially, the optimal design scheme, distribution methods, and catalyst loading strategies for the micro channel FT reactor are derived from the various case studies.

2.2.2. Model construction

As shown in Fig. 2-11, a model for the five reactor design was constructed. For all the cases in the figure, syngas flows vertically down through the 1,110 process channels whose dimensions are 10 mm (width), 5 mm (height), and 510 mm (length). The main difference for each case is the coolant flow configuration, which is illustrated by red arrows in the figure. For example, in the first structure (Fig. 2-11(a), Structure S1), the coolant flows into a header distributor at the bottom of the reactor, counter current flow up the reactor body, through a footer plenum at the top

of the reactor, with entrance and exit flows on the same side of the reactor. We call this first case cross-counter-cross with the same side. Naming of other cases is similar: Cross-co-cross with the same side (Fig. 2-11(b), Structure S2), cross-counter-cross with the different side (Fig. 2-11(c), Structure S3), cross-co-cross with the different side (Fig. 2-11(d), Structure S4), and fully cross current (Fig. 2-11(e), Structure S5).

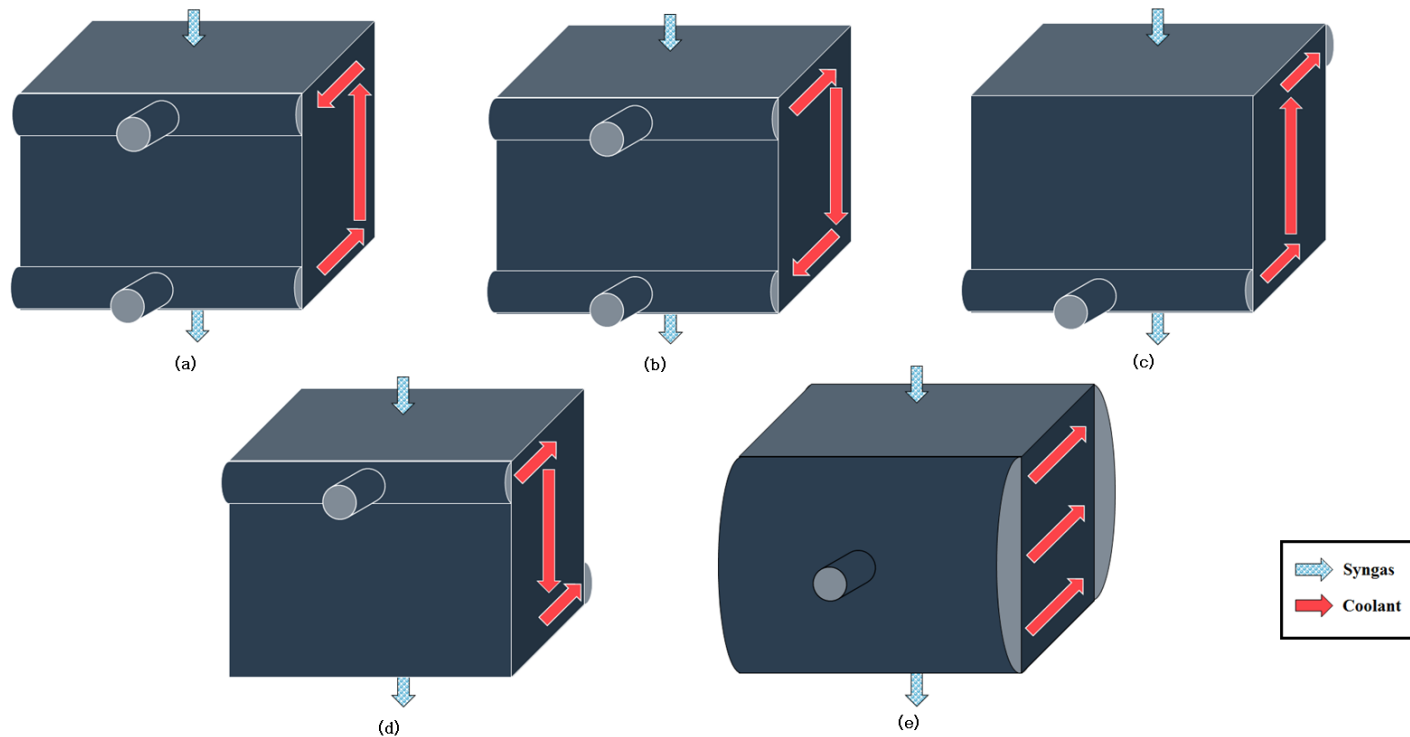
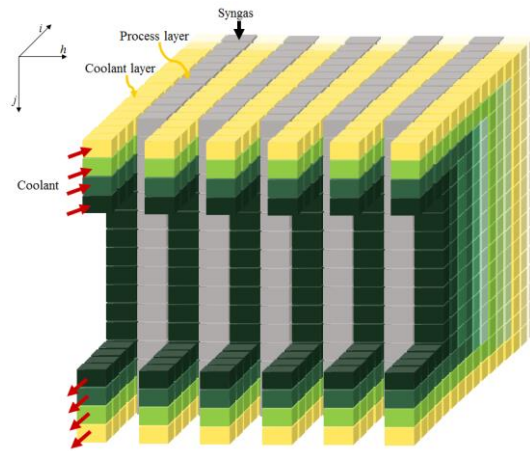


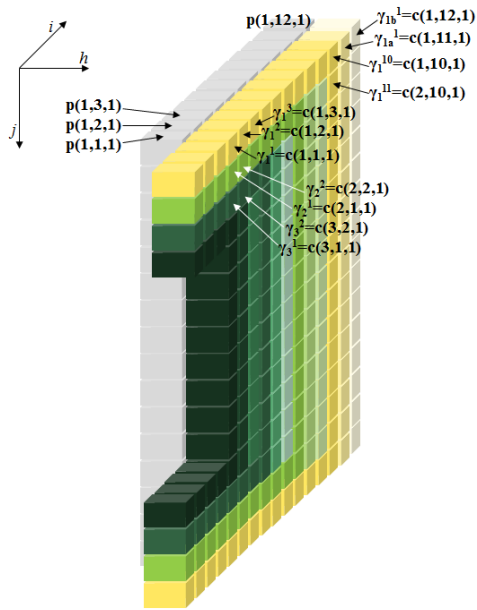
Figure 2-11. Flow configuration of multi-channel reactor: (a) Structure S1. Cross-counter-cross current with the same side; (b) Structure S2. Cross-co-cross current with the same side; (c) Structure S3. Cross-counter-cross with the different side; (d) Structure S4. Cross-co-cross current with the different side; (e) Structure S5. Fully cross-current

When the overall reactor geometry is determined, then the computation domain is defined by the cell coupling method. Figure 2-12(a) shows how the channels are decomposed and the cells are configured for the structure S2. All the process and cooling channels in the reactor core are decomposed into the i , j , and h -directions. Every cell is then matched to all the neighboring cells that interact each other. The communication between each cell is mathematically described by the heat and mass balance equations.

The next step is to define the flow configurations: A route for the coolant flow is constructed in the entire cell arrangement. This is the main part that distinguishes the present model from the previous one. As can be seen from Fig. 2-12(b), each flow path γ is denoted by different colors. We define the path segment γ_s^t as the t -th segment of flow path s . It is a $\mathbb{R}^2 \rightarrow \mathbb{R}^3$ mapping function that relates the route information to the 3 dimensional coolant cell space $c(j, i, h)$. For example, in Fig 2-12(b), γ_1 is the first coolant flow path starting from the top inlet channel to the bottom outlet channel (yellow color). The first segment of the path, γ_1^1 then becomes $c(1, 1, 1)$ in the 3-D cell coordinate. The second segment γ_1^2 is $c(1, 2, 1)$ as the coolant flows cross currently against the syngas flow (to the i -direction). All other cells are assigned to each path's segment in the same way.



(a)



(b)

Figure 2-12. Conceptual diagram of a cell coupling model: (a) Cell domain construction for the entire reactor of cross-co-cross current with the same side scheme; (b) Flow path construction

Figure 2-13 shows the overall procedure for the model computation. As explained above, it starts with defining channel geometry and cell coupling, followed by the flow configuration. The next step is to implement flow distribution data obtained from CFD calculation on the entire cell domain. In the CFD environment, two continuity equations are solved to obtain local velocity profiles for the coolant flow:

$$\nabla \cdot (\rho \mathbf{u}) = 0 \quad (2 - 5)$$

$$\rho(\mathbf{u} \cdot \nabla)\mathbf{u} = \nabla \cdot [-p\mathbf{I} + \boldsymbol{\tau}] + \mathbf{F} \quad (2 - 6)$$

Equation (2-5) and (2-6) describe mass and momentum conservation in the reactor's local boundary, where ρ is fluid density [kg/m^3], \mathbf{u} is velocity vector [m/s], p is pressure [bar], \mathbf{I} is identity matrix, $\boldsymbol{\tau}$ is viscous stress tensor [bar], and \mathbf{F} is volume force [N/m^3]. It is assumed that there's no reaction and no phase change in the coolant channel. Because of the computational load, the CFD cannot be applied to the whole reactor domain. (More than 5,000 channels are involved.) So it is simulated over the decomposed regions. In other words, the reactor was divided into two parts: 1) the header and/or the footer plenum, and 2) the channel plate inside the reactor (Figure 2-14). Each part is related to the flow distribution for the h - and i -direction. As shown in the figure, the velocity profile is obtained by solving equation (2-5) and (2-6). Then, the data is regressed with non-linear functions. By using the result of the CFD simulation, the coolant flow rates for each cell could be obtained: They were calculated by multiplying the total coolant flowrate and the flow fractions of the two parts. The results –the coolant flowrate on each cell position- are then incorporated into the entire cell domain.

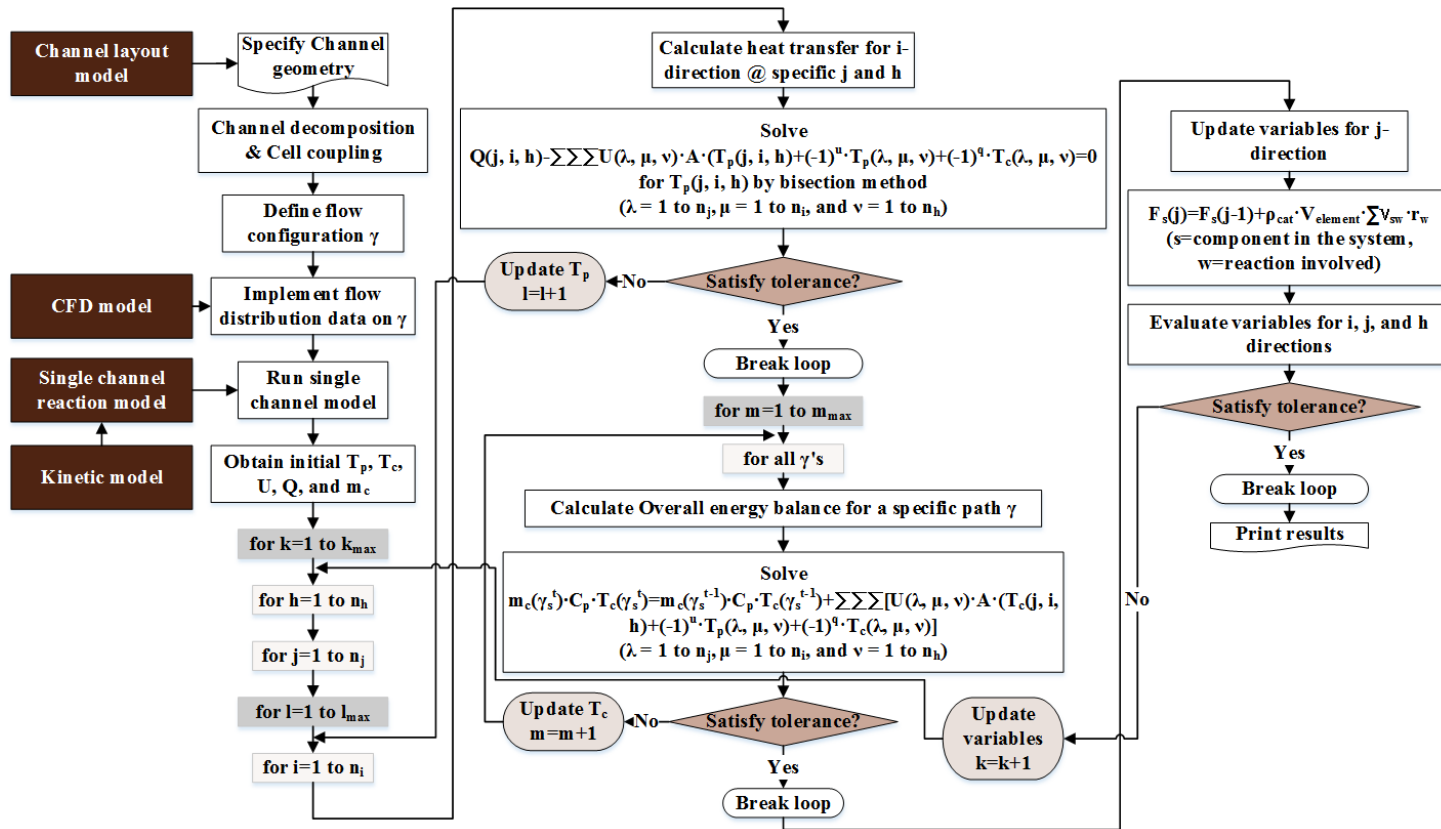


Figure 2-13. Overall procedure for the computation of the integrated model

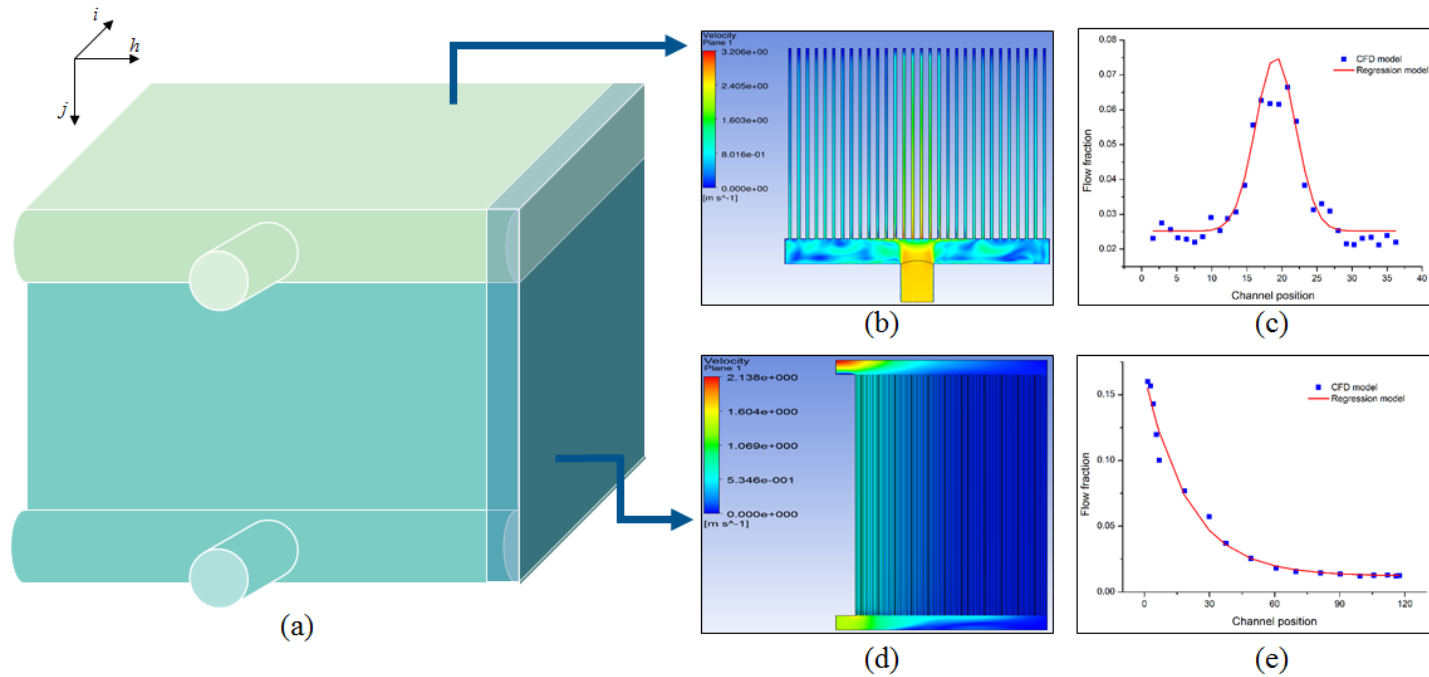


Figure 2-14. Flow distribution effect for the inlet/outlet of the channel and the channel plate inside the reactor: (a) Conceptual diagram representing the domain decomposition of the reactor geometry, ((b) and (d)) velocity profiles obtained from CFD simulation for the decomposed plates, and ((c) and (e)) the result of the data fitting with non-linear

function.

The remaining parts of the procedure are devoted to computing mass and energy balances, and heat transfer phenomena. First, the single channel reaction model is run for the whole process channel cells. Empirical kinetic parameters obtained from kinetic experiment, which will be described in section 2.2.3.1., are implemented on the model to describe the catalyst's performances. The results of the temperature, pressure, and heat generation profile along the single channel will be the initial values for the next calculation. The heat transfer equation between cells (Equation 2-7) and the overall energy balance equation (Equation 2-8) for the flow paths are then solved:

$$Q(j, i, h) - \sum_{\lambda} \sum_{\mu} \sum_{\nu} [U(\lambda, \mu, \nu) \cdot A \cdot \{T_p(j, i, h) + (-1)^u \cdot T_p(\lambda, \mu, \nu) + (-1)^q \cdot T_c(\lambda, \mu, \nu)\}] = 0 \quad (2-7)$$

$$\begin{aligned} m_c(\gamma_s^t) \cdot C_p \cdot T_c(\gamma_s^t) \\ = m_c(\gamma_s^{t-1}) \cdot C_p \cdot T_c(\gamma_s^{t-1}) \\ + \sum_{\lambda} \sum_{\mu} \sum_{\nu} [U(\lambda, \mu, \nu) \cdot A \cdot \{T_c(j, i, h) + (-1)^u \cdot T_p(\lambda, \mu, \nu) \\ + (-1)^q \cdot T_c(\lambda, \mu, \nu)\}] \quad (2-8) \end{aligned}$$

where Q is heat generation [kW], U is the overall heat transfer coefficient [kW/(m² K)], A is characteristic area for the heat transfer [m²], T_p is the temperature in the process channel cell [°C], T_c is the temperature in the coolant channel cell [°C], m_c is the coolant flow rate [kg/s], and C_p is the heat capacity of the coolant [kJ/(kg K)]. The u and q in the exponent of (-1) is used to describe the direction of the heat flow. For example, if the temperature of a certain cell ($T_p(j, i, h)$) is higher than that of the adjacent cell ($T_p(\lambda, \mu, \nu)$ where $\lambda \neq j, \mu \neq i, \nu \neq h$), then the exponent is 1 because heat flows from $p(j, i, h)$ to $p(\lambda, \mu, \nu)$. The j -th vector

component of T_p and T_c at a particular i and h is obtained by solving eq (2-7) and eq (2-8), respectively. The model performs iterative calculations to update the variables until the errors are satisfactory within the tolerance.

It subsequently computes the molar flow rate of each chemical species along the j -direction:

$$F_s(j, i, h) = F_s(j - 1, i, h) + \rho_{cat} \cdot V_{element} \cdot \sum_w \nu_{sw} \cdot r_w \quad (2 - 9)$$

where F_s is the molar flow rate of component s [mol/s], ρ_{cat} is bulk catalyst packing density [g/m³], $V_{element}$ is the volume of unit cell [m³], ν_{sw} is the stoichiometric coefficient of component s in reaction w , and r_w is the reaction rate [mol/(g s)]. The above equation accounts for the generation or consumption of each component. The model conducts the same calculations iteratively until the relative error between the previous and present values are within the pre-specified tolerance value (10^{-6}). The computation terminates when the final versions of each variable matrices are obtained.

2.2.3. Model validation

2.2.3.1. Kinetic model

In order to obtain kinetic model, several experiments were conducted by using conventional FT synthesis experimental equipments consisting of feed gas vessels, a feed gas preheater, single channel reactor, two product receiving tanks, back pressure regulator, and gas chromatography device. The flow rate of the feed gas (nitrogen, hydrogen, and carbon monoxide) is controlled by mass flow controllers. It is heated by the preheater before flowing down through the reactor. The reactor is a single channel reactor with the diameter of 7.75 mm and the channel length of

140 mm. It is surrounded by the electric heater, which is used for maintaining the operation temperature. A 12 wt% cobalt catalyst supported on $\gamma\text{Al}_2\text{O}_3$ was prepared by impregnation method, where a particular organic-based acid solution was used to improve the dispersion of cobalt on the support. The catalysts were calcined at 350°C and then loaded into the reactor, together with the inert quartz powder. Their volumetric mixing ratio was catalyst:inert bead=1:4. Prior to the reaction, the catalyst (0.3 g) was reduced *in situ* by flowing hydrogen gas at 350°C for 24 hours. The hot trap and the cold trap were used to collect the wax product and light oil, respectively. Back pressure regulator was used to maintain the operating pressure. The effluent gas was analyzed by gas chromatography (YoungLin YL6100GC) equipped with the 45/60 molecular sieve 13X, 80/100 PORAPAK N 10 ft \times 1/8 in, thermal conductivity detector (TCD) and flame ionization detector (FID) to quantify the unreacted CO, N₂, and light gas products including CH₄, CO₂, ethylene, ethane, propane, and propylene. The selectivity of the light hydrocarbons such as methane, ethane, propane, and butane, is particularly important in case of the Fischer-Tropsch synthesis because an unsuitable reaction temperature can lead to an excessive production of undesired light hydrocarbons. Their molar distribution in the effluent gas was obtained by gas chromatography. It was assumed that the product distribution in the wax (C₅⁺) follows the well-known Anderson-Schulz-Flowry (ASF) distribution, characterized by the probability of chain growth (α).

To obtain a robust kinetic model, the reaction rates were determined over a range conditions and these are specified in Table 2-4. For all the cases, the pressure was set to 20 bar, and the molar ratio of H₂ to CO in the feed gas was set to 2. The reactor was tested by changing the temperature from 220 °C to 240 °C. The

concentration of the reactants was changed by using different N₂ dilution in the feed gas, and the gas hourly space velocity (GHSV) was varied by changing the feed gas flowrate.

For the regression, the commonly-used kinetic model for the low temperature Fischer Tropsch (LTFT) synthesis on cobalt catalyst presented by Yates and Satterfield (1991) was considered in this study³⁹. The model is derived from Langmuir-Hinshelwood-type equation, and it was modified to allow for variation in the exponents of the partial pressure of CO and H₂:

$$-r_{CO} = \frac{k_0 \exp\left(-\frac{E_a}{RT}\right) p_{CO}^a p_{H_2}^b}{(1 + c \cdot p_{CO})^2} \quad (2 - 10)$$

where k_0 is the frequency factor and E_a is the activation energy [J/(mol K)]. The `fmincon` subroutine in Matlab R2014b was used to minimize the sum of square error (SSE) between the CO conversion data and the model estimation.

$$SSE = \sum \left(\frac{X_{CO,measured} - X_{CO,estimated}}{X_{CO,measured}} \right)^2 \quad (2 - 11)$$

where $X_{CO,estimated}$ is obtained from 1-D pseudo-homogeneous single channel model. In the `fmincon` subroutine, five kinetic parameters, i.e., k_0 , E_a , a , b , and c in eq(2-10), are the decision variables, while the sum of square error (eq (2-11)) is the objective function.

Table 2-4. Operating conditions^a for the kinetic experiment

ID	Temperature (°C)	N₂ dilution^b (vol%)	GHSV (mL/(gcat hr))	CO conversion (%)
1	200	4.00	4,000	16.40
2	220	4.00	4,000	42.00
3	240	4.00	4,000	86.20
4	230	3.96	10,000	30.87
5	230	3.96	15,000	17.90
6	230	3.96	20,000	11.59
7	230	3.96	25,000	7.78
8	230	3.96	30,000	7.37
9	230	3.96	35,000	5.19
10	240	3.96	30,000	13.39
11	220	71.14	23,000	21.32
12	230	71.14	23,000	33.65
13	240	71.14	23,000	48.46
14	220	37.70	23,000	10.88
15	230	37.70	23,000	20.39
16	240	37.70	23,000	31.88
17	220	3.96	23,000	7.76
18	230	3.96	23,000	11.90
19	240	3.96	23,000	16.42

^aFor all the cases, total pressure is 20 bar, and H₂/CO=2 in the feed gas.

^bVolume fraction of the nitrogen in the feed gas.

Figure 2-15 illustrates the result of the regression. It shows the comparison of the experimental data with the model prediction. As presented in the figure, the modified version of Yates and Saterfield model well fits to the experimental data. The result of kinetic parameters is presented in Table 2-5. It is noted that the value of the estimated activation energy and the exponents of the partial pressure of the reactants are within the range of 80~100 kJ/mol and -0.5~+0.5, respectively, which are typically found in literatures³⁹⁻⁴¹. It can be said that the obtained kinetic model is applicable for discription of the typical LTFT system without losing much physicochemical validity. The model is valid for the wide operating range as specified in Table 2-4.

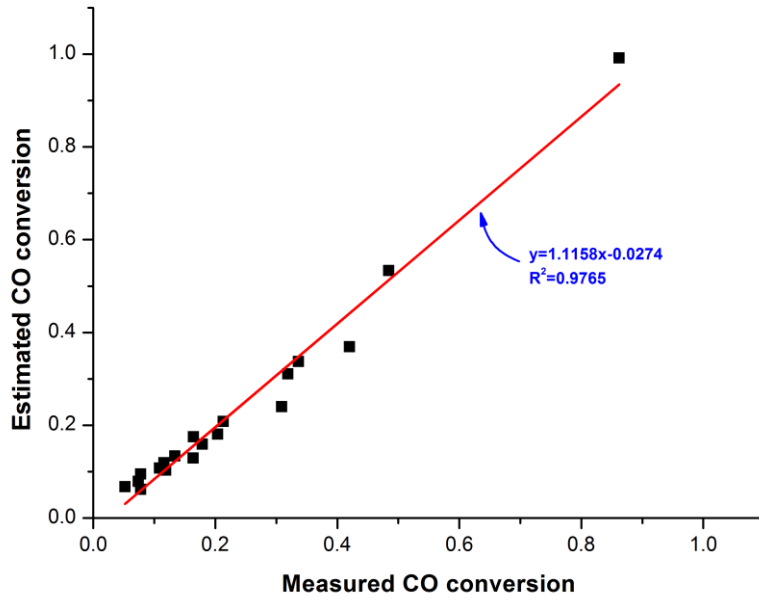


Figure 2-15. Comparison of the CO conversion between the measurement and the model estimation. The red line in the plot represents the trend line obtained from the regression.

Table 2-5. Kinetic parameters^a for Fischer–Tropsch catalyst used in this article

k_0	E_a^b	a	b	c
5.0 $\times 10^7$	95	0.50	0.50	0.30

^aThe parameters correspond to what is presented in eq(2-10)

^bActivation energy in kJ/(mol K)

2.2.3.2. Multichannel reactor model

The validation of the multichannel model was performed based on the kinetic data taken from the literature²⁷. Although the kinetic is different from what is used in 2.2.3.1., it is enough to validate the multi-channel model itself because the system is similar: both are the LTFT system having cobalt as a catalyst. Moreover, the reactor evaluated in the article has the cross-current flow configuration and the channel with micro scale, which means that the geometry is also comparable to the structure of the multi-channel reactor considered in this paper.

Operating data of a pilot scale micro-channel FT reactor tested by Deshmukh et al. (2011)¹¹ was used to validate the cell coupling model. The reactor consists of 274 process channels, which is oriented orthogonally with coolant channels (Fig. 2-11(e)). It was packed with 66.5 grams of the cobalt catalyst for low temperature Fischer-Tropsch synthesis.

Table 2-6 shows a comparison of the model estimation of the CO conversion with the operating data for the various conditions. Errors are less than 10 % for all cases, which implies that the model could handle multiple channels without severe inaccuracies. The errors are believed to arise due to the uncertainties in kinetics, catalyst packing pattern, flow distribution, and plug flow operation. The model is robust in that it is applicable for the various operating conditions as presented in Table 2-6.

Table 2-6. Comparison of CO conversion between model estimation and the data reported in literature (Deshmukh et al., 2011¹¹)

ID	Contact time (ms)	Temperature (°C)	Measured conversion	Estimated conversion	Error
1	290	207	0.741	0.681	0.081
2	210	215	0.722	0.684	0.053
3	150	222	0.710	0.671	0.055
4	100	241	0.702	0.722	-0.029
5	85	253	0.710	0.737	-0.037
6	70	263	0.696	0.733	-0.053

2.2.4. Case studies

In this part, several case studies are carried out to clarify the influence of three variables on the design: Flow configuration, flow distribution, and overlapping zone of the catalyst.

2.2.4.1. Flow configuration

As illustrated in Figure 2-11, the flow configuration will directly affect the velocity profiles of the coolant. It will affect the coolant flow rate, and hence, the cooling capacity at each position. For example, in the structure S1 (Fig. 2-11(a)), the coolant flowrate at the cross current part is higher than that at the counter current region because of the narrow inlet and outlet stream. So, the cooling capacity there is higher than the cooling capacity at the counter current region.

The flow configuration also affect the temperature profile. Some channel paths are longer than others. For example, for the U-shape flow path, the length of the coolant channel that is on the periphery of the plate is longer than that of the channel near the center. So the coolant flowing along the longer path gets more heat from the reaction channel because the contact area for the heat transfer is larger than that of the short path.

Figure 2-16 illustrates the result of representative base case study. The configuration of cross-counter-cross current with the same side (structure S1) was used, and it was assumed that the uniform distribution of the coolant is achieved, which will be explained in next section. Catalyst loading ratio was 0.2 (lump), and the operating temperature and pressure were 220°C and 20 bar, respectively. The coolant flow rate was 217 L/min, gas hourly space velocity (GHSV) was 4,000 mL/(g hr), and the number of process channel was 1,110. The size of the channel was 10 mm (width), 5 mm (height), and 510 mm (length). It was assumed that 370

coolant channels with 3 mm (width) x 3mm (height) was oriented orthogonally with the process channels at the inlet and outlet, respectively. At other part, where the flow is counter current, 4,440 coolant channels with 2.5 mm (width) x 3 mm (height) was placed parallel with the process channels. The inlet temperature of the syngas and coolant was 220.5°C and 220°C, respectively. The weight of packed catalyst was 5.04 kg, and the inlet flow rate of the syngas was 20.15 Nm³/h. The overall CO conversion was computed to be 0.44, and the total wax production rate was 0.26 barrels per day.

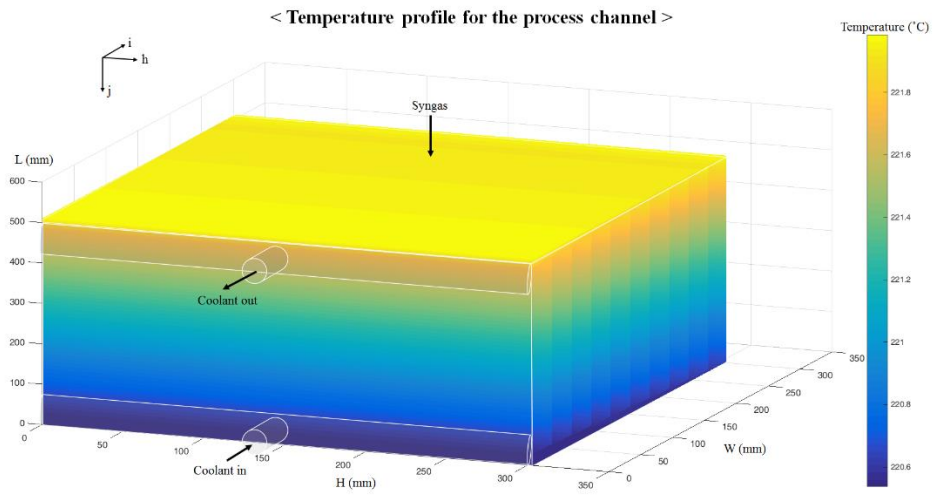


Figure 2-16. Temperature profile of the process channel for the cross-counter-cross current with the same side scheme

As illustrated in Figure 2-16, the temperature profile is influenced by the coolant's flow configuration. As the coolant flows into the channel (positive i -direction), it absorbs the reaction heat from the outlet of the process channel. The temperature increases along the channel until it encounters intersections, where the flow changes its direction to the negative j -direction. (There are 10 intersections. So 10 imaginary discontinuous boundaries are formed due to the characteristics of the cell coupling model, where it computes the energy balance equation for every pre-defined flow path as described in eq. (2-8). In the real operation, however, no such boundaries will be formed because the heat is dissipated along the channel wall.) The temperature increases for the negative j -direction as the coolant flows counter currently against the process channel. The coolant continuously absorbs the heat until its flow direction is changed to the negative i -direction at the intersections. The temperature is subsequently increased along that direction as the coolant flows cross currently against the process channel until it flows out through the footer plenum at the top of the reactor. The temperature has the maximum value at the outlet stream of the coolant. At that point, the syngas flows into the process channel and the FT reaction starts. The reaction rate is the highest due to the high concentration of the reactant, so the heat generation is the highest. Heat released there must be carefully controlled to prevent thermal runaway situation.

A sensitivity analysis was conducted to see the effect of flow configuration on the thermal performance of the reactor, as presented in Table 2-7. For the five cases studied (case C1~C5), the same operating conditions, except for the catalyst loading and coolant flowrate, with the operating conditions of the base case design were used: the reaction temperature and pressure was 220 °C, and 20 bar, respectively, and GHSV was 4,000mL/(g hr), whereas the catalyst loading ratio and

the coolant flowrate was 1.0 and 1086 L/min, respectively. The maximum temperature difference (ΔT_{max}), defined as the difference between the maximum temperature of the process channel cell and the inlet temperature of the syngas, is used for the comparison of each design. If ΔT_{max} is too high, it means that at some point the reaction is taking place at a condition that is far from the desirable operating point, and there is a chance for undesirable situation such as thermal runaway of the reactor, or deactivation of the catalyst. So, ΔT_{max} should be maintained as low as possible for the safe isothermal operation.

Table 2-7. Result of simulation for the five different flow configurations

Case number	Flow configuration^a	Maximum temperature difference (°C)
C1	Cross-counter-cross with the same side (S1)	5.57
C2	Cross-co-cross with the same side (S2)	4.11
C3	Cross-counter-cross with the different side (S3)	5.51
C4	Cross-co-cross with the different side (S4)	4.11
C5	Full cross current (S5)	5.71

^aThe flow configuration correspond to the cases presented in Figure 2-11.

As presented in Table 2-7, the maximum temperature difference is the highest for the full cross current design. The number of inlet coolant channels of that design is more than the others due to the increased contact area for the inlet (Fig. 2-11(e)). So the cooling capacity *per channel* is reduced, which makes the ΔT_{max} increase. The second and the third highest ΔT_{max} is found in the case C1 (Fig. 2-11(a)) and C3 (Fig. 2-11(c)), respectively. Both designs have the inlet coolant stream at the bottom and outlet at the top, so the coolant remove the maximum heat generated at the top after having swept the other part of the channel. The coolant's temperature has already increased at the outlet stream due to this sweeping effect, so the driving force for the heat transfer is decreased. This results in decrease in cooling capacity and increase in the temperature of the process channel inlet stream. The temperature is slightly higher for the case C1 than the temperature of C3 because the coolant path is longer: It brings more heat to the coolant outlet stream after flowing through the long path.

ΔT_{max} for the case C2 (Fig. 2-11(b)) and C4 (Fig. 2-11(d)) is the lowest among the all cases. Both have the exactly same numerical value of ΔT_{max} . In these cases, the inlet of the coolant flow is located at the top and the outlet at the bottom. The coolant first absorbs heat from the top where the reaction rate is the highest. It flows cross currently against the process channel with bearing the heat released at each point, until it encounters the final intersection at the corner, where the temperature reaches the maximum value. The value of ΔT_{max} for the case C2 and C4 is lower than that for C1 and C3 because the driving force for the heat transfer is higher: The fresh coolant at the inlet stream directly removes the maximum heat generation. Both C2 and C4 have the same coolant geometry at the initial part of the coolant channel (cross current region). So the model calculations result in the

same value of ΔT_{max} .

The difference between the values of ΔT_{max} in Table 2-7 is less than 2°C. This small difference is due to the compactness of the system considered in this work. Accordingly, the heat transfer schemes were extremely compact, making the values of ΔT_{max} for the cases so close. Despite the small difference, the difference itself is remarkable: The flow path inside the channel directly affects to the maximum temperature difference, and hence, to the thermal stability of the reactor.

In summary, different coolant flow configuration give the result of different temperature profiles. In most cases, it is desirable to remove the heat as soon as the reaction takes place. Unless the coolant absorbs the generated heat immediately, ΔT_{max} increases due to the sweeping effect and the operation becomes more dangerous. The temperature profile is also affected by the length of the flow path. So if all conditions being same, it is advantageous to make the coolant flow path as short as possible to prevent it from absorbing more heat: If the residence time for the coolant is short, then the heat is more effectively removed and the heat does not accumulate inside the reactor core.

2.2.4.2. Coolant flow distribution

In this context, the flow distribution is meant to be the distribution of the coolant flow at the inlet pipeline or inside the channel. The distribution of the syngas flow is assumed to be uniform, which is achievable by using particular equipment such as demister-like-distributor and a special header packed with bead materials like alumina ball.

The flow distribution plays an important role for the reactor control because it is directly related with the coolant flowrate, and hence, the cooling capacity at every

location inside the coolant channel. If the distribution system is improperly designed, then that will affect the local cooling efficiency, causing mal-function and thermal runaway of the reactor.

There are two local boundaries of interest for design of the coolant flow distribution: Inlet pipeline and inside the channel. First, the distribution at the inlet pipeline affects the flow distribution for each channel layer, as illustrated in Fig 2-14(b). Because of the momentum inertia, coolant tends to flow to the layer located at the center. A bell-shaped curve, similar to the normal Gaussian distribution plot, is obtained by CFD simulation. Less coolant flows into the layers at the edges means less cooling capacity available at those spots. Therefore, the flow profile should be made as flat as possible to have equal cooling capacity for each cooling channel layer.

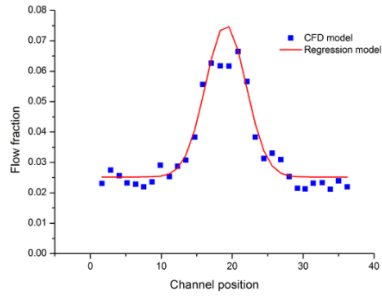
The diameter of the inlet pipe is the main variable that determines the shape of the profile. For the analysis, CFD computation was performed by changing inlet pipe diameter from 40 mm to 60 mm. A commercial available Syltherm 800[®] was used as a coolant, and the total flowrate of 180 L/min, which was determined from the overall energy balance equation was used. At the operating condition, the coolant's specific heat is 1.95 kJ/(kg K), density is 754.11 kg/m³, thermal conductivity is 0.0974 W/(m K), and the viscosity is 0.88 mPa·s. The vapor pressure of the coolant is 142.4 kPa, slightly higher than the ambient pressure at the reaction temperature. So the coolant was assumed to be pressurized to around 10 bar before the operation to avoid the partial evaporation.

Ansys CFX 15.0 was used to solve the mass and momentum balance equations. The results are shown as the blue data points in Fig. 2-17. A non-negligible dispersion of the data is due to the turbulence in the inlet header. As presented in

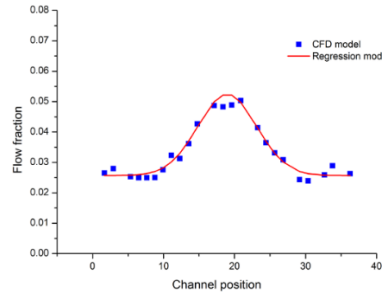
the figure, the velocity profile becomes more flat as the inlet pipe diameter increases. This is because the inertia towards the center is dispersed as the coolant flows for the wide area. The obtained profile is then regressed with the nonlinear function:

$$u_i(h_k) = a \cdot \exp(-b \cdot (h_k - c)^2) + d \quad (2 - 12)$$

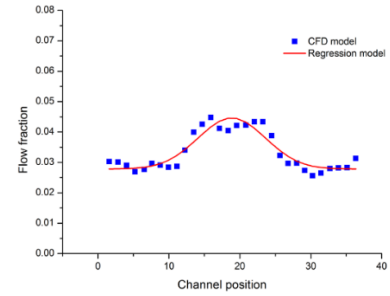
where u_i is the coolant velocity for i -direction. It is a function of the layer position h_k , where the subscript k ($k=1$ to 37 in this case study) is used for counting the number of channel layers which is located along the h -direction. The a , b , c , and d are the parameters that determine the shape, displacement, and the axis of symmetry of the bell-shaped curve. The structure of the function was conferred from the normal Gaussian distribution. The `nlinfit` subroutine in Matlab R2014b was used to regress the data taken from the CFD simulation to the above nonlinear function. The results are shown in Figure 2-17. As can be seen from the figure, the model function well fits to the CFD data.



(a)



(b)

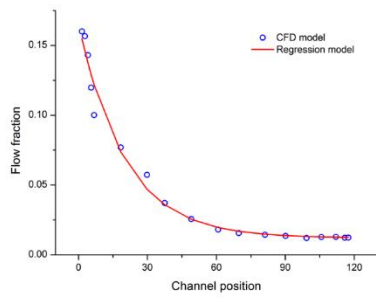
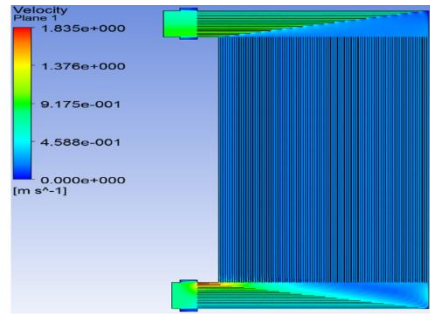
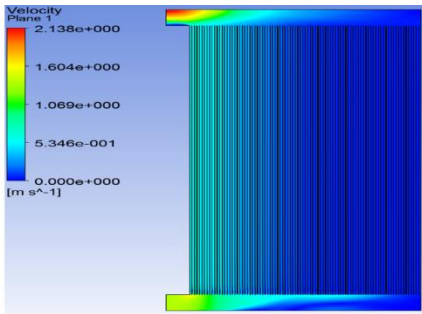


(c)

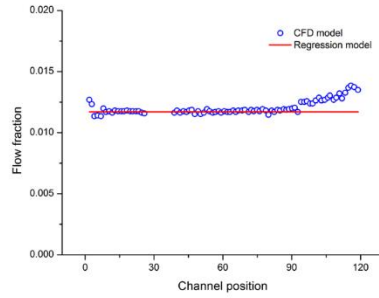
Figure 2-17. Result of the regression of the velocity profile for the inlet pipeline whose diameter is (a) 40 mm, (b) 50 mm, and (c) 60 mm.

Next, the distribution inside the channel affects the internal coolant flow and cooling capacity for a specific layer as illustrated in Figure 2-14(d). In the channel layer, the coolant flowing for a short path undergoes less resistance than the coolant flowing for a long path. So more coolant flows along the short channel, showing skewed velocity profile. From one particular case study, the ratio of maximum to minimum velocity (u_{max}/u_{min}), which is commonly used criteria for evaluation of the flow distribution, was around 13 for the worst scenario. That means the cooling capacity for some region can be less than 1/13 of other region if the distribution system is improperly designed. In that case, the reactor control would be so difficult that thermal runaway or local overcooling can occur. Such a mal-distribution must be prevented for the safe operation.

One strategy for making the skewed flow distribution uniform is to use inlet guiding fin, which transports the coolant to a certain point without losing its momentum. Figure 2-18(b) illustrates the result of the CFD simulation for the case of inlet guiding fin. Each guiding fin has different length so that the coolant that flows along the long channel path flow through the long fin, and short path through the short fin. As depicted in the figure, the distribution becomes nearly uniform when the guiding fin is used.



(a)



(b)

Figure 2-18. Result of CFD simulation and data regression for the flow distribution of the coolant channel plate (a) without inlet guiding fin and (b) with inlet guiding fin.

The obtained CFD data was then regressed with the nonlinear function:

$$u_j(i_m) = p \cdot \exp(-q \cdot i_m) + r \quad (2 - 13)$$

where u_j is the coolant velocity for the j -direction. It is a function of the channel position i_m , where the subscript m ($m=1$ to 120 in this case study) is used for counting the number of coolant channels comprising one layer. And p , q , and r is the parameters that determine the shape of the function. The `nlinfit` subroutine in Matlab R2014b was used to regress the data to the above exponential form. The result is shown in Fig 2-18, and the function well fits to the CFD data.

After obtaining the parameters in eq (2-12) and (2-13), the function values, i.e., the coolant velocity, are evaluated for every cell position. They are implemented to the cell coupling model (especially to the equation (2-8)) as a 3-D array of the $m_c(\gamma_s^t)$. Subsequently, the mass and energy balance, and the heat transfer equation are solved based on the implemented flow distribution data.

Figure 2-19 shows a comparison between the temperature profile of the uniform distribution and the mal-distribution case. It is assumed that perfectly uniform distribution, i.e., flat profile for both inlet pipe and inside the channel, is achieved for an ideal case. Practically, it is attainable by using inlet pipe whose diameter is greater than 80 mm and the inlet guiding fin. And in the mal-distribution case, narrow (40 mm) inlet pipe and no inlet guiding fin were used. As shown in the figure, ΔT_{max} becomes greater than 4 times of the ideal case, if mal-distribution occurs. It is also noted that the overcooling is expected at the center of the reactor core where the most fraction of the coolant flows, whereas the heat is accumulated at the two edges where almost no coolant flows. The flow distribution model was successfully integrated with the cell coupling model. The integrated model could be run without severe computational load, and also giving the physically

reasonable result. The model can be used to clarify the influence of the flow distribution and realistic structure on the reactor performances, even if more than 5,000 channels are involved.

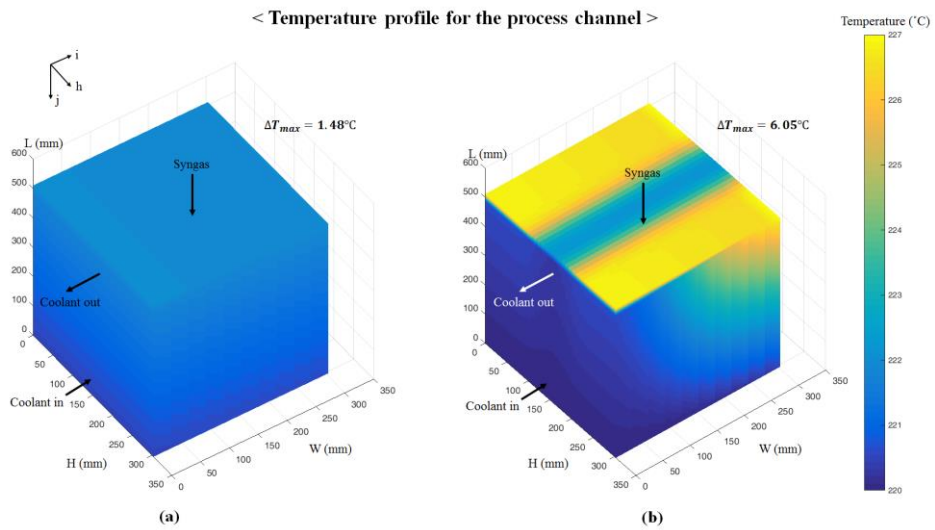


Figure 2-19. Temperature profile for the case of (a) uniform distribution and (b) non-uniform distribution

2.2.4.3. Catalyst-coolant overlapping zone

As mentioned in section 2.2.4.1, it is important to remove the maximum heat generated at the inlet of the process channel because in most cases, the temperature reaches the maximum value near the inlet as shown in the previous case studies. The amount of heat generation is related to the reaction rate [mol/gcat s], which is dependent on the catalyst loading density [gcat/L]. So it is a common technique to reduce the catalyst loading amount by mixing the catalyst particle with inert bead, when a large amount of heat generation is expected. Heat can be removed more easily although the productivity (per unit channel) is reduced. So it can be said that there is a trade-off relationship between the heat generation (safety) and production rate (efficiency). In the previous report³⁸, we studied the effect of zone division with catalyst loading ratio. Both the high heat removal rate and the high wax productivity could be achieved simultaneously by using zone division method, where the low amount of catalyst is packed in the initial part of the channel zone and the high amount of catalyst is filled in the next remaining part of the zone. Higher productivity could be accomplished without severe heat generation despite the larger catalyst amount in the second zone. Because some fraction of the reactants has been already consumed in the first zone so that the reaction rate is not that fast.

In this study, another strategy for the efficient heat removal is proposed. The main objective is to successfully control the heat generation for the particular region that shows complicated flow distribution profiles. Such region includes the inlet and outlet of the coolant channel, and the intersections where the flow momentum changes drastically. As mentioned in the previous section, it is difficult to predict the exact coolant velocity profile and evaluate the local cooling capacity

for such complicated structures. Therefore, one can say that it is reasonable to make those unpredictable regions inactive, or dead, for the safe operation. If there is no reaction, then no heat will be generated, and no effort is needed to remove the heat. So, no catalyst is loaded on purpose for the channel zones that overlaps with the complicated cooling regions, which is just a small fraction of the entire part. As shown in Fig 2-20(a), the catalyst is packed only for the zone that overlaps with the well-defined, predictable, and accountable cooling region.

Two cases were simulated for the comparison on the basis of the flow configuration of cross-counter-cross current with the same side (Structure S1). In the first case, the partial overlapping zone scheme, 50% diluted catalyst was packed in a fractional, i.e., only counter current part of the channels, and in the second case, the full overlapping zone scheme, the same diluted catalyst was filled in the entire part of the channels. The operating temperature was 220°C, and the pressure was 20 bar. The GHSV was 4,000 mL/gcat-hr, and the coolant flow rate was set to 500 L/min. The worst scenario for the coolant flow distribution was assumed: The sharpest bell-shaped profile for the inlet pipe region, and the most steeply decaying exponential profile for the inside channel layer out of all distribution scenarios were implemented into the model.

The results are presented in Figure 2-21. As shown in the figure, the first case (Fig 2-21(a)) has no hot spot at the inlet, because no catalyst is packed there. On the other hand, the second case (Fig 2-21(b)) has hot spot at two sides of the inlet of the process channel, where the cooling capacity is low due to the poor distribution performance. For the first case, although the zone is inactive with respect to reaction at the inlet of the process channel, the temperature increased slightly due to the coolant's sweeping effect, as discussed in the previous chapters.

The maximum temperature difference (ΔT_{max}) for both cases is 7.04°C, and 8.79°C, respectively, which shows the effectiveness of the strategy of partial overlapping zone. When the operating condition is changed to more harsh condition, for example, the high catalyst loading, high temperature, and high pressure, the difference of ΔT_{max} between two cases becomes bigger. The productivity for the partial overlapping case decreased by 11.7% because of the dead zone. Although the productivity is reduced, the design became more predictable, operable, and reliable in terms of safety, which is regarded as the most important issue in the detail reactor design. The integrated model suggested in this article could successfully handle such problems, and give results of most favorable and feasible design out of many design candidates through the efficient computational procedure.

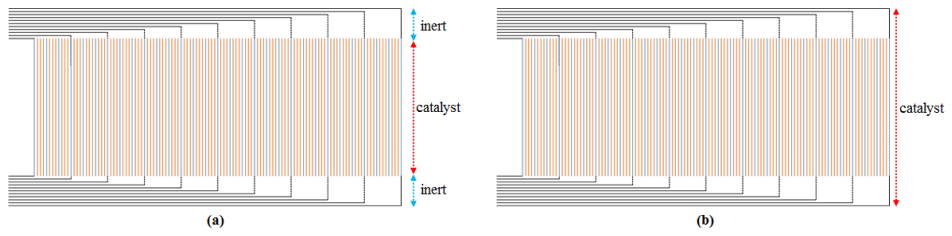


Figure 2-20. Conceptual diagram of (a) partial-overlapping and (b) full-overlapping zone scheme

< Temperature profile for the process channel >

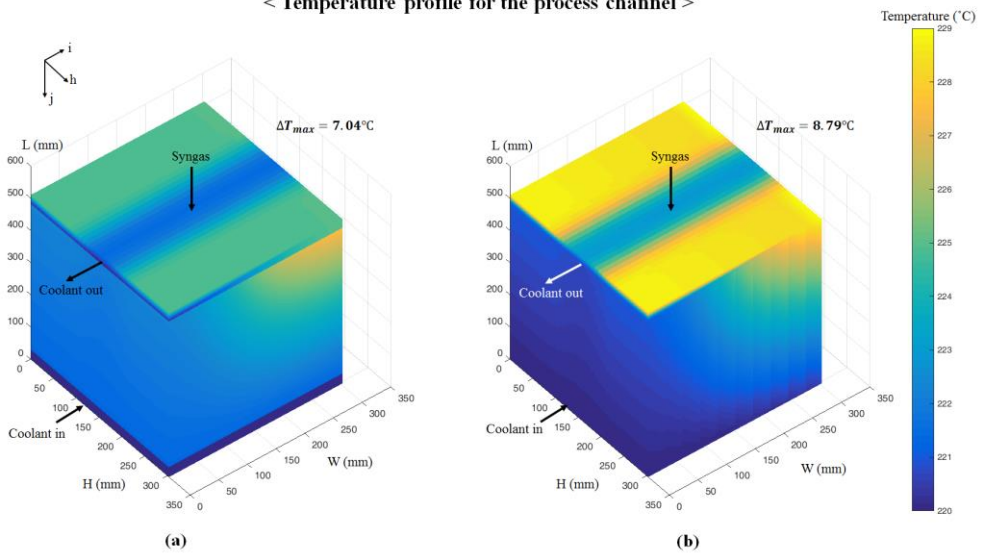


Figure 2-21. Temperature profile for the case of (a) partial-overlapping and (b) full-overlapping zone scheme

2.2.5. Conclusion

In this study, an integrated model for designing large-scale micro-channel Fischer-Tropsch reactor was developed. The effects of flow configuration, flow distribution, and strategic catalyst loading zone adjustment on the temperature profile of the reactor were analyzed by using cell-coupling approach and the results obtained from external computational fluid dynamics model.

Temperature control is of utmost importance in the reactor design, especially for the highly exothermic reaction systems. When more than 1,000 channels are involved, which is a common situation in designing the pilot- or industrial-scale micro-channel reactor, it is very hard to predict what is going on in the entire reactor domain. Interaction between each channel should be carefully analyzed in the design phase, in order to prevent undesirable situation such as thermal runaway, catalyst deactivation, and acceleration of side reactions. The present study contributes to designing such large-scale multi-channel reactor by modelling approach. The model incorporates kinetic parameters, flow configuration, and flow distribution data. This integration made it possible to analyze the whole scale reactor, which is not practicable if the conventional model, such as computational fluid dynamics, is used.

The design strategies and philosophy obtained from the case studies presented in this paper can be used for evaluating the feasibility of particular design. Moreover, the model in general can be extensively applied for designing other exothermic- or endothermic-reaction systems.

CHAPTER 3 : Optimization for GTL process

3.3. Introduction

GTL technology is known to be a highly energy-intensive process: It consumes a large amount of energy for reforming, compression, and separation, which is provided in the form of fuel energy of the natural gas, heat energy of the steam, or pure electricity. However, some of the energy can be recovered in the process: For example, the outlet stream from the reformer should be cooled down before going to a separation unit. The heat contained by this hot stream can be recovered through a heat exchanger. In addition, the heat generated in the FT reactor also can be utilized because the reaction is highly exothermic, and the reaction temperature is high enough to generate the medium-pressure steam. For this reason, it can be said that there is an opportunity for optimization of the GTL process.

Panahi et al. developed a model for optimal operation of the GTL process⁴². They developed a steady state model using autothermal reformer (ATR) and slurry bubble column Fischer-Tropsch reactor. Based on that steady model, an optimization problem was formulated, where the objective function was defined as an total income. Six design variables were used: H_2O/C (hydro carbon), O_2/C (hydrocarbon), fired heater duty, CO_2 recover percentage, purge ratio, and recycle ratio to FT reactor. Although optimal solution was obtained, other important variables, i.e., reaction pressure and temperature, were not taken into account in the model. The reaction condition directly affects to the reactor performances and recycle efficiency, so still there is an opportunity for process

improvement. The process can be further optimized by utilizing micro-channel FT reactor because the capital cost of this type reactor is lower than conventional ones, and it removes heat more efficiently.

This chapter discusses optimization of the overall GTL process with implementing the micro-channel FT reactor. Reaction temperature and pressure, as well as purge ratio and recycle ratio were taken into account as design variables. In section 3.2, the steady-state process model, and the regressed reactor model will be addressed. In section 3.3, the optimization problem will be briefly introduced. The resulting solution will be analyzed and discussed in section 3.4. In section 3.5, concluding remarks will be addressed.

3.4. Model description

3.4.6. Steady-state process model

The flowsheet for the process is shown in Figure 3-1. The process is divided into three sub-processes; Reforming, separation, and Fischer-Tropsch synthesis. In the reforming part, the natural gas feed and the recycle gas is converted into syngas, mainly composed of H_2 and CO . The molar ratio of H_2 to CO is an important factor for FT synthesis. The optimal value for H_2/CO is known to be 2, which is achieved by adjusting O_2 flow rate to the auto-thermal reformer (ATR). In the separation part, H_2O and CO_2 content in the syngas product stream is reduced before it going to the FT reactor. Water is removed by simple flash drum, and the CO_2 is separated by absorption with monoethanolamine (MEA). The resulting syngas is sent to the FT reactor where FT synthetic fuel is produced. In this study, the micro-channel FT

reactor presented in the previous chapters is used. The unconverted gas is purged or recycled to either ATR or FT reactor. The natural gas feed flow rate is fixed at 8195 kmol/h. The molar composition of the feed gas is $\text{CH}_4=95.5\%$, $\text{C}_2\text{H}_6=3\%$, $\text{C}_3\text{H}_8=0.5\%$, $\text{n-C}_4\text{H}_{10}=0.4\%$, $\text{N}_2=0.6\%$. A commercial process simulator Aspen plus V7.3 was used to calculate the steady-state mass and energy balance for this overall GTL process.

The reforming process is configured by a pre-reformer, fired heater, and an ATR. Pre-reformer is used to decompose all the heavier hydrocarbon into methane. The reactor is assumed to be adiabatic with operating pressure of 30bar, and in chemical-equilibrium. It was simulated with an RGibbs equilibrium reactor model, where Gibbs free energy of the product stream is minimized subject to atom balance constraints. The temperature of the inlet stream to the reactor was set to 445°C by preheating the feed gas in the fired heater. Methane, nitrogen, oxygen, steam, hydrogen, carbon monoxide, and carbon dioxide were specified as chemical components in the product stream. The resulting outlet temperature of the pre-reformer was 463.4°C.

The product stream of the pre-reformer is sent to the ATR with pure O₂, which is assumed to be provided by an air separation unit (ASU). The temperature of the inlet stream of the ATR unit was set to 675°C by using fired heater. The ATR was operated with adiabatic condition and the pressure of 30 bar. It was also simulated with the RGibbs model in the simulator. The outlet stream of the ATR was 1290°C.

This syngas is cooled down to 38°C in the heat exchanger (HTRC-HX in Figure 3-1), where the water absorbs the heat from the syngas and the MP steam is generated. It then expands through VLV1 to 10 bar, and the gas is sent to the flash drum where the water is drained out in the liquid stream. The dry gas (stream 16) is subsequently sent to the CO₂ separation unit, where CO₂ is absorbed by MEA solvent. The reboiler duty for stripping CO₂ gas is provided by the heat contained by the coolant outlet from the FT reactor. The MP steam generated from the HTRC-HX is provided as a feed for the prereformer, feed for the gas turbine for ASU drive, or steam export to the utility system.

The effluent gas from the CO₂ separator (stream 19 in Figure 3-1) is pressurized and heated up before being introduced into the FT reactor. The pressure and temperature of the feed gas to the FT reactor are the main design variables in optimization problem, which will be described in section 3.3. Representative values for those variables are 20 bar and 220°C, respectively. The micro-channel reactor model presented in the previous chapters are used for FT synthesis. The customized reactor model was implemented onto the process model using Fortran language. Detailed description of the regressed model will be addressed in section 3.2.2. The coolant used for thermal control of the FT reactor is sent to the flash drum, where it is separated by phase equilibrium. The resulting hot vapor (FTCOOL5) is sent to the reboiler of the CO₂ separator, where the latent heat of vaporization of the coolant vapor is utilized for the heat recovery.

The product of the FT reactor (FTOUT in Figure 3-1) is sent to the 3-phase separator, where aqueous product, FT synfuel, and tailgas are separated. The tail gas is subsequently sent to the first splitter (SPLIT1), where some fraction of the unreacted gas is purged out. The remainder of the gas is further sent to another splitter (SPLIT2), where the gas is recycled back to either FT reactor or reformer. The split ratio of those two splitters are also the main design variables in optimization problem. Representative values for those variables are 0.04 (to PURGE from SPLIT1) and 0.82 (to RECTOFT from SPLIT2), respectively.

The result of the mass and energy balance calculation for the steady-state model is shown in Table 3-1.

	NGFEED	O2FEED	ATR0UT	H2O0UT	CO20UT	FTIN	FTOUT	AQEU0UT	OILOUT	PURGE	RECTOFT	RECTOREF	FTCOOL5
Temperature C	40	25	1290	38	38	220	220	30	30	30	30	30	220
Pressure bar	30.00	30.00	30.00	10.00	10.00	23.75	23.75	23.75	23.75	23.75	23.75	23.75	23.30
Vapor Frac	1.00	1.00	1.00	0.00	1.00	1.00	0.98	0.00	0.00	1.00	1.00	1.00	1.00
Mole Flow kmol/hr	8195	5319	31241	5871	981	28752	13754	7637	574	222	4364	958	35134
Mass Flow kg/hr	138036	170189	412830	105773	43189	334233	334228	137576	107266	3575	70365	15446	632958
Mole Flow kmol/hr													
C1	7826	0	11	0	0	47	47	0	1	2	37	8	0
C2	246	0	0	0	0	0	0	0	0	0	0	0	0
C3	41	0	0	0	0	0	0	0	0	0	0	0	0
NC4	33	0	0	0	0	0	0	0	0	0	0	0	0
N2	49	0	237	0	0	1091	1091	0	6	43	854	188	0
O2	0	5319	0	0	0	0	0	0	0	0	0	0	0
H2O	0	0	6019	5871	0	155	7654	7636	9	0	7	2	35134
NC14	0	0	0	0	0	0	536	0	536	0	0	0	0
H2	0	0	16099	0	0	18170	2636	0	5	105	2071	455	0
CO	0	0	7843	0	0	9083	1583	0	8	63	1240	272	0
CO2	0	0	1033	0	981	206	206	0	10	8	155	34	0

Table 3-1. Stream table for the GTL process

3.4.7. Micro-channel reactor model

The micro-channel FT reactor model presented in the previous chapters are implemented onto the steady-state model for more realistic process design. The detailed reactor model is required to analyze the effect of the reaction conditions such as temperature, pressure, and space velocity on the reaction performances. Although many researchers conducted optimization work for the GTL process, such variables were not taken into account in the problem formulation. For example, Panahi et al. simulated FT reactor as an RStoic model, where the simple mass balance for the reaction system is computed using a lumped conversion parameter⁴². Such simplification is necessary when the (process) model becomes too large.

However, both physical rigors and simplicity should be retained to consider the effect of operating conditions in the optimization problem. In this study, those were satisfied by implementing a regressed reactor model onto the steady-state process model.

For that purpose, artificial neural network, a well known nonlinear regression technique, was applied to the regression of the 3D cell-coupling reactor model. First, 200 data points were obtained by conducting sensitivity analysis for the reactor model: Three input variables, i.e., temperature (T), pressure (P), and GHSV were set as one of the combination of the values from $T [^{\circ}\text{C}] = \{215, 220, 225, 230\}$, $P [\text{bar}] = \{18, 21, 24\}$, and $\text{GHSV} [\text{mL}/(\text{gcat}\cdot\text{h})] = \{25600, 32000, 41600, 48000\}$. The cell coupling model was then conducted using every 48 input data, and the resulting CO conversion was recorded. The used layout of the reactor for this sensitivity analysis is as follows: 133 process channels of 1mm (width) x 3mm

(height) x 500mm (length), and 1001 coolant channels (2mm x 2mm x 85mm) orthogonally arranged with the process channels to produce cross-current flow scheme.

Next, an artificial neural network was configured as shown in Figure 3-2: First, 3 input variables are introduced into the input layer and sent to 10 neurons in the hidden layer after multiplication with the adaptive weighting factors. The weighted input signal for each neuron enters the pre-defined activation function, where the signal is converted into its output activation. The activation function used in this study is a sigmoid function:

$$y = \frac{1}{1 + e^{-x}} \quad (3 - 1)$$

In the output layer, there is only one neuron that accepts activation signal from 10 hidden neurons. This final neuron calculates the weighted sum of the signal and the bias term (b_2 in Figure 3-2) and returns the estimated CO conversion value.

The sum of square errors (SSE) between CO conversion values calculated from cell coupling model ($X_{CO,data}$) and those estimated from ANN model ($X_{CO,estimated}$) are minimized by adjusting 51 ANN regression parameters:

$$SSE = \sum_{i=1}^{48} (X_{CO,data} - X_{CO,estimated}) \quad (3 - 2)$$

The optimization problem was solved by *fmincon* procedure built in Matlab R2014b with the training data set. This data set was composed of 28 data, that was randomly selected from the total 48 data points. Remaining 42% data was used as a test set to examine the performance and validity of the regression model. As a result, the estimated data well fits to the original data, as illustrated in Figure 3-3.

The obtained optimal ANN parameters were implemented onto the Aspen model by using Fortran code.

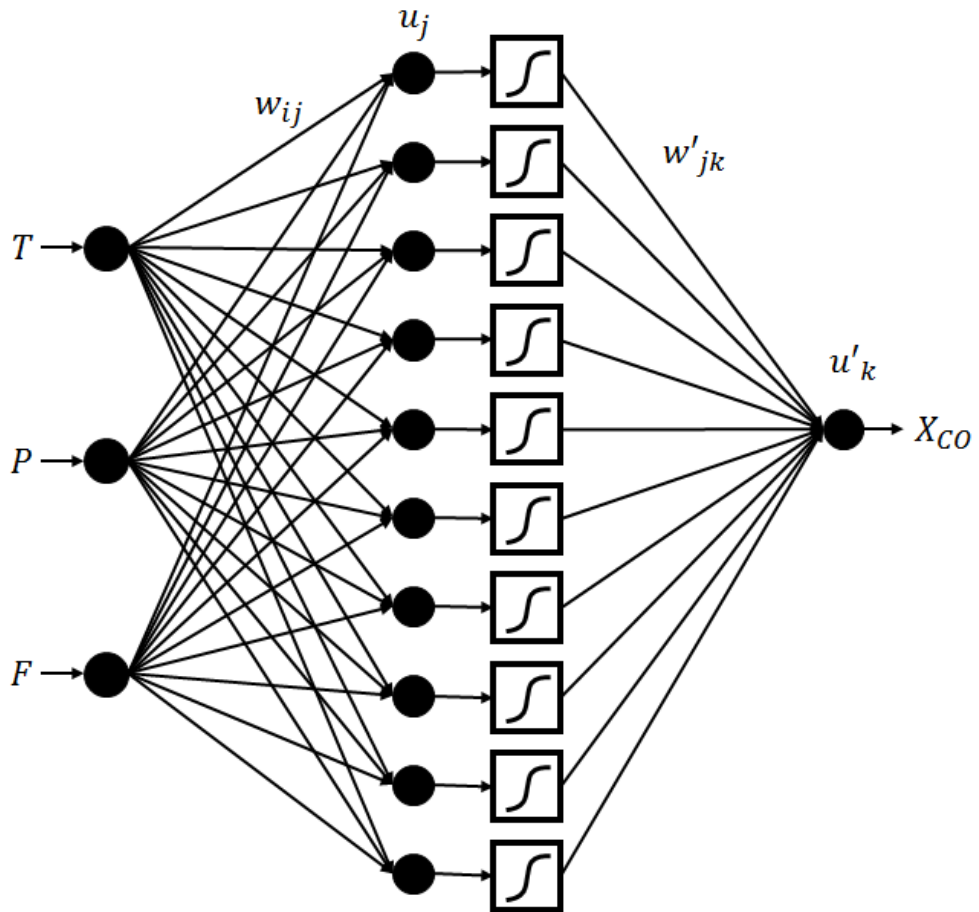
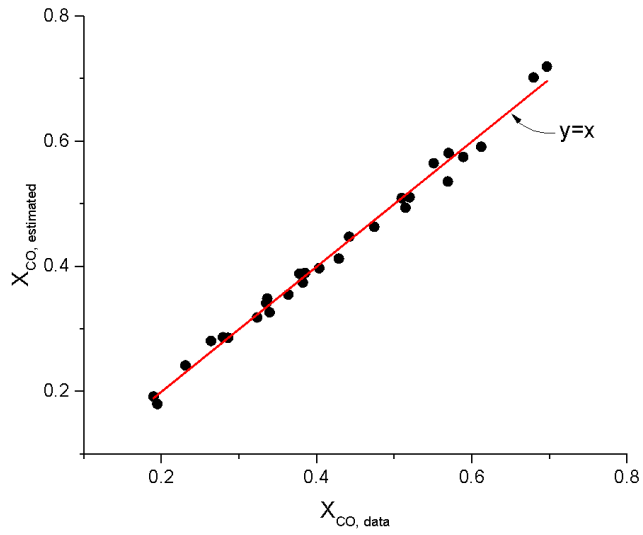
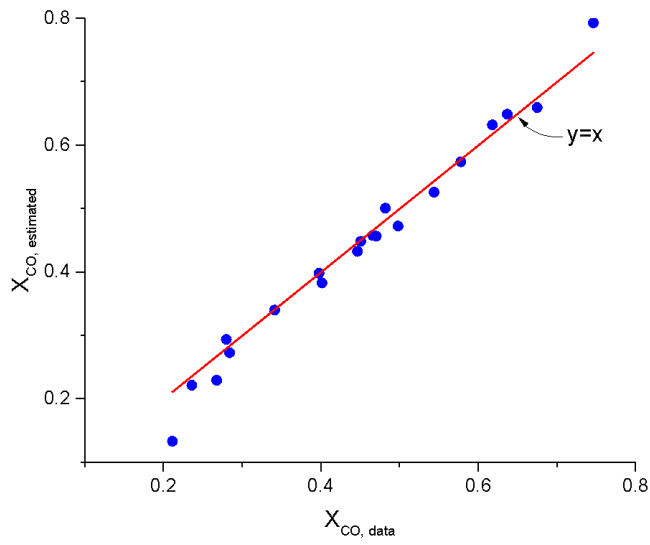


Figure 3-2. Structure of the artificial neural network for the micro-channel FT reactor



(a)



(b)

Figure 3-3. Results for the artificial neural network model: (a) Training set and (b) test set

3.5. Optimization for the steady-state model

Now that the steady state model (section 3.3.1) and regressed reactor model (section 3.3.2) has been obtained, the optimization for the GTL process can be performed. This section covers the formulation of the optimization problem and solving algorithm.

3.5.1. Cost model

First, a cost model that evaluates the total capital cost (CAPEX) and operating cost (OPEX) for the steady-state model was developed referring to the literature. CE index of 394 and the expected life time of 3 years were used for annualized capital cost calculation for all the equipments. The capital cost evaluation is as follows:

For the fired heater,

$$C_{cap,FIRED\ HEATER} (\$) = C_B F_P F_M \quad (3 - 3)$$

where C_B , the base cost, is a function of the heat duty.

$$C_B = \exp(0.8505 + 0.766 \cdot \ln(Q)) \quad (3 - 4)$$

where Q is in Btu/hr. F_P and F_M are for the pressure and material effect, and both were assumed to be 1 in this study. For the pre-reformer and ATR,

$$C_{cap,PRE-REFORMER} (\$) = 10 \cdot 17640 \cdot D^{1.066} L^{0.802} \quad (3 - 5)$$

$$C_{cap,ATR} (\$) = 10 \cdot 17640 \cdot D^{1.066} L^{0.802} \quad (3 - 6)$$

where D (m) and L (m) represent the diameter and length of the cylindrical vessel. The size of the reformer was decided by assuming the gas residence time(τ)=5 seconds and $L/D=10$. For the heat exchangers (HTRC-HX and PREHEAFT in Figure 3-1),

$$C_{cap,Heat\ exchanger} (\$) = 7296 \cdot A^{0.65} \quad (3 - 7)$$

where A is required heat exchanger area (m²). For the water separator (H2OSEP in Figure 3-1),

$$C_{cap,H2OSEP} = C_V F_M + C_{PL} \quad (3 - 8)$$

where C_V is the vessel cost, which is the function of the vessel weight:

$$C_V = \exp(6.775 + 0.18255 \cdot \ln(W) + 0.02297 \cdot \ln(W)^2) \quad (3 - 9)$$

where W in lb. C_{PL} is the cost for platforms and ladders, which depends on the vessel layout:

$$C_{PL} = 285.1 \cdot (D_i)^{0.7396} \cdot (L)^{0.70684} \quad (3 - 10)$$

where D_i (inner diameter) and L (length) are in ft. For the CO₂ separation unit, it was assumed that the capture cost is 50\$/tonCO₂. The total cost (both capital and operating cost) is calculated by multiplying it with the total CO₂ flowrate into the separator. 10% of the total cost is assumed to be the column capital cost, and remaining 90% is the fuel cost for the reboiler duty (operating cost). For the compressors,

$$C_{cap,COMPRESSOR} = F_D \cdot F_M \cdot \exp(7.2223 + 0.8 \cdot \ln(W_{HP})) \quad (3 - 11)$$

where F_D and F_M are for motor drive type and material effect respectively, and they are assumed to be 1 in this study. W_{HP} (hp) is a brake horse power for compressor driving. The capital cost for the FT reactor was assumed to be 10 times the cost of the simple vessel:

$$C_{cap,FTRXTOR} = 10 \cdot (C_V \cdot F_M + C_{PL}) \quad (3 - 12)$$

where C_V and C_{PL} are computed using eq. (3-9) and eq. (3-10), respectively. F_M is assumed to be 1. The capital cost for the 3 phase separator (3PHASESEP in Figure 3-1) was assumed to be 3 times the cost of the normal vessel:

$$C_{cap,FTRXTOR} = 3 \cdot (C_V \cdot F_M + C_{PL}) \quad (3 - 13)$$

where C_V , F_M , and C_{PL} are computed in the same manner with the FT reactor cost calculation. For the ASU turbine (ASUTURB in Figure 3-1),

$$C_{cap,ASUTURB} = 7400 \cdot (W_{HP})^{0.41}$$

where W_{HP} (hp) is generated horse power.

Operating cost for the energy-consuming equipments were computed based on the required amount of energy (MW) and the cost of the natural gas (5\$/1000scf of NG), whose lower heating value (LHV) is assumed to be used for that energy consumption. First, for the compressors and ASU turbine, with an overall thermal efficiency of 33% and LHV of natural gas of 50 MJ/kg, 1 MW of electricity requires the combustion of 0.00379 kmol/s of natural gas⁴³. For all other equipments, fired heater, reboiler in the stripping column, and preheater, a thermal efficiency of 75% was assumed. So 1MW of the heat duty requires the combustion of 0.001667 kmol/s of natural gas⁴³.

Results for the economic analysis for the base case (optimal design) are summarized in Table 3-2. The CAPEX and OPEX for the process equipments were 11.68×10^6 \$/yr and 75.95×10^6 \$/yr, respectively. Other costs, the feed gas price and O₂ import from ASU, and the earning from FT wax, MP steam export, and electricity generated from ASU turbine are shown in Table 3-2(b). As a result, the total income was calculated to be $592.81 + 38.43 + 36.02 - (314.07 + 37.48 + 11.68 + 75.95) = 228.09 \times 10^6$ \$/yr.

Table 3-2. Results for the economic evaluation for the optimal design; (a) CAPEX and OPEX for the process equipment and (b) Other cost and earning

(a)

Equipment^a	Capital cost (10⁶ \$/yr)	Operating cost (10⁶ \$/yr)
FIRHEATK1		11.50
FIRHEATK2	Sum of 3 fired heaters=1.30	1.84
FIRHEATK3		11.02
PREREFOR	1.02	
ATR	2.70	
HTRC-HX	0.71	
FIRHEATZ1		8.92
FIRHEATZ2	Sum of 2 fired heaters=1.75	26.73
H2OSEP	0.01	
CO2SEP	1.87	
CMPRSS1	1.69	11.21
PREHEAFT	0.20	4.59
FTRXTOR	0.07	
3PHASESEP	0.05	
CMPRSS2	0.05	0.13
ASUTURB	0.27	

^aThe names of the equipments are those shown in Figure 3-1.

(b)

Cost (10⁶ \$/yr)	Earning (10⁶ \$/yr)
------------------------------------	---------------------------------------

NG feed	314.07	FT wax	592.81
O ₂ import	37.48	Steam export	38.43
		electricity (ASU turbine)	36.02

3.5.2. Problem formulation

The optimization problem was formulated based on the steady state model (Section 3.2.1) and the cost model (3.3.1). The objective function, which should be minimized in the optimization problem, was defined as “-(minus) total income”:

$$\begin{aligned} \text{total income} &= \text{Revenue} - \text{Cost} \\ &= (\text{Wax price} + \text{Steam export}) - (\text{NG feed price} + \text{O}_2 \text{ price} \\ &\quad + \text{CAPEX} + \text{OPEX}) \end{aligned}$$

The decision variables were the operating temperature (T) and pressure (P) of the FT reactor, purge ratio (s_1), and recycle ratio (s_2). s_1 is the ratio of the mole flow rate of the purge stream to that of the inlet stream of the first splitter (SPLIT1 in Figure 3-1). And s_2 is the ratio of the mole flow rate of the recycle stream for the FT reactor (RECTOFT in Figure 3-1) to that of the inlet stream of the second splitter (SPLIT2 in Figure 3-1). The upper and lower bound for each variable were $215 \leq T \leq 230$, $21.5 \leq P \leq 24$, $0.04 \leq s_1 \leq 0.09$, and $0.67 \leq s_2 \leq 0.87$, respectively.

In addition, there are two process specifications that must be satisfied. First, H₂/CO molar ratio of the inlet stream to the FT reactor should be 2 for optimal FT synthesis. This can be satisfied by changing O₂ flow rate. Next, S/C ratio, the ratio of the mole flow rate of H₂O to that of the hydrocarbons in the inlet stream to the pre-reformer, was specified as 0.61, which was met by varying the split ratio of the SPLIT3 in Figure 3-1.

In summary, the optimization problem was formulated as:

$$\text{minimize } (-\text{total income})$$

subject to

$$215 \leq T \leq 230$$

$$21.5 \leq P \leq 24$$

$$0.04 \leq s_1 \leq 0.09$$

$$0.67 \leq s_2 \leq 0.87$$

$$H_2/CO = 2.0$$

$$H_2O/C(\text{hydro carbon}) = 0.61$$

The Nelder-Mead algorithm was applied to solving this problem. It is also known as the downhill simplex method, where the concept of a simplex, having (n+1) vertices in n dimensions, is used to find the optimum of an objective function. This algorithm is commonly applied to derivative-free optimization problems, for which the derivatives for the objective function may not be known. It requires small number of function evaluation, which is essential for optimization of a large process model.

The method determines search direction by evaluating function values for each vertex of the current simplex: If the point of interest is better than the current best point, then search further to that direction; If the point of interest is worse than the current worst point, then stop searching to that direction and reduce the searching area. To be more specific, the method begins with sorting (n+1) initial points in an ascending order.

$$f(x_1) \leq f(x_2) \leq \dots \leq f(x_n) \leq f(x_{n+1})$$

where $x \in \mathbb{R}^n$. Let us define x_1 , x_n , and x_{n+1} as the best point (B), good point (G), and worst point (W), respectively (Figure 3-4). Then compute the centered point (M) and reflected point (R):

$$M = \frac{x_1 + x_2 + \dots + x_n}{n}$$

$$R = M + \alpha \cdot (M - W)$$

Evaluate the function at point R. If $f(B) \leq f(R) < f(G)$, then replace W with R to obtain a new simplex and do the ordering again. If $f(R) < f(B)$, then compute the expanded point (E) and evaluate $f(E)$:

$$R = M + \gamma(M - W)$$

If $f(E) < f(R)$, replace W with E and go to the ordering step. If not, i.e., $f(E) > f(R)$, then replace W with R and do the ordering again. Expansion is finished here.

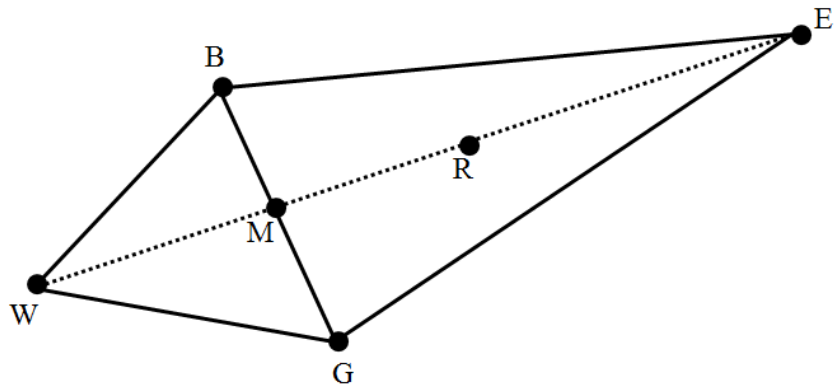
If $f(R) \geq f(G)$, compute the contracted point (C):

$$C = M + \rho(M - W)$$

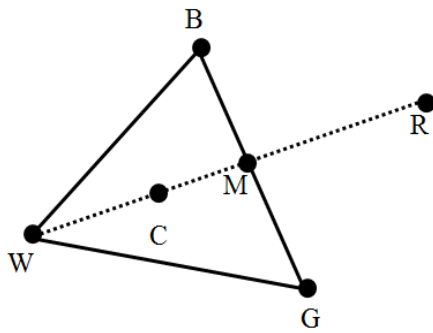
If $f(C) < f(W)$, then replace W with C and go to the ordering step. If $f(C) \geq f(W)$, compute the shrink point(S_i) except for B:

$$S_i = B + \sigma(x_i - B), \quad i = 2, 3, \dots, n + 1$$

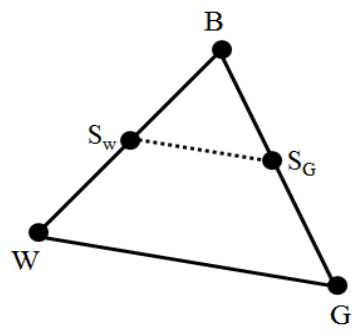
And then replace x_i with S_i and go to the ordering step. The Nelder-Mead algorithm stops if the pre-defined criteria such as the tolerance for the relative error between previous and updated function values or the maximum number of function evaluation are met.



(a)



(b)



(c)

Figure 3-4. Concept of Nelder-Mead algorithm: (a) Reflection and expansion, (b) Contraction, (c) Shrink

3.6. Results and discussion

In this section, the results for the economic evaluation for two process models are compared; M1, the process model taken from literature, M2, the process alternative with optimization.

The major differences between M1 and M2 are that 1) M1 used slurry bubble column FT reactor, whereas M2 used the micro-channel FT reactor, 2) M1 used the simple Rstoic model for the FT reactor, which is not realistic and optimal, while M2 used the ANN regression model that was proven to be reliable as addressed in section 2.1.3 and 2.2.3 of this thesis, and 3) M1 does not utilize the FT reaction heat, whereas M2 uses that heat as a reboiler duty for CO₂ stripping column.

The results for the CAPEX and OPEX computation for each process are illustrated in Figure 3-5. As presented in the figure, the sum of OPEX and annualized CAPEX for the optimal process (M2) is decreased by 17% compared to that for the reference process (M1). The reduction in fuel cost for the CO₂ separation unit mainly caused this improvement.

The overall economic evaluation for the two cases are presented in Table 3-3. It is noted that the cost for optimal case is reduced by 4.1% due to the energy saving in CO₂ separation, and the earning increased by 2.4% due to the improvement in FT wax production. As a result, the total income increased by 17.9% compared to the reference case.

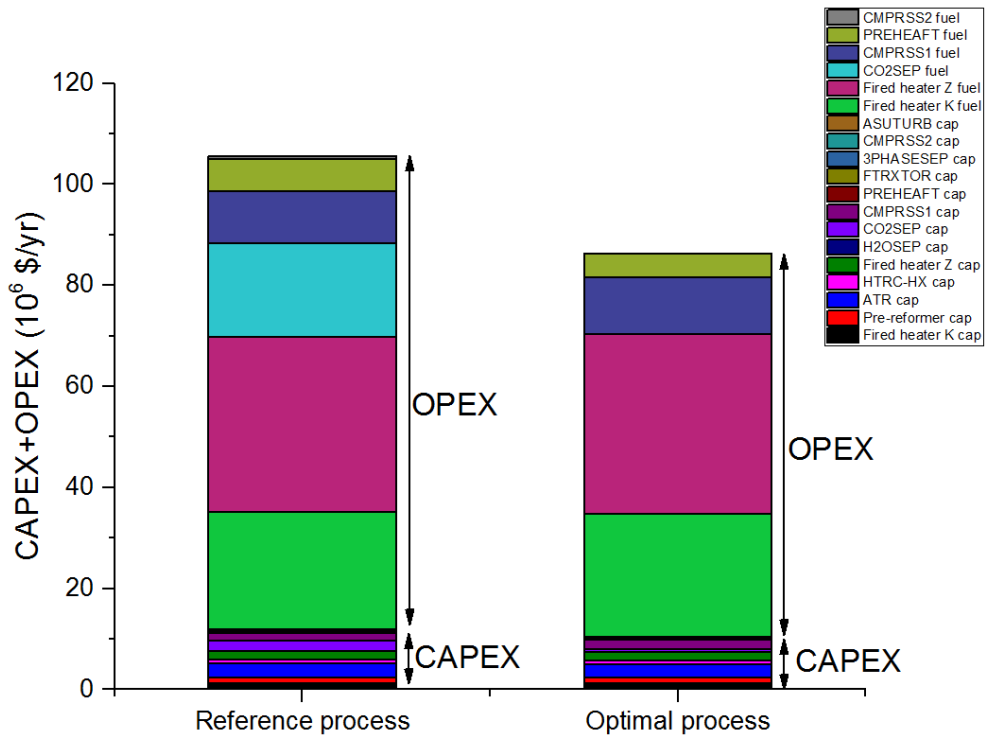


Figure 3-5. CAPEX and OPEX for reference process and optimal process

Table 3-3. Overall economic evaluation for reference process and optimal process

		Reference process	Optimal process
Cost (10⁶\$/yr)	CAPEX	12.02	11.68
	OPEX	93.57	75.95
	NG feed	314.07	314.07
	O ₂ import	38.43	37.48
Earning (10⁶\$/yr)	FT wax	576.16	592.81
	Steam export	38.43	38.43
	electricity (ASU turbine)	36.91	36.02
Total income (10⁶\$/yr)		193.41	228.08

3.7. Conclusion

Optimal design for steady-state GTL process was performed in this chapter. The GTL process is known to be highly capital intensive process mainly due to the syngas reforming unit, CO₂ separation, and gas compression system. Hence, the optimization for this process is important for process efficiency and economic feasibility.

The steady state model utilizing the micro-channel FT reactor was developed by implementing this reactor model onto the process model. Both the model simplicity and physical rigors were attained by development of customized reactor model using artificial neural network regression technique.

The economic evaluation for the processes was conducted based on the cost model referring to literature. Then the optimization problem was formulated by defining objective function as “minus total income”, and decision variables as the operating temperature and pressure for the FT reactor, purge ratio, and recycle ratio to the FT reactor. Nelder-Mead simplex algorithm was applied to solving this derivative-free optimization problem without much time consumption.

The total income for the optimal design increased by approximately 18% compared to that for the reference design, mainly due to the energy saving in CO₂ separation and improvement in wax production. This work could contribute to designing an optimal and reliable GTL process based on micro-channel Fischer-Tropsch reactor.

CHAPTER 4 : Dynamic simulation for microchannel Fischer-Tropsch reactor

4.1. Introduction

FT synthesis is known as an strongly exothermic reaction: A large amount of heat, ca. 165kJ per mol of converted CO is generated during the reaction. Care must be taken when operating this exothermic reactor for the process safety: If improperly controlled, the reactor would cause undesired situation such as thermal runaway and catalyst deactivation. Other safety issue includes wax-clogging, back-flow, and reactor rupture.

In that sense, rigorous dynamic analysis is essential part for preparation for the operation of the reactor. Many researchers conducted the research on dynamic analysis for many types of reactor. For example, Asteasuanin et al. performed dynamic simulation an optimization of tubular polymerization reactors to suggest optimal start-up strategies⁴⁴. Dynamic modeling of styrene/butadiene emulsion polymerization reactors was conducted by Sayer et al⁴⁵. They studied the system's dynamic behavior by analyzing the open loop response and closed loop control performances. Morud et al. did dynamic simulation for the analysis of instability in an industrial ammonia reactor⁴⁶. They analyzed steady state operating conditions and developed the dynamic model that describes oscillatory behavior in outlet temperature of the reactor. Studies on the transient behavior of the micro-channel FT reaction system, however, have not been done extensively.

Several researchers studied on operating procedure for the conventional FT reactor. Arcuri et al. suggested an efficient and stable start-up procedure for the FT reactor by accounting for the H₂/CO molar ratio as a main manipulating variable⁴⁷. While maintaining low H₂/CO ratio, pressure and temperature was increased to line-out condition. After that, the H₂/CO ratio was raised. In that manner, the start-up time period could be reduced and the thermal stability was greatly improved. Also, Sumerford et al. conducted the research on start-up operating strategy to prevent the carbon formation⁴⁸. By adjusting H₂ flow rate during the start-up phase, they could achieve the stable temperature control, resulting in soot-free operation. Song et al. performed a model-directed study for suggesting the operating procedures for FT reactors that prevents the reactor multiplicity⁴⁹. A strategy for high speed shut-down for the FT reactor was suggested by Bezemer et al⁵⁰. The high speed shut-down was achieved by blocking provision of feed to the reactor and simultaneously blocking the withdrawal of effluent from the reactor. Operating procedures for the normal start-up and shut-down of the micro-channel reactor, however, have not been studied extensively.

In this chapter, first, the development of the dynamic model for the micro-channel FT reactor presented in the previous chapters is addressed. The transient behavior for the 3D reactor is analyzed. Then the dynamic simulations for the micro-channel FT reactor are performed. Optimal start-up and shut-down strategies for the FT reactor operation is suggested.

4.2. Dynamic modeling for 3D reactor

4.2.1. Model description

In order to simulate the transient behavior of the 3-dimensional micro-channel FT reactor, one should solve both mass balance and energy balance equation simultaneously:

$$\frac{\partial N_i}{\partial t} = \sum F_i|_{in} - \sum F_i|_{out} + \int r_i dV \quad (4-1)$$

$$\frac{\partial \hat{E}_{sys}}{\partial t} = \sum F_i H_i|_{in} - \sum F_i H_i|_{out} + \dot{Q} - \dot{W}_s \quad (4-2)$$

where chemical species i flows into and out from the control volume dV . N is the amount of the mole of the species i in the control volume, F is the flow rate, r is the reaction rate, \hat{E}_{sys} is the total energy of the system, H is the enthalpy, Q is the heat flowing into the control volume, and W_s is the shaft work done by the system. The above equations can be converted into the form of partial differential equations by taking limit of $dV \rightarrow 0$, whereby spatial and temporal variations of the mass and energy are computed. However, solving such partial differential equations is challenging, particularly when the dimension of the domain becomes so large that many unit control volumes are to be generated. Thus, in that case, it is necessary to simplify those equations to obtain the solution of the dynamic model.

In this study, the simplification of the model was made by taking the structure of the cell coupling model developed so far, where the bias of the flow direction was allowed for the computation. The dynamic model was developed on the basis of the existing cell coupling model:

$$N_x^{u+1} = N_x^u + \Delta t \left[F_x^u(j, i, h) - F_x^u(j + 1, i, h) + \rho A \sum_w r_{wx}^{u+1} \right] \quad (4-3)$$

$$\begin{aligned} T_p^{u+1}(j, i, h) = & T_p^u(j, i, h) \\ & + \frac{\Delta t}{\sum N_x C_{px}} \left[UA \{ T_p^{u+1}(j, i, h) - T_c^{u+1}(j, i, h) \} - \Delta H_r \right. \\ & \left. \cdot \sum_w \left(k_{w0} \exp \left(-\frac{E_w}{RT_p^{u+1}(j, i, h)} \right) C_x \right) \cdot \rho V \right] \quad (4-4) \end{aligned}$$

$$\begin{aligned} T_c^{u+1}(j, i, h) = & T_c^u(j, i, h) \\ & + \frac{\Delta t}{\rho_c V C_{p,c}} \left[\Delta H_r \cdot \sum_w \left(k_{w0} \exp \left(-\frac{E_w}{RT_p^{u+1}(j, i, h)} \right) C_x \right) \cdot \rho V \right. \\ & \left. - \dot{m}_c C_{p,c} (T_c^{u+1}(j, i, h) - T_c^u(j, i - 1, h)) \right] \quad (4-5) \end{aligned}$$

Eq. 4-3, 4-4, and 4-5 represent the mole balance of the chemical species x in the process channel cell, energy balance in the process channel cell, and energy balance in the cooling channel cell, respectively. The superscript denoted by u is the specified time u . These equations are driven from eq. 4-1 and 4-2 by using backward Euler method. Parameters j , i , and h in the parenthesis represent the cell position. The same coordinate system was used as that used in Chapter 2 and 3.

First, the initial points at time $u=0$ were specified as the solution obtained from steady state simulation of the cell-coupling model in Chapter 2 (or 3). With those points, T_p^1 and T_c^1 are computed by solving eq. 4-4 and 4-5 simultaneously. In Matlab R2014b environment, the built-in *fsolve* function was used to solve these two nonlinear equations. The nested function structure was utilized to separate the parameters (old values such as T_p^u and T_c^u) and variables (updated values such as T_p^{u+1} and T_c^{u+1}) when the *fsolve* function is called. After obtaining all the updated

values of $T_p^{u+1}(j, i, h)$ and $T_c^{u+1}(j, i, h)$, the material balance equation (eq. 4-3) is solved, where the reaction rate (r_{wx}^{u+1}) is evaluated by the updated cell temperature and the mole of the component x at time $u+1$ is computed. These are iteratively calculated until the error between the values (at time= $u+1$) of the previous and present step becomes negligible.

4.2.2. Results and analysis

Several case studies were conducted for the analysis of the dynamic behavior of the reactor on the basis of the same layout: process channel size of $1\text{mm} \times 3\text{mm} \times 500\text{mm}$, coolant channel size of $2\text{mm} \times 2\text{mm} \times 103\text{mm}$, 352 process channels and 1573 coolant channels with fully cross current scheme. Total number of cells generated by channel decomposition method was $32 \times 143 \times 11 = 50336$. The initial point was obtained by solving the steady-state cell coupling model based on the reaction condition specified: The temperature of the syngas and coolant inlet stream was 230°C , reaction pressure was 24.13 bar, WHSV was 32,000 ml/gcat-h, the catalyst loading was 70 vol%, and the coolant's flow rate was 175.4 L/min. The same kinetic parameters were used as those used in section 2.1. The result of overall CO conversion was 0.6975, and the maximum process temperature was 232.66°C .

With the initial condition obtained, the dynamic model was simulated. The step size of the time was specified as 300 s. In this simulation, it was assumed that at a certain time the flow rate of the coolant was suddenly reduced to 1/4 of the initial value. Such situation was assumed to simulate the abnormal condition in cooling

utility.

The result of the simulation is illustrated in Figure 4-1.

<Temperature profile for the process channels>

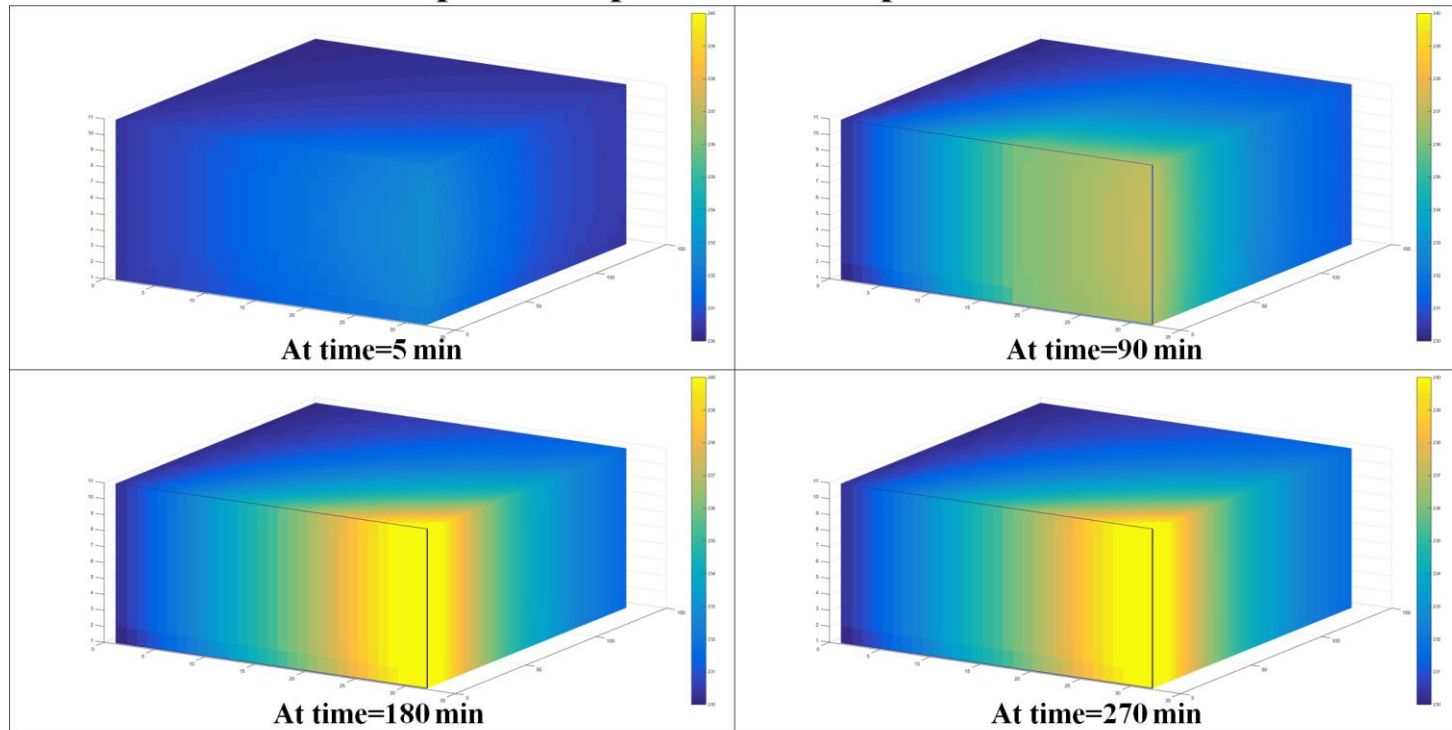


Figure 4-1. Changes of the temperature profile with time (Scenario 1). The color bar of the same scale (230°C - 240°C) was used for all the subplots.

The transient temperature profile was obtained as shown in the figure. For all the subplots in the figure, the color bar of the same scale was used. As can be seen from the figure, the temperature of the process channels increases immediately after the flow rate of the coolant is reduced. It is also noted that the temperature reaches a new steady state after 180 minutes. The maximum temperature value at that time was 241.96°C. Thereafter, this new steady state value was maintained.

Next, another case study was performed to check the model's ability to simulate the control action. In the simulation, the coolant flow rate was reduced to 1/4 of the initial flow rate, which was maintained for 150 minutes, after which the flow rate was increased back again to the original value. The results are illustrated in Figure 4-2, where the maximum temperature difference (ΔT_{max}) in Fig. 4-2(c) takes place at the cell position of $(i, j, h)=(32, 1, 11)$. In this case study, $n_i=32$, $n_j=142$, and $n_h=11$, respectively. When the coolant's flow rate is reduced, the temperature of the process channel is increased as in the previous case study. As the coolant's flow rate is recovered back to the original value at 150 minutes, the temperature decreases going back to its original state. From these results, the developed dynamic model can be utilized to study the response of the reactor to the changes in the input (manipulated) variables.

<Temperature profile for the process channels>

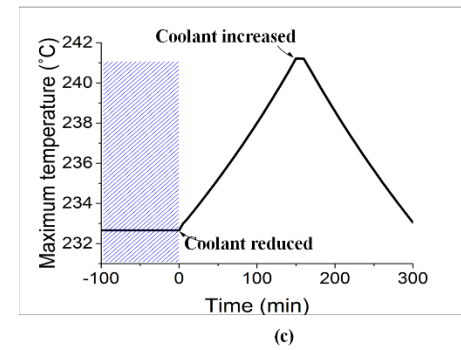
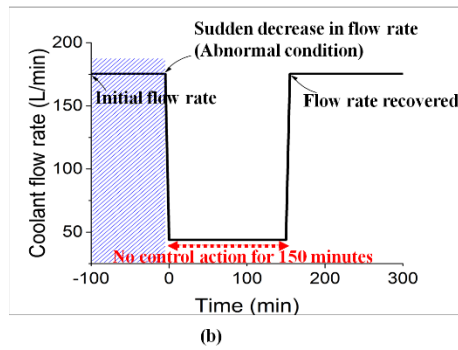
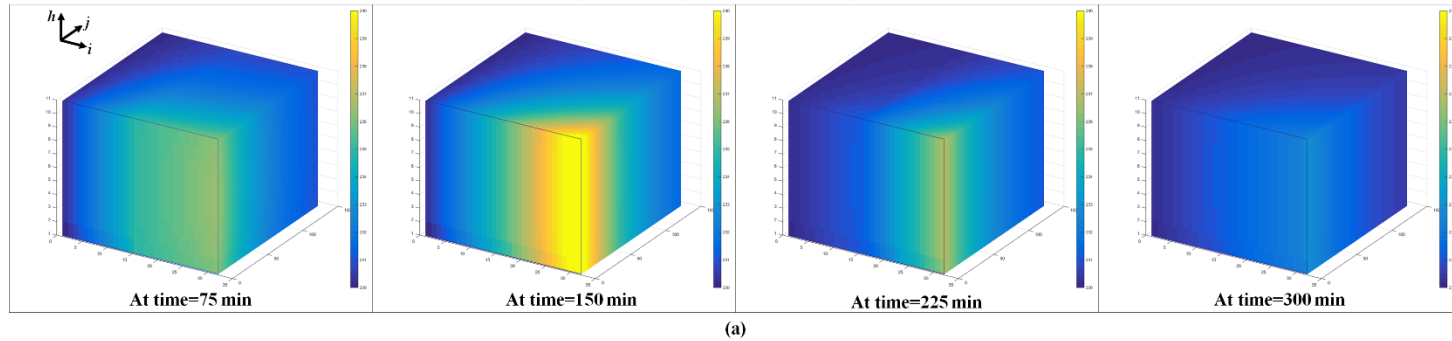


Figure 4-2. Changes of the temperature profile with time (Scenario 2).

4.3. Optimal operating strategies for FT reactor

4.3.3. Model description

The dynamic simulations were performed to suggest the optimal operating strategies for the micro-channel FT reactor. For this purpose, a process model for the FT reaction was developed by using Aspen Hysys software. Instead of using the 3-D cell coupling model, the built-in one-dimensional plug flow reactor model was used for simplification. The process flow diagram (PFD) used is shown in Figure 4-3.

The feed gas flows in the stream 1. It was assumed that the syngas is provided from a storage tank large enough to meet the target operating demand. The syngas is also assumed to be introduced into the process at 220°C and 2000 kPa.

The feed gas flows through the inlet valve (VLV-100) controlled by the flow controller (FIC-100). It then flows into the reactor (PFR-100), where the FT reaction takes place and the reaction heat is removed. The product gas subsequently flows into the two separation tanks. In the first separator, the wax product is mainly separated, whereas in the second separator, the light oil product is collected. The stream 13 consists of a pure N₂ used as purging or diluting agent in the start-up or shut-down procedure. All the boundary streams and intermediate streams connecting each unit are connected to the valves where the gas flow rate is controlled by the flow controllers.

The steady state simulation was performed to calculate the equipment sizing. For the valves, the conductance (C_v) was calculated based on the 50% valve opening at the normal flow rate with pressure drop of 70 kPa. Sizing of the reactor and the

separation tank was based on the target wax production rate of 0.2 BPD. The size information of the process units is summarized in Table 4-1.

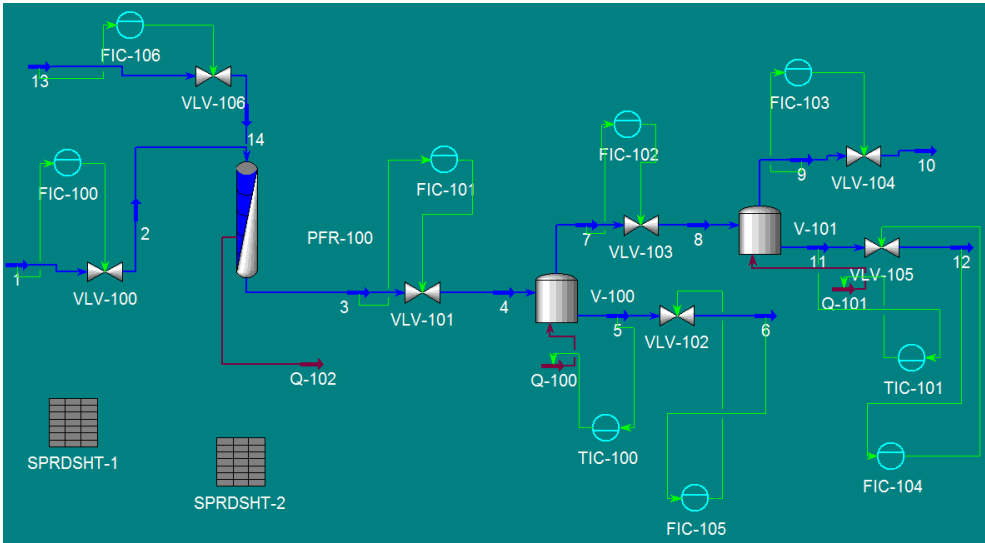


Figure 4-3. Process flow diagram for the dynamic simulation

Table 4-1. Size of the process equipments

		Size	Unit
Valve	VLV-100, C _v	0.6315	USGPM (60F, 1psi)
	VLV-101, C _v	0.1183	USGPM (60F, 1psi)
	VLV-102, C _v	0.1575	USGPM (60F, 1psi)
	VLV-103, C _v	0.1575	USGPM (60F, 1psi)
	VLV-104, C _v	0.1141	USGPM (60F, 1psi)
	VLV-105, C _v	0.1141	USGPM (60F, 1psi)
	VLV-106, C _v	0.6315	USGPM (60F, 1psi)
Reactor	PFR-100, length	0.4470	m
	PFR-100, diameter	0.2314	m
	PFR-100, volume	0.0188	m ³
Separator	V-100, volume	0.0800	m ³
	V-101, volume	0.0800	m ³

4.3.4. Start-up

During the start-up, care should be taken to prevent the thermal runaway of the reactor. In this phase, usually the catalyst is already reduced and in the fresh state. If the operating procedure is improperly configured, this highly active catalyst may lead to a sudden reaction occurrences.

There are many variables that can affect to the start-up state. In this study, we analyze the effect of five variables, i.e., temperature and pressure of the reactor, feed gas flowrate, H_2/CO ratio of the feed gas, and external N_2 flow rate, on the operating performances. To be more specific, nine representative scenarios are generated with the different sequence of those five variables as shown in Table 4-2. For example, in the scenario 1, first the temperature of the reactor is increased gradually (ramp) from initial temperature to the reaction temperature. Then the pressure is increased by closing back pressure regulator in step manner, followed by the step increase in the feed gas flow rate. The sequence of the other scenarios described in the table can be interpreted in the similar manner. Scenario 7 and 8 are comprised of the manipulation of pressure, temperature, and H_2/CO ratio. After the pressure is increased to the reaction condition, the syngas with low H_2/CO is introduced by valve opening. Then the temperature is increased by heating the reactor with the preheated cooling oil. When the heating is finished, the ratio of H_2/CO is increased by adding hydrogen gas imported from other processes.

Scenario 9 uses pure nitrogen instead of the hydrogen.

Table 4-2. Description for start-up scenarios

Description	
1	T (ramp)→P(step)→F(step)
2	T(ramp)→P(step)→F(ramp)
3	P(step)→F(step)→T(ramp)
4	P(step)→F(ramp)→T(ramp)
5	P(step)→F(step)→T(step)
6	P(step)→F(ramp)→T(step)
7^a	P(step)→F ₁ (step, low H ₂ /CO)→T(ramp)→F ₂ (step, high H ₂ /CO)
8	P(step)→F ₁ (ramp, low H ₂ /CO)→T(ramp)→F ₂ (ramp, high H ₂ /CO)
9	P(step)→F(ramp, high N ₂)→T(ramp)→F(ramp, low N ₂)

^aThis scenario was taken from the patent document⁴⁷

The result of two extreme cases are illustrated in Figure 4-4. For Scenario 1, a sudden increase in heat generation occurred when the valve for the inlet stream of the feed gas opened. Because the temperature and pressure has already reached the reaction condition, the FT reaction takes place as the feed gas is introduced abruptly into the reactor. Similar heat generation trend was obtained for Scenario 2. On the other hand, such rapid heat generation does not occur for Scenario 9, where the nitrogen gas was utilized as a diluting agent in the start-up period. In the scenario, the nitrogen is introduced with the syngas after the pressure reaches the reaction pressure. High nitrogen contents inhibit the rapid, or abrupt FT reaction by acting as an inert gas.

The results of all 9 scenarios are shown in Figure 4-5. As can be seen from the figure, Scenario 1 showed the largest heat generation, whereas Scenario 9 resulted in the least heat generation. For Scenario 7 and 8, the heat generation has decreased as compared to Scenario 1 due to the lower concentration of the reactant in feed gas. However, it is higher than the heat generated in Scenario 9. Meanwhile, the controllability of Scenario 7, 8, and 9 is better than that of the others because those three cases use the flow rate as the final manipulating variable, which shows faster responses than temperature or pressure. From this analysis, it is concluded that the optimal start-up procedure for the FT reactor is the procedure used in Scenario 9.

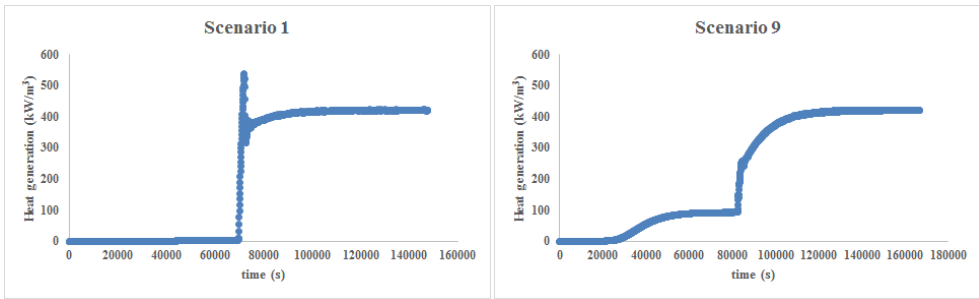


Figure 4-4. Comparison between two extreme cases: Scenario 1 and 9.

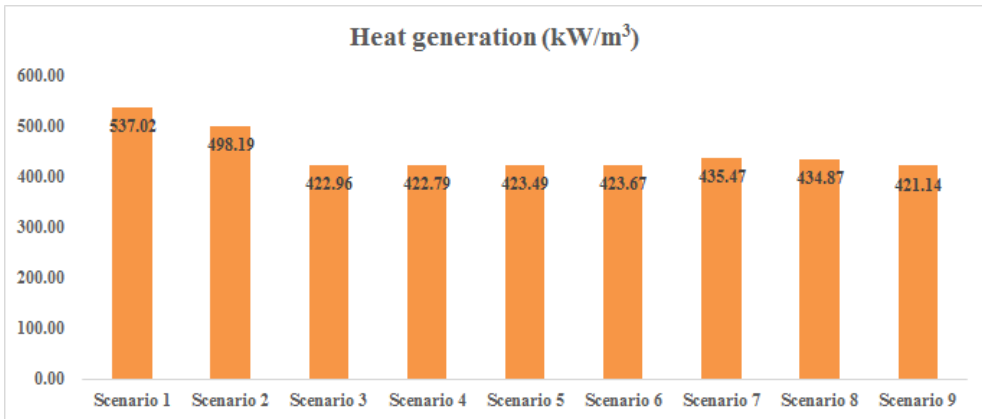


Figure 4-5. Results of the case studies: Scenario 1 through 9

4.3.5. Shut-down

Wax clogging is the main issue in the shut-down procedure of the FT reactor. During the shut-down, temperature and pressure of the reactor are reduced to the room temperature and atmospheric pressure, respectively, at which the FT product is in the liquid phase. If the reactor improperly shut down, this may cause the wax-clogging in the reactor channel. If the wax is clogged inside the channel, it is difficult to take it off from the channel. Therefore, care must be taken to keep the wax from clogging inside the micro-channels so that the reactor can be easily re-commissioned after the shut-down.

In this study, 8 shut down scenarios were studied, where different sequences for the main manipulating variables were incorporated. The description for the scenarios is shown in Table 4-3. For example, in Scenario 1, first the flow rate of the syngas is reduced from steady state value to zero in step manner. Then the temperature is gradually (ramp) decreased to room temperature, followed by the step decrease of the pressure. The other scenarios can be interpreted in the similar manner. For Scenario 7, first the N₂ gas is introduced into the reactor. The reaction pressure and temperature are subsequently reduced to the room conditions. In the final step, the flow rate of the syngas, diluted with the nitrogen gas, is decreased. In scenario 8, the order of the temperature and pressure is altered.

All the scenarios were evaluated with the same criteria, the liquid fraction in the channel. The liquid fraction increases when more and more wax component builds up in the channel. The result of the representative scenarios, scenario 1, 3, and 7, is illustrated in Figure 4-6. As can be seen from the figure, Scenario 1 showed the highest liquid fraction, whereas Scenario 8 showed nearly zero liquid fraction.

Table 4-3. Description for shut-down scenarios

Description	
1	F(step)->T(ramp)->P(step)
2	F(step)->P(step)->T(ramp)
3	T(ramp)->P(ramp)->F(step)
4	T(ramp)->P(step)->F(step)
5	P(step)->T(ramp)->F(step)
6	P(ramp)->T(ramp)->F(step)
7	N2->P(ramp)->T(ramp)->F(step)
8	N2->T(ramp)->P(ramp)->F(step)

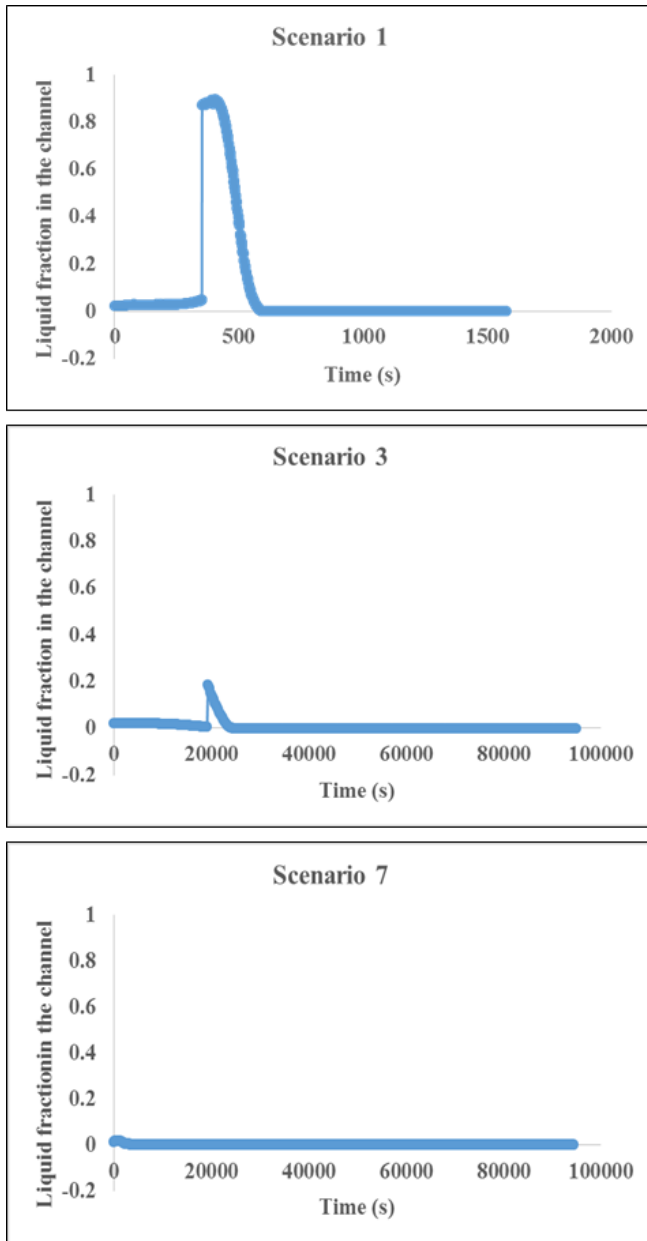


Figure 4-6. Result of dynamic simulation for three shut-down scenarios: Scenario 1, 3, and 8

For Scenario 1, the liquid fraction abruptly increased when the flow rate was being decreased. This phenomenon can be explained with Figure 4-7. Before the temperature decrease, the flow rate has been reduced. As a result, the conversion was increased due to the decrease in space velocity, changing the phase envelope curve in Figure 4-7 from the one at the middle ($X_{CO}=0.7$) to the one at the right ($X_{CO}=1.0$). The phase of the resulting mixture suddenly changed to the liquid phase at this operating condition. The liquid fraction increased abruptly in this step. In the next step, as the temperature decreased, the reaction rate was reduced, and hence, the conversion decreased. The conversion became nearly zero when the temperature reaches the room temperature. The phase envelope moves from right ($X_{CO}=1.0$) to the left ($X_{CO}=0.1$), and the operating point also moves from right to the left. The liquid fraction becomes nearly zero in this step. After that, the pressure is reduced and the shut-down is completed.

For Scenario 3, also the liquid fraction suddenly increased (the second plot in Figure 4-6), but the value is lower than that in Scenario 1. In this case, the temperature of the reactor was reduced first. As the temperature decreases, the operating point moves from right to the left, which is illustrated as the black arrow in Figure 4-7. The phase envelope also changes from the one at the middle ($X_{CO}=0.7$) to the one at the left ($X_{CO}=0.1$). The operating point is placed under the two-phase region of the envelope, causing the liquid fraction to increase. Next, the pressure was reduced, which corresponds to the black arrow vertically down in Figure 4-7. The operating point is now located under the dew point curve. As a result, the liquid fraction becomes zero at this step. After that, the flow rate is decreased, and the shut-down is completed.

For scenario 7, nitrogen gas is first introduced into the process. As this diluent gas is fed into the reactor, the reaction rate is decreased, changing the phase envelope from the one in the middle ($X_{CO}=0.7$) to the one in the left ($X_{CO}=0.1$). For operating point remaining unchanged in this step, no liquid is generated. Then the pressure is reduced to 1 bar, which corresponds to the blue arrow vertically down in Figure 4-7. In this step also, the operating point is placed under the dew point curve and the liquid fraction remains zero. Then, the temperature is decreased to the target point (the horizontal blue arrow in Figure 4-7), which is also located under the dew point curve. and no liquid is generated. The shut-down is completed by reducing the gas flow rate.

Among the all shut-down scenarios, scenario 7 is the best in that the liquid fraction remains almost zero, and the controllability is also good because the final manipulating variable is the gas flow rate. The inert nitrogen gas can be also used as a purge gas at the end of the shut-down procedure, which removes the remaining wax component in the channel. From this analysis, it is concluded that the optimal shut-down procedure for the FT reactor is the procedure used in Scenario 7.

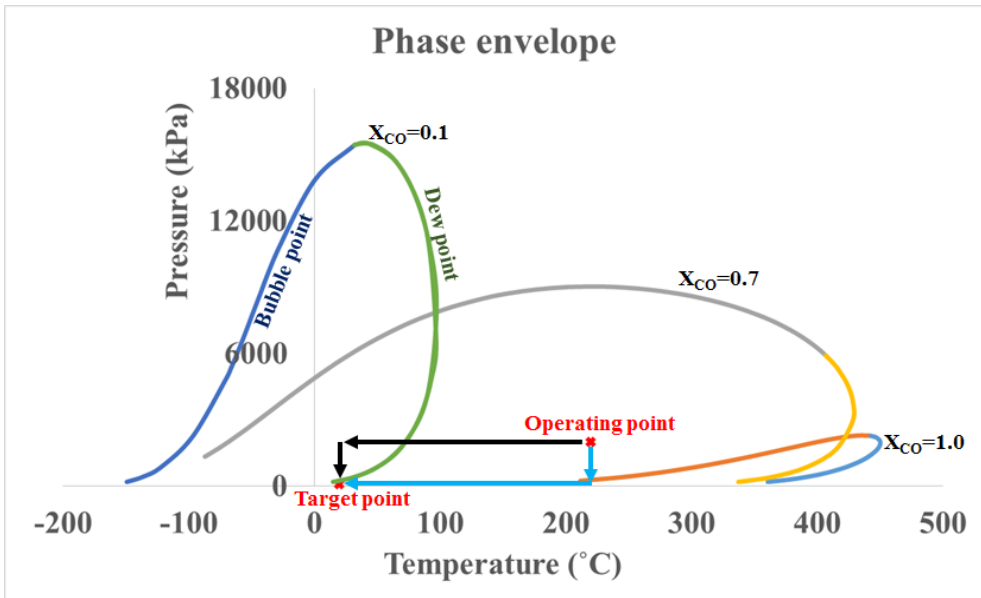


Figure 4-7. Phase envelope

4.4. Conclusion

In this chapter, the dynamic model for the micro-channel FT reactor was developed and the analysis on the transient behavior of the model was addressed. The model could simulate the response of the reactor in step change of some important manipulating variable, e.g., the coolant flow rate. It is also able to describe the situation in which the input variables are changed and recovered back by the user's control action. The dynamic simulation for the micro-channel FT reactor system was also performed. By analyzing several operating scenarios, optimal strategies for start-up and shut-down could be derived. The developed dynamic model and the suggested operating procedure further can be used in the control logic design and real plant operation.

CHAPTER 5 : Concluding Remarks

5.5. Conclusions

This thesis has addressed issues in design of optimal GTL processes based on the micro-channel FT reactor: Reactor design, steady-state process design, and dynamic simulation. All of the developed models were based on the new reactor model, which was validated against the real pilot reactor data.

The model for the micro-channel Fischer-Tropsch reactor was developed by using the new method, where every channel is decomposed into a number of unit cells that interact each other to solve the mass and energy balance equations. This model was validated against the multi-channel reactor data taken from the literature. Sensitivity analyses were performed on the important variables such as catalyst loading ratio, coolant's flow rate, and channel layout.

The improved version of this cell-coupling reactor model was developed, where the effect of the flow configuration, flow distribution, and catalyst overlapping zone was considered. The model was also validated by using the operation data of various operating conditions. With the help of this realistic model, optimal flow configuration, distribution, and catalyst loading strategies for the micro-channel FT reactor could be derived. The barrels-per-day scale pilot reactor has been fabricated, and is now prepared for the commissioning.

Based on the reactor model, an optimal steady-state GTL process was suggested. The steady state model utilizing the micro-channel FT reactor was developed by

implementing this reactor model onto the process model. The derivative-free optimization problem, minimizing the objective function of the overall cost, was formulated and solve by using Nelder-Mead algorithm. The total income for the optimal design increased by approximately 18% compared to that for the reference design, mainly due to the energy saving in CO₂ separation and improvement in wax production.

The dynamic modeling for the 3-D reactor was performed by solving the modified cell-coupling reactor model, where the temporal variation was taken into account. The model could simulate the response of the reactor in step change of some important manipulating variable, e.g., the coolant flow rate. It was also able to describe the situation in which the input variables are changed and recovered back by the user's control action. The dynamic simulation for the micro-channel FT reactor system was also performed. Optimal strategies for start-up and shut-down could be derived by analyzing several operating scenarios. The developed dynamic model and the suggested operating procedure further can be used in the control logic design and real plant operation.

Hopefully, the proposed modeling and design work in this thesis will be helpful to those who want to solve similar design problems.

5.6. Future works

In the future, the developed reactor model will be applied to demonstrating its validity with predicting the pilot-scale micro-channel FT reactor which is now prepared for the commissioning under various circumstances. The reactor was designed and fabricated for the purpose of achieving the production of 1 barrelper-day of wax. Temporal and spatial temperature profiles for the reactor will be measured, which will then be utilized for the demonstration and parameter-tuning of the developed reactor model.

Extension of the optimization methodologies in this thesis will be made to other GTL process alternatives such as tri-reformer, steam-methane-reformer, steam-CO₂-reformer, etc, in order to find the best process configuration. In addition, future work will continue to evaluate the effect of other design variables, such as reformer's outlet temperature, CO₂ recovery, and steam-to-carbon ratio.

For the dynamic model part, further analyses on the various variables that affect the reactor's performances will be conducted. Such variables include the reactant's inlet temperature, syngas flow rate, or catalyst deactivation. More detailed analysis will help us to understand the dynamics and transient behavior of the micro-channel reactors. Furthermore, the dynamic simulation will be extended to the whole GTL process by integrating the FT reaction subprocess with the syngas production process, which will allow us to develop more rigorous, robust, and realistic operating strategies and control logic for the entire process.

Nomenclature

T_P – Matrix of temperatures (K) of process channel cells for every element

T_C – Matrix of temperatures (K) of cooling channel cells for every element

U – Matrix of overall heat-transfer coefficients [$W/(m^2 K)$] between two paired cells for every element

Q – Matrix of heat generation values (kJ) from process channel cells for every element

$h_{process}$ – Convective heat-transfer coefficient [$W/(m^2 K)$] in process channel cell

$h_{coolant}$ – Convective heat-transfer coefficient [$W/(m^2 K)$] in coolant channel cell

$k_{channel}$ – Thermal conductivity [$W/(m K)$] of channel material

Δx – Gap (m) between two paired cells

m_c – Mass flow rate (kg/s) of coolant

\widehat{h}_c – Specific enthalpy (kJ/kg) of coolant

ΔH_r – Heat of reaction (kJ/mol)

r_{CO} – CO consumption rate [$mol/(g-cat s)$]

E_a – Activation energy (kJ/mol)

C_x – Concentration (mol/L) of component x

γ_s – Flow path s

γ_s^t – t -th segment of flow path s

\mathbb{R}^n – n -dimensional vector space

$c(j, i, h)$ – A coolant cell at the position of (j, i, h) in the cell coordinate

$p(j, i, h)$ – A process cell at the position of (j, i, h) in the cell coordinate

ρ – Fluid density (kg/m³)

\mathbf{u} – Velocity vector (m/s)

p – Pressure (bar)

\mathbf{I} – Identity matrix

τ – Viscous stress tensor (bar)

\mathbf{F} – Volume force (N/m³)

p_i – Partial pressure of component i (bar)

$X_{CO,measured}$ – Conversion of carbon monoxide measured (and calculated) from kinetic experiment

$X_{CO,estimated}$ – Conversion of carbon monoxide estimated from 1-D pseudo-homogeneous single channel model

ΔT_{max} – Difference between the maximum temperature of the process

channel cell and the inlet temperature of the syngas

C_B – Base cost

D – Diameter of the vessel

L – Length of the vessel

A – Area of the heat exchanger

C_V – Vessel cost

C_{PL} – Cost for platforms and ladders

D_i – Inner diameter

F_P – Effect of pressure when calculating capital cost

F_M – Effect of material when calculating capital cost

Q – Heat duty for a fired heater

W_{HP} – Brake horse power for a compressor

s_1 – Split ratio for purge stream

s_2 – Split ratio for the FT reactor

M – Centered point

R – Reflected point

W – Worst point

B – Best point

N_i – Mole of component i in a control volume

F_i – Flow rate of component i into/out from a control volume

r_i – Reaction rate of generation of component i in a control volume

\hat{E}_{sys} – Total energy of the system

H_i – Enthalpy of component i

\dot{Q} – Heat flowing into the control volume

\dot{W}_s – Shaft work done by the system

N_x^u – Mole of component x at a time u

Δt – Step change of time

r_{wx}^u – Reaction rate of generation of component x by reaction w at a time

u

C_{px} – Heat capacity of component x

ΔH_r – Heat of reaction

k_{w0} – Frequency factor for reaction w

E_w – Activation energy for reaction w

$C_{p,c}$ – Heat capacity of coolant

ρ_c – Density of coolant

Abbreviations

ANN – Artificial neural network

ASU – Air separation unit

ATR – Autothermal reformer

CAPEX – Capital cost

CFD – Computational fluid dynamics

FID – Flame ionization detector

FPSO – Floating, production, storage, and offloading

FT – Fischer–Tropsch

GHSV – Gas hourly space velocity

GTL – Gas to liquid

LHV – Low heating value

MEA – Monoethanolamine

NG – Natural gas

OPEX – Operating cost

PFD – Process flow diagram

SSE – Sum of square error

TCD – Thermal conductivity detector

Literature cited

- (1) Bao, B.; El-Halwagi, M. M.; Elbashir, N. O., Simulation, integration, and economic analysis of gas-to-liquid processes. *Fuel Processing Technology* **2010**, 91, (7), 703-713.
- (2) Cao, C.; Hu, J.; Li, S.; Wilcox, W.; Wang, Y., Intensified Fischer–Tropsch synthesis process with microchannel catalytic reactors. *Catalysis Today* **2009**, 140, (3), 149-156.
- (3) Deshmukh, S. R.; Tonkovich, A. L. Y.; Jarosch, K. T.; Schrader, L.; Fitzgerald, S. P.; Kilanowski, D. R.; Lerou, J. J.; Mazanec, T. J., Scale-up of microchannel reactors for Fischer–Tropsch synthesis. *Industrial & Engineering Chemistry Research* **2010**, 49, (21), 10883-10888.
- (4) Kim, Y. H.; Jun, K.-W.; Joo, H.; Han, C.; Song, I. K., A simulation study on gas-to-liquid (natural gas to Fischer–Tropsch synthetic fuel) process optimization. *Chemical Engineering Journal* **2009**, 155, (1), 427-432.
- (5) Knochen, J.; Güttel, R.; Knobloch, C.; Turek, T., Fischer–Tropsch synthesis in milli-structured fixed-bed reactors: Experimental study and scale-up considerations. *Chemical Engineering and Processing: Process Intensification* **2010**, 49, (9), 958-964.
- (6) Lee, C.-J.; Lim, Y.; Kim, H. S.; Han, C., Optimal gas-to-liquid product selection from natural gas under uncertain price scenarios. *Industrial & Engineering Chemistry Research* **2008**, 48, (2), 794-800.
- (7) Lee, Y. J.; Hong, S.-I.; Moon, D. J., Studies on the steam and CO₂ reforming of methane for GTL-FPSO applications. *Catalysis Today* **2011**,

174, (1), 31-36.

- (8) Park, D.; Moon, D. J.; Kim, T., Steam-CO₂ reforming of methane on Ni/ γ -Al₂O₃-deposited metallic foam catalyst for GTL-FPSO process. *Fuel Processing Technology* **2013**, 112, 28-34.
- (9) Cao, C.; Xia, G.; Holladay, J.; Jones, E.; Wang, Y., Kinetic studies of methanol steam reforming over Pd/ZnO catalyst using a microchannel reactor. *Applied Catalysis A: General* **2004**, 262, (1), 19-29.
- (10) Chin, Y.-h.; Hu, J.; Cao, C.; Gao, Y.; Wang, Y., Preparation of a novel structured catalyst based on aligned carbon nanotube arrays for a microchannel Fischer-Tropsch synthesis reactor. *Catalysis today* **2005**, 110, (1), 47-52.
- (11) Deshmukh, S.; Keyes, L. W.; Luzenski, R. J.; Marchiando, M. A.; Marco, J. L.; Marco, J. D.; Neagle, P. W.; Tonkovich, A. L.; Yuschak, T., Laminated, Leak-Resistant Chemical Processors; Methods of Making, and Methods of Operating. In United States Patent: 2011.
- (12) Arzamendi, G.; Diéguez, P.; Montes, M.; Odriozola, J.; Falabella Sousa-Aguiar, E.; Gandía, L., Computational fluid dynamics study of heat transfer in a microchannel reactor for low-temperature Fischer–Tropsch synthesis. *Chemical Engineering Journal* **2010**, 160, (3), 915-922.
- (13) Arzamendi, G.; Diéguez, P.; Montes, M.; Odriozola, J.; Sousa-Aguiar, E. F.; Gandía, L., Methane steam reforming in a microchannel reactor for GTL intensification: A computational fluid dynamics simulation study. *Chemical Engineering Journal* **2009**, 154, (1), 168-173.
- (14) Jeon, S. W.; Yoon, W. J.; Baek, C.; Kim, Y., Minimization of hot spot in a microchannel reactor for steam reforming of methane with the stripe combustion

catalyst layer. *International Journal of Hydrogen Energy* **2013**, 38, (32), 13982-13990.

(15) Mohammadi, M.; Jovanovic, G. N.; Sharp, K. V., Numerical study of flow uniformity and pressure characteristics within a microchannel array with triangular manifolds. *Computers & Chemical Engineering* **2013**, 52, 134-144.

(16) Shin, M.-S.; Park, N.; Park, M.-J.; Jun, K.-W.; Ha, K.-S., Computational fluid dynamics model of a modular multichannel reactor for Fischer–Tropsch synthesis: Maximum utilization of catalytic bed by microchannel heat exchangers. *Chemical Engineering Journal* **2013**, 234, (0), 23-32.

(17) Troshko, A. A.; Zdravistch, F., CFD modeling of slurry bubble column reactors for Fisher–Tropsch synthesis. *Chemical Engineering Science* **2009**, 64, (5), 892-903.

(18) Uriz, I.; Arzamendi, G.; López, E.; Llorca, J.; Gandía, L., Computational fluid dynamics simulation of ethanol steam reforming in catalytic wall microchannels. *Chemical Engineering Journal* **2011**, 167, (2), 603-609.

(19) Gumuslu, G.; Avci, A. K., Parametric analysis of Fischer-tropsch synthesis in a catalytic microchannel reactor. *AIChE Journal* **2012**, 58, (1), 227-235.

(20) Guettel, R.; Turek, T., Comparison of different reactor types for low temperature Fischer–Tropsch synthesis: a simulation study. *Chemical Engineering Science* **2009**, 64, (5), 955-964.

(21) Park, S.; Jung, I.; Lee, Y.; Kshetrimayum, K. S.; Na, J.; Park, S.; Shin, S.; Ha, D.; Lee, Y.; Chung, J.; Lee, C.-J.; Han, C., Design of Microchannel Fischer-Tropsch Reactor Using Cell-Coupling Method: Effect of Flow Configurations and Distribution. *Chemical Engineering Science* **accepted**.

- (22) Gabriel, K. J.; Linke, P.; Jiménez-Gutiérrez, A.; Martínez, D. Y.; Noureldin, M.; El-Halwagi, M. M., Targeting of the Water-Energy Nexus in Gas-to-Liquid Processes: A Comparison of Syngas Technologies. *Industrial & Engineering Chemistry Research* **2014**, *53*, (17), 7087-7102.
- (23) Hall, K. R., A new gas to liquids (GTL) or gas to ethylene (GTE) technology. *Catalysis Today* **2005**, *106*, (1–4), 243-246.
- (24) Lee, C.-J.; Lim, Y.; Kim, H. S.; Han, C., Optimal Gas-To-Liquid Product Selection from Natural Gas under Uncertain Price Scenarios. *Industrial & Engineering Chemistry Research* **2009**, *48*, (2), 794-800.
- (25) Castelo Branco, D. A.; Szklo, A. S.; Schaeffer, R., CO₂e emissions abatement costs of reducing natural gas flaring in Brazil by investing in offshore GTL plants producing premium diesel. *Energy* **2010**, *35*, (1), 158-167.
- (26) Dillerop, C.; van den Berg, H.; van der Ham, A. G. J., Novel Syngas Production Techniques for GTL-FT Synthesis of Gasoline Using Reverse Flow Catalytic Membrane Reactors. *Industrial & Engineering Chemistry Research* **2010**, *49*, (24), 12529-12537.
- (27) Deshmukh, S. R.; Tonkovich, A. L. Y.; Jarosch, K. T.; Schrader, L.; Fitzgerald, S. P.; Kilanowski, D. R.; Lerou, J. J.; Mazanec, T. J., Scale-Up of Microchannel Reactors For Fischer–Tropsch Synthesis. *Industrial & Engineering Chemistry Research* **2010**, *49*, (21), 10883-10888.
- (28) Mancaruso, E.; Sequino, L.; Vaglieco, B. M., GTL (Gas To Liquid) and RME (Rapeseed Methyl Ester) combustion analysis in a transparent CI (compression ignition) engine by means of IR (infrared) digital imaging. *Energy* **2013**, *58*, (0), 185-191.

- (29) Rahimpour, M. R.; Mirvakili, A.; Paymooni, K., A novel water perm-selective membrane dual-type reactor concept for Fischer–Tropsch synthesis of GTL (gas to liquid) technology. *Energy* **2011**, 36, (2), 1223-1235.
- (30) Sharma, A.; Philippe, R.; Luck, F.; Schweich, D., A simple and realistic fixed bed model for investigating Fischer–Tropsch catalyst activity at lab-scale and extrapolating to industrial conditions. *Chemical Engineering Science* **2011**, 66, (24), 6358-6366.
- (31) de Klerk, A.; Furimsky, E., Catalysis in the refining of Fischer–Tropsch syncrude. *A quarterly journal of research on the science and technology of the platinum group metals and developments in their application in industry* **2011**, 55, (4), 263-267.
- (32) Pratt, J. W., A Fischer-Tropsch synthesis reactor model framework for liquid biofuels production. *Sandia National Laboratories, California* **2012**.
- (33) Cao, C.; Palo, D. R.; Tonkovich, A. L. Y.; Wang, Y., Catalyst screening and kinetic studies using microchannel reactors. *Catalysis Today* **2007**, 125, (1–2), 29-33.
- (34) Butcher, H.; Quenzel, C. J. E.; Breziner, L.; Mettes, J.; Wilhite, B. A.; Bossard, P., Design of an annular microchannel reactor (AMR) for hydrogen and/or syngas production via methane steam reforming. *International Journal of Hydrogen Energy* **2014**, 39, (31), 18046-18057.
- (35) Irani, M., EXPERIMENTAL AND CFD MODELING OF A BENCH-SCALE GTL PACKED-BED REACTOR BASED ON FE/CU CATALYST. *Petroleum & Coal* **2014**, 56, (1), 62-73.
- (36) Deshmukh, S. R.; Vlachos, D. G., Effect of flow configuration on the

- operation of coupled combustor/reformer microdevices for hydrogen production. *Chemical Engineering Science* **2005**, 60, (21), 5718-5728.
- (37) Agrawal, G.; Kaisare, N. S.; Pushpavanam, S.; Ramanathan, K., Modeling the effect of flow mal-distribution on the performance of a catalytic converter. *Chemical Engineering Science* **2012**, 71, (0), 310-320.
- (38) Park, S.; Jung, I.; Lee, U.; Na, J.; Kshetrimayum, K. S.; Lee, Y.; Lee, C.-J.; Han, C., Design and modeling of large-scale cross-current multichannel Fischer–Tropsch reactor using channel decomposition and cell-coupling method. *Chemical Engineering Science* **2015**, 134, 448-456.
- (39) Yates, I. C.; Satterfield, C. N., Intrinsic kinetics of the Fischer-Tropsch synthesis on a cobalt catalyst. *Energy & Fuels* **1991**, 5, (1), 168-173.
- (40) Eliason, S.; Bartholomew, C., Reaction and deactivation kinetics for Fischer–Tropsch synthesis on unpromoted and potassium-promoted iron catalysts. *Applied Catalysis A: General* **1999**, 186, (1), 229-243.
- (41) Iglesia, E.; Reyes, S. C.; Madon, R. J.; Soled, S. L., Selectivity control and catalyst design in the Fischer-Tropsch synthesis: sites, pellets, and reactors. *Advances in Catalysis* **1993**, 39, 221-302.
- (42) Panahi, M.; Rafiee, A.; Skogestad, S.; Hillestad, M., A natural gas to liquids process model for optimal operation. *Industrial & Engineering Chemistry Research* **2011**, 51, (1), 425-433.
- (43) Baltrusaitis, J.; Luyben, W. L., Methane Conversion to Syngas for Gas-to-Liquids (GTL): Is Sustainable CO₂ Reuse via Dry Methane Reforming (DMR) Cost Competitive with SMR and ATR Processes? *ACS Sustainable Chemistry & Engineering* **2015**, 3, (9), 2100-2111.

- (44) Asteasuain, M.; Tonelli, S.; Brandolin, A.; Bandoni, J., Dynamic simulation and optimisation of tubular polymerisation reactors in gPROMS. *Computers & Chemical Engineering* **2001**, 25, (4), 509-515.
- (45) Sayer, C.; Lima, E.; Pinto, J., Dynamic modeling of SBR emulsion polymerization reactors refrigerated by thermosyphons. *Chemical engineering science* **1997**, 52, (3), 341-356.
- (46) Morud, J. C.; Skogestad, S., Analysis of instability in an industrial ammonia reactor. *AIChE Journal* **1998**, 44, (4), 888-895.
- (47) Arcuri, K. B., Process for the start-up of a Fischer-Tropsch reactor. In United States Patent: 1986.
- (48) Sumerford, S. D.; Moise, J. E.; Rouge, B.; La., Starting up procedure for the synthesis of hydrocarbons. In United States Patent: 1958.
- (49) Song, H.-S.; Ramkrishna, D.; Trinh, S.; Wright, H., Operating strategies for Fischer-Tropsch reactors: A model-directed study. *Korean Journal of Chemical Engineering* **2004**, 21, (2), 308-317.
- (50) Bezemer, G. L.; Mesters, C. M. A. M.; Remans, T. J.; Smits, J. T. M., High-speed stop in Fischer-Tropsch process. In United States Patent: 2015.

Abstract in Korean (요약)

지난 수십년간 Gas-to-Liquid (GTL) 공정은 천연가스를 청정 합성연료로 전환할 수 있는 기술로 많은 주목을 받아왔다. GTL 공정에서 우선 개질기에서 천연가스가 수소와 일산화탄소로 구성된 합성가스로 전환된다. 이후 합성가스는 피셔-트롭쉬 (FT) 반응기에서 반응을 일으켜 탄소 사슬수가 긴 탄화수소로 전환된다. 탄소수가 1개부터 30개 이상인 탄화수소는 FT 합성 연료라고도 불리는데, 옥탄가와 세탄가가 높고 질소 성분과 황 성분이 거의 없어 고급 청정 연료로 활용된다.

FT 반응은 일산화탄소 1몰 반응당 약 165kJ만큼의 반응열이 나오는 고발열 반응이다. 이 반응열은 반응기의 thermal-runaway와 같은 불안정성과 직접적인 연관이 있기 때문에 반응기 내에서 효율적으로 제거되어야 한다. 이를 위해 많은 종류의 반응기, 이를테면 슬러리 버블 반응기, 고정층 반응기, 유동층 반응기들이 GTL 공정에 적용되어 왔으나, 해양 플랫폼 등 특수한 상황에서는 이보다 더 작고 생산 효율이 높은 반응기가 필요하다는 의견이 꾸준히 제기되어왔다.

이에 최근 마이크로채널 FT 반응기의 개념이 대두하였는데, 마이크로채널 반응기는 채널 사이즈가 매우 작기 때문에 단위부피당 열교환 면적이 커서 반응열을 빠르고 효율적으로 제거할 수 있다는 특징이 있다. 한 문헌에서는 일반적인 고정층 반응기보다 마이크로채널 반응기가 약 15배 가량 열 제거 속도가 빠르다고 나와있다. 또한 마이크로 채널 반응기는 모듈화가 가능하기 때문에 scale-up에서도 유리하다. 이러한 열교환

효율성과 모듈화 덕분에 스케일이 작은 단일 채널의 반응기와 파일럿 스케일의 반응기의 성능이 거의 동일하다고 알려져 있다.

본 논문에서는 마이크로채널 반응기를 기반으로 한 최적 GTL공정의 설계를 다룬다. 이를 위해 마이크로 채널 FT 반응기의 모델을 수립하였고, 그 반응기 모델을 바탕으로 한 GTL 공정의 모델을 만들어 최적화를 수행했으며, 마이크로 채널 FT 반응기의 동적 모사를 통한 최적 운전 절차를 제안하였다. 반응기 모델은 실제 반응기의 운전 데이터로부터 실증(validation) 하였다.

첫째로, 반응기에 대한 distributed-parameter 모델을 채널 분해와 셀 결합이라는 새로운 방식으로 구성했다. 셀 결합 모델에서는 인접한 반응 채널과 냉각채널간의 상호 작용, 즉 물질 수지와 열 수지, 열전달에 대한 방정식을 전체 셀 공간 내에서 세우고 해를 구한다. 그 모델 계산 결과와 실제 파일럿 스케일 반응기 데이터를 비교해보니 서로 경향성과 크기가 거의 일치함을 확인했다. 또한, 촉매의 충전량, 냉매의 유량, 그리고 채널의 사이즈에 대한 효과를 파악하기 위해 cross-current 반응기에 대해 민감도 분석을 수행했다.

나아가 유로의 구성과 흐름 분배 효과를 반영해 개선된 셀 결합 모델을 개발했다. 이를 위해 각각의 유로 구성에 대해 셀의 영역을 재정의하였고, 전산유체역학의 결과를 모델에 이식해 흐름 분배에 대한 효과를 반영했다. 개선된 모델을 통해 유로의 구성, 흐름 분배, 그리고 촉매의 충전 구간에 대한 민감도 분석을 수행하였다. 그 결과 cross-co-cross

current 구조가 다른 구조들에 비해 열 제거 측면에서 가장 성능이 좋았다.

다음으로 개발된 마이크로채널 반응기 모델을 이용해 최적 GTL 공정에 대한 연구를 수행했다. 우선 정상 상태의 GTL 공정을 모델링 했는데, 이 때 반응기 모델은 인공 신경망으로 모사하였다. 이후 순이익의 음수 값을 최소화하는 최적화 문제를 구성했다. 이 문제에서 설계 변수로는 FT 반응기의 온도, 압력, purge 비율, 그리고 FT반응기로 들어가는 비율을 사용했다. 본 최적화 문제를 풀기 위해 Nelder-Mead 알고리즘을 사용하였고, 그 결과 FT 반응기의 반응열을 이산화탄소 분리에 필요한 재기화기의 열량을 보충해줘서 효율이 증가했다. 얻어진 최적 해는 기존 공정보다 경제적으로 더 나은 성능을 보였다.

끝으로 FT 반응기의 동적 모델을 개발했다. 셀 결합 모델의 구조를 이용해 편미분방정식을 단순화하여 시간에 대한 반응기 내의 3차원적인 온도 프로파일을 구할 수 있었다. 이 모델을 이용해 마이크로채널 반응기의 동적 거동을 분석했다. 또한 별도로 FT 반응기 시스템에 대한 동적 모사를 수행하여 공정의 최적 start-up과 shut-down 절차를 제안했다.

본 연구는 마이크로채널 피셔-트롭쉬 반응기를 기반으로 한 최적 GTL 공정을 설계하는 데 기여할 수 있을 것이다. 개발된 반응기 모델, 정상 상태의 모델과 동적 모델, 실제 GTL 시스템을 설계하고 운전하는 데 이용하고 거기에서 발생하는 수많은 문제점을 해결하는 데 활용할

수 있을 것으로 기대한다.

주요어: 마이크로채널 반응기, 피셔-트롭쉬, 반응기 모델링, GTL 공정,
공정 최적화, 동적 모사

학번: 2011-21036

성명: 박 성 호



저작자표시-비영리-변경금지 2.0 대한민국

이용자는 아래의 조건을 따르는 경우에 한하여 자유롭게

- 이 저작물을 복제, 배포, 전송, 전시, 공연 및 방송할 수 있습니다.

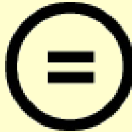
다음과 같은 조건을 따라야 합니다:



저작자표시. 귀하는 원저작자를 표시하여야 합니다.



비영리. 귀하는 이 저작물을 영리 목적으로 이용할 수 없습니다.



변경금지. 귀하는 이 저작물을 개작, 변형 또는 가공할 수 없습니다.

- 귀하는, 이 저작물의 재이용이나 배포의 경우, 이 저작물에 적용된 이용허락조건을 명확하게 나타내어야 합니다.
- 저작권자로부터 별도의 허가를 받으면 이러한 조건들은 적용되지 않습니다.

저작권법에 따른 이용자의 권리는 위의 내용에 의하여 영향을 받지 않습니다.

이것은 [이용허락규약\(Legal Code\)](#)을 이해하기 쉽게 요약한 것입니다.

[Disclaimer](#)

공학박사학위논문

**A Study on Optimal Design for Gas-to-Liquid Process by
Utilizing Micro-channel Fischer-Tropsch Reactor**

마이크로채널 피셔-트롭쉬 반응기를 활용한 Gas-to-Liquid
공정의 최적 설계에 관한 연구

2015년 12월

서울대학교 대학원

화학생물공학부

박 성 호

Abstract

A Study on Optimal Design for Gas-to-Liquid Process by Utilizing Micro-channel Fischer- Tropsch Reactor

Seongho Park

School of Chemical & Biological Engineering

The Graduate School of Seoul National University

For several decades, a gas-to-liquid (GTL) process has been identified as a promising technology for converting abundant natural gas (NG) to clean synthetic fuel. Throughout the GTL process, NG is firstly converted to synthesis gas, mainly composed of hydrogen and carbon monoxide by a syngas reforming process. Syngas is then chemically converted into the liquid fuel by Fischer-Tropsch (FT) reaction process, wherein several carbon atoms in the syngas are oligomerized to form a long chain hydrocarbon product. This hydrocarbon product is also known as FT synfuel, and it contains many hydrocarbon species of carbon number ranging from 1 (methane) to more than 30 (FT wax). FT synfuel has high research octane number (RON) and cetane number (CN) and almost nitrogen and sulfur free. So it is taking a premium position in the fuel market.

FT synthesis reaction is known as a strongly exothermic reaction: A large amount of heat, ca. 165kJ per mol of converted CO is generated during the reaction. This heat must be removed to prevent runaway situation and achieve safe isothermal operation of the reactor. Various types of reactors, such as fixed bed, slurry bubble column, circulating fluidized bed, and fixed fluidized bed FT reactors, have been developed and applied to the GTL industries. In order to utilize the FT reaction in off-shore platform, however, more compact, but highly productive, FT reactor is essential.

Recently, the concept of micro channel FT reactor has evolved because it can effectively handle large amount of heat based on the high heat exchange surface area per unit volume. It was reported that the heat removal rate in the micro-channel reactor was around 15 times higher than that in a conventional fixed bed reactor. Moreover, micro-channel reactors are good for scale-up perspectives because the wax production can be easily increased by simply adding modularized reactors. It has been reported that the performance of the pilot scale micro-channel reactor was consistent with that of a single micro-channel reactor due to the achievement in isothermal operation.

This thesis has addressed the optimal design for GTL processes based on the micro-channel Fischer-Tropsch reactor technology: Modeling of the micro-channel FT reactor, optimization of the GTL process based on the developed reactor model, and dynamic simulation and optimal operating procedures for the micro-channel FT reaction system. The reactor models were validated against the real operation data.

A distributed parameter model for micro-channel FT reactor was developed by using a new method, in which all the process and cooling channels are decomposed

into a number of unit cells. Each neighboring process and cooling channel unit cells are coupled to set up material and energy balance equations, including heat-transfer equations for the entire reactor domain, which are then solved simultaneously. The model results were compared with the experimental data for a pilot-scale reactor described in the literature, and were found to be in good agreement. Several case studies were performed to see the effect of variables such as catalyst loading ratio, coolant flow rate, and channel layout on design of a cross-current type reactor with state-of-the-art Fischer–Tropsch catalyst.

The cell-coupling model was then modified to consider more realistic type of flow configurations and flow distribution effect. Cell domain was re-defined for each flow configuration, and the realistic flow distribution effect was incorporated into the model by using results obtained from computational fluid dynamics (CFD). Several case studies were conducted to see the effect of flow configurations, flow distribution, and catalyst loading zones. It was observed that the geometry of cross-co-current was found to give the best performance among the designs considered.

Optimal GTL process was suggested by conducting steady-state simulations where the developed micro-channel FT reactor model was implemented in the form of regressed artificial neural network (ANN) model. First, steady state model for a conventional GTL process was developed. Then, an optimization problem was formulated by defining objective function as the net profit. Design variables for this problem were the pressure and temperature of the FT reactor, split ratio for purge, and recycle flowrate to the FT reactor. Nelder-Mead algorithm was used to solve this derivative-free optimization problem. It can be said that by utilizing the reaction heat of the FT reactor, the reboiler duty for the CO₂ separation was

reduced, and the overall efficiency was increased. Optimal solution showed better economic performances over the base case design.

A dynamic model for the FT reactor was developed. A partial differential equation for the 3D cell-coupling model was formulated and solved to obtain time dependent temperature profile in the entire reactor domain. Several case studies were performed to analyze dynamic behavior of the micro-channel reactor. Separate dynamic simulations were also conducted to suggest optimal start-up and shut-down procedure for the FT reactor system. Several scenarios were generated to analyze the thermal and hydrodynamic behavior of the reactor. Optimal operating strategies for both start-up and shut-down of the reactor could be obtained.

This work could contribute to designing optimal GTL process, especially using a large-scale micro-channel Fischer-Tropsch reactor containing more than 1,000 process channels. The developed reactor model, steady-state model, and dynamic model could be utilized for designing and operation of the GTL system.

Keywords: Micro-channel reactor, Fischer-Tropsch, Reactor modeling, Gas-to-Liquid process, Process optimization, Dynamic simulation

Student ID: 2011-21036

Contents

Abstract	i
Contents.....	v
List of Figures	vii
List of Tables.....	x
CHAPTER 1 : Introduction.....	11
1.1. Research motivation.....	11
1.2. Research objectives.....	13
1.3. Outline of the thesis.....	14
CHAPTER 2 : Reactor model using cell-coupling method.....	15
2.1. Cross-current reactor model.....	15
2.1.1. Introduction	15
2.1.2. Model description.....	17
2.1.3. Model validation.....	27
2.1.4. Case studies	32
2.1.5. Conclusion.....	45
2.2. Improved reactor model	47
2.2.1. Introduction	47
2.2.2. Model construction.....	50
2.2.3. Model validation.....	60
2.2.4. Case studies	69
2.2.5. Conclusion.....	90

CHAPTER 3 : Optimization for GTL process	91
3.1. Introduction	91
3.2. Model description.....	92
3.2.1. Steady-state process model.....	92
3.2.2. Micro-channel reactor model	99
3.3. Optimization for the steady-state model	103
3.3.1. Cost model.....	103
3.3.2. Problem formulation.....	108
3.4. Results and discussion.....	112
3.5. Conclusion.....	115
CHAPTER 4 : Dynamic simulation for microchannel Fischer-Tropsch reactor ...	116
4.1. Introduction	116
4.2. Dynamic modeling for 3D reactor	118
4.2.1. Model description.....	118
4.2.2. Results and anlysis	120
4.3. Optimal operating strategies for FT reactor	125
4.3.1. Model description.....	125
4.3.2. Start-up	129
4.3.3. Shut-down	134
4.4. Conclusion.....	141
CHAPTER 5 : Concluding Remarks.....	142
5.1. Conclusions	142
5.2. Future works.....	144
Nomenclature	145

Literature cited	150
Abstract in Korean (요약).....	157

List of Figures

Figure 2-1. Conceptual diagrams of cross-current heat-exchange reactor, and channel decomposition and cell-coupling method.	19
Figure 2-2. Algorithm for computing material balance, energy balance, and heat transfer in model domain.....	21
Figure 2-3. Comparison of plots of literature experimental data (Deshmukh et al., 2010) (a) and the model estimations (b).....	28
Figure 2-4. Comparison between the model estimation and the experimental data of the conversion and selectivity	30
Figure 2-5. Results for base-case model simulation.....	34
Figure 2-6. Heat generation profiles for different catalyst loading ratio: 0.2(a), 0.7(b), and 1.0(c).	36
Figure 2-7. Heat generation and heat removal rate at various reaction temperature and catalyst loading ratio.....	38
Figure 2-8. Heat generation profile for the different catalyst loading at divided zones: Catalyst loading ratio of 0.2 and 0.7 for the 50% length of the channel, respectively. Same scale of color bar as in the Figure 2-5 was used.	41
Figure 2-9. Sensitivities of maximum temperature of process channels to coolant flow rate for different catalyst loading ratio.....	42
Figure 2-10. Sensitivities of maximum temperature difference and reactor volume	

to the process channel size	44
Figure 2-11. Flow configuration of multi-channel reactor: (a) Structure S1. Cross-counter-cross current with the same side; (b) Structure S2. Cross-co-cross current with the same side; (c) Structure S3. Cross-counter-cross with the different side; (d) Structure S4. Cross-co-cross current with the different side; (e) Structure S5. Fully cross-current	52
Figure 2-12. Conceptual diagram of a cell coupling model: (a) Cell domain construction for the entire reactor of cross-co-cross current with the same side scheme; (b) Flow path construction	54
Figure 2-13. Overall procedure for the computation of the integrated model.....	56
Figure 2-14. Flow distribution effect for the inlet/outlet of the channel and the channel plate inside the reactor: (a) Conceptual diagram representing the domain decomposition of the reactor geometry, ((b) and (d)) velocity profiles obtained from CFD simulation for the decomposed plates, and ((c) and (e)) the result of the data fitting with non-linear function.....	57
Figure 2-15. Comparison of the CO conversion between the measurement and the model estimation. The red line in the plot represents the trend line obtained from the regression.....	65
Figure 2-16. Temperature profile of the process channel for the cross-counter-cross current with the same side scheme	71
Figure 2-17. Result of the regression of the velocity profile for the inlet pipeline whose diameter is (a) 40 mm, (b) 50 mm, and (c) 60 mm.	79
Figure 2-18. Result of CFD simulation and data regression for the flow distribution of the coolant channel plate (a) without inlet guiding fin and (b) with inlet guiding	

fin.	81
Figure 2-19. Temperature profile for the case of (a) uniform distribution and (b) mal-distribution	84
Figure 2-20. Conceptual diagram of (a) partial-overlapping and (b) full-overlapping zone scheme	88
Figure 2-21. Temperature profile for the case of (a) partial-overlapping and (b) full-overlapping zone scheme	89
Figure 3-1. Process flow diagram for overall GTL process	94
Figure 3-2. Structure of the artificial neural network for the micro-channel FT reactor	101
Figure 3-3. Results for the artificial neural network model: (a) Training set and (b) test set	102
Figure 3-4. Concept of Nelder-Mead algorithm: (a) Reflection and expansion, (b) Contraction, (c) Shrink	111
Figure 3-5. CAPEX and OPEX for reference process and optimal process.....	113
Figure 4-1. Changes of the temperature profile with time (Scenario 1). The color bar of the same scale (230°C - 240°C) was used for all the subplots.	122
Figure 4-2. Changes of the temperature profile with time (Scenario 2).....	124
Figure 4-3. Process flow diagram for the dynamic simulation.....	127
Figure 4-4. Comparison between two extreme cases: Scenario 1 and 9.	132
Figure 4-5. Results of the case studies: Scenario 1 through 9.....	133
Figure 4-6. Result of dynamic simulation for three shut-down scenarios: Scenario 1, 3, and 8	137
Figure 4-7. Phase envelope	140

List of Tables

Table 2-1. Reaction Schemes and Kinetic Parameters for Fischer–Tropsch Catalyst Reported in Literature (Deshmukh et al., 2011).....	25
Table 2-2. Reaction conditions for the operation of multichannel Fischer Tropsch reactor.....	31
Table 2-3. Comparison of Sizes of Existing Computational Fluid Dynamic (CFD) ^a and Cell-Coupling Models	46
Table 2-4. Operating conditions ^a for the kinetic experiment.....	63
Table 2-5. Kinetic parameters ^a for Fischer–Tropsch catalyst used in this article....	66
Table 2-6. Comparison of CO conversion between model estimation and the data reported in literature (Deshmukh et al., 2011 ¹¹)	68
Table 2-7. Result of simulation for the five different flow configurations.....	74
Table 3-1. Stream table for the GTL process.....	97
Table 3-2. Results for the economic evaluation for the optimal design; (a) CAPEX and OPEX for the process equipment and (b) Other cost and earning.....	106
Table 3-3. Overall economic evaluation for reference process and optimal process	114
Table 4-1. Size of the process equipments	128
Table 4-2. Description for start-up scenarios	130
Table 4-3. Description for shut-down scenarios.....	136

CHAPTER 1 : Introduction

1.1. Research motivation

Gas-to-liquid (GTL) processes have been identified as promising processes for converting abundant natural gas (NG) to a clean synthetic fuel. The NG is first converted to syngas, which consists mainly of carbon monoxide (CO) and hydrogen, through a reforming process, and then the synthetic liquid fuel is chemically synthesized via a Fischer–Tropsch (FT) reaction. FT synfuel is almost sulfur and nitrogen free, and is therefore considered to be a clean energy fuel.

FT synthesis is known as a strongly exothermic reaction: A large amount of heat, ca. 165kJ per mol of converted CO is generated during the reaction. This heat must be removed to prevent runaway situation and achieve safe isothermal operation of the reactor. In that sense, micro-channel FT reactors are spotlighted as an alternative reactors because its heat removal performance is much better than that of conventional reactors such as fixed bed reactor or slurry-bubble reactor. The micro-channel reactors are also known to be good for scale-up perspectives due to its compactness and ease of manufacturing by modularization.

Although many researchers studied FT reaction performances in the micro-channel environment experimentally, few studies on the design of the micro-channel Fischer-Tropsch reactor can be found from the literature. In order to design a robust and reliable micro-channel reactor, the effect of design variables such as channel layout, reactant inlet temperature, coolant flow rate, catalyst loading ratio, flow configuration, and flow distribution on the reactor performances should be rigorously analyzed. In that perspectives, computational fluid dynamics (CFD) has

been widely used for such detailed evaluation of reaction systems. However, when many process and coolant channels are involved, for large-scale reactors, CFD is highly computationally intensive and time consuming. CFD therefore may not be able to handle all the channels; the problem is unrealistically large, because it deals with rigorous physics such as flow patterns over the entire domain, the shear stress and viscous effects of the flowing entity, and material and energy balances, rather than using simple empirical equations. The current research trend in FT reaction design in a CFD environment is towards reduction of the problem size and analysis of the effects of key variables in the newly defined reduced domain.

When dealing with the design problem of micro-channel reactors, where typically more than 1,000 channels are involved, more efficient way of modeling and solving approach should be considered so that we can practically conduct the design work such as sensitivity analysis, optimization, and dynamic simulations. The reactor model should be simplified in order to reduce the heavy computational load, without losing much physical rigors that are of main concern in the preliminary design of micro-channel FT reactor.

To find an optimal structure and operating conditions for GTL process is an important issue for economic process design. To be more specific, development of more efficient process by analyzing overall heat and mass flow, and design of better process alternatives by changing several important design variables play an important role in process optimization for entire GTL process. Such optimization problem, particularly for a GTL process with the micro-channel FT reactor, is hardly found from the literature.

Development of a dynamic model for the micro-channel FT reactor is essential part for safe operation of the GTL process. FT reaction is considered to be one of

the most exothermic reaction, so the dynamic behavior of the reaction system should be rigorously analyzed for safety. When the reaction heat is improperly controlled, abnormal situation such as thermal runaway takes place. Such undesirable situation is more likely to occur in transient state, for example, start-up and shut-down period of the reactor. It is therefore necessary to find the optimal, robust, and reliable operating procedure for the process safety.

1.2. Research objectives

The objective of this thesis is to suggest an optimal design for GTL process based on the micro-channel Fischer-Tropsch reactor. When a micro-channel reactor is to be scaled-up, more than 1,000 channels are involved, which makes it hard to handle such a large number of channels in conventional CFD environment. In order to solve that problem, a novel micro-channel FT reactor model was developed by using channel decomposition and cell coupling method. The model was validated against the pilot reactor operation data. An improved model that could handle variations in channel configuration and flow distribution. GTL process is known to be one of the most energy-intensive process. Improved versions of the process should be suggested for ensuring economic feasibility. For this purpose, an optimization problem for the GTL process was formulated and solved. A steady state model was developed with implementation of the aforementioned reactor model. Heat from the reformer's outlet stream and FT reactor's outlet stream was utilized to generate excess steam, and to provide required energy for CO₂ separation, respectively. For the safe operation of the FT reaction system, a dynamic model for the FT reactor was developed. Optimal start-up and shut-down procedure for the FT reactor was suggested to prevent thermal runaway or wax

clogging.

1.3. Outline of the thesis

The thesis is organized as follows. Chapter 1 provides motivation and objectives of this study. Chapter 2 describes the micro-channel FT reactor model using channel decomposition and cell coupling method. It includes validation with data from a pilot scale FT reactor. Furthermore, in this chapter, an improved model for the FT reactor which takes flow configuration and distribution effect into account is suggested. In chapter 3, an optimal structure and operating condition for the overall GTL process with the micro-channel FT reactor is suggested. The formulation of the optimization problem is stated, and the solution to that problem is analyzed. Chapter 4 describes the dynamic model for the micro-channel reactor. It also includes the optimal operating strategies for the FT reactor. Chapter 5 presents the conclusion and an outline for the future works.

CHAPTER 2 : Reactor model using cell-coupling method¹

2.1. Cross-current reactor model

2.1.1. Introduction

Gas-to-liquid (GTL) processes have been identified as promising processes for converting abundant natural gas (NG) to a clean synthetic fuel¹⁻⁶. The NG is first converted to syngas, which consists mainly of carbon monoxide (CO) and hydrogen, through a reforming process, and then the synthetic liquid fuel is chemically synthesized via a Fischer–Tropsch (FT) reaction. FT synfuel is almost sulfur and nitrogen free, and is therefore considered to be a clean energy fuel.

Recently, the GTL-FPSO (floating, production, storage, and offloading) process has been considered as an alternative process for exploiting NG from stranded gas reserves or for using associated gases in conventional oil fields^{7,8}. The design of compact, but highly productive, FT reactors will play a central role in the commercialization of GTL-FPSO. The large amount of heat generated during the FT reaction, ca. 165 kJ/mol, must be removed to achieve isothermal operation of the reactor and prevent runaway situations. Novel microchannel heat-exchange FT reactors have received much attention because of their high heat-transfer efficiencies and high production rates per unit volume of reactor^{2, 9-11}. A microchannel FT reactor was studied by Chin et al., using a novel engineered catalyst¹⁰, which improved mass- and heat-transfers and enabled safe operation of

¹ The partial part of this chapter is taken from the author's published paper.

the reactor without increasing undesired methane formation. Cao et al. evaluated the FT reaction performance of a supported cobalt catalyst in a microchannel catalytic reactor². Heat was effectively removed, enabling the reaction to be performed at a high gas hourly space velocity (GHSV).

Many variables such as channel layout, reactant inlet temperature, coolant flow rate, catalyst loading ratio, and space velocity are involved in multichannel FT reactor design. For successful reactor design, the effect of each important variable should be estimated and analyzed in the design step, and computational fluid dynamics (CFD) is widely used for detailed evaluation of reaction systems¹²⁻¹⁸. However, when many process and coolant channels are involved, for large-scale reactors, CFD is highly computationally intensive and time consuming. CFD therefore may not be able to handle all the channels; the problem is unrealistically large, because it deals with rigorous physics such as flow patterns over the entire domain, the shear stress and viscous effects of the flowing entity, and material and energy balances, rather than using simple empirical equations. The current research trend in FT reaction design in a CFD environment is towards reduction of the problem size and analysis of the effects of key variables in the newly defined reduced domain^{12, 19}.

A quick check of the effect of some variable changes is essential for decision making in the preliminary design phase. Sensitivity analyses of the channel layout such as channel width and height, gaps between channels, and wall thickness should be conducted to determine the feasible range of the channel size before the detailed design phase. The influences of some important variables such as reactant inlet temperature, coolant velocity, and feed composition on other related variables, e.g., heat generation, heat removal rate, reaction kinetics, and heat-transfer

coefficient, should be rapidly estimated throughout the entire channel.

In this study, a new method for modeling large-scale cross-current microchannel FT reactors using a channel decomposition and cell-coupling method was developed. External models such as the channel layout model, kinetic model, single-channel model, and empirical heat-transfer model were used to constitute an integrated multichannel distributed model. First, the method and algorithm for model construction were developed, and then the developed model was validated against literature data. Several case studies of the design of cross-current FT reactors with use of the state-of-the-art FT catalyst¹¹ were performed to determine design criteria, analyses, and strategies.

2.1.2. Model description

As will be described in the following sections, a distributed model for the cross-current FT reactor was developed to handle all the channels in the system. It is supported by four external models: a channel layout model that defines channel geometries, a kinetic model that provides kinetic information on the catalytic FT reaction, an empirical heat-transfer model that calculates the heat removal rate, and a single-channel model that evaluates the heat and mass balances for the reaction system in one dimension. Especially, in the channel layout model, structural information such as the number of both process and cooling channels, and the overall size of the reactor core is obtained by specifying the width, height, length, and wall thickness of the process and cooling channels, target wax production rate, space velocity of the reactant, and the catalyst loading amount.

Figure 2-1 shows a diagram of channel decomposition and cell coupling in the cross-current heat-exchange reactor. From the channel configuration, which was

predefined based on the channel layout model, all the process and cooling channels are decomposed in the i , j , and h directions. All the decomposed channel cells are then matched not only to the adjacent cells, but also to the distant cells that interact each other: A process cell located at an arbitrary position (j, i, h) is firstly coupled to every neighboring cells located at the position e.g., $(j, i \pm 1, h)$, $(j, i \pm 2, h)$, $(j, i, h \pm 1)$, $(j, i, h \pm 2)$, etc, to set up heat and material balance equations, which are then solved to obtain the solution. It is assumed that the heat transfer rate is in inverse relationship with the distance between each cell. The lower figure in Figure 2-1 illustrates this pairing concept over an arbitrary cell domain.

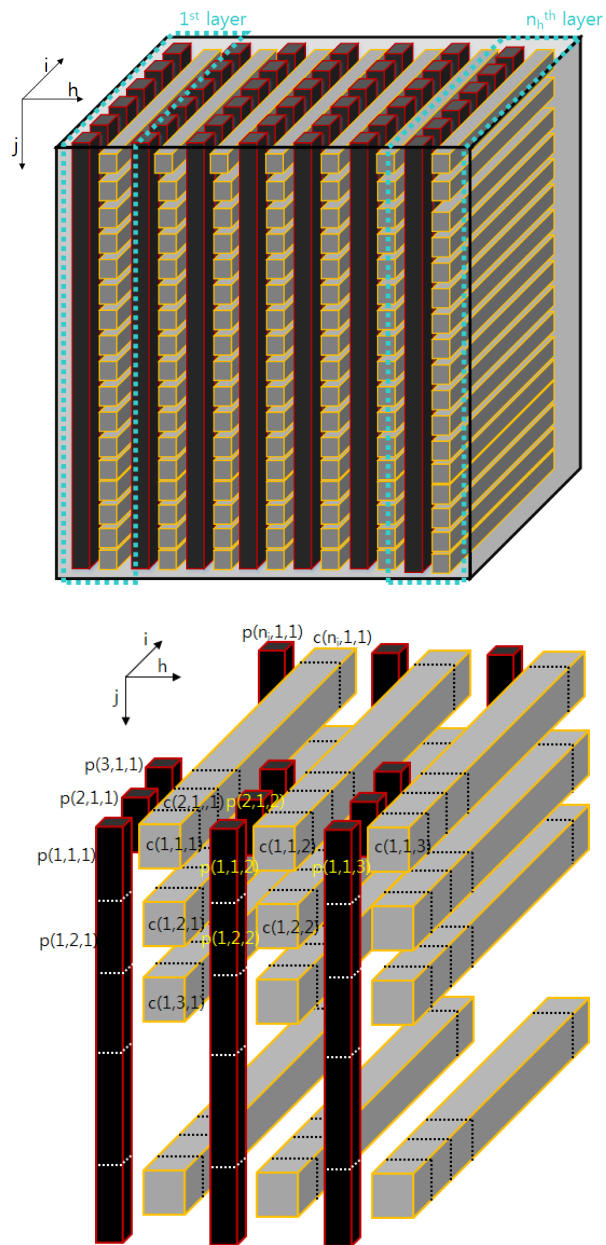


Figure 2-1. Conceptual diagrams of cross-current heat-exchange reactor, and channel decomposition and cell-coupling method.

Figure 2-2 shows the algorithm for computing the mass and energy balance and heat-transfer equations involved in the model. First, it decides the channel configurations over the entire reaction core, followed by the channel decomposition and cell-coupling procedure. It then runs the single channel reaction model, with the help of a predeveloped external kinetic model, to obtain initial values for all the decomposed cells. T_p , T_c , U , and Q in Figure 2-2 are $n_j \times n_i \times n_h$ matrices of the temperature of the process channel cells, temperature of the coolant channel cells, overall heat-transfer coefficient for every pair of matched cells, and amount of heat generated by the exothermic FT reaction in the process channel cells, respectively. U is evaluated using an empirical heat-transfer model:

$$U(j, i, h) = \left(\frac{1}{h_{\text{process}}(j, i, h)} + \frac{\Delta x}{k_{\text{channel}}} + \frac{1}{h_{\text{coolant}}(j, i, h)} \right)^{-1} \quad (2 - 1)$$

where $h_{\text{process}}(j, i, h)$ and $h_{\text{coolant}}(j, i, h)$ are the convective heat-transfer coefficients in a process channel cell and coolant channel cell, respectively, located at position (j, i, h) . In the conductive heat-transfer resistance term, Δx and k_{channel} represent the gap between two matched channel cells and the thermal conductivity of the reactor material, respectively.

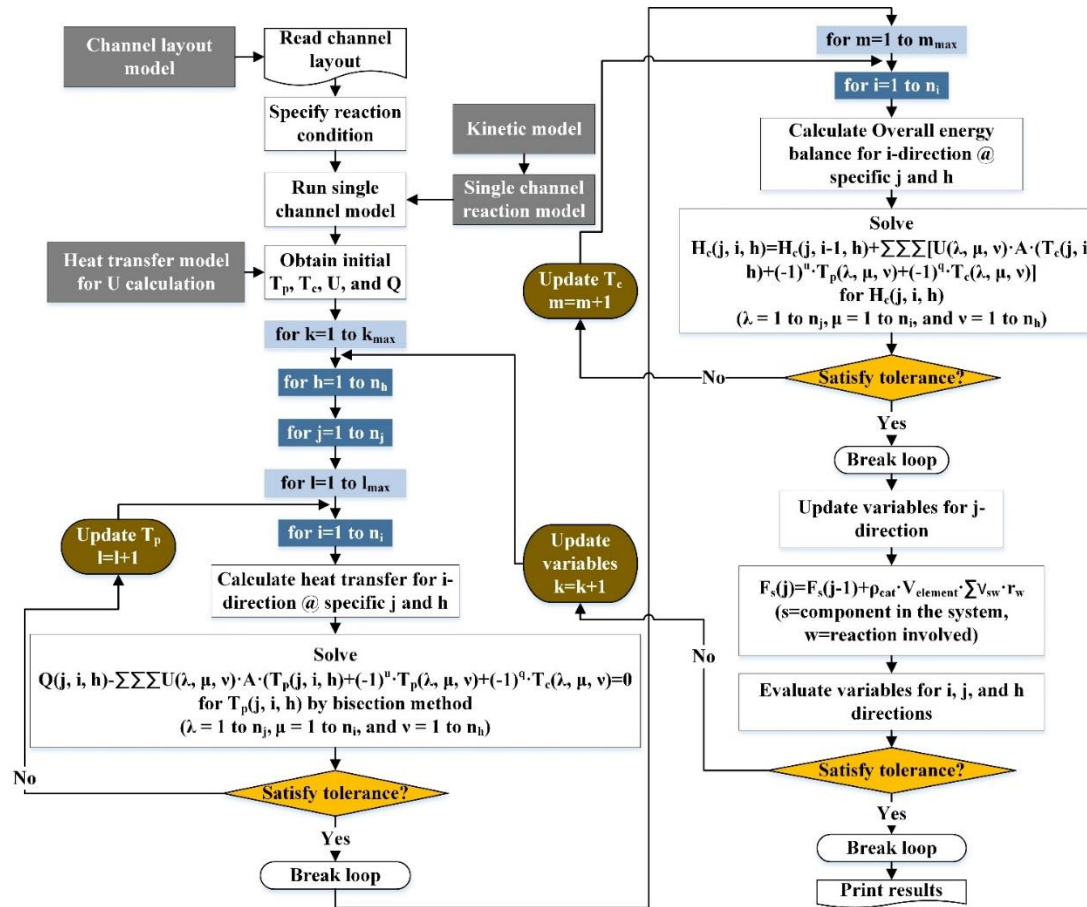


Figure 2-2. Algorithm for computing material balance, energy balance, and heat transfer in model domain.

After specifying the initial values, the model iteratively computes the heat transfer between cells (eq 2-2), and the overall energy balance (eq 2-3) along the i and j direction, respectively.

$$Q(j, i, h) - \sum_{\lambda} \sum_{\mu} \sum_{\nu} [U(\lambda, \mu, \nu) \cdot A \cdot (T_p(j, i, h) + (-1)^u \cdot T_p(\lambda, \mu, \nu) + (-1)^q \cdot T_c(\lambda, \mu, \nu)] = 0 \quad (2-2)$$

$$m_c \widehat{h}_c(j, i, h) = m_c \widehat{h}_c(j, i-1, h) + \sum_{\lambda} \sum_{\mu} \sum_{\nu} [U(\lambda, \mu, \nu) \cdot A \cdot (T_c(j, i, h) + (-1)^u \cdot T_p(\lambda, \mu, \nu) + (-1)^q \cdot T_c(\lambda, \mu, \nu)] \quad (2-3)$$

where the λ , μ , and ν in the sigma are evaluated from 1 to n_j , 1 to n_i , and 1 to n_h , except for j , i , and h , respectively. The u and q in the exponent of (-1) are used to decide the direction of the heat flow. The m_c and \widehat{h}_c are the coolant flow rate and specific enthalpy of the coolant, respectively. First, in the first loop with iteration variable i (Figure 2-2), the j th-vector component of T_p along the i -direction at a particular h is updated, using the bisection method, to solve eq 2-2. The model then evaluates the corresponding vectors of Q and U with a new T_p , and iteratively solves eq 2-2 with updated variables until the errors between the previous and present values are satisfactory within the tolerance. After finishing specification of the variables related to the process channels, i.e., T_p , Q , and U , the coolant channel temperature T_c is updated using the overall energy balance (eq 2-3). Eq 2-3 evaluates the enthalpy changes of the coolant along the i -direction and the heat flow into and out of the cell. In the second loop with iteration variable i (Figure 2-2), the model performs iterative calculations to update j th-vector component of T_c along the i -direction at a specific h until the errors are satisfactory within the

tolerance.

It then updates variables for j -direction using pseudo homogeneous 1-D reaction model (eq 2-4) which accounts for the net generation of all the chemical species in the system.

$$F_s(j, i, h) = F_s(j - 1, i, h) + \rho_{cat} \cdot V_{element} \cdot \sum_w \nu_{sw} \cdot r_w \quad (2 - 4)$$

where F_s , ρ_{cat} , $V_{element}$, and ν_{sw} are the molar flowrate of component s [mol/s], bulk catalyst packing density [gcat/m³], volume of unit element [m³], and stoichiometric coefficient of component s in reaction w , respectively. The reaction schemes considered in this study are presented in Table 2-1, so the $w = 1$ to 6. The same calculation is conducted for all other h s (the layer counting number for h -direction) to obtain the final versions of the variable matrices. The model iterates the computation until the error between the values in the present and previous step becomes negligible.

In summary, this cell decomposition model computes the heat and material balances for the process channel (j -direction), and the overall energy balance and heat transfer equation for the coolant channel (i -direction). It accounts for the heat flow for the j - and h -direction as well. Pseudo homogeneous 1-D reaction model can be applied because the reactions are taking place in the micro channel environment. Detailed computations such as flow viscous effect, heat dissipation along the construction material, and shear stress were not considered because they have negligible effect on the overall heat and mass balances. This simplification greatly reduces computational load without losing much physical rigors that are of main concern in the preliminary design of cross current micro channel FT reactor.

Table 2-1. Reaction Schemes and Kinetic Parameters for Fischer–Tropsch Catalyst
Reported in Literature (Deshmukh et al., 2011)

ID	Reaction	Reaction rate expression ^a
1	$3H_2 + CO \rightarrow H_2O + CH_4$	$r_{CH_4} = k_1 \exp(-E_1/RT) C_{H_2}$
2	$5H_2 + 2CO \rightarrow 2H_2O + C_2H_6$	$r_{C_2H_6} = k_2 \exp(-E_2/RT) C_{H_2}$
3	$7H_2 + 3CO \rightarrow 3H_2O + C_3H_8$	$r_{C_3H_8} = k_3 \exp(-E_3/RT) C_{H_2}$
4	$9H_2 + 4CO \rightarrow 4H_2O + C_4H_{10}$	$r_{C_4H_{10}} = k_4 \exp(-E_4/RT) C_{H_2}$
5	$H_2O + CO \rightarrow H_2 + CO_2$	$r_{CO_2} = k_5 \exp(-E_5/RT) C_{CO} C_{H_2O}$
6	$29H_2 + 14CO \rightarrow 14H_2O + C_{14}H_{30}$	$r_{C_{14}H_{30}} = \frac{k_6 \exp(-E_6/RT) C_{H_2} C_{CO}}{[1 + k_{ad} \exp(-E_{ad}/RT) C_{CO}]^2}$

(a) Reaction schemes and rate expressions

^aConcentrations in kmol/m³.

(b) Kinetic parameters

ID	k_i [rate in kmol/(kg-cat s)]	E_i (J/kmol)
1	2.509×10^9	1.30×10^8
2	3.469×10^7	1.25×10^8
3	1.480×10^7	1.20×10^8
4	1.264×10^7	1.20×10^8
5	2.470×10^7	1.20×10^8
6	3.165×10^4	8.0×10^7
	$k_{ad} = 63.5$	$E_{ad} = 8.0 \times 10^7$

2.1.3. Model validation

The model was validated using the experimental data reported by Deshmukh et al. for a pilot-scale FT reactor with 276 process channels, tested with a cobalt-based catalyst³. Two-phase boiling water was used as a coolant to maximize the heat removal rate. The process and cooling channels were oriented orthogonally to produce a cross-current flow scheme. Kinetic information for the catalyst are presented in Table 2-1; the data are taken from the literature¹¹. The cell-coupling model was constructed using these data.

The process channel, of width 3 mm and height 1 mm, was assumed to be packed with catalyst for 171 mm along the channel length. The size of the catalyst was 280 μ m and the pressure drop was 0.09 bar, which was calculated from Ergun equation. The widths, heights, and wall thicknesses of the cooling channels were all assumed to be 0.5 mm. A feed gas flow rate of 12 400 h⁻¹ GHSV was used. It was also assumed that the feed gas composition (H₂/CO molar ratio) was 2.0, the inlet pressure was 25 bar, the inlet coolant temperature was 210 °C, and the molar fraction of nitrogen in the feed gas was 16.5%.

Figure 2-3 shows a comparison of plots of the experimental data taken from the literature and the model results. The plots represent the temperature profiles in the process channels, and, as can be seen from the figure, the two contours are similar in both trend and values. The estimated results are in good agreement with the experimental data.

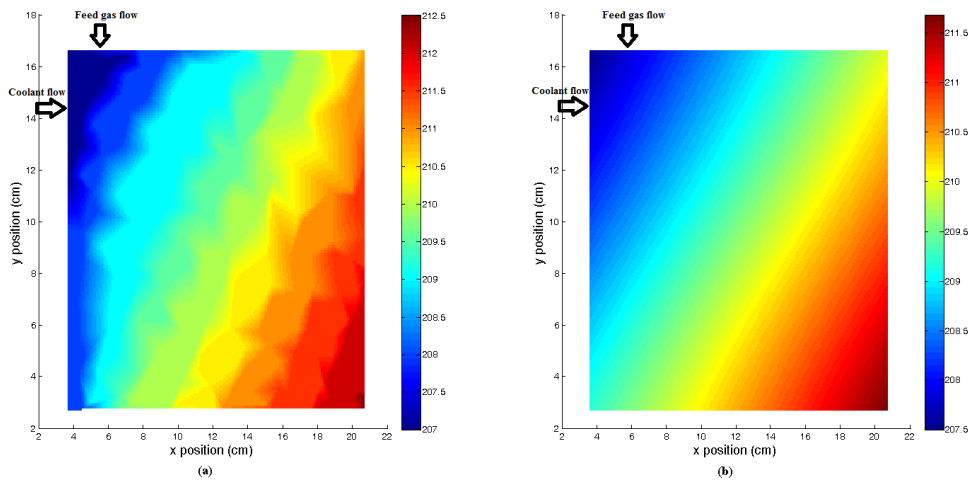


Figure 2-3. Comparison of plots of literature experimental data (Deshmukh et al., 2010) (a) and the model estimations (b).

The robustness of the model was also checked so that it can be applied for the various operating conditions. That is, the model estimation of the CO conversion and methane selectivity were compared with the experimental data taken from the literature¹¹, where the performance of the cross current FT reactor was tested at various reaction temperature (Figure 2-4). In the experiment, the contact time was adjusted to maintain CO conversion of ca. 0.7. Methane selectivity increased as the temperature increased, which is a common phenomenon in the FT reaction systems. The reactor consisted of 274 process channels whose width, height, and length are 0.95 mm, 6.35 mm, and 76.2 mm, respectively. The device was loaded with 66.5 grams of the catalyst with the bulk packing density of 1.054 g/mL. Detailed description of the operating conditions are in Table 2-2.

As can be seen from the figure, the model well predicts both conversion and selectivity for the wide operating range. They are very sensitive to the reaction conditions, so it can be concluded that the model is robust enough to evaluate the performance of the reactor design in terms of safety, operability, and production rate, as well as the temperature distribution over the entire domain.

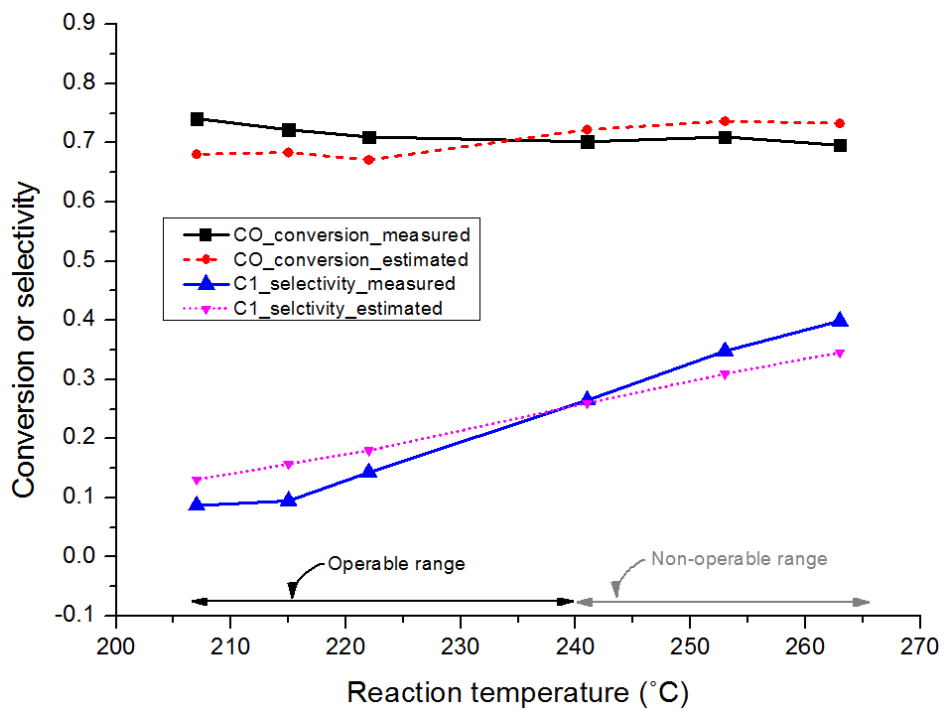


Figure 2-4. Comparison between the model estimation and the experimental data of the conversion and selectivity

Table 2-2. Reaction conditions for the operation of multichannel Fischer Tropsch reactor

Experimental number	Temperature (°C)	GHSV (mL/gcat-hr)
1	207	11,800
2	215	16,200
3	222	22,800
4	241	34,200
5	253	40,200
6	263	48,800

For all the cases, the pressure is 24.13 bar, volume ratio of H₂/CO is 2, volume percent of N₂ in the feed gas is 16.8%, catalyst packing density is 1.054 gcat/cm³.

2.1.4. Case studies

In this section, several case studies for the preliminary design of a FT reactor using the state-of-the-art FT catalyst¹¹ were carried out to clarify the influence of some variables on the design. First, a base-case model was developed, and the results are presented. Sensitivity analyses of the process catalyst loading ratio, coolant flow rate, and channel layout were then conducted to see how the model responded to variations in the design variables.

2.1.4.1. Base-case model

In this base-case study, it is assumed that the highly active cobalt catalyst is used for the low temperature FT reaction in the micro channel reactor. It is therefore a preliminary design study based on the kinetics for the catalyst.

A production rate of 1 barrel per day of FT wax was aimed at in this study. The process channel, of width 1 mm and height 3 mm, was assumed to be packed with the catalyst for 500 mm along the channel length. The widths, heights, and wall thicknesses of the cooling channels were assumed to be 2, 2, and 1 mm, respectively. A feed gas space velocity of 32 000 mL/gcat-hr was used. Assuming 70% CO conversion and 80% wax selectivity, a total of 1704 process channels and 3432 coolant channels with 24 layers was required to achieve the production rate.

The same catalyst in the previous section (model validation part), which follows the kinetics in Table 2-1 was used. Liquid oil was assumed to be used as the coolant, so the coolant phase did not change in the normal operating range. It was also assumed that the H₂/CO molar ratio in the feed was 2.0, and the molar fraction of nitrogen in the feed gas was 16.8 vol%. The reaction pressure and temperature were 24.13 bar and 230 °C respectively. The catalyst loading ratio, defined as the

ratio of the volume of the supported catalyst beads to the sum of the volumes of inert beads and supported catalyst bead, was 70%. The proposed cell-coupling algorithm was implemented in Matlab R2012a to solve the problem.

The simulation results are shown in Figure 2-5, where the temperature profile of the process channel cells are presented. First, for the i-direction, in which the coolant flows, the temperature increases as it takes up the reaction heat. Then the temperatures of the adjacent process channel cells also increase under the influence of the heated coolant cells. For the j-direction in which the reactant flows, however, the temperature decreases as the reaction proceeds: The reaction rate decreases because the syngas concentration decreases as it is consumed by FT synthesis. The decrease in reaction rate reduces the amount of heat generation, which results in the decrease in the process channel cell's temperature for the j-direction. Parabolic temperature profile is found for the h-direction in which the subassemblies of process and cooling channel plates are stacked up: For the vertical direction in the figure, the temperature at the center is higher than those at the two edges because the coolant channel cell at the center is influenced by more process channel cells than the other positions. It therefore absorbs more heat from the process cells, and the heated coolant cell gives that heat to the adjacent process cell resulting in acceleration of reaction heat generation.

A maximum temperature difference (ΔT_{\max}), defined as the difference between the maximum temperature value and the inlet temperature, was 2.55°C for this design. The increase in overall reaction temperature increased the catalyst activity. And as a result, the actual wax production rate of 1.15 barrel per day, which is 15% higher than the target production rate was achieved. The CPU time requirements of this model calculation was 943 s based on the Intel Core i5-2500 3.30GHz.

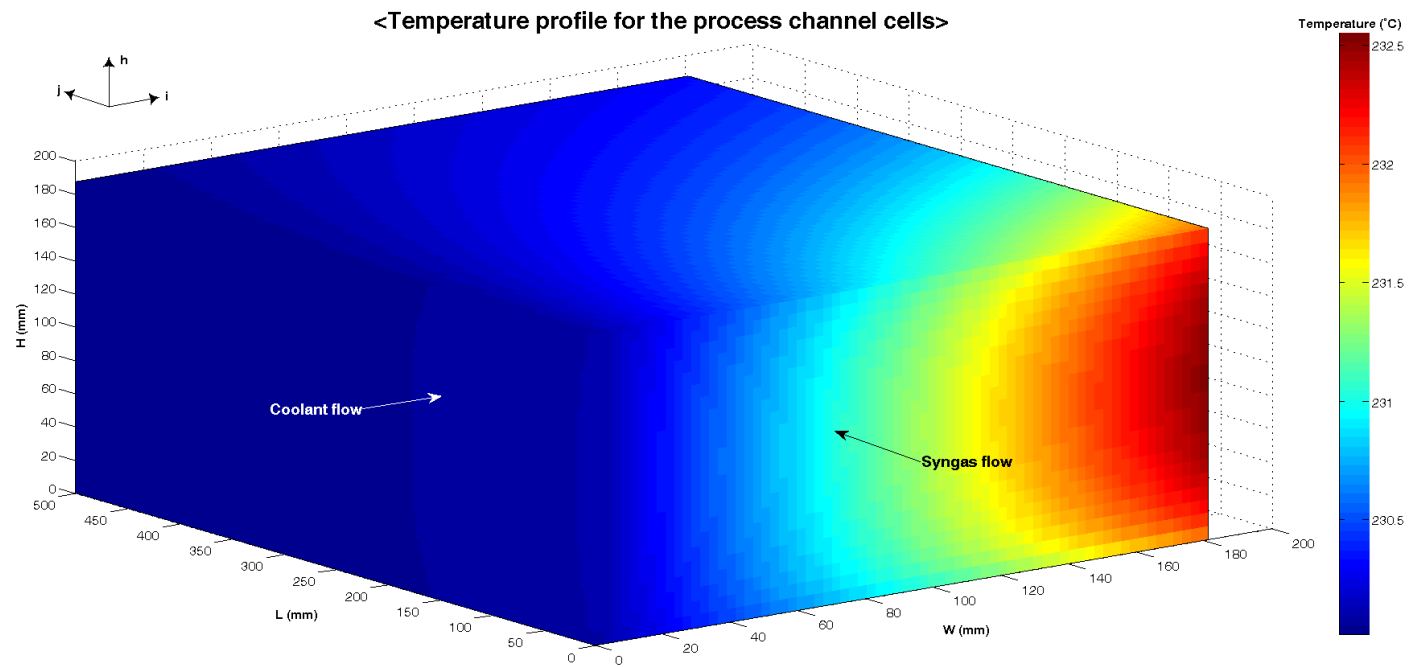


Figure 2-5. Results for base-case model simulation.

2.1.4.2. Sensitivity Analysis.

Sensitivity analyses were performed to determine the effects of three variables: the process catalyst loading ratio, coolant flow rate, and channel layout. Those are the main variables that we can control in the design phase.

First, the effects of model changes were examined by setting the catalyst loading ratio at 0.2, 0.7, or 1.0, with all the remaining operational variables fixed. And for the basis, the same wax production rate of 1 barrel per day was aimed for each case. The catalyst loading amount is controlled so as to control the heat generation, because it directly affects the quantity of the reaction heat per unit volume [kW/m^3]. So the loading ratio should be carefully controlled for a stable and isothermal operation of the reactor.

Figure 2-6 is a graphic representation of the results of the analysis. As can be seen from the figure, the amount of heat generation increases as the catalyst loading increases. So, the case with the low catalyst loading ratio is better design than the case with higher catalyst loading ratio in terms of the heat removal: More stable and safe operation is possible with low catalyst loading. When the loading ratio is 1, however, a large amount of heat is generated from the inlet of the process channels where the concentration of the syngas is the highest. Heat generation there should be carefully controlled to prevent undesired situation such as thermal runaway of the reactor, thermal degradation of the catalyst, or acceleration of the side reaction such as methane formation.

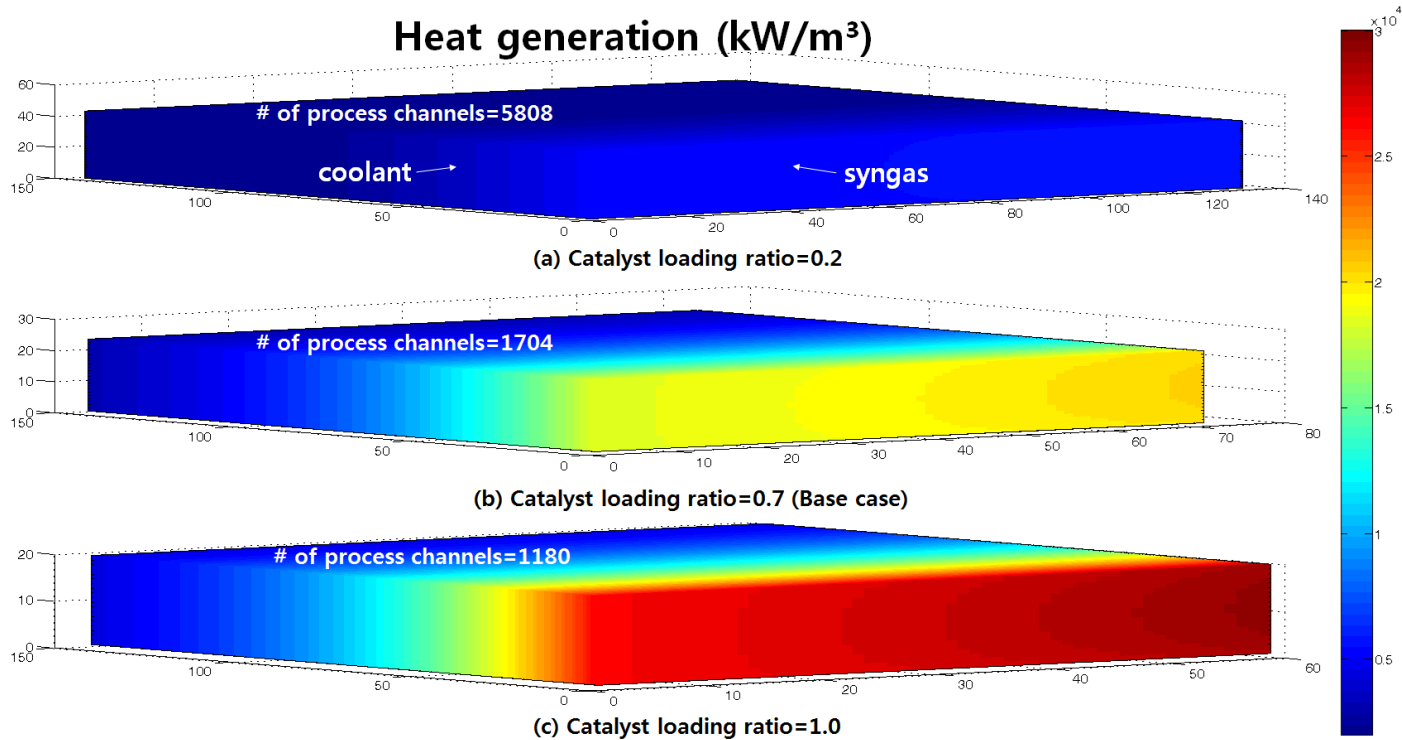


Figure 2-6. Heat generation profiles for different catalyst loading ratio: 0.2(a), 0.7(b), and 1.0(c).

Figure 2-7 is a comparison of the plot of heat generation and heat removal rate at the various operating conditions. First, the reaction heat increases exponentially with the temperature increase because of the activation energy term in reaction constants. The curve should be below the heat removal line for the feasible operation. As the catalyst loading ratio increases, the heat generation curve is moved in vertical direction, and at some point it is located at the upper side of the heat removal line. In that case, heat cannot be perfectly removed, resulting in thermal runaway of the reactor.

For the productivity, however, it is less effective to use low amount of catalyst. As presented in the Figure 2-6, more number of process channels are required to achieve the same amount wax production rate of 1 barrel per day. The productivity per unit volume was reduced as the catalyst loading amount decreased. So, there is a trade-off relationship between safety (heat generation) and economic efficiency (number of channels). (Note that if the reactor is operated at lower catalyst amount and thus smaller hot spot, one can operate the reactor at higher temperature to achieve higher productivity, as discussed by Guettel et al²⁰. But in this study, the operating temperature was fixed at 230°C for the comparison.)

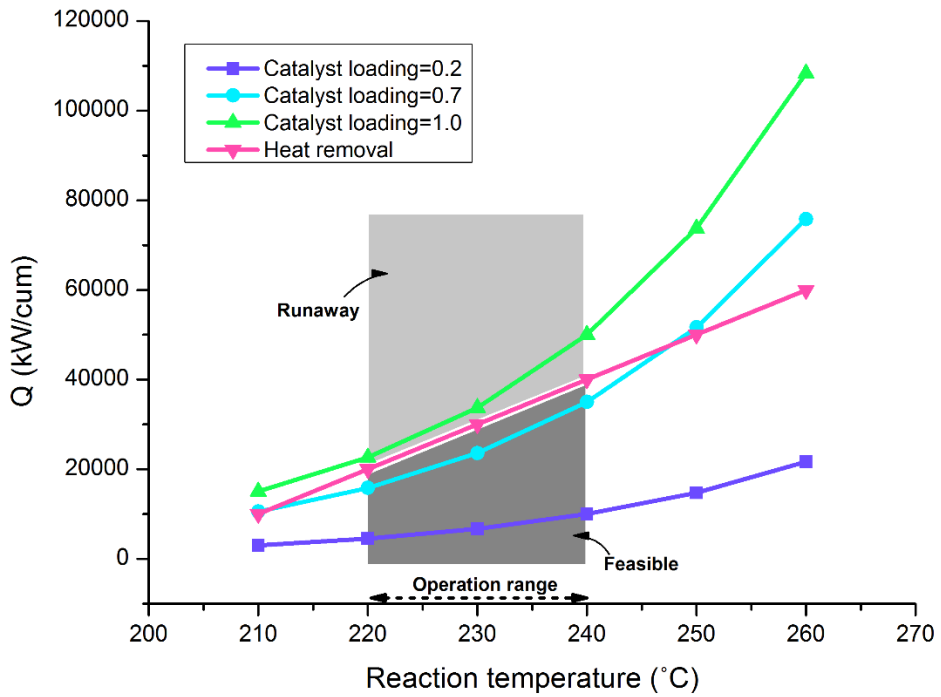


Figure 2-7. Heat generation and heat removal rate at various reaction temperature and catalyst loading ratio.

One way to achieve the high productivity, as well as satisfying the safety problem is to utilize different catalyst loading with zone division. When the high amount of heat generation is expected in the channel inlet, more diluted catalyst is loaded in the zone, after which the higher amount of catalyst is loaded to achieve high productivity. In other words, in the first part of the reaction zone filled with low amount of catalyst, the reaction proceeds to some extent with low heat generation. And in the next zone with high catalyst loading, high productivity can be accomplished without severe heat generation because some amount of reactants has been consumed in the earlier zone: The reaction can start with low concentration. Figure 2-8 illustrates this idea. For the first 50% of the process channel length, the catalyst was filled with the loading ratio of 0.2, and for the next 50%, loading ratio of 0.7. The number of process channels was reduced to 2555 (zone division) from 5808 (lumped loading ratio of 0.2), which means higher productivity is achieved. The maximum heat generation was also reduced to $1.39 \times 10^4 \text{ kJ/m}^3$ (zone division) from $2.05 \times 10^4 \text{ kJ/m}^3$ (lumped loading ratio of 0.7), which means more safe operation could be accomplished.

Next, an analysis of the coolant flow rate was performed. The model was run several times with various coolant flow rates to observe the changes in the results. Figure 2-9 shows the response of the maximum temperature in the process channels to the coolant flow rate for different catalyst loading ratio. First, if the coolant flow rate is increased, the maximum process temperature decreases due to the enhancement of the cooling capacity. The temperature decreases dramatically at the low flow rate region where the temperature difference between the process and the cooling channel is large, whereas it slowly decreases to converge to the inlet temperature of 230°C as the coolant flow rate is increased. The extent of change in

the slope becomes steeper for the high catalyst loading ratio, because the amount of heat generation increases as the catalyst loading amount is increased. The catalyst loading also affects to the minimum requirement of the coolant flow rate: For example, as in the Figure 2-9, if ΔT_{\max} is set to 5°C, then the minimum coolant flow rate requirement is 137 L/min and 439 L/min for the catalyst loading ratio of 0.2 and 0.7, respectively. The higher the catalyst loading, the more the coolant is required. So, for the feasible reactor design, the utility requirement should be checked to prevent thermal runaway. The developed model could decide the feasible range taking into account the interaction among all the process and cooling channel cells.

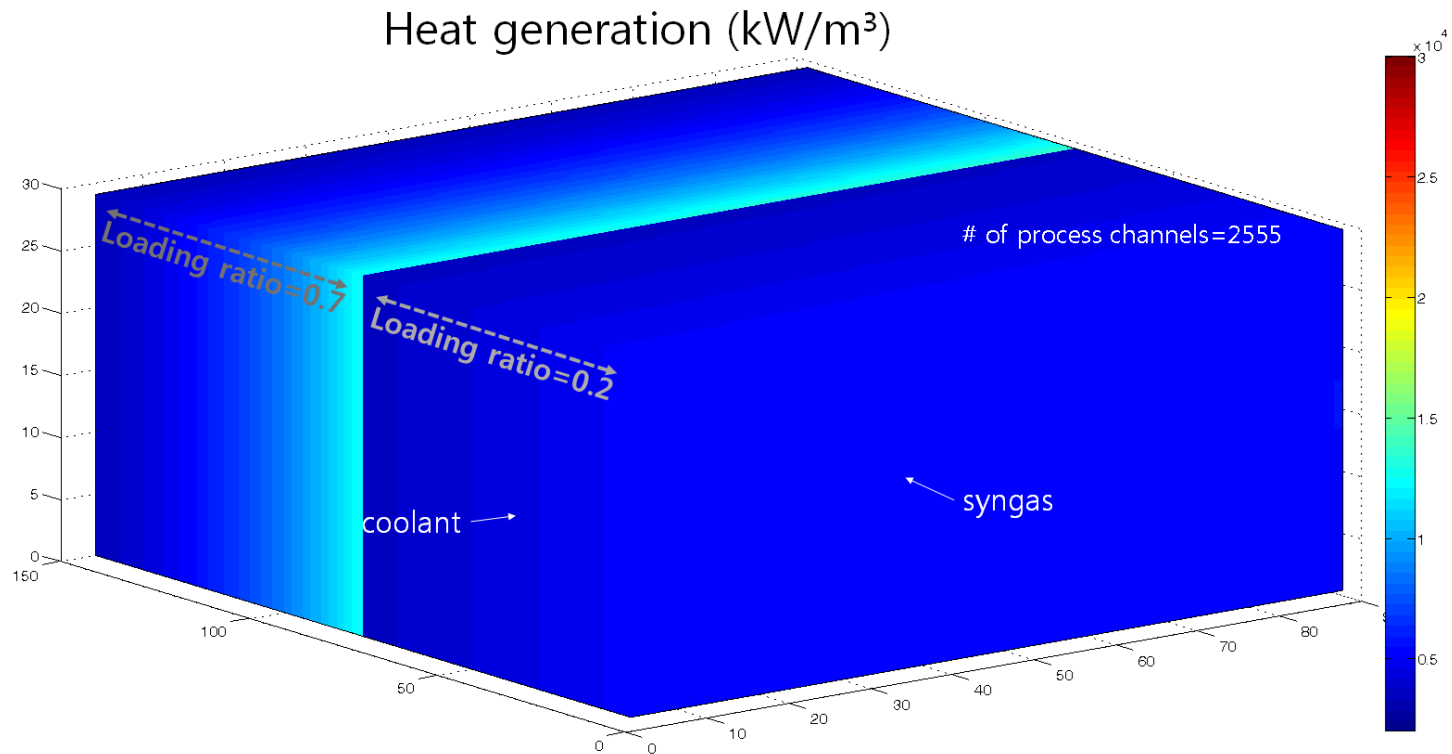


Figure 2-8. Heat generation profile for the different catalyst loading at divided zones: Catalyst loading ratio of 0.2 and 0.7 for the 50% length of the channel, respectively. Same scale of color bar as in the Figure 2-5 was used.

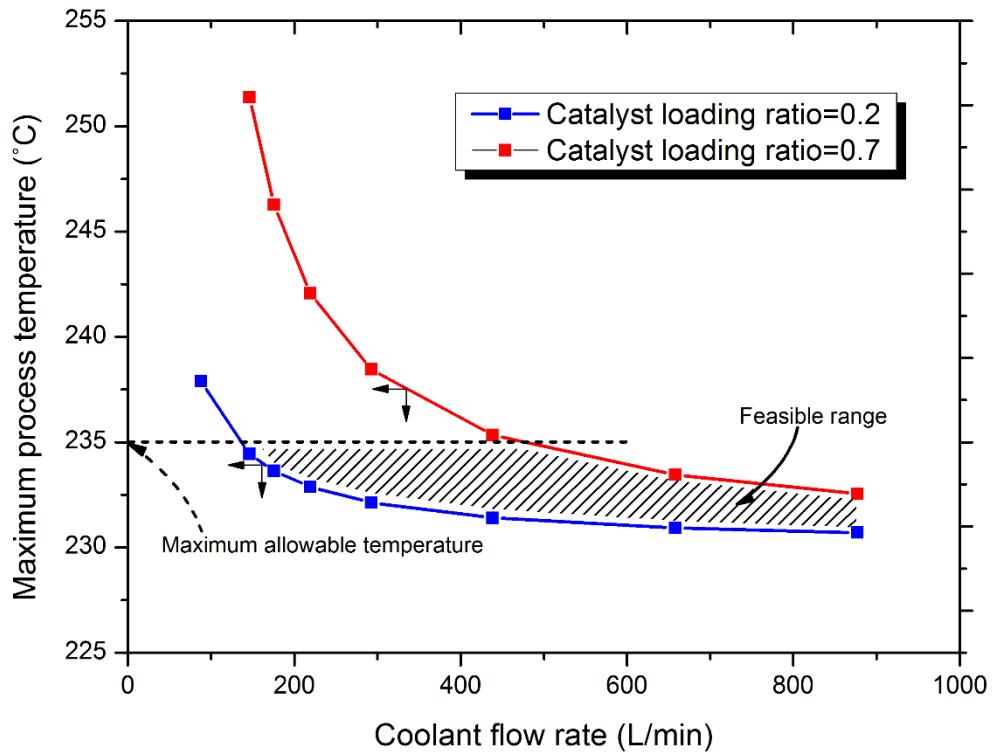


Figure 2-9. Sensitivities of maximum temperature of process channels to coolant flow rate for different catalyst loading ratio.

Finally, a sensitivity analysis was performed on the channel geometry. The characteristic length for heat removal, which is defined by the channel volume divided by the surface area responsible for heat removal, was changed from 0.75 mm to 1.97 mm by varying the width and height. Figure 2-10 shows the result of the analysis. First, as the channel size increases, ΔT_{\max} increases because of the reaction heat. The amount of heat generation increased due to the increase in the unit cell size. The figure illustrates that there is a limit on the characteristic length of 1.20 mm, above which ΔT_{\max} becomes larger than the predefined upper limit of 5°C. So, for the safe operation, it is better to use the channel with small size.

The coolant flow rate affects to the feasibility of the design. For example, the case with the characteristic length of 1.36 mm in Figure 2-10 does not satisfy ΔT_{\max} specification when the normal coolant flow rate (m_{c0}) is used. However, when the coolant flow rate is increased by 20%, it meets the specification. The design, or the operation becomes more dangerous when the flow rate is decreased.

Although ΔT_{\max} decreases when the small channel size is used, the volume of the reactor core becomes large because more number of channels are required to meet the production specification. Also, the core volume increases due to the increase in the free space, where the construction material such as process wall seam should be filled to divide the process channels. As can be seen from the figure, there is a limit on the channel size, below which the reactor volume becomes too large for the fabrication. So, the trade-off relationship between safety (ΔT_{\max}) and economic efficiency (reactor volume) should be considered when deciding the feasible and optimal channel geometry. The cell coupling model could easily determine the feasibility of the design by accounting for the interaction among the variables involved in the reactor design.

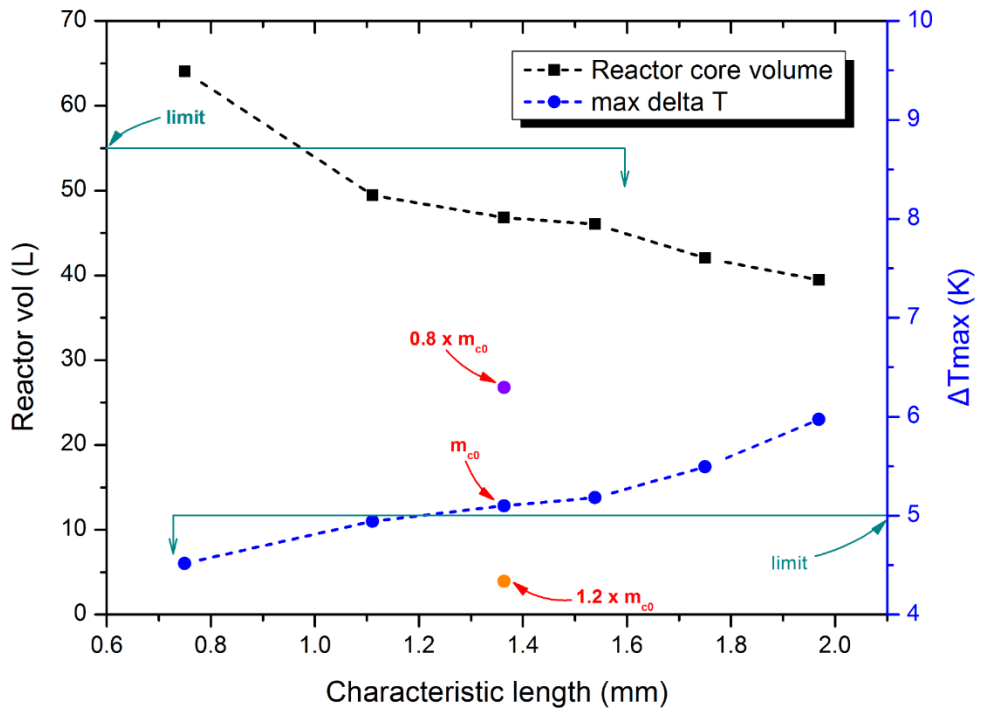


Figure 2-10. Sensitivities of maximum temperature difference and reactor volume to the process channel size

2.1.5. Conclusion

In this study, a new modeling method was developed for the design of a multichannel cross-current heat-exchange micro FT reactor. The model was constructed using the channel decomposition and cell-coupling approach, and was validated with literature data. A case study for design of a FT reactor with the state-of-the-art catalyst was also conducted, followed by sensitivity analyses of the main design variables.

Several external empirical models were incorporated into the integrated model. As a result, the design problem was significantly simplified, without losing physical validity, and the model was able to handle more channels, larger reactor volumes, and more complex reactions compared with existing models¹² (Table 2-3).

The model can be extensively used for preliminary FT reactor design, in which sensitivity analyses of many design variables, and a study of the correlation and causal relationships among variables should be carried out. It can be applied not only to FT reaction systems, but also to other endo- or exo-thermic reaction systems. The model can also be modified to handle more complex flow schemes, and co-current or counter-current architectures with cell rearrangement.

Table 2-3. Comparison of Sizes of Existing Computational Fluid Dynamic (CFD)^a and Cell-Coupling Models

	Existing CFD model ^a	Cell-coupling model
Number of process channels	40	5800 ^b
Number of cooling channels	40	7500 ^c
Number of layers	4	130 ^b
Reactor volume (mm³)	7.5×10^3	6.4×10^{7c}
Number of reactions involved	0	6 ^{b, c}

^aThe compared CFD model is based on the model reported in the reference (Arzamendi et al., 2010).

^bThe numbers correspond to the values used in section 3 of this article.

^cThe numbers correspond to the values used in section 4 of this article.

2.2. Improved reactor model[†]

2.2.1. Introduction

In recent years, gas-to-liquid (GTL) process has attracted considerable attention because it can produce a high quality, clean synthetic liquid product from abundant natural gas (NG) resources^{1, 22-24}. The process consists of two main sub processes. First, the NG is converted into the syngas, mainly composed of carbon monoxide (CO) and hydrogen by a reforming process. The syngas then flows into the Fischer-Tropsch (FT) process, where it is chemically synthesized into a liquid product, also known as a FT synfuel. FT synfuel has high research octane (RON) and cetane number (CN) and almost nitrogen and sulfur free. So it is taking a premium position in the fuel market²⁴⁻²⁶.

FT synthesis is known as an strongly exothermic reaction: A large amount of heat, ca. 165kJ per mol of converted CO is generated during the reaction²⁷⁻³⁰. This heat must be removed to prevent runaway situation and achieve safe isothermal operation of the reactor. Various types of reactors, such as fixed bed, slurry bubble column, circulating fluidized bed, and fixed fluidized bed FT reactors, have been developed and applied to the GTL industries^{31, 32}. Recently, the concept of micro channel FT reactor has evolved because it can effectively handle large amount of heat based on the high heat exchange surface area per unit volume. Cao et al. studied micro-channel reactor for screening several FT catalyst³³. The heat removal rate in the micro-channel reactor was around 15 times higher than that in a conventional fixed bed reactor. Moreover, a scale-up of micro-channel FT reactor was successfully performed by Deshmukh et al²⁷. It was shown that the

[†] The partial part of this chapter is taken from the author's publications.

performance of the pilot scale reactor was consistent with that of a single micro-channel reactor due to the achievement in isothermal operation.

Several design studies for the multi micro-channel reactor have been reported in literatures^{12, 13, 18, 34, 35}. Arzamendi et al. evaluated the effectiveness of the heat removal of micro-channel FT reactor by using computational fluid dynamics (CFD) tools¹². They clarified an important role of the buoyancy effects on the thermal performance of the reactor having cross-current channel structure. Uriz et al. also conducted CFD simulations for designing micro-channel ethanol steam reformer¹⁸. They changed the size of the square channels from 0.1 mm to 0.7 mm and it was shown that the reactor with high surface area-to-volume ratio could remove the heat more effectively. But only four channels were considered due to the complicated kinetic systems implemented onto the CFD environment.

Structural variables such as flow configuration, channel geometry inside the reactor, and the flow distribution play an important role in the reactor performances. For example, Deshmukh and Vlachos analyzed the effect of co-current and counter-current flow configurations on the operation of micro devices for hydrogen production using 2-D CFD model³⁶. The co-current configuration showed the better performance when using medium and low thermal conductivity materials, while the counter-current configuration showed a slightly superior performance in a rather narrow operating region of high space velocity and high thermal conductivity materials. Agrawal et al. investigated the effect of mal-distribution on the reaction and thermal performance of the multi-channel reactor composed of 85 channels³⁷. They simulated 2-D CFD model which accounts for the momentum, material, and energy balance equations simultaneously. Flow mal-distribution affected the reactor performances significantly, especially at high space velocity.

To the best of our knowledge, however, few attempts have been made to model a large scale reactor consisting of more than 1,000 channels. In most cases, the results obtained from simple- or small-scale model and the bench-scale experiment are extrapolated to design the pilot- or industrial-scale reactors due to the practical reason. When developing a large scale multi-channel reactor, many decision variables such as flow configuration, channel geometry, channel layout, flow distribution strategy, catalyst loading, and cooling capacity are involved. In that case, even CFD cannot be utilized for the analysis due to the heavy computational load. A new modeling approach is needed to clarify the interaction among each variable in the entire reactor domain. Especially, some structural variables related to the reactor's cooling capacity are of utmost importance because they directly affect the heat removal rate and safety. Therefore, the effects should be precisely analyzed for design of the large scale, highly exothermic FT reactor.

In the previous work³⁸, we reported the design methods and strategies for the large-scale multichannel FT reactor. A cell-coupling modeling approach was proposed to handle the design problem, where a number of process and coolant channels were oriented orthogonally to produce a cross-current flow scheme. Several case studies were carried out to clarify the effect of some variables such as the process catalyst loading ratio, coolant flow rate, and the size of the process channel. The analysis was performed only based on the cross current configuration, in order to precisely determine the influence of the variables on the *pre-defined* flow scheme.

In this study, we develop the cell-coupling model to handle various flow configurations, so that the design can be conducted at the higher (more conceptual) level. In other words, the improved model is extended to wider searching area:

Several, not only one, flow configurations are considered. This extension helps to determine the optimal flow configuration out of the whole design candidates, which cannot be achieved by using the previous model. We design and evaluate the micro channel FT reactor having more than 5,000 channels based on five representative flow configurations: Cross-counter-cross current with the same side (Fig. 2-11(a)), cross-co-cross current with the same side (Fig. 2-11(b)), cross-counter-cross with the different side (Fig. 2-11(c)), cross-co-cross with the different side (Fig. 2-11(d)), and fully cross current (Fig. 2-11(e)). The modelling approach was slightly modified to apply the cell-coupling model to the various configurations, which will be explained in the following section. The improved model was used to construct the entire 3D domain and set up the material and energy balance equations for the five flow schemes. Moreover, the results from flow simulation using CFD were incorporated into the model to examine the effect of the flow distribution on the temperature profile inside the reactor. Essentially, the optimal design scheme, distribution methods, and catalyst loading strategies for the micro channel FT reactor are derived from the various case studies.

2.2.2. Model construction

As shown in Fig. 2-11, a model for the five reactor design was constructed. For all the cases in the figure, syngas flows vertically down through the 1,110 process channels whose dimensions are 10 mm (width), 5 mm (height), and 510 mm (length). The main difference for each case is the coolant flow configuration, which is illustrated by red arrows in the figure. For example, in the first structure (Fig. 2-11(a), Structure S1), the coolant flows into a header distributor at the bottom of the reactor, counter current flow up the reactor body, through a footer plenum at the top

of the reactor, with entrance and exit flows on the same side of the reactor. We call this first case cross-counter-cross with the same side. Naming of other cases is similar: Cross-co-cross with the same side (Fig. 2-11(b), Structure S2), cross-counter-cross with the different side (Fig. 2-11(c), Structure S3), cross-co-cross with the different side (Fig. 2-11(d), Structure S4), and fully cross current (Fig. 2-11(e), Structure S5).

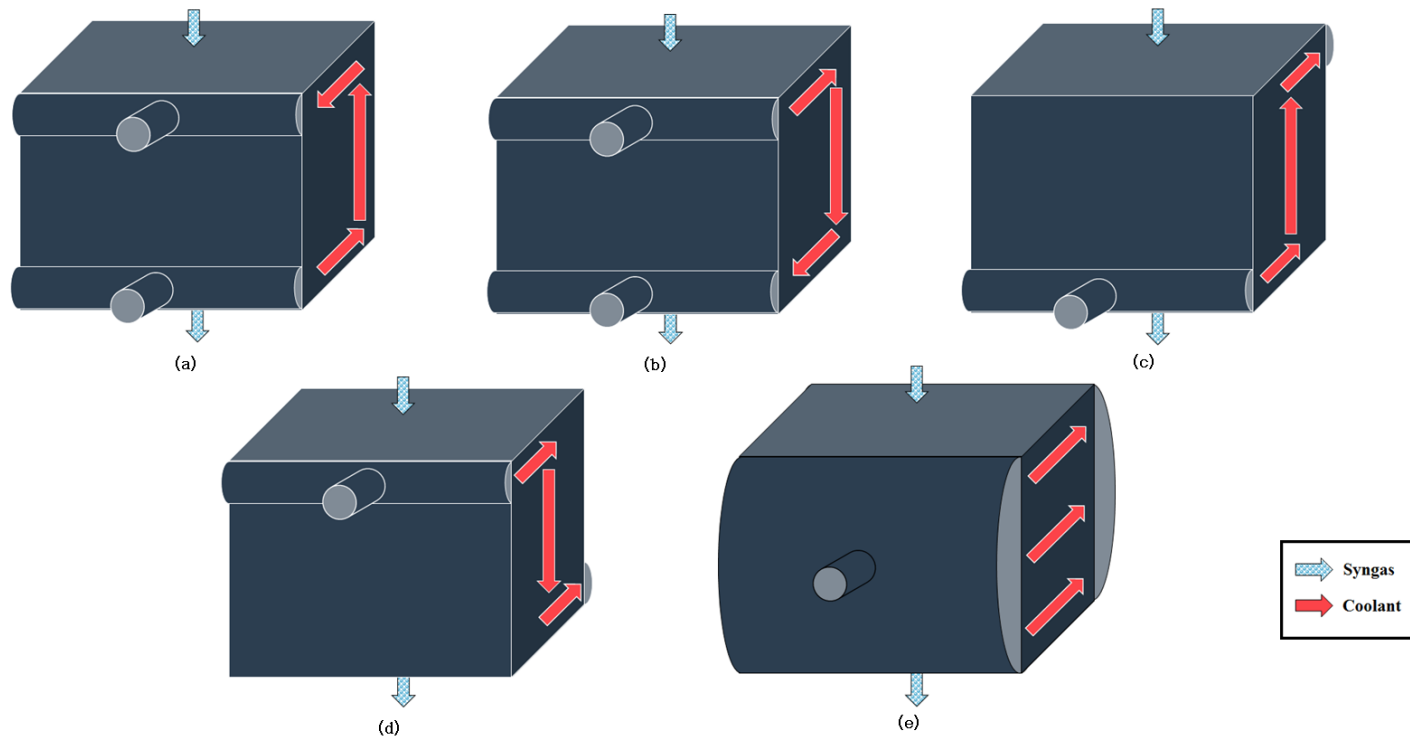
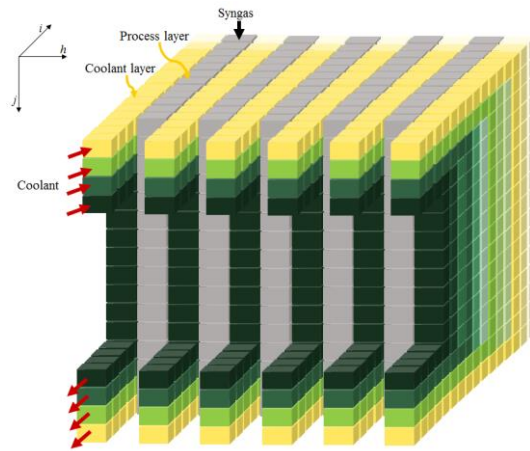


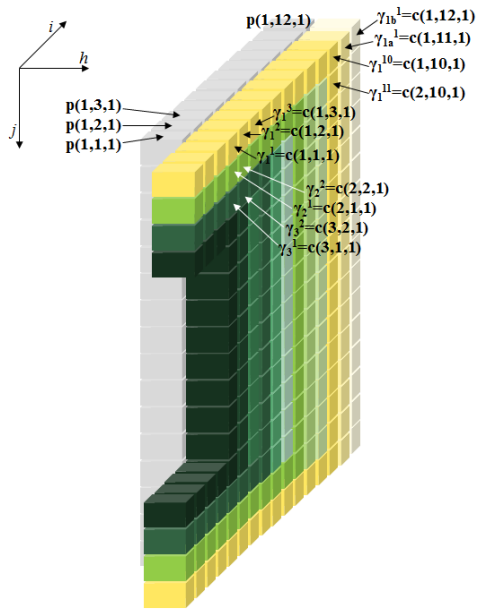
Figure 2-11. Flow configuration of multi-channel reactor: (a) Structure S1. Cross-counter-cross current with the same side; (b) Structure S2. Cross-co-cross current with the same side; (c) Structure S3. Cross-counter-cross with the different side; (d) Structure S4. Cross-co-cross current with the different side; (e) Structure S5. Fully cross-current

When the overall reactor geometry is determined, then the computation domain is defined by the cell coupling method. Figure 2-12(a) shows how the channels are decomposed and the cells are configured for the structure S2. All the process and cooling channels in the reactor core are decomposed into the i , j , and h -directions. Every cell is then matched to all the neighboring cells that interact each other. The communication between each cell is mathematically described by the heat and mass balance equations.

The next step is to define the flow configurations: A route for the coolant flow is constructed in the entire cell arrangement. This is the main part that distinguishes the present model from the previous one. As can be seen from Fig. 2-12(b), each flow path γ is denoted by different colors. We define the path segment γ_s^t as the t -th segment of flow path s . It is a $\mathbb{R}^2 \rightarrow \mathbb{R}^3$ mapping function that relates the route information to the 3 dimensional coolant cell space $c(j, i, h)$. For example, in Fig 2-12(b), γ_1 is the first coolant flow path starting from the top inlet channel to the bottom outlet channel (yellow color). The first segment of the path, γ_1^1 then becomes $c(1, 1, 1)$ in the 3-D cell coordinate. The second segment γ_1^2 is $c(1, 2, 1)$ as the coolant flows cross currently against the syngas flow (to the i -direction). All other cells are assigned to each path's segment in the same way.



(a)



(b)

Figure 2-12. Conceptual diagram of a cell coupling model: (a) Cell domain construction for the entire reactor of cross-co-cross current with the same side scheme; (b) Flow path construction

Figure 2-13 shows the overall procedure for the model computation. As explained above, it starts with defining channel geometry and cell coupling, followed by the flow configuration. The next step is to implement flow distribution data obtained from CFD calculation on the entire cell domain. In the CFD environment, two continuity equations are solved to obtain local velocity profiles for the coolant flow:

$$\nabla \cdot (\rho \mathbf{u}) = 0 \quad (2 - 5)$$

$$\rho(\mathbf{u} \cdot \nabla)\mathbf{u} = \nabla \cdot [-p\mathbf{I} + \boldsymbol{\tau}] + \mathbf{F} \quad (2 - 6)$$

Equation (2-5) and (2-6) describe mass and momentum conservation in the reactor's local boundary, where ρ is fluid density [kg/m^3], \mathbf{u} is velocity vector [m/s], p is pressure [bar], \mathbf{I} is identity matrix, $\boldsymbol{\tau}$ is viscous stress tensor [bar], and \mathbf{F} is volume force [N/m^3]. It is assumed that there's no reaction and no phase change in the coolant channel. Because of the computational load, the CFD cannot be applied to the whole reactor domain. (More than 5,000 channels are involved.) So it is simulated over the decomposed regions. In other words, the reactor was divided into two parts: 1) the header and/or the footer plenum, and 2) the channel plate inside the reactor (Figure 2-14). Each part is related to the flow distribution for the h - and i -direction. As shown in the figure, the velocity profile is obtained by solving equation (2-5) and (2-6). Then, the data is regressed with non-linear functions. By using the result of the CFD simulation, the coolant flow rates for each cell could be obtained: They were calculated by multiplying the total coolant flowrate and the flow fractions of the two parts. The results –the coolant flowrate on each cell position- are then incorporated into the entire cell domain.

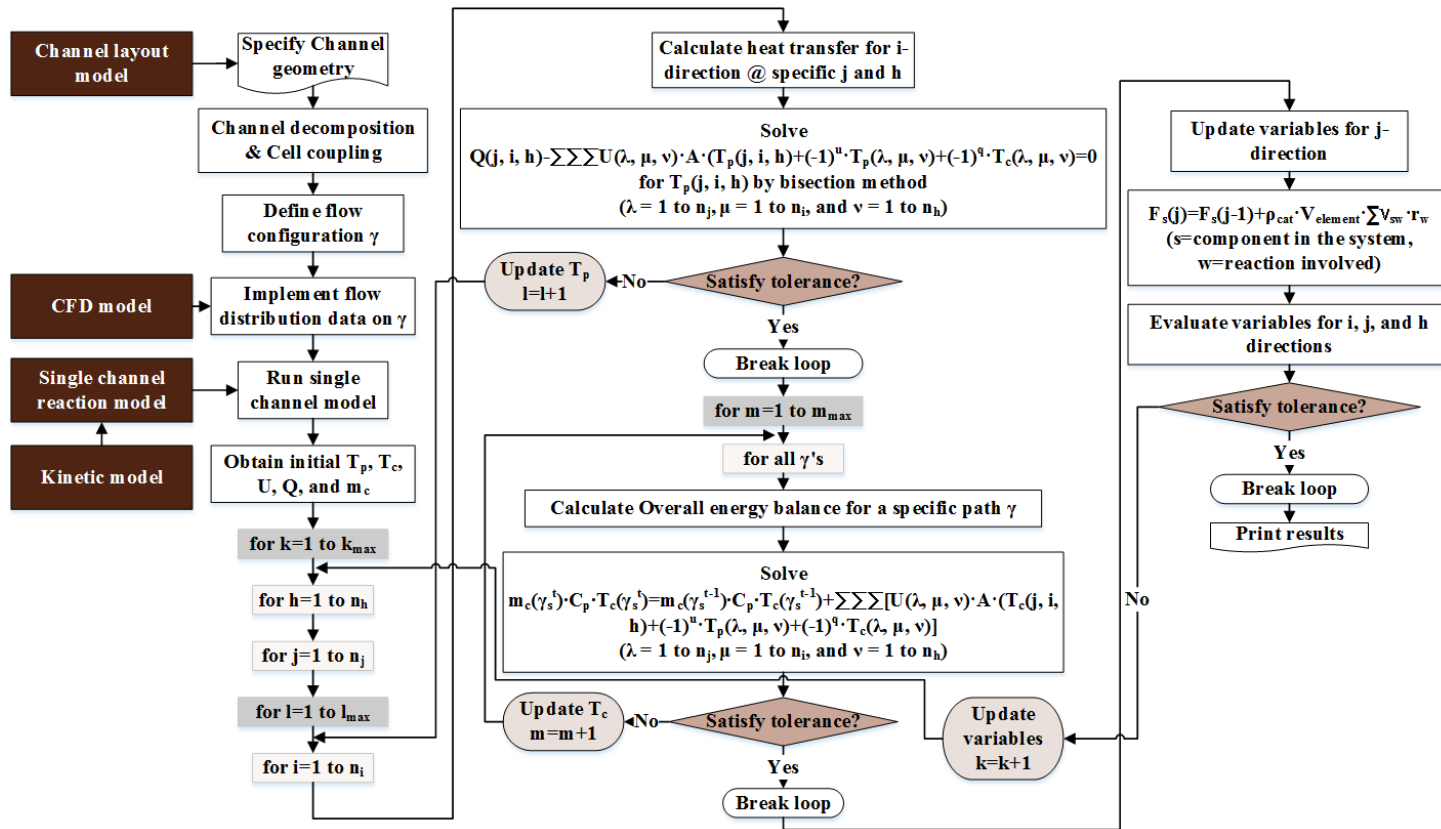


Figure 2-13. Overall procedure for the computation of the integrated model

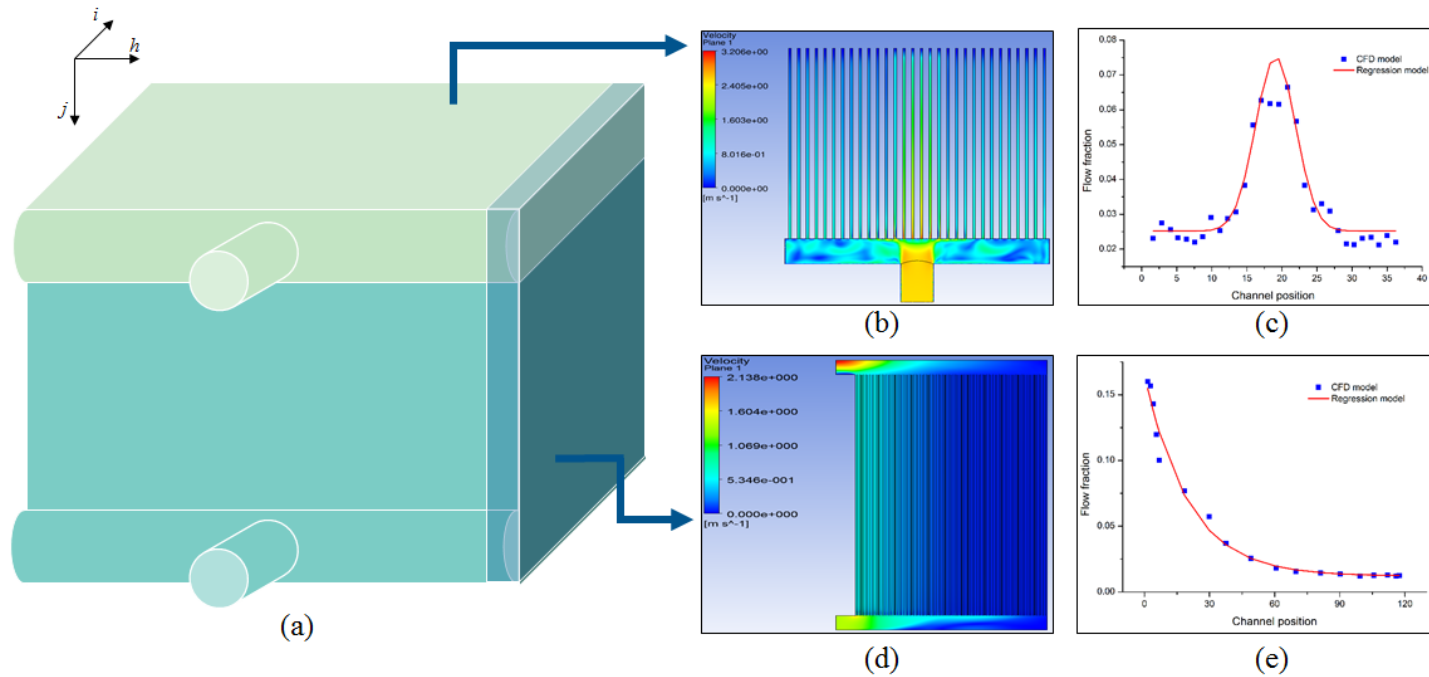


Figure 2-14. Flow distribution effect for the inlet/outlet of the channel and the channel plate inside the reactor: (a) Conceptual diagram representing the domain decomposition of the reactor geometry, ((b) and (d)) velocity profiles obtained from CFD simulation for the decomposed plates, and ((c) and (e)) the result of the data fitting with non-linear

function.

The remaining parts of the procedure are devoted to computing mass and energy balances, and heat transfer phenomena. First, the single channel reaction model is run for the whole process channel cells. Empirical kinetic parameters obtained from kinetic experiment, which will be described in section 2.2.3.1., are implemented on the model to describe the catalyst's performances. The results of the temperature, pressure, and heat generation profile along the single channel will be the initial values for the next calculation. The heat transfer equation between cells (Equation 2-7) and the overall energy balance equation (Equation 2-8) for the flow paths are then solved:

$$Q(j, i, h) - \sum_{\lambda} \sum_{\mu} \sum_{\nu} [U(\lambda, \mu, \nu) \cdot A \cdot \{T_p(j, i, h) + (-1)^u \cdot T_p(\lambda, \mu, \nu) + (-1)^q \cdot T_c(\lambda, \mu, \nu)\}] = 0 \quad (2-7)$$

$$\begin{aligned} m_c(\gamma_s^t) \cdot C_p \cdot T_c(\gamma_s^t) \\ = m_c(\gamma_s^{t-1}) \cdot C_p \cdot T_c(\gamma_s^{t-1}) \\ + \sum_{\lambda} \sum_{\mu} \sum_{\nu} [U(\lambda, \mu, \nu) \cdot A \cdot \{T_c(j, i, h) + (-1)^u \cdot T_p(\lambda, \mu, \nu) \\ + (-1)^q \cdot T_c(\lambda, \mu, \nu)\}] \quad (2-8) \end{aligned}$$

where Q is heat generation [kW], U is the overall heat transfer coefficient [kW/(m² K)], A is characteristic area for the heat transfer [m²], T_p is the temperature in the process channel cell [°C], T_c is the temperature in the coolant channel cell [°C], m_c is the coolant flow rate [kg/s], and C_p is the heat capacity of the coolant [kJ/(kg K)]. The u and q in the exponent of (-1) is used to describe the direction of the heat flow. For example, if the temperature of a certain cell ($T_p(j, i, h)$) is higher than that of the adjacent cell ($T_p(\lambda, \mu, \nu)$ where $\lambda \neq j, \mu \neq i, \nu \neq h$), then the exponent is 1 because heat flows from $p(j, i, h)$ to $p(\lambda, \mu, \nu)$. The j -th vector

component of T_p and T_c at a particular i and h is obtained by solving eq (2-7) and eq (2-8), respectively. The model performs iterative calculations to update the variables until the errors are satisfactory within the tolerance.

It subsequently computes the molar flow rate of each chemical species along the j -direction:

$$F_s(j, i, h) = F_s(j - 1, i, h) + \rho_{cat} \cdot V_{element} \cdot \sum_w \nu_{sw} \cdot r_w \quad (2 - 9)$$

where F_s is the molar flow rate of component s [mol/s], ρ_{cat} is bulk catalyst packing density [g/m³], $V_{element}$ is the volume of unit cell [m³], ν_{sw} is the stoichiometric coefficient of component s in reaction w , and r_w is the reaction rate [mol/(g s)]. The above equation accounts for the generation or consumption of each component. The model conducts the same calculations iteratively until the relative error between the previous and present values are within the pre-specified tolerance value (10^{-6}). The computation terminates when the final versions of each variable matrices are obtained.

2.2.3. Model validation

2.2.3.1. Kinetic model

In order to obtain kinetic model, several experiments were conducted by using conventional FT synthesis experimental equipments consisting of feed gas vessels, a feed gas preheater, single channel reactor, two product receiving tanks, back pressure regulator, and gas chromatography device. The flow rate of the feed gas (nitrogen, hydrogen, and carbon monoxide) is controlled by mass flow controllers. It is heated by the preheater before flowing down through the reactor. The reactor is a single channel reactor with the diameter of 7.75 mm and the channel length of

140 mm. It is surrounded by the electric heater, which is used for maintaining the operation temperature. A 12 wt% cobalt catalyst supported on $\gamma\text{Al}_2\text{O}_3$ was prepared by impregnation method, where a particular organic-based acid solution was used to improve the dispersion of cobalt on the support. The catalysts were calcined at 350°C and then loaded into the reactor, together with the inert quartz powder. Their volumetric mixing ratio was catalyst:inert bead=1:4. Prior to the reaction, the catalyst (0.3 g) was reduced *in situ* by flowing hydrogen gas at 350°C for 24 hours. The hot trap and the cold trap were used to collect the wax product and light oil, respectively. Back pressure regulator was used to maintain the operating pressure. The effluent gas was analyzed by gas chromatography (YoungLin YL6100GC) equipped with the 45/60 molecular sieve 13X, 80/100 PORAPAK N 10 ft \times 1/8 in, thermal conductivity detector (TCD) and flame ionization detector (FID) to quantify the unreacted CO, N₂, and light gas products including CH₄, CO₂, ethylene, ethane, propane, and propylene. The selectivity of the light hydrocarbons such as methane, ethane, propane, and butane, is particularly important in case of the Fischer-Tropsch synthesis because an unsuitable reaction temperature can lead to an excessive production of undesired light hydrocarbons. Their molar distribution in the effluent gas was obtained by gas chromatography. It was assumed that the product distribution in the wax (C₅⁺) follows the well-known Anderson-Schulz-Flowry (ASF) distribution, characterized by the probability of chain growth (α).

To obtain a robust kinetic model, the reaction rates were determined over a range of conditions and these are specified in Table 2-4. For all the cases, the pressure was set to 20 bar, and the molar ratio of H₂ to CO in the feed gas was set to 2. The reactor was tested by changing the temperature from 220 °C to 240 °C. The

concentration of the reactants was changed by using different N₂ dilution in the feed gas, and the gas hourly space velocity (GHSV) was varied by changing the feed gas flowrate.

For the regression, the commonly-used kinetic model for the low temperature Fischer Tropsch (LTFT) synthesis on cobalt catalyst presented by Yates and Satterfield (1991) was considered in this study³⁹. The model is derived from Langmuir-Hinshelwood-type equation, and it was modified to allow for variation in the exponents of the partial pressure of CO and H₂:

$$-r_{CO} = \frac{k_0 \exp\left(-\frac{E_a}{RT}\right) p_{CO}^a p_{H_2}^b}{(1 + c \cdot p_{CO})^2} \quad (2 - 10)$$

where k_0 is the frequency factor and E_a is the activation energy [J/(mol K)]. The `fmincon` subroutine in Matlab R2014b was used to minimize the sum of square error (SSE) between the CO conversion data and the model estimation.

$$SSE = \sum \left(\frac{X_{CO,measured} - X_{CO,estimated}}{X_{CO,measured}} \right)^2 \quad (2 - 11)$$

where $X_{CO,estimated}$ is obtained from 1-D pseudo-homogeneous single channel model. In the `fmincon` subroutine, five kinetic parameters, i.e., k_0 , E_a , a , b , and c in eq(2-10), are the decision variables, while the sum of square error (eq (2-11)) is the objective function.

Table 2-4. Operating conditions^a for the kinetic experiment

ID	Temperature (°C)	N₂ dilution^b (vol%)	GHSV (mL/(gcat hr))	CO conversion (%)
1	200	4.00	4,000	16.40
2	220	4.00	4,000	42.00
3	240	4.00	4,000	86.20
4	230	3.96	10,000	30.87
5	230	3.96	15,000	17.90
6	230	3.96	20,000	11.59
7	230	3.96	25,000	7.78
8	230	3.96	30,000	7.37
9	230	3.96	35,000	5.19
10	240	3.96	30,000	13.39
11	220	71.14	23,000	21.32
12	230	71.14	23,000	33.65
13	240	71.14	23,000	48.46
14	220	37.70	23,000	10.88
15	230	37.70	23,000	20.39
16	240	37.70	23,000	31.88
17	220	3.96	23,000	7.76
18	230	3.96	23,000	11.90
19	240	3.96	23,000	16.42

^aFor all the cases, total pressure is 20 bar, and H₂/CO=2 in the feed gas.

^bVolume fraction of the nitrogen in the feed gas.

Figure 2-15 illustrates the result of the regression. It shows the comparison of the experimental data with the model prediction. As presented in the figure, the modified version of Yates and Saterfield model well fits to the experimental data. The result of kinetic parameters is presented in Table 2-5. It is noted that the value of the estimated activation energy and the exponents of the partial pressure of the reactants are within the range of 80~100 kJ/mol and -0.5~+0.5, respectively, which are typically found in literatures³⁹⁻⁴¹. It can be said that the obtained kinetic model is applicable for discription of the typical LTFT system without losing much physicochemical validity. The model is valid for the wide operating range as specified in Table 2-4.

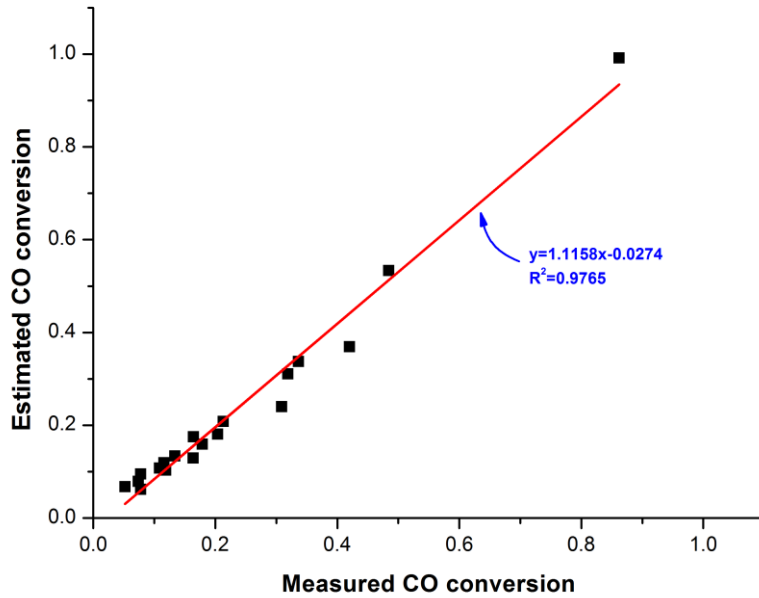


Figure 2-15. Comparison of the CO conversion between the measurement and the model estimation. The red line in the plot represents the trend line obtained from the regression.

Table 2-5. Kinetic parameters^a for Fischer–Tropsch catalyst used in this article

k_0	E_a^b	a	b	c
5.0 $\times 10^7$	95	0.50	0.50	0.30

^aThe parameters correspond to what is presented in eq(2-10)

^bActivation energy in kJ/(mol K)

2.2.3.2. Multichannel reactor model

The validation of the multichannel model was performed based on the kinetic data taken from the literature²⁷. Although the kinetic is different from what is used in 2.2.3.1., it is enough to validate the multi-channel model itself because the system is similar: both are the LTFT system having cobalt as a catalyst. Moreover, the reactor evaluated in the article has the cross-current flow configuration and the channel with micro scale, which means that the geometry is also comparable to the structure of the multi-channel reactor considered in this paper.

Operating data of a pilot scale micro-channel FT reactor tested by Deshmukh et al. (2011)¹¹ was used to validate the cell coupling model. The reactor consists of 274 process channels, which is oriented orthogonally with coolant channels (Fig. 2-11(e)). It was packed with 66.5 grams of the cobalt catalyst for low temperature Fischer-Tropsch synthesis.

Table 2-6 shows a comparison of the model estimation of the CO conversion with the operating data for the various conditions. Errors are less than 10 % for all cases, which implies that the model could handle multiple channels without severe inaccuracies. The errors are believed to arise due to the uncertainties in kinetics, catalyst packing pattern, flow distribution, and plug flow operation. The model is robust in that it is applicable for the various operating conditions as presented in Table 2-6.

Table 2-6. Comparison of CO conversion between model estimation and the data reported in literature (Deshmukh et al., 2011¹¹)

ID	Contact time (ms)	Temperature (°C)	Measured conversion	Estimated conversion	Error
1	290	207	0.741	0.681	0.081
2	210	215	0.722	0.684	0.053
3	150	222	0.710	0.671	0.055
4	100	241	0.702	0.722	-0.029
5	85	253	0.710	0.737	-0.037
6	70	263	0.696	0.733	-0.053

2.2.4. Case studies

In this part, several case studies are carried out to clarify the influence of three variables on the design: Flow configuration, flow distribution, and overlapping zone of the catalyst.

2.2.4.1. Flow configuration

As illustrated in Figure 2-11, the flow configuration will directly affect the velocity profiles of the coolant. It will affect the coolant flow rate, and hence, the cooling capacity at each position. For example, in the structure S1 (Fig. 2-11(a)), the coolant flowrate at the cross current part is higher than that at the counter current region because of the narrow inlet and outlet stream. So, the cooling capacity there is higher than the cooling capacity at the counter current region.

The flow configuration also affect the temperature profile. Some channel paths are longer than others. For example, for the U-shape flow path, the length of the coolant channel that is on the periphery of the plate is longer than that of the channel near the center. So the coolant flowing along the longer path gets more heat from the reaction channel because the contact area for the heat transfer is larger than that of the short path.

Figure 2-16 illustrates the result of representative base case study. The configuration of cross-counter-cross current with the same side (structure S1) was used, and it was assumed that the uniform distribution of the coolant is achieved, which will be explained in next section. Catalyst loading ratio was 0.2 (lump), and the operating temperature and pressure were 220°C and 20 bar, respectively. The coolant flow rate was 217 L/min, gas hourly space velocity (GHSV) was 4,000 mL/(g hr), and the number of process channel was 1,110. The size of the channel was 10 mm (width), 5 mm (height), and 510 mm (length). It was assumed that 370

coolant channels with 3 mm (width) x 3mm (height) was oriented orthogonally with the process channels at the inlet and outlet, respectively. At other part, where the flow is counter current, 4,440 coolant channels with 2.5 mm (width) x 3 mm (height) was placed parallel with the process channels. The inlet temperature of the syngas and coolant was 220.5°C and 220°C, respectively. The weight of packed catalyst was 5.04 kg, and the inlet flow rate of the syngas was 20.15 Nm³/h. The overall CO conversion was computed to be 0.44, and the total wax production rate was 0.26 barrels per day.

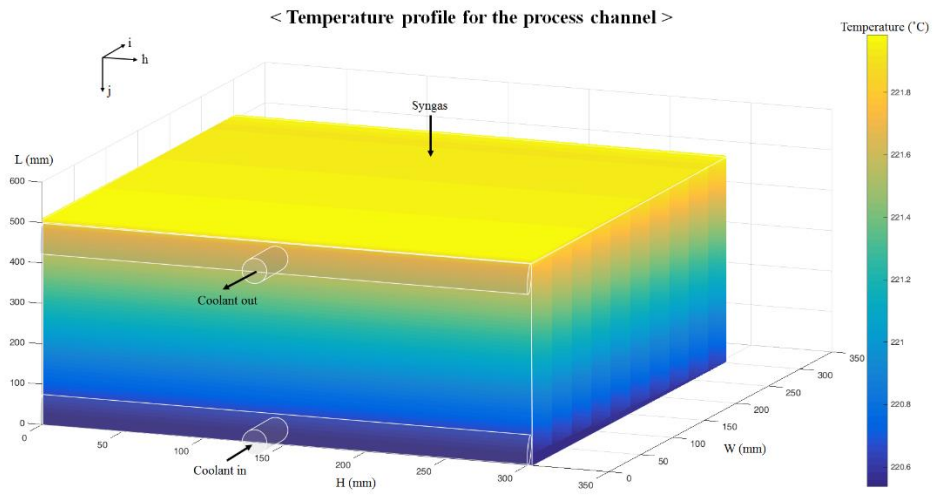


Figure 2-16. Temperature profile of the process channel for the cross-counter-cross current with the same side scheme

As illustrated in Figure 2-16, the temperature profile is influenced by the coolant's flow configuration. As the coolant flows into the channel (positive i -direction), it absorbs the reaction heat from the outlet of the process channel. The temperature increases along the channel until it encounters intersections, where the flow changes its direction to the negative j -direction. (There are 10 intersections. So 10 imaginary discontinuous boundaries are formed due to the characteristics of the cell coupling model, where it computes the energy balance equation for every pre-defined flow path as described in eq. (2-8). In the real operation, however, no such boundaries will be formed because the heat is dissipated along the channel wall.) The temperature increases for the negative j -direction as the coolant flows counter currently against the process channel. The coolant continuously absorbs the heat until its flow direction is changed to the negative i -direction at the intersections. The temperature is subsequently increased along that direction as the coolant flows cross currently against the process channel until it flows out through the footer plenum at the top of the reactor. The temperature has the maximum value at the outlet stream of the coolant. At that point, the syngas flows into the process channel and the FT reaction starts. The reaction rate is the highest due to the high concentration of the reactant, so the heat generation is the highest. Heat released there must be carefully controlled to prevent thermal runaway situation.

A sensitivity analysis was conducted to see the effect of flow configuration on the thermal performance of the reactor, as presented in Table 2-7. For the five cases studied (case C1~C5), the same operating conditions, except for the catalyst loading and coolant flowrate, with the operating conditions of the base case design were used: the reaction temperature and pressure was 220 °C, and 20 bar, respectively, and GHSV was 4,000mL/(g hr), whereas the catalyst loading ratio and

the coolant flowrate was 1.0 and 1086 L/min, respectively. The maximum temperature difference (ΔT_{max}), defined as the difference between the maximum temperature of the process channel cell and the inlet temperature of the syngas, is used for the comparison of each design. If ΔT_{max} is too high, it means that at some point the reaction is taking place at a condition that is far from the desirable operating point, and there is a chance for undesirable situation such as thermal runaway of the reactor, or deactivation of the catalyst. So, ΔT_{max} should be maintained as low as possible for the safe isothermal operation.

Table 2-7. Result of simulation for the five different flow configurations

Case number	Flow configuration^a	Maximum temperature difference (°C)
C1	Cross-counter-cross with the same side (S1)	5.57
C2	Cross-co-cross with the same side (S2)	4.11
C3	Cross-counter-cross with the different side (S3)	5.51
C4	Cross-co-cross with the different side (S4)	4.11
C5	Full cross current (S5)	5.71

^aThe flow configuration correspond to the cases presented in Figure 2-11.

As presented in Table 2-7, the maximum temperature difference is the highest for the full cross current design. The number of inlet coolant channels of that design is more than the others due to the increased contact area for the inlet (Fig. 2-11(e)). So the cooling capacity *per channel* is reduced, which makes the ΔT_{max} increase. The second and the third highest ΔT_{max} is found in the case C1 (Fig. 2-11(a)) and C3 (Fig. 2-11(c)), respectively. Both designs have the inlet coolant stream at the bottom and outlet at the top, so the coolant remove the maximum heat generated at the top after having swept the other part of the channel. The coolant's temperature has already increased at the outlet stream due to this sweeping effect, so the driving force for the heat transfer is decreased. This results in decrease in cooling capacity and increase in the temperature of the process channel inlet stream. The temperature is slightly higher for the case C1 than the temperature of C3 because the coolant path is longer: It brings more heat to the coolant outlet stream after flowing through the long path.

ΔT_{max} for the case C2 (Fig. 2-11(b)) and C4 (Fig. 2-11(d)) is the lowest among the all cases. Both have the exactly same numerical value of ΔT_{max} . In these cases, the inlet of the coolant flow is located at the top and the outlet at the bottom. The coolant first absorbs heat from the top where the reaction rate is the highest. It flows cross currently against the process channel with bearing the heat released at each point, until it encounters the final intersection at the corner, where the temperature reaches the maximum value. The value of ΔT_{max} for the case C2 and C4 is lower than that for C1 and C3 because the driving force for the heat transfer is higher: The fresh coolant at the inlet stream directly removes the maximum heat generation. Both C2 and C4 have the same coolant geometry at the initial part of the coolant channel (cross current region). So the model calculations result in the

same value of ΔT_{max} .

The difference between the values of ΔT_{max} in Table 2-7 is less than 2°C. This small difference is due to the compactness of the system considered in this work. Accordingly, the heat transfer schemes were extremely compact, making the values of ΔT_{max} for the cases so close. Despite the small difference, the difference itself is remarkable: The flow path inside the channel directly affects to the maximum temperature difference, and hence, to the thermal stability of the reactor.

In summary, different coolant flow configuration give the result of different temperature profiles. In most cases, it is desirable to remove the heat as soon as the reaction takes place. Unless the coolant absorbs the generated heat immediately, ΔT_{max} increases due to the sweeping effect and the operation becomes more dangerous. The temperature profile is also affected by the length of the flow path. So if all conditions being same, it is advantageous to make the coolant flow path as short as possible to prevent it from absorbing more heat: If the residence time for the coolant is short, then the heat is more effectively removed and the heat does not accumulate inside the reactor core.

2.2.4.2. Coolant flow distribution

In this context, the flow distribution is meant to be the distribution of the coolant flow at the inlet pipeline or inside the channel. The distribution of the syngas flow is assumed to be uniform, which is achievable by using particular equipment such as demister-like-distributor and a special header packed with bead materials like alumina ball.

The flow distribution plays an important role for the reactor control because it is directly related with the coolant flowrate, and hence, the cooling capacity at every

location inside the coolant channel. If the distribution system is improperly designed, then that will affect the local cooling efficiency, causing mal-function and thermal runaway of the reactor.

There are two local boundaries of interest for design of the coolant flow distribution: Inlet pipeline and inside the channel. First, the distribution at the inlet pipeline affects the flow distribution for each channel layer, as illustrated in Fig 2-14(b). Because of the momentum inertia, coolant tends to flow to the layer located at the center. A bell-shaped curve, similar to the normal Gaussian distribution plot, is obtained by CFD simulation. Less coolant flows into the layers at the edges means less cooling capacity available at those spots. Therefore, the flow profile should be made as flat as possible to have equal cooling capacity for each cooling channel layer.

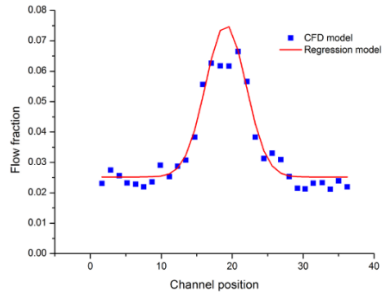
The diameter of the inlet pipe is the main variable that determines the shape of the profile. For the analysis, CFD computation was performed by changing inlet pipe diameter from 40 mm to 60 mm. A commercial available Syltherm 800[®] was used as a coolant, and the total flowrate of 180 L/min, which was determined from the overall energy balance equation was used. At the operating condition, the coolant's specific heat is 1.95 kJ/(kg K), density is 754.11 kg/m³, thermal conductivity is 0.0974 W/(m K), and the viscosity is 0.88 mPa·s. The vapor pressure of the coolant is 142.4 kPa, slightly higher than the ambient pressure at the reaction temperature. So the coolant was assumed to be pressurized to around 10 bar before the operation to avoid the partial evaporation.

Ansys CFX 15.0 was used to solve the mass and momentum balance equations. The results are shown as the blue data points in Fig. 2-17. A non-negligible dispersion of the data is due to the turbulence in the inlet header. As presented in

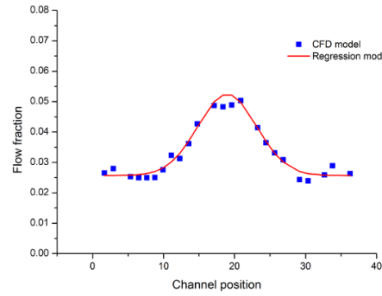
the figure, the velocity profile becomes more flat as the inlet pipe diameter increases. This is because the inertia towards the center is dispersed as the coolant flows for the wide area. The obtained profile is then regressed with the nonlinear function:

$$u_i(h_k) = a \cdot \exp(-b \cdot (h_k - c)^2) + d \quad (2 - 12)$$

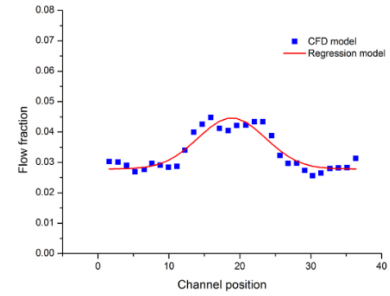
where u_i is the coolant velocity for i -direction. It is a function of the layer position h_k , where the subscript k ($k=1$ to 37 in this case study) is used for counting the number of channel layers which is located along the h -direction. The a , b , c , and d are the parameters that determine the shape, displacement, and the axis of symmetry of the bell-shaped curve. The structure of the function was conferred from the normal Gaussian distribution. The `nlinfit` subroutine in Matlab R2014b was used to regress the data taken from the CFD simulation to the above nonlinear function. The results are shown in Figure 2-17. As can be seen from the figure, the model function well fits to the CFD data.



(a)



(b)

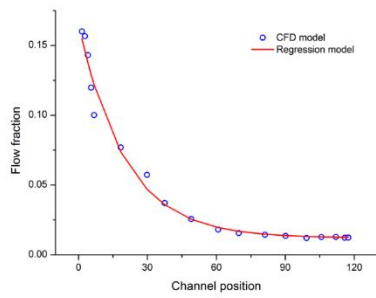
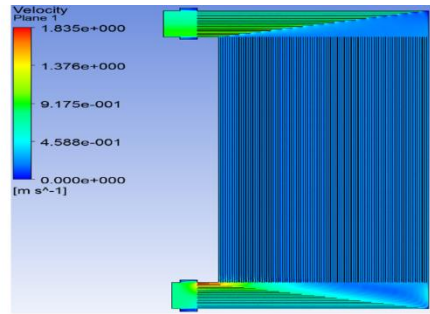
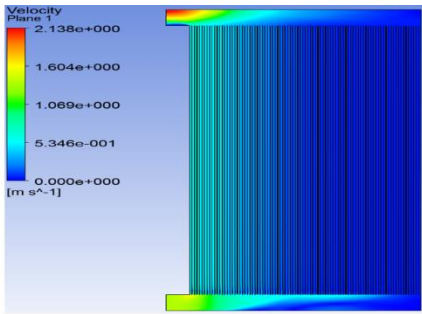


(c)

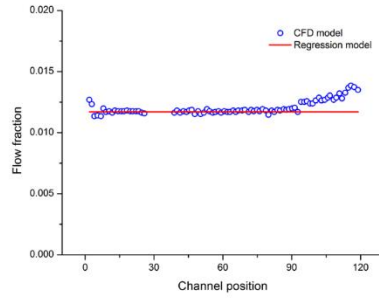
Figure 2-17. Result of the regression of the velocity profile for the inlet pipeline whose diameter is (a) 40 mm, (b) 50 mm, and (c) 60 mm.

Next, the distribution inside the channel affects the internal coolant flow and cooling capacity for a specific layer as illustrated in Figure 2-14(d). In the channel layer, the coolant flowing for a short path undergoes less resistance than the coolant flowing for a long path. So more coolant flows along the short channel, showing skewed velocity profile. From one particular case study, the ratio of maximum to minimum velocity (u_{max}/u_{min}), which is commonly used criteria for evaluation of the flow distribution, was around 13 for the worst scenario. That means the cooling capacity for some region can be less than 1/13 of other region if the distribution system is improperly designed. In that case, the reactor control would be so difficult that thermal runaway or local overcooling can occur. Such a mal-distribution must be prevented for the safe operation.

One strategy for making the skewed flow distribution uniform is to use inlet guiding fin, which transports the coolant to a certain point without losing its momentum. Figure 2-18(b) illustrates the result of the CFD simulation for the case of inlet guiding fin. Each guiding fin has different length so that the coolant that flows along the long channel path flow through the long fin, and short path through the short fin. As depicted in the figure, the distribution becomes nearly uniform when the guiding fin is used.



(a)



(b)

Figure 2-18. Result of CFD simulation and data regression for the flow distribution of the coolant channel plate (a) without inlet guiding fin and (b) with inlet guiding fin.

The obtained CFD data was then regressed with the nonlinear function:

$$u_j(i_m) = p \cdot \exp(-q \cdot i_m) + r \quad (2 - 13)$$

where u_j is the coolant velocity for the j -direction. It is a function of the channel position i_m , where the subscript m ($m=1$ to 120 in this case study) is used for counting the number of coolant channels comprising one layer. And p , q , and r is the parameters that determine the shape of the function. The `nlinfit` subroutine in Matlab R2014b was used to regress the data to the above exponential form. The result is shown in Fig 2-18, and the function well fits to the CFD data.

After obtaining the parameters in eq (2-12) and (2-13), the function values, i.e., the coolant velocity, are evaluated for every cell position. They are implemented to the cell coupling model (especially to the equation (2-8)) as a 3-D array of the $m_c(\gamma_s^t)$. Subsequently, the mass and energy balance, and the heat transfer equation are solved based on the implemented flow distribution data.

Figure 2-19 shows a comparison between the temperature profile of the uniform distribution and the mal-distribution case. It is assumed that perfectly uniform distribution, i.e., flat profile for both inlet pipe and inside the channel, is achieved for an ideal case. Practically, it is attainable by using inlet pipe whose diameter is greater than 80 mm and the inlet guiding fin. And in the mal-distribution case, narrow (40 mm) inlet pipe and no inlet guiding fin were used. As shown in the figure, ΔT_{max} becomes greater than 4 times of the ideal case, if mal-distribution occurs. It is also noted that the overcooling is expected at the center of the reactor core where the most fraction of the coolant flows, whereas the heat is accumulated at the two edges where almost no coolant flows. The flow distribution model was successfully integrated with the cell coupling model. The integrated model could be run without severe computational load, and also giving the physically

reasonable result. The model can be used to clarify the influence of the flow distribution and realistic structure on the reactor performances, even if more than 5,000 channels are involved.

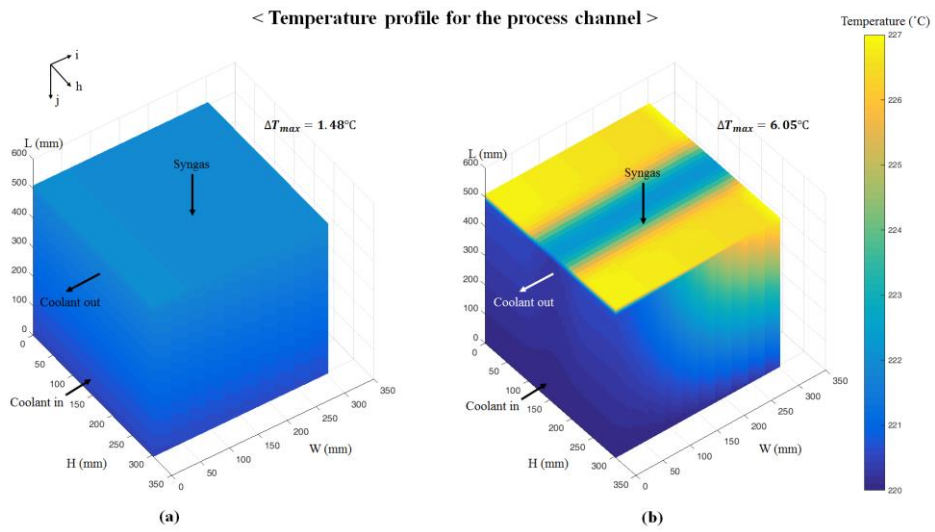


Figure 2-19. Temperature profile for the case of (a) uniform distribution and (b) non-uniform distribution

2.2.4.3. Catalyst-coolant overlapping zone

As mentioned in section 2.2.4.1, it is important to remove the maximum heat generated at the inlet of the process channel because in most cases, the temperature reaches the maximum value near the inlet as shown in the previous case studies. The amount of heat generation is related to the reaction rate [mol/gcat s], which is dependent on the catalyst loading density [gcat/L]. So it is a common technique to reduce the catalyst loading amount by mixing the catalyst particle with inert bead, when a large amount of heat generation is expected. Heat can be removed more easily although the productivity (per unit channel) is reduced. So it can be said that there is a trade-off relationship between the heat generation (safety) and production rate (efficiency). In the previous report³⁸, we studied the effect of zone division with catalyst loading ratio. Both the high heat removal rate and the high wax productivity could be achieved simultaneously by using zone division method, where the low amount of catalyst is packed in the initial part of the channel zone and the high amount of catalyst is filled in the next remaining part of the zone. Higher productivity could be accomplished without severe heat generation despite the larger catalyst amount in the second zone. Because some fraction of the reactants has been already consumed in the first zone so that the reaction rate is not that fast.

In this study, another strategy for the efficient heat removal is proposed. The main objective is to successfully control the heat generation for the particular region that shows complicated flow distribution profiles. Such region includes the inlet and outlet of the coolant channel, and the intersections where the flow momentum changes drastically. As mentioned in the previous section, it is difficult to predict the exact coolant velocity profile and evaluate the local cooling capacity

for such complicated structures. Therefore, one can say that it is reasonable to make those unpredictable regions inactive, or dead, for the safe operation. If there is no reaction, then no heat will be generated, and no effort is needed to remove the heat. So, no catalyst is loaded on purpose for the channel zones that overlaps with the complicated cooling regions, which is just a small fraction of the entire part. As shown in Fig 2-20(a), the catalyst is packed only for the zone that overlaps with the well-defined, predictable, and accountable cooling region.

Two cases were simulated for the comparison on the basis of the flow configuration of cross-counter-cross current with the same side (Structure S1). In the first case, the partial overlapping zone scheme, 50% diluted catalyst was packed in a fractional, i.e., only counter current part of the channels, and in the second case, the full overlapping zone scheme, the same diluted catalyst was filled in the entire part of the channels. The operating temperature was 220°C, and the pressure was 20 bar. The GHSV was 4,000 mL/gcat-hr, and the coolant flow rate was set to 500 L/min. The worst scenario for the coolant flow distribution was assumed: The sharpest bell-shaped profile for the inlet pipe region, and the most steeply decaying exponential profile for the inside channel layer out of all distribution scenarios were implemented into the model.

The results are presented in Figure 2-21. As shown in the figure, the first case (Fig 2-21(a)) has no hot spot at the inlet, because no catalyst is packed there. On the other hand, the second case (Fig 2-21(b)) has hot spot at two sides of the inlet of the process channel, where the cooling capacity is low due to the poor distribution performance. For the first case, although the zone is inactive with respect to reaction at the inlet of the process channel, the temperature increased slightly due to the coolant's sweeping effect, as discussed in the previous chapters.

The maximum temperature difference (ΔT_{max}) for both cases is 7.04°C, and 8.79°C, respectively, which shows the effectiveness of the strategy of partial overlapping zone. When the operating condition is changed to more harsh condition, for example, the high catalyst loading, high temperature, and high pressure, the difference of ΔT_{max} between two cases becomes bigger. The productivity for the partial overlapping case decreased by 11.7% because of the dead zone. Although the productivity is reduced, the design became more predictable, operable, and reliable in terms of safety, which is regarded as the most important issue in the detail reactor design. The integrated model suggested in this article could successfully handle such problems, and give results of most favorable and feasible design out of many design candidates through the efficient computational procedure.

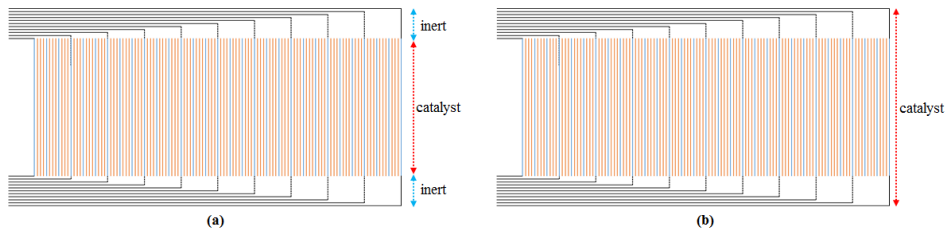


Figure 2-20. Conceptual diagram of (a) partial-overlapping and (b) full-overlapping zone scheme

< Temperature profile for the process channel >

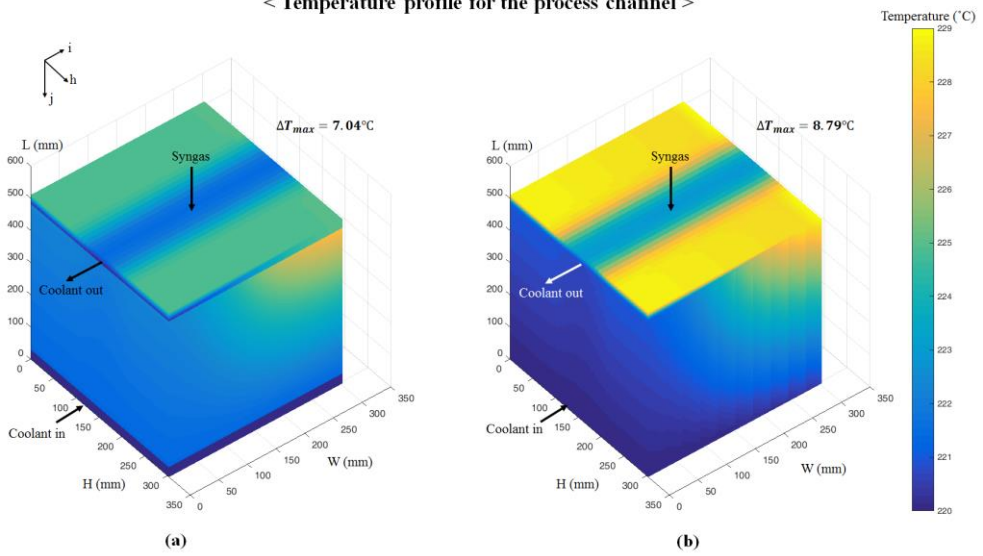


Figure 2-21. Temperature profile for the case of (a) partial-overlapping and (b) full-overlapping zone scheme

2.2.5. Conclusion

In this study, an integrated model for designing large-scale micro-channel Fischer-Tropsch reactor was developed. The effects of flow configuration, flow distribution, and strategic catalyst loading zone adjustment on the temperature profile of the reactor were analyzed by using cell-coupling approach and the results obtained from external computational fluid dynamics model.

Temperature control is of utmost importance in the reactor design, especially for the highly exothermic reaction systems. When more than 1,000 channels are involved, which is a common situation in designing the pilot- or industrial-scale micro-channel reactor, it is very hard to predict what is going on in the entire reactor domain. Interaction between each channel should be carefully analyzed in the design phase, in order to prevent undesirable situation such as thermal runaway, catalyst deactivation, and acceleration of side reactions. The present study contributes to designing such large-scale multi-channel reactor by modelling approach. The model incorporates kinetic parameters, flow configuration, and flow distribution data. This integration made it possible to analyze the whole scale reactor, which is not practicable if the conventional model, such as computational fluid dynamics, is used.

The design strategies and philosophy obtained from the case studies presented in this paper can be used for evaluating the feasibility of particular design. Moreover, the model in general can be extensively applied for designing other exothermic- or endothermic-reaction systems.

CHAPTER 3 : Optimization for GTL process

3.3. Introduction

GTL technology is known to be a highly energy-intensive process: It consumes a large amount of energy for reforming, compression, and separation, which is provided in the form of fuel energy of the natural gas, heat energy of the steam, or pure electricity. However, some of the energy can be recovered in the process: For example, the outlet stream from the reformer should be cooled down before going to a separation unit. The heat contained by this hot stream can be recovered through a heat exchanger. In addition, the heat generated in the FT reactor also can be utilized because the reaction is highly exothermic, and the reaction temperature is high enough to generate the medium-pressure steam. For this reason, it can be said that there is an opportunity for optimization of the GTL process.

Panahi et al. developed a model for optimal operation of the GTL process⁴². They developed a steady state model using autothermal reformer (ATR) and slurry bubble column Fischer-Tropsch reactor. Based on that steady model, an optimization problem was formulated, where the objective function was defined as an total income. Six design variables were used: H_2O/C (hydro carbon), O_2/C (hydrocarbon), fired heater duty, CO_2 recover percentage, purge ratio, and recycle ratio to FT reactor. Although optimal solution was obtained, other important variables, i.e., reaction pressure and temperature, were not taken into account in the model. The reaction condition directly affects to the reactor performances and recycle efficiency, so still there is an opportunity for process

improvement. The process can be further optimized by utilizing micro-channel FT reactor because the capital cost of this type reactor is lower than conventional ones, and it removes heat more efficiently.

This chapter discusses optimization of the overall GTL process with implementing the micro-channel FT reactor. Reaction temperature and pressure, as well as purge ratio and recycle ratio were taken into account as design variables. In section 3.2, the steady-state process model, and the regressed reactor model will be addressed. In section 3.3, the optimization problem will be briefly introduced. The resulting solution will be analyzed and discussed in section 3.4. In section 3.5, concluding remarks will be addressed.

3.4. Model description

3.4.6. Steady-state process model

The flowsheet for the process is shown in Figure 3-1. The process is divided into three sub-processes; Reforming, separation, and Fischer-Tropsch synthesis. In the reforming part, the natural gas feed and the recycle gas is converted into syngas, mainly composed of H_2 and CO. The molar ratio of H_2 to CO is an important factor for FT synthesis. The optimal value for H_2/CO is known to be 2, which is achieved by adjusting O_2 flow rate to the auto-thermal reformer (ATR). In the separation part, H_2O and CO_2 content in the syngas product stream is reduced before it going to the FT reactor. Water is removed by simple flash drum, and the CO_2 is separated by absorption with monoethanolamine (MEA). The resulting syngas is sent to the FT reactor where FT synthetic fuel is produced. In this study, the micro-channel FT

reactor presented in the previous chapters is used. The unconverted gas is purged or recycled to either ATR or FT reactor. The natural gas feed flow rate is fixed at 8195 kmol/h. The molar composition of the feed gas is $\text{CH}_4=95.5\%$, $\text{C}_2\text{H}_6=3\%$, $\text{C}_3\text{H}_8=0.5\%$, $\text{n-C}_4\text{H}_{10}=0.4\%$, $\text{N}_2=0.6\%$. A commercial process simulator Aspen plus V7.3 was used to calculate the steady-state mass and energy balance for this overall GTL process.

The reforming process is configured by a pre-reformer, fired heater, and an ATR. Pre-reformer is used to decompose all the heavier hydrocarbon into methane. The reactor is assumed to be adiabatic with operating pressure of 30bar, and in chemical-equilibrium. It was simulated with an RGibbs equilibrium reactor model, where Gibbs free energy of the product stream is minimized subject to atom balance constraints. The temperature of the inlet stream to the reactor was set to 445°C by preheating the feed gas in the fired heater. Methane, nitrogen, oxygen, steam, hydrogen, carbon monoxide, and carbon dioxide were specified as chemical components in the product stream. The resulting outlet temperature of the pre-reformer was 463.4°C.

The product stream of the pre-reformer is sent to the ATR with pure O₂, which is assumed to be provided by an air separation unit (ASU). The temperature of the inlet stream of the ATR unit was set to 675°C by using fired heater. The ATR was operated with adiabatic condition and the pressure of 30 bar. It was also simulated with the RGibbs model in the simulator. The outlet stream of the ATR was 1290°C.

This syngas is cooled down to 38°C in the heat exchanger (HTRC-HX in Figure 3-1), where the water absorbs the heat from the syngas and the MP steam is generated. It then expands through VLV1 to 10 bar, and the gas is sent to the flash drum where the water is drained out in the liquid stream. The dry gas (stream 16) is subsequently sent to the CO₂ separation unit, where CO₂ is absorbed by MEA solvent. The reboiler duty for stripping CO₂ gas is provided by the heat contained by the coolant outlet from the FT reactor. The MP steam generated from the HTRC-HX is provided as a feed for the prereformer, feed for the gas turbine for ASU drive, or steam export to the utility system.

The effluent gas from the CO₂ separator (stream 19 in Figure 3-1) is pressurized and heated up before being introduced into the FT reactor. The pressure and temperature of the feed gas to the FT reactor are the main design variables in optimization problem, which will be described in section 3.3. Representative values for those variables are 20 bar and 220°C, respectively. The micro-channel reactor model presented in the previous chapters are used for FT synthesis. The customized reactor model was implemented onto the process model using Fortran language. Detailed description of the regressed model will be addressed in section 3.2.2. The coolant used for thermal control of the FT reactor is sent to the flash drum, where it is separated by phase equilibrium. The resulting hot vapor (FTCOOL5) is sent to the reboiler of the CO₂ separator, where the latent heat of vaporization of the coolant vapor is utilized for the heat recovery.

The product of the FT reactor (FTOUT in Figure 3-1) is sent to the 3-phase separator, where aqueous product, FT synfuel, and tailgas are separated. The tail gas is subsequently sent to the first splitter (SPLIT1), where some fraction of the unreacted gas is purged out. The remainder of the gas is further sent to another splitter (SPLIT2), where the gas is recycled back to either FT reactor or reformer. The split ratio of those two splitters are also the main design variables in optimization problem. Representative values for those variables are 0.04 (to PURGE from SPLIT1) and 0.82 (to RECTOFT from SPLIT2), respectively.

The result of the mass and energy balance calculation for the steady-state model is shown in Table 3-1.

	NGFEED	O2FEED	ATR0UT	H2O0UT	CO20UT	FTIN	FT0UT	AQEU0UT	OILOUT	PURGE	RECTOFT	RECTOREF	FTCOOL5
Temperature C	40	25	1290	38	38	220	220	30	30	30	30	30	220
Pressure bar	30.00	30.00	30.00	10.00	10.00	23.75	23.75	23.75	23.75	23.75	23.75	23.75	23.30
Vapor Frac	1.00	1.00	1.00	0.00	1.00	1.00	0.98	0.00	0.00	1.00	1.00	1.00	1.00
Mole Flow kmol/hr	8195	5319	31241	5871	981	28752	13754	7637	574	222	4364	958	35134
Mass Flow kg/hr	138036	170189	412830	105773	43189	334233	334228	137576	107266	3575	70365	15446	632958
Mole Flow kmol/hr													
C1	7826	0	11	0	0	47	47	0	1	2	37	8	0
C2	246	0	0	0	0	0	0	0	0	0	0	0	0
C3	41	0	0	0	0	0	0	0	0	0	0	0	0
NC4	33	0	0	0	0	0	0	0	0	0	0	0	0
N2	49	0	237	0	0	1091	1091	0	6	43	854	188	0
O2	0	5319	0	0	0	0	0	0	0	0	0	0	0
H2O	0	0	6019	5871	0	155	7654	7636	9	0	7	2	35134
NC14	0	0	0	0	0	0	536	0	536	0	0	0	0
H2	0	0	16099	0	0	18170	2636	0	5	105	2071	455	0
CO	0	0	7843	0	0	9083	1583	0	8	63	1240	272	0
CO2	0	0	1033	0	981	206	206	0	10	8	155	34	0

Table 3-1. Stream table for the GTL process

3.4.7. Micro-channel reactor model

The micro-channel FT reactor model presented in the previous chapters are implemented onto the steady-state model for more realistic process design. The detailed reactor model is required to analyze the effect of the reaction conditions such as temperature, pressure, and space velocity on the reaction performances. Although many researchers conducted optimization work for the GTL process, such variables were not taken into account in the problem formulation. For example, Panahi et al. simulated FT reactor as an RStoic model, where the simple mass balance for the reaction system is computed using a lumped conversion parameter⁴². Such simplification is necessary when the (process) model becomes too large.

However, both physical rigors and simplicity should be retained to consider the effect of operating conditions in the optimization problem. In this study, those were satisfied by implementing a regressed reactor model onto the steady-state process model.

For that purpose, artificial neural network, a well known nonlinear regression technique, was applied to the regression of the 3D cell-coupling reactor model. First, 200 data points were obtained by conducting sensitivity analysis for the reactor model: Three input variables, i.e., temperature (T), pressure (P), and GHSV were set as one of the combination of the values from $T [^{\circ}\text{C}] = \{215, 220, 225, 230\}$, $P [\text{bar}] = \{18, 21, 24\}$, and $\text{GHSV} [\text{mL}/(\text{gcat}\cdot\text{h})] = \{25600, 32000, 41600, 48000\}$. The cell coupling model was then conducted using every 48 input data, and the resulting CO conversion was recorded. The used layout of the reactor for this sensitivity analysis is as follows: 133 process channels of 1mm (width) x 3mm

(height) x 500mm (length), and 1001 coolant channels (2mm x 2mm x 85mm) orthogonally arranged with the process channels to produce cross-current flow scheme.

Next, an artificial neural network was configured as shown in Figure 3-2: First, 3 input variables are introduced into the input layer and sent to 10 neurons in the hidden layer after multiplication with the adaptive weighting factors. The weighted input signal for each neuron enters the pre-defined activation function, where the signal is converted into its output activation. The activation function used in this study is a sigmoid function:

$$y = \frac{1}{1 + e^{-x}} \quad (3 - 1)$$

In the output layer, there is only one neuron that accepts activation signal from 10 hidden neurons. This final neuron calculates the weighted sum of the signal and the bias term (b_2 in Figure 3-2) and returns the estimated CO conversion value.

The sum of square errors (SSE) between CO conversion values calculated from cell coupling model ($X_{CO,data}$) and those estimated from ANN model ($X_{CO,estimated}$) are minimized by adjusting 51 ANN regression parameters:

$$SSE = \sum_{i=1}^{48} (X_{CO,data} - X_{CO,estimated}) \quad (3 - 2)$$

The optimization problem was solved by *fmincon* procedure built in Matlab R2014b with the training data set. This data set was composed of 28 data, that was randomly selected from the total 48 data points. Remaining 42% data was used as a test set to examine the performance and validity of the regression model. As a result, the estimated data well fits to the original data, as illustrated in Figure 3-3.

The obtained optimal ANN parameters were implemented onto the Aspen model by using Fortran code.

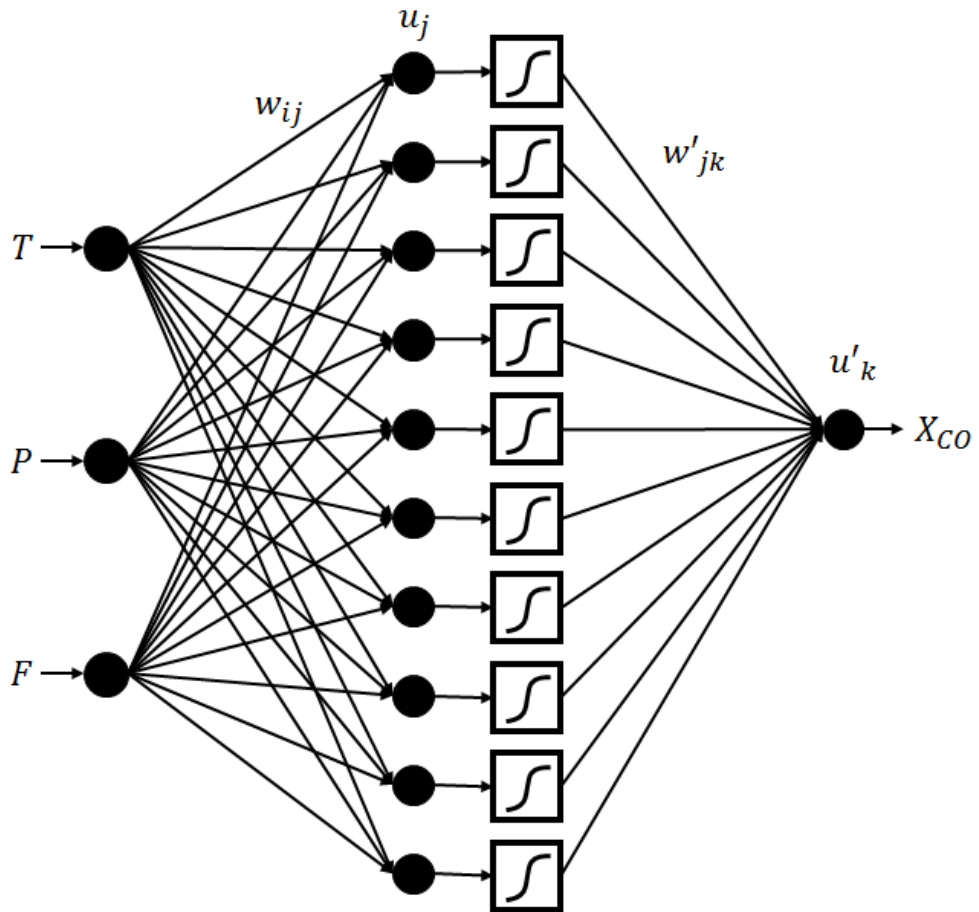
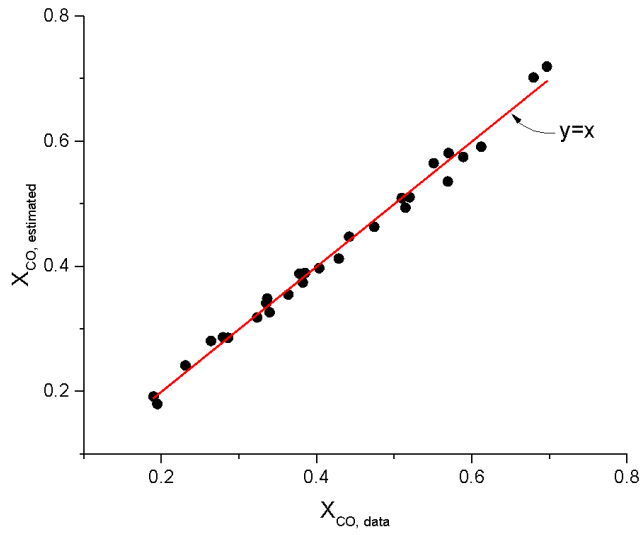
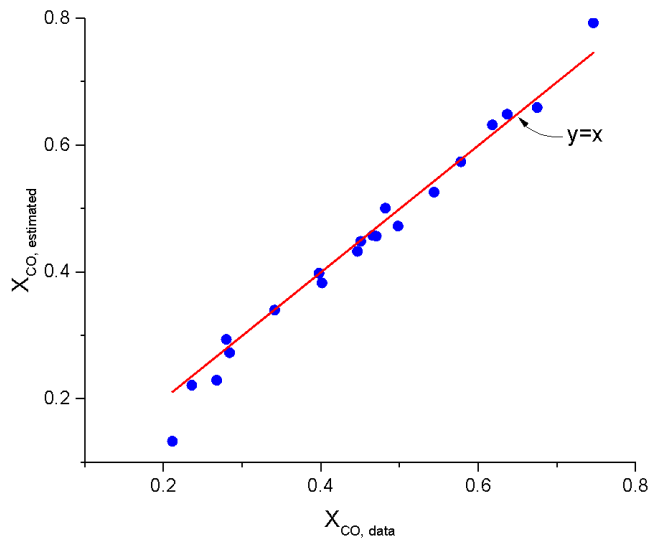


Figure 3-2. Structure of the artificial neural network for the micro-channel FT reactor



(a)



(b)

Figure 3-3. Results for the artificial neural network model: (a) Training set and (b) test set

3.5. Optimization for the steady-state model

Now that the steady state model (section 3.3.1) and regressed reactor model (section 3.3.2) has been obtained, the optimization for the GTL process can be performed. This section covers the formulation of the optimization problem and solving algorithm.

3.5.1. Cost model

First, a cost model that evaluates the total capital cost (CAPEX) and operating cost (OPEX) for the steady-state model was developed referring to the literature. CE index of 394 and the expected life time of 3 years were used for annualized capital cost calculation for all the equipments. The capital cost evaluation is as follows:

For the fired heater,

$$C_{cap,FIRED\ HEATER} (\$) = C_B F_P F_M \quad (3 - 3)$$

where C_B , the base cost, is a function of the heat duty.

$$C_B = \exp(0.8505 + 0.766 \cdot \ln(Q)) \quad (3 - 4)$$

where Q is in Btu/hr. F_P and F_M are for the pressure and material effect, and both were assumed to be 1 in this study. For the pre-reformer and ATR,

$$C_{cap,PRE-REFORMER} (\$) = 10 \cdot 17640 \cdot D^{1.066} L^{0.802} \quad (3 - 5)$$

$$C_{cap,ATR} (\$) = 10 \cdot 17640 \cdot D^{1.066} L^{0.802} \quad (3 - 6)$$

where D (m) and L (m) represent the diameter and length of the cylindrical vessel. The size of the reformer was decided by assuming the gas residence time(τ)=5 seconds and $L/D=10$. For the heat exchangers (HTRC-HX and PREHEAFT in Figure 3-1),

$$C_{cap,Heat\ exchanger} (\$) = 7296 \cdot A^{0.65} \quad (3 - 7)$$

where A is required heat exchanger area (m²). For the water separator (H2OSEP in Figure 3-1),

$$C_{cap,H2OSEP} = C_V F_M + C_{PL} \quad (3 - 8)$$

where C_V is the vessel cost, which is the function of the vessel weight:

$$C_V = \exp(6.775 + 0.18255 \cdot \ln(W) + 0.02297 \cdot \ln(W)^2) \quad (3 - 9)$$

where W in lb. C_{PL} is the cost for platforms and ladders, which depends on the vessel layout:

$$C_{PL} = 285.1 \cdot (D_i)^{0.7396} \cdot (L)^{0.70684} \quad (3 - 10)$$

where D_i (inner diameter) and L (length) are in ft. For the CO₂ separation unit, it was assumed that the capture cost is 50\$/tonCO₂. The total cost (both capital and operating cost) is calculated by multiplying it with the total CO₂ flowrate into the separator. 10% of the total cost is assumed to be the column capital cost, and remaining 90% is the fuel cost for the reboiler duty (operating cost). For the compressors,

$$C_{cap,COMPRESSOR} = F_D \cdot F_M \cdot \exp(7.2223 + 0.8 \cdot \ln(W_{HP})) \quad (3 - 11)$$

where F_D and F_M are for motor drive type and material effect respectively, and they are assumed to be 1 in this study. W_{HP} (hp) is a brake horse power for compressor driving. The capital cost for the FT reactor was assumed to be 10 times the cost of the simple vessel:

$$C_{cap,FTRXTOR} = 10 \cdot (C_V \cdot F_M + C_{PL}) \quad (3 - 12)$$

where C_V and C_{PL} are computed using eq. (3-9) and eq. (3-10), respectively. F_M is assumed to be 1. The capital cost for the 3 phase separator (3PHASESEP in Figure 3-1) was assumed to be 3 times the cost of the normal vessel:

$$C_{cap,FTRXTOR} = 3 \cdot (C_V \cdot F_M + C_{PL}) \quad (3 - 13)$$

where C_V , F_M , and C_{PL} are computed in the same manner with the FT reactor cost calculation. For the ASU turbine (ASUTURB in Figure 3-1),

$$C_{cap,ASUTURB} = 7400 \cdot (W_{HP})^{0.41}$$

where W_{HP} (hp) is generated horse power.

Operating cost for the energy-consuming equipments were computed based on the required amount of energy (MW) and the cost of the natural gas (5\$/1000scf of NG), whose lower heating value (LHV) is assumed to be used for that energy consumption. First, for the compressors and ASU turbine, with an overall thermal efficiency of 33% and LHV of natural gas of 50 MJ/kg, 1 MW of electricity requires the combustion of 0.00379 kmol/s of natural gas⁴³. For all other equipments, fired heater, reboiler in the stripping column, and preheater, a thermal efficiency of 75% was assumed. So 1MW of the heat duty requires the combustion of 0.001667 kmol/s of natural gas⁴³.

Results for the economic analysis for the base case (optimal design) are summarized in Table 3-2. The CAPEX and OPEX for the process equipments were 11.68×10^6 \$/yr and 75.95×10^6 \$/yr, respectively. Other costs, the feed gas price and O₂ import from ASU, and the earning from FT wax, MP steam export, and electricity generated from ASU turbine are shown in Table 3-2(b). As a result, the total income was calculated to be $592.81 + 38.43 + 36.02 - (314.07 + 37.48 + 11.68 + 75.95) = 228.09 \times 10^6$ \$/yr.

Table 3-2. Results for the economic evaluation for the optimal design; (a) CAPEX and OPEX for the process equipment and (b) Other cost and earning

(a)

Equipment^a	Capital cost (10⁶ \$/yr)	Operating cost (10⁶ \$/yr)
FIRHEATK1		11.50
FIRHEATK2	Sum of 3 fired heaters=1.30	1.84
FIRHEATK3		11.02
PREREFOR	1.02	
ATR	2.70	
HTRC-HX	0.71	
FIRHEATZ1		8.92
FIRHEATZ2	Sum of 2 fired heaters=1.75	26.73
H2OSEP	0.01	
CO2SEP	1.87	
CMPRSS1	1.69	11.21
PREHEAFT	0.20	4.59
FTRXTOR	0.07	
3PHASESEP	0.05	
CMPRSS2	0.05	0.13
ASUTURB	0.27	

^aThe names of the equipments are those shown in Figure 3-1.

(b)

Cost (10⁶ \$/yr)	Earning (10⁶ \$/yr)
------------------------------------	---------------------------------------

NG feed	314.07	FT wax	592.81
O ₂ import	37.48	Steam export	38.43
		electricity (ASU turbine)	36.02

3.5.2. Problem formulation

The optimization problem was formulated based on the steady state model (Section 3.2.1) and the cost model (3.3.1). The objective function, which should be minimized in the optimization problem, was defined as “-(minus) total income”:

$$\begin{aligned} \text{total income} &= \text{Revenue} - \text{Cost} \\ &= (\text{Wax price} + \text{Steam export}) - (\text{NG feed price} + \text{O}_2 \text{ price} \\ &\quad + \text{CAPEX} + \text{OPEX}) \end{aligned}$$

The decision variables were the operating temperature (T) and pressure (P) of the FT reactor, purge ratio (s_1), and recycle ratio (s_2). s_1 is the ratio of the mole flow rate of the purge stream to that of the inlet stream of the first splitter (SPLIT1 in Figure 3-1). And s_2 is the ratio of the mole flow rate of the recycle stream for the FT reactor (RECTOFT in Figure 3-1) to that of the inlet stream of the second splitter (SPLIT2 in Figure 3-1). The upper and lower bound for each variable were $215 \leq T \leq 230$, $21.5 \leq P \leq 24$, $0.04 \leq s_1 \leq 0.09$, and $0.67 \leq s_2 \leq 0.87$, respectively.

In addition, there are two process specifications that must be satisfied. First, H₂/CO molar ratio of the inlet stream to the FT reactor should be 2 for optimal FT synthesis. This can be satisfied by changing O₂ flow rate. Next, S/C ratio, the ratio of the mole flow rate of H₂O to that of the hydrocarbons in the inlet stream to the pre-reformer, was specified as 0.61, which was met by varying the split ratio of the SPLIT3 in Figure 3-1.

In summary, the optimization problem was formulated as:

$$\text{minimize } (-\text{total income})$$

subject to

$$215 \leq T \leq 230$$

$$21.5 \leq P \leq 24$$

$$0.04 \leq s_1 \leq 0.09$$

$$0.67 \leq s_2 \leq 0.87$$

$$H_2/CO = 2.0$$

$$H_2O/C(\text{hydro carbon}) = 0.61$$

The Nelder-Mead algorithm was applied to solving this problem. It is also known as the downhill simplex method, where the concept of a simplex, having (n+1) vertices in n dimensions, is used to find the optimum of an objective function. This algorithm is commonly applied to derivative-free optimization problems, for which the derivatives for the objective function may not be known. It requires small number of function evaluation, which is essential for optimization of a large process model.

The method determines search direction by evaluating function values for each vertex of the current simplex: If the point of interest is better than the current best point, then search further to that direction; If the point of interest is worse than the current worst point, then stop searching to that direction and reduce the searching area. To be more specific, the method begins with sorting (n+1) initial points in an ascending order.

$$f(x_1) \leq f(x_2) \leq \dots \leq f(x_n) \leq f(x_{n+1})$$

where $x \in \mathbb{R}^n$. Let us define x_1 , x_n , and x_{n+1} as the best point (B), good point (G), and worst point (W), respectively (Figure 3-4). Then compute the centered point (M) and reflected point (R):

$$M = \frac{x_1 + x_2 + \dots + x_n}{n}$$

$$R = M + \alpha \cdot (M - W)$$

Evaluate the function at point R. If $f(B) \leq f(R) < f(G)$, then replace W with R to obtain a new simplex and do the ordering again. If $f(R) < f(B)$, then compute the expanded point (E) and evaluate $f(E)$:

$$R = M + \gamma(M - W)$$

If $f(E) < f(R)$, replace W with E and go to the ordering step. If not, i.e., $f(E) > f(R)$, then replace W with R and do the ordering again. Expansion is finished here.

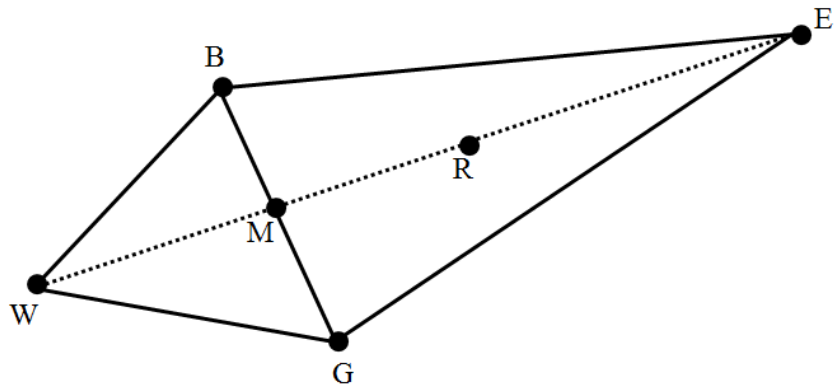
If $f(R) \geq f(G)$, compute the contracted point (C):

$$C = M + \rho(M - W)$$

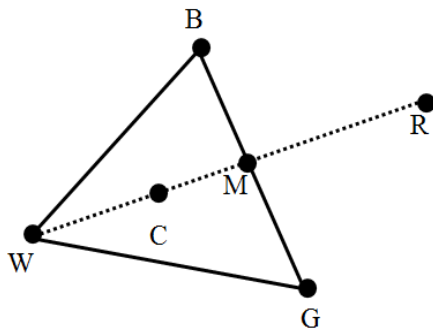
If $f(C) < f(W)$, then replace W with C and go to the ordering step. If $f(C) \geq f(W)$, compute the shrink point(S_i) except for B:

$$S_i = B + \sigma(x_i - B), \quad i = 2, 3, \dots, n + 1$$

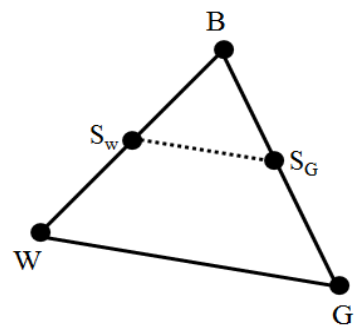
And then replace x_i with S_i and go to the ordering step. The Nelder-Mead algorithm stops if the pre-defined criteria such as the tolerance for the relative error between previous and updated function values or the maximum number of function evaluation are met.



(a)



(b)



(c)

Figure 3-4. Concept of Nelder-Mead algorithm: (a) Reflection and expansion, (b) Contraction, (c) Shrink

3.6. Results and discussion

In this section, the results for the economic evaluation for two process models are compared; M1, the process model taken from literature, M2, the process alternative with optimization.

The major differences between M1 and M2 are that 1) M1 used slurry bubble column FT reactor, whereas M2 used the micro-channel FT reactor, 2) M1 used the simple Rstoic model for the FT reactor, which is not realistic and optimal, while M2 used the ANN regression model that was proven to be reliable as addressed in section 2.1.3 and 2.2.3 of this thesis, and 3) M1 does not utilize the FT reaction heat, whereas M2 uses that heat as a reboiler duty for CO₂ stripping column.

The results for the CAPEX and OPEX computation for each process are illustrated in Figure 3-5. As presented in the figure, the sum of OPEX and annualized CAPEX for the optimal process (M2) is decreased by 17% compared to that for the reference process (M1). The reduction in fuel cost for the CO₂ separation unit mainly caused this improvement.

The overall economic evaluation for the two cases are presented in Table 3-3. It is noted that the cost for optimal case is reduced by 4.1% due to the energy saving in CO₂ separation, and the earning increased by 2.4% due to the improvement in FT wax production. As a result, the total income increased by 17.9% compared to the reference case.

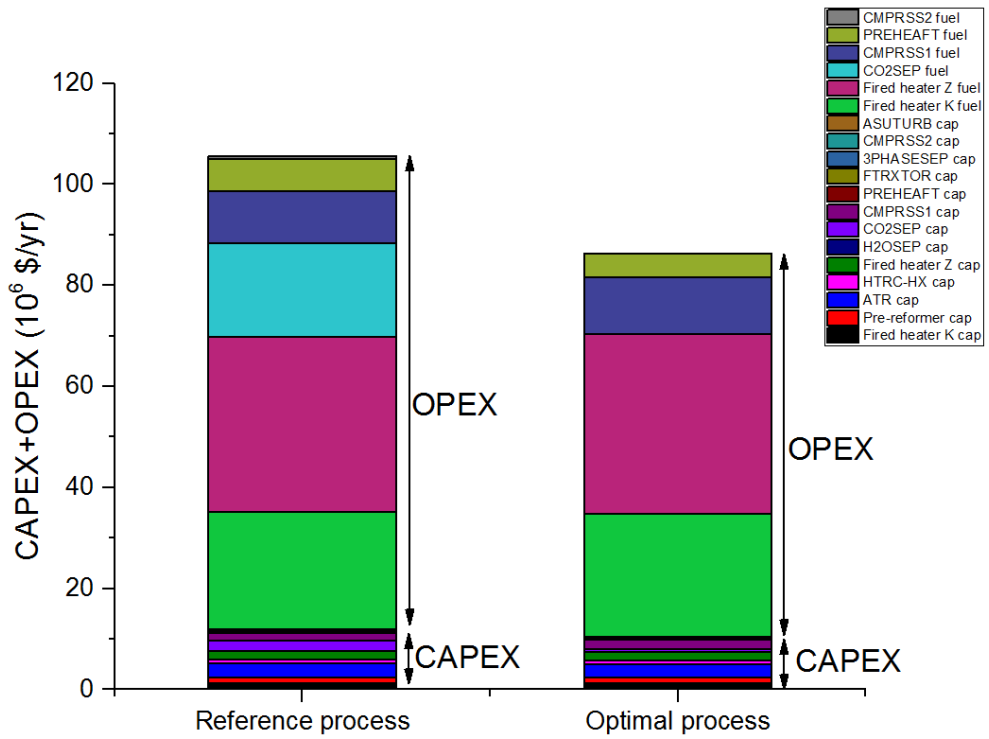


Figure 3-5. CAPEX and OPEX for reference process and optimal process

Table 3-3. Overall economic evaluation for reference process and optimal process

		Reference process	Optimal process
Cost (10⁶\$/yr)	CAPEX	12.02	11.68
	OPEX	93.57	75.95
	NG feed	314.07	314.07
	O ₂ import	38.43	37.48
Earning (10⁶\$/yr)	FT wax	576.16	592.81
	Steam export	38.43	38.43
	electricity (ASU turbine)	36.91	36.02
Total income (10⁶\$/yr)		193.41	228.08

3.7. Conclusion

Optimal design for steady-state GTL process was performed in this chapter. The GTL process is known to be highly capital intensive process mainly due to the syngas reforming unit, CO₂ separation, and gas compression system. Hence, the optimization for this process is important for process efficiency and economic feasibility.

The steady state model utilizing the micro-channel FT reactor was developed by implementing this reactor model onto the process model. Both the model simplicity and physical rigors were attained by development of customized reactor model using artificial neural network regression technique.

The economic evaluation for the processes was conducted based on the cost model referring to literature. Then the optimization problem was formulated by defining objective function as “minus total income”, and decision variables as the operating temperature and pressure for the FT reactor, purge ratio, and recycle ratio to the FT reactor. Nelder-Mead simplex algorithm was applied to solving this derivative-free optimization problem without much time consumption.

The total income for the optimal design increased by approximately 18% compared to that for the reference design, mainly due to the energy saving in CO₂ separation and improvement in wax production. This work could contribute to designing an optimal and reliable GTL process based on micro-channel Fischer-Tropsch reactor.

CHAPTER 4 : Dynamic simulation for microchannel Fischer-Tropsch reactor

4.1. Introduction

FT synthesis is known as an strongly exothermic reaction: A large amount of heat, ca. 165kJ per mol of converted CO is generated during the reaction. Care must be taken when operating this exothermic reactor for the process safety: If improperly controlled, the reactor would cause undesired situation such as thermal runaway and catalyst deactivation. Other safety issue includes wax-clogging, back-flow, and reactor rupture.

In that sense, rigorous dynamic analysis is essential part for preparation for the operation of the reactor. Many researchers conducted the research on dynamic analysis for many types of reactor. For example, Asteasuanin et al. performed dynamic simulation an optimization of tubular polymerization reactors to suggest optimal start-up strategies⁴⁴. Dynamic modeling of styrene/butadiene emulsion polymerization reactors was conducted by Sayer et al⁴⁵. They studied the system's dynamic behavior by analyzing the open loop response and closed loop control performances. Morud et al. did dynamic simulation for the analysis of instability in an industrial ammonia reactor⁴⁶. They analyzed steady state operating conditions and developed the dynamic model that describes oscillatory behavior in outlet temperature of the reactor. Studies on the transient behavior of the micro-channel FT reaction system, however, have not been done extensively.

Several researchers studied on operating procedure for the conventional FT reactor. Arcuri et al. suggested an efficient and stable start-up procedure for the FT reactor by accounting for the H₂/CO molar ratio as a main manipulating variable⁴⁷. While maintaining low H₂/CO ratio, pressure and temperature was increased to line-out condition. After that, the H₂/CO ratio was raised. In that manner, the start-up time period could be reduced and the thermal stability was greatly improved. Also, Sumerford et al. conducted the research on start-up operating strategy to prevent the carbon formation⁴⁸. By adjusting H₂ flow rate during the start-up phase, they could achieve the stable temperature control, resulting in soot-free operation. Song et al. performed a model-directed study for suggesting the operating procedures for FT reactors that prevents the reactor multiplicity⁴⁹. A strategy for high speed shut-down for the FT reactor was suggested by Bezemer et al⁵⁰. The high speed shut-down was achieved by blocking provision of feed to the reactor and simultaneously blocking the withdrawal of effluent from the reactor. Operating procedures for the normal start-up and shut-down of the micro-channel reactor, however, have not been studied extensively.

In this chapter, first, the development of the dynamic model for the micro-channel FT reactor presented in the previous chapters is addressed. The transient behavior for the 3D reactor is analyzed. Then the dynamic simulations for the micro-channel FT reactor are performed. Optimal start-up and shut-down strategies for the FT reactor operation is suggested.

4.2. Dynamic modeling for 3D reactor

4.2.1. Model description

In order to simulate the transient behavior of the 3-dimensional micro-channel FT reactor, one should solve both mass balance and energy balance equation simultaneously:

$$\frac{\partial N_i}{\partial t} = \sum F_i|_{in} - \sum F_i|_{out} + \int r_i dV \quad (4-1)$$

$$\frac{\partial \hat{E}_{sys}}{\partial t} = \sum F_i H_i|_{in} - \sum F_i H_i|_{out} + \dot{Q} - \dot{W}_s \quad (4-2)$$

where chemical species i flows into and out from the control volume dV . N is the amount of the mole of the species i in the control volume, F is the flow rate, r is the reaction rate, \hat{E}_{sys} is the total energy of the system, H is the enthalpy, Q is the heat flowing into the control volume, and W_s is the shaft work done by the system. The above equations can be converted into the form of partial differential equations by taking limit of $dV \rightarrow 0$, whereby spatial and temporal variations of the mass and energy are computed. However, solving such partial differential equations is challenging, particularly when the dimension of the domain becomes so large that many unit control volumes are to be generated. Thus, in that case, it is necessary to simplify those equations to obtain the solution of the dynamic model.

In this study, the simplification of the model was made by taking the structure of the cell coupling model developed so far, where the bias of the flow direction was allowed for the computation. The dynamic model was developed on the basis of the existing cell coupling model:

$$N_x^{u+1} = N_x^u + \Delta t \left[F_x^u(j, i, h) - F_x^u(j + 1, i, h) + \rho A \sum_w r_{wx}^{u+1} \right] \quad (4-3)$$

$$\begin{aligned} T_p^{u+1}(j, i, h) = & T_p^u(j, i, h) \\ & + \frac{\Delta t}{\sum N_x C_{px}} \left[UA \{ T_p^{u+1}(j, i, h) - T_c^{u+1}(j, i, h) \} - \Delta H_r \right. \\ & \left. \cdot \sum_w \left(k_{w0} \exp \left(-\frac{E_w}{RT_p^{u+1}(j, i, h)} \right) C_x \right) \cdot \rho V \right] \quad (4-4) \end{aligned}$$

$$\begin{aligned} T_c^{u+1}(j, i, h) = & T_c^u(j, i, h) \\ & + \frac{\Delta t}{\rho_c V C_{p,c}} \left[\Delta H_r \cdot \sum_w \left(k_{w0} \exp \left(-\frac{E_w}{RT_p^{u+1}(j, i, h)} \right) C_x \right) \cdot \rho V \right. \\ & \left. - \dot{m}_c C_{p,c} (T_c^{u+1}(j, i, h) - T_c^u(j, i - 1, h)) \right] \quad (4-5) \end{aligned}$$

Eq. 4-3, 4-4, and 4-5 represent the mole balance of the chemical species x in the process channel cell, energy balance in the process channel cell, and energy balance in the cooling channel cell, respectively. The superscript denoted by u is the specified time u . These equations are driven from eq. 4-1 and 4-2 by using backward Euler method. Parameters j , i , and h in the parenthesis represent the cell position. The same coordinate system was used as that used in Chapter 2 and 3.

First, the initial points at time $u=0$ were specified as the solution obtained from steady state simulation of the cell-coupling model in Chapter 2 (or 3). With those points, T_p^1 and T_c^1 are computed by solving eq. 4-4 and 4-5 simultaneously. In Matlab R2014b environment, the built-in *fsolve* function was used to solve these two nonlinear equations. The nested function structure was utilized to separate the parameters (old values such as T_p^u and T_c^u) and variables (updated values such as T_p^{u+1} and T_c^{u+1}) when the *fsolve* function is called. After obtaining all the updated

values of $T_p^{u+1}(j, i, h)$ and $T_c^{u+1}(j, i, h)$, the material balance equation (eq. 4-3) is solved, where the reaction rate (r_{wx}^{u+1}) is evaluated by the updated cell temperature and the mole of the component x at time $u+1$ is computed. These are iteratively calculated until the error between the values (at time= $u+1$) of the previous and present step becomes negligible.

4.2.2. Results and analysis

Several case studies were conducted for the analysis of the dynamic behavior of the reactor on the basis of the same layout: process channel size of $1\text{mm} \times 3\text{mm} \times 500\text{mm}$, coolant channel size of $2\text{mm} \times 2\text{mm} \times 103\text{mm}$, 352 process channels and 1573 coolant channels with fully cross current scheme. Total number of cells generated by channel decomposition method was $32 \times 143 \times 11 = 50336$. The initial point was obtained by solving the steady-state cell coupling model based on the reaction condition specified: The temperature of the syngas and coolant inlet stream was 230°C , reaction pressure was 24.13 bar, WHSV was 32,000 ml/gcat-h, the catalyst loading was 70 vol%, and the coolant's flow rate was 175.4 L/min. The same kinetic parameters were used as those used in section 2.1. The result of overall CO conversion was 0.6975, and the maximum process temperature was 232.66°C .

With the initial condition obtained, the dynamic model was simulated. The step size of the time was specified as 300 s. In this simulation, it was assumed that at a certain time the flow rate of the coolant was suddenly reduced to 1/4 of the initial value. Such situation was assumed to simulate the abnormal condition in cooling

utility.

The result of the simulation is illustrated in Figure 4-1.

<Temperature profile for the process channels>

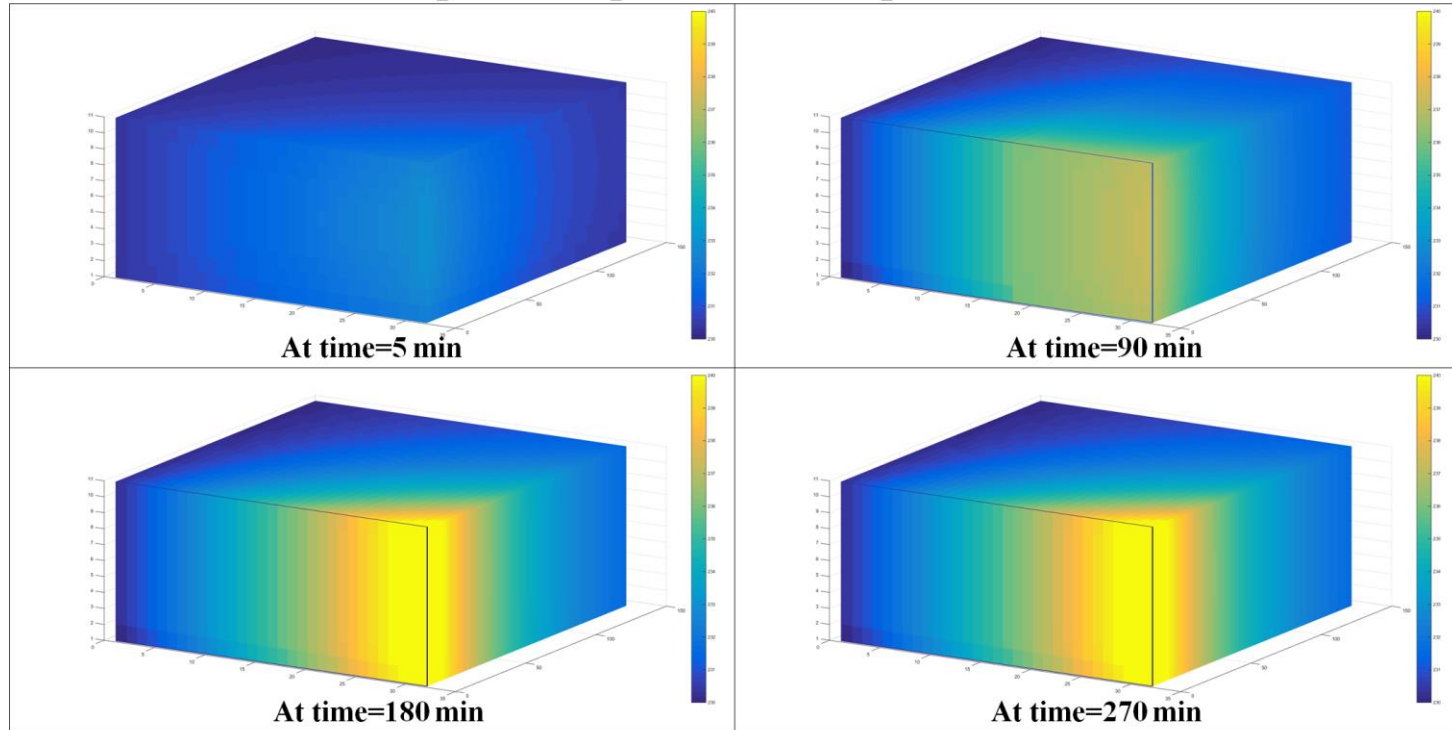


Figure 4-1. Changes of the temperature profile with time (Scenario 1). The color bar of the same scale (230°C - 240°C) was used for all the subplots.

The transient temperature profile was obtained as shown in the figure. For all the subplots in the figure, the color bar of the same scale was used. As can be seen from the figure, the temperature of the process channels increases immediately after the flow rate of the coolant is reduced. It is also noted that the temperature reaches a new steady state after 180 minutes. The maximum temperature value at that time was 241.96°C. Thereafter, this new steady state value was maintained.

Next, another case study was performed to check the model's ability to simulate the control action. In the simulation, the coolant flow rate was reduced to 1/4 of the initial flow rate, which was maintained for 150 minutes, after which the flow rate was increased back again to the original value. The results are illustrated in Figure 4-2, where the maximum temperature difference (ΔT_{max}) in Fig. 4-2(c) takes place at the cell position of $(i, j, h)=(32, 1, 11)$. In this case study, $n_i=32$, $n_j=142$, and $n_h=11$, respectively. When the coolant's flow rate is reduced, the temperature of the process channel is increased as in the previous case study. As the coolant's flow rate is recovered back to the original value at 150 minutes, the temperature decreases going back to its original state. From these results, the developed dynamic model can be utilized to study the response of the reactor to the changes in the input (manipulated) variables.

<Temperature profile for the process channels>

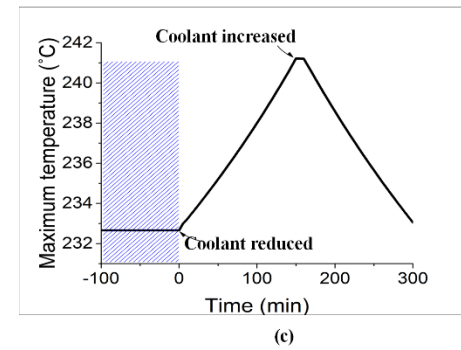
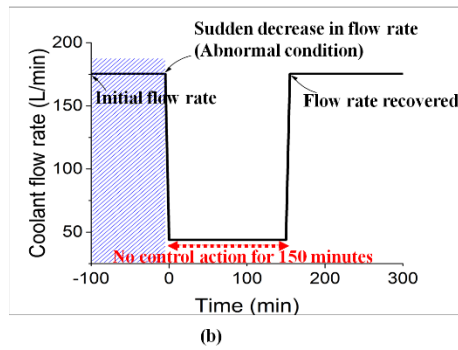
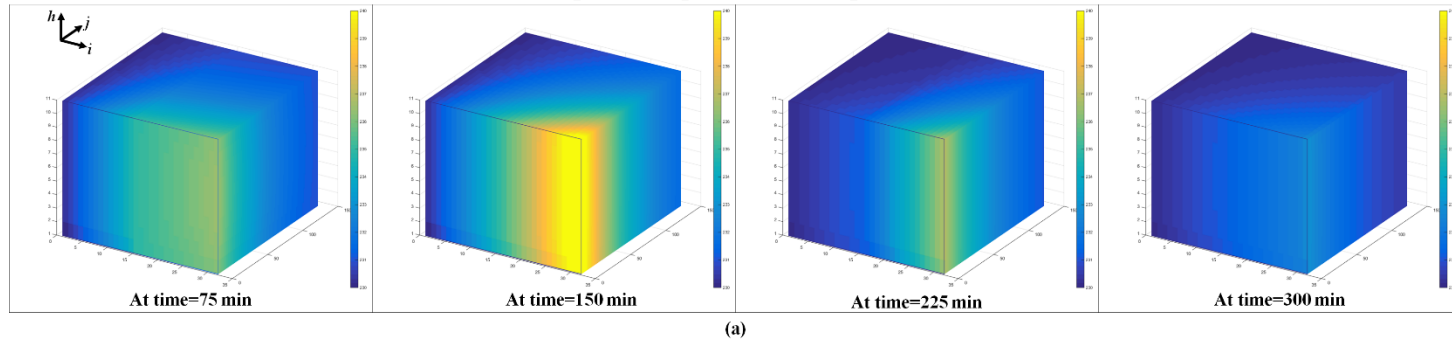


Figure 4-2. Changes of the temperature profile with time (Scenario 2).

4.3. Optimal operating strategies for FT reactor

4.3.3. Model description

The dynamic simulations were performed to suggest the optimal operating strategies for the micro-channel FT reactor. For this purpose, a process model for the FT reaction was developed by using Aspen Hysys software. Instead of using the 3-D cell coupling model, the built-in one-dimensional plug flow reactor model was used for simplification. The process flow diagram (PFD) used is shown in Figure 4-3.

The feed gas flows in the stream 1. It was assumed that the syngas is provided from a storage tank large enough to meet the target operating demand. The syngas is also assumed to be introduced into the process at 220°C and 2000 kPa.

The feed gas flows through the inlet valve (VLV-100) controlled by the flow controller (FIC-100). It then flows into the reactor (PFR-100), where the FT reaction takes place and the reaction heat is removed. The product gas subsequently flows into the two separation tanks. In the first separator, the wax product is mainly separated, whereas in the second separator, the light oil product is collected. The stream 13 consists of a pure N₂ used as purging or diluting agent in the start-up or shut-down procedure. All the boundary streams and intermediate streams connecting each unit are connected to the valves where the gas flow rate is controlled by the flow controllers.

The steady state simulation was performed to calculate the equipment sizing. For the valves, the conductance (C_v) was calculated based on the 50% valve opening at the normal flow rate with pressure drop of 70 kPa. Sizing of the reactor and the

separation tank was based on the target wax production rate of 0.2 BPD. The size information of the process units is summarized in Table 4-1.

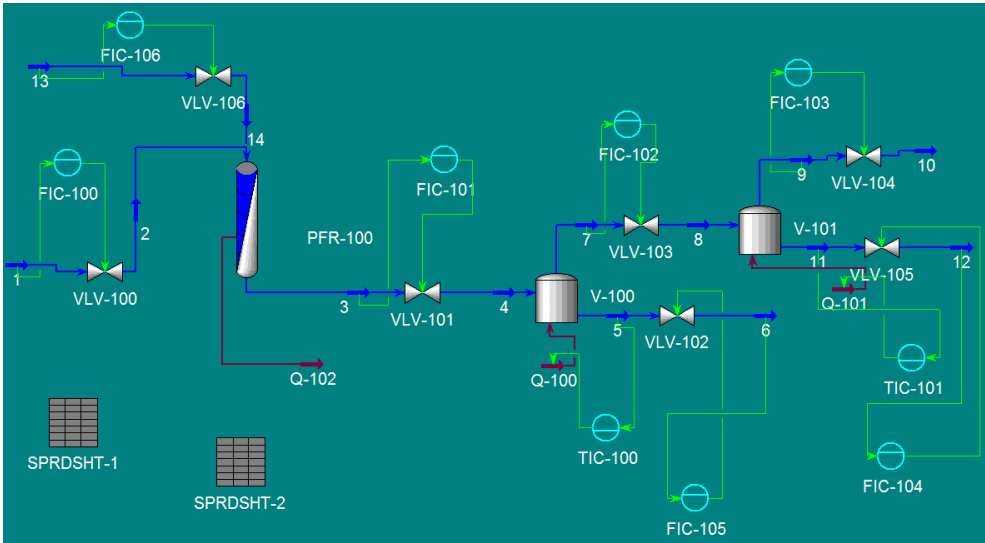


Figure 4-3. Process flow diagram for the dynamic simulation

Table 4-1. Size of the process equipments

		Size	Unit
Valve	VLV-100, C _v	0.6315	USGPM (60F, 1psi)
	VLV-101, C _v	0.1183	USGPM (60F, 1psi)
	VLV-102, C _v	0.1575	USGPM (60F, 1psi)
	VLV-103, C _v	0.1575	USGPM (60F, 1psi)
	VLV-104, C _v	0.1141	USGPM (60F, 1psi)
	VLV-105, C _v	0.1141	USGPM (60F, 1psi)
	VLV-106, C _v	0.6315	USGPM (60F, 1psi)
Reactor	PFR-100, length	0.4470	m
	PFR-100, diameter	0.2314	m
	PFR-100, volume	0.0188	m ³
Separator	V-100, volume	0.0800	m ³
	V-101, volume	0.0800	m ³

4.3.4. Start-up

During the start-up, care should be taken to prevent the thermal runaway of the reactor. In this phase, usually the catalyst is already reduced and in the fresh state. If the operating procedure is improperly configured, this highly active catalyst may lead to a sudden reaction occurrences.

There are many variables that can affect to the start-up state. In this study, we analyze the effect of five variables, i.e., temperature and pressure of the reactor, feed gas flowrate, H_2/CO ratio of the feed gas, and external N_2 flow rate, on the operating performances. To be more specific, nine representative scenarios are generated with the different sequence of those five variables as shown in Table 4-2. For example, in the scenario 1, first the temperature of the reactor is increased gradually (ramp) from initial temperature to the reaction temperature. Then the pressure is increased by closing back pressure regulator in step manner, followed by the step increase in the feed gas flow rate. The sequence of the other scenarios described in the table can be interpreted in the similar manner. Scenario 7 and 8 are comprised of the manipulation of pressure, temperature, and H_2/CO ratio. After the pressure is increased to the reaction condition, the syngas with low H_2/CO is introduced by valve opening. Then the temperature is increased by heating the reactor with the preheated cooling oil. When the heating is finished, the ratio of H_2/CO is increased by adding hydrogen gas imported from other processes.

Scenario 9 uses pure nitrogen instead of the hydrogen.

Table 4-2. Description for start-up scenarios

Description	
1	T (ramp)→P(step)→F(step)
2	T(ramp)→P(step)→F(ramp)
3	P(step)→F(step)→T(ramp)
4	P(step)→F(ramp)→T(ramp)
5	P(step)→F(step)→T(step)
6	P(step)→F(ramp)→T(step)
7^a	P(step)→F ₁ (step, low H ₂ /CO)→T(ramp)→F ₂ (step, high H ₂ /CO)
8	P(step)→F ₁ (ramp, low H ₂ /CO)→T(ramp)→F ₂ (ramp, high H ₂ /CO)
9	P(step)→F(ramp, high N ₂)→T(ramp)→F(ramp, low N ₂)

^aThis scenario was taken from the patent document⁴⁷

The result of two extreme cases are illustrated in Figure 4-4. For Scenario 1, a sudden increase in heat generation occurred when the valve for the inlet stream of the feed gas opened. Because the temperature and pressure has already reached the reaction condition, the FT reaction takes place as the feed gas is introduced abruptly into the reactor. Similar heat generation trend was obtained for Scenario 2. On the other hand, such rapid heat generation does not occur for Scenario 9, where the nitrogen gas was utilized as a diluting agent in the start-up period. In the scenario, the nitrogen is introduced with the syngas after the pressure reaches the reaction pressure. High nitrogen contents inhibit the rapid, or abrupt FT reaction by acting as an inert gas.

The results of all 9 scenarios are shown in Figure 4-5. As can be seen from the figure, Scenario 1 showed the largest heat generation, whereas Scenario 9 resulted in the least heat generation. For Scenario 7 and 8, the heat generation has decreased as compared to Scenario 1 due to the lower concentration of the reactant in feed gas. However, it is higher than the heat generated in Scenario 9. Meanwhile, the controllability of Scenario 7, 8, and 9 is better than that of the others because those three cases use the flow rate as the final manipulating variable, which shows faster responses than temperature or pressure. From this analysis, it is concluded that the optimal start-up procedure for the FT reactor is the procedure used in Scenario 9.

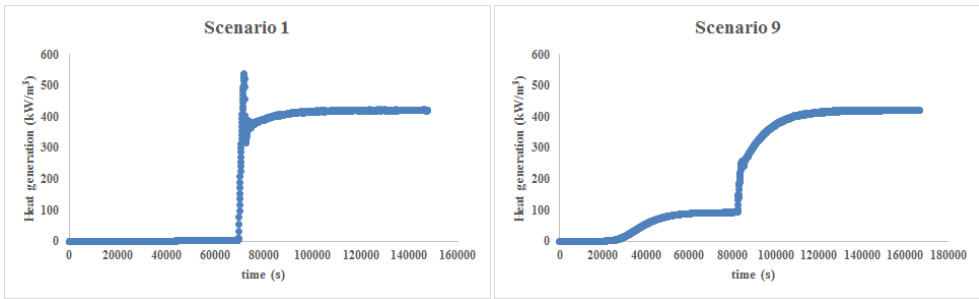


Figure 4-4. Comparison between two extreme cases: Scenario 1 and 9.

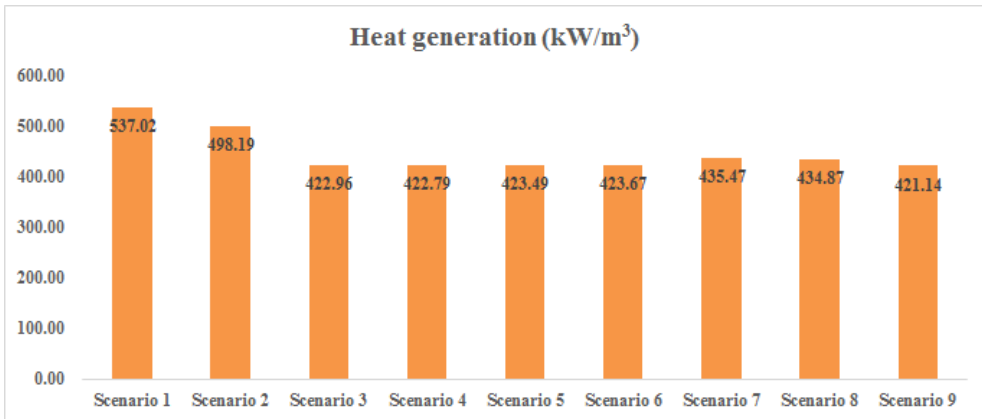


Figure 4-5. Results of the case studies: Scenario 1 through 9

4.3.5. Shut-down

Wax clogging is the main issue in the shut-down procedure of the FT reactor. During the shut-down, temperature and pressure of the reactor are reduced to the room temperature and atmospheric pressure, respectively, at which the FT product is in the liquid phase. If the reactor improperly shut down, this may cause the wax-clogging in the reactor channel. If the wax is clogged inside the channel, it is difficult to take it off from the channel. Therefore, care must be taken to keep the wax from clogging inside the micro-channels so that the reactor can be easily re-commissioned after the shut-down.

In this study, 8 shut down scenarios were studied, where different sequences for the main manipulating variables were incorporated. The description for the scenarios is shown in Table 4-3. For example, in Scenario 1, first the flow rate of the syngas is reduced from steady state value to zero in step manner. Then the temperature is gradually (ramp) decreased to room temperature, followed by the step decrease of the pressure. The other scenarios can be interpreted in the similar manner. For Scenario 7, first the N₂ gas is introduced into the reactor. The reaction pressure and temperature are subsequently reduced to the room conditions. In the final step, the flow rate of the syngas, diluted with the nitrogen gas, is decreased. In scenario 8, the order of the temperature and pressure is altered.

All the scenarios were evaluated with the same criteria, the liquid fraction in the channel. The liquid fraction increases when more and more wax component builds up in the channel. The result of the representative scenarios, scenario 1, 3, and 7, is illustrated in Figure 4-6. As can be seen from the figure, Scenario 1 showed the highest liquid fraction, whereas Scenario 8 showed nearly zero liquid fraction.

Table 4-3. Description for shut-down scenarios

	Description
1	F(step)->T(ramp)->P(step)
2	F(step)->P(step)->T(ramp)
3	T(ramp)->P(ramp)->F(step)
4	T(ramp)->P(step)->F(step)
5	P(step)->T(ramp)->F(step)
6	P(ramp)->T(ramp)->F(step)
7	N2->P(ramp)->T(ramp)->F(step)
8	N2->T(ramp)->P(ramp)->F(step)

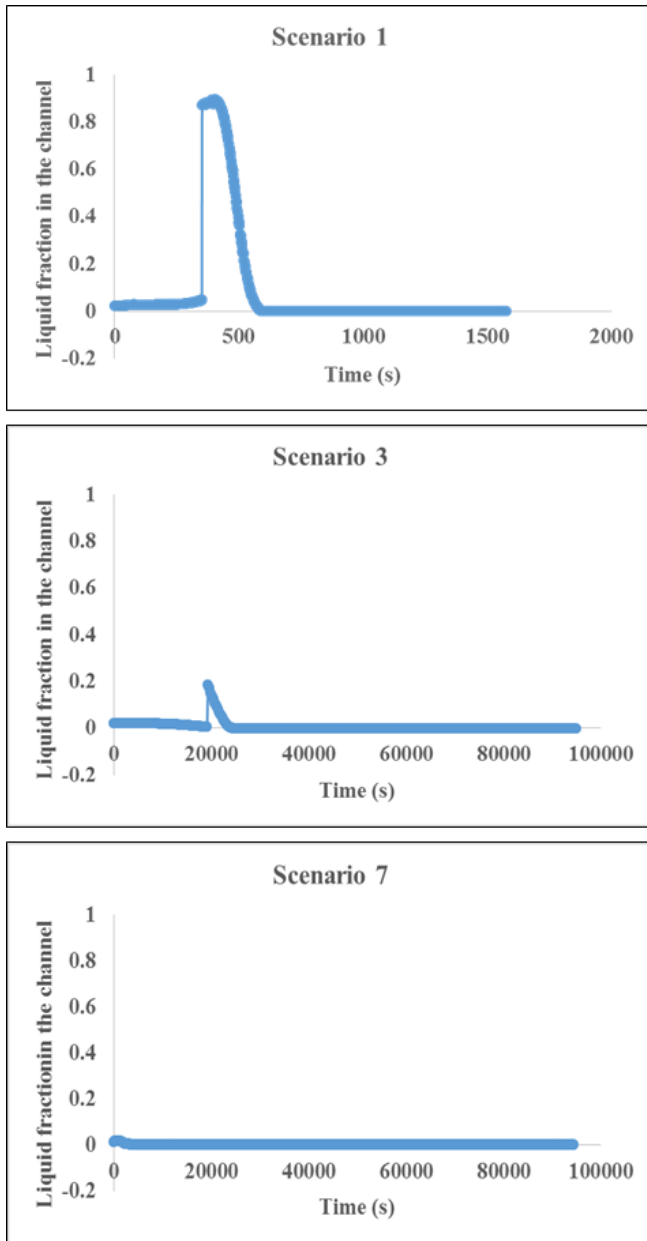


Figure 4-6. Result of dynamic simulation for three shut-down scenarios: Scenario 1, 3, and 8

For Scenario 1, the liquid fraction abruptly increased when the flow rate was being decreased. This phenomenon can be explained with Figure 4-7. Before the temperature decrease, the flow rate has been reduced. As a result, the conversion was increased due to the decrease in space velocity, changing the phase envelope curve in Figure 4-7 from the one at the middle ($X_{CO}=0.7$) to the one at the right ($X_{CO}=1.0$). The phase of the resulting mixture suddenly changed to the liquid phase at this operating condition. The liquid fraction increased abruptly in this step. In the next step, as the temperature decreased, the reaction rate was reduced, and hence, the conversion decreased. The conversion became nearly zero when the temperature reaches the room temperature. The phase envelope moves from right ($X_{CO}=1.0$) to the left ($X_{CO}=0.1$), and the operating point also moves from right to the left. The liquid fraction becomes nearly zero in this step. After that, the pressure is reduced and the shut-down is completed.

For Scenario 3, also the liquid fraction suddenly increased (the second plot in Figure 4-6), but the value is lower than that in Scenario 1. In this case, the temperature of the reactor was reduced first. As the temperature decreases, the operating point moves from right to the left, which is illustrated as the black arrow in Figure 4-7. The phase envelope also changes from the one at the middle ($X_{CO}=0.7$) to the one at the left ($X_{CO}=0.1$). The operating point is placed under the two-phase region of the envelope, causing the liquid fraction to increase. Next, the pressure was reduced, which corresponds to the black arrow vertically down in Figure 4-7. The operating point is now located under the dew point curve. As a result, the liquid fraction becomes zero at this step. After that, the flow rate is decreased, and the shut-down is completed.

For scenario 7, nitrogen gas is first introduced into the process. As this diluent gas is fed into the reactor, the reaction rate is decreased, changing the phase envelope from the one in the middle ($X_{CO}=0.7$) to the one in the left ($X_{CO}=0.1$). For operating point remaining unchanged in this step, no liquid is generated. Then the pressure is reduced to 1 bar, which corresponds to the blue arrow vertically down in Figure 4-7. In this step also, the operating point is placed under the dew point curve and the liquid fraction remains zero. Then, the temperature is decreased to the target point (the horizontal blue arrow in Figure 4-7), which is also located under the dew point curve. and no liquid is generated. The shut-down is completed by reducing the gas flow rate.

Among the all shut-down scenarios, scenario 7 is the best in that the liquid fraction remains almost zero, and the controllability is also good because the final manipulating variable is the gas flow rate. The inert nitrogen gas can be also used as a purge gas at the end of the shut-down procedure, which removes the remaining wax component in the channel. From this analysis, it is concluded that the optimal shut-down procedure for the FT reactor is the procedure used in Scenario 7.

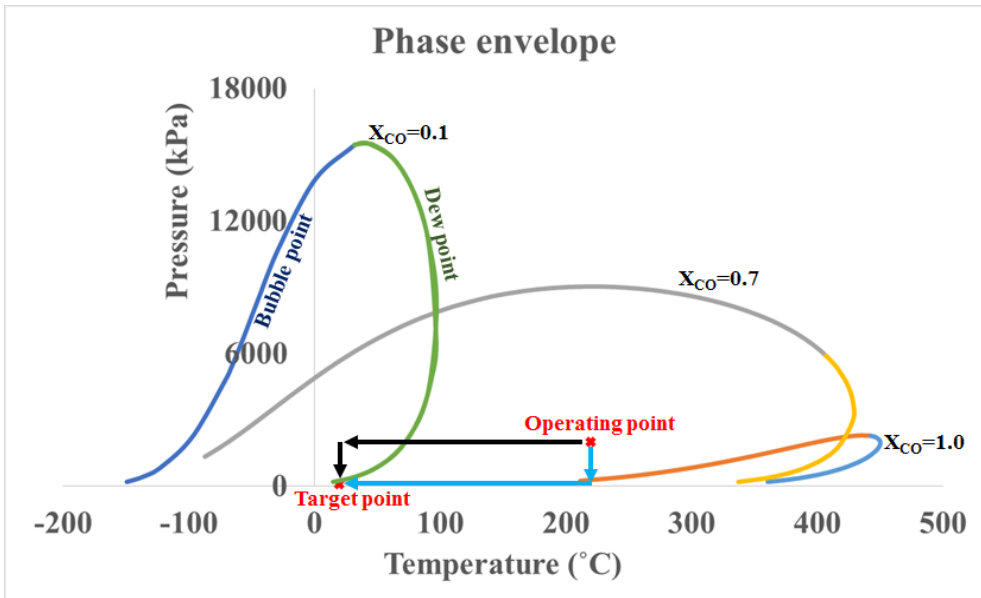


Figure 4-7. Phase envelope

4.4. Conclusion

In this chapter, the dynamic model for the micro-channel FT reactor was developed and the analysis on the transient behavior of the model was addressed. The model could simulate the response of the reactor in step change of some important manipulating variable, e.g., the coolant flow rate. It is also able to describe the situation in which the input variables are changed and recovered back by the user's control action. The dynamic simulation for the micro-channel FT reactor system was also performed. By analyzing several operating scenarios, optimal strategies for start-up and shut-down could be derived. The developed dynamic model and the suggested operating procedure further can be used in the control logic design and real plant operation.

CHAPTER 5 : Concluding Remarks

5.5. Conclusions

This thesis has addressed issues in design of optimal GTL processes based on the micro-channel FT reactor: Reactor design, steady-state process design, and dynamic simulation. All of the developed models were based on the new reactor model, which was validated against the real pilot reactor data.

The model for the micro-channel Fischer-Tropsch reactor was developed by using the new method, where every channel is decomposed into a number of unit cells that interact each other to solve the mass and energy balance equations. This model was validated against the multi-channel reactor data taken from the literature. Sensitivity analyses were performed on the important variables such as catalyst loading ratio, coolant's flow rate, and channel layout.

The improved version of this cell-coupling reactor model was developed, where the effect of the flow configuration, flow distribution, and catalyst overlapping zone was considered. The model was also validated by using the operation data of various operating conditions. With the help of this realistic model, optimal flow configuration, distribution, and catalyst loading strategies for the micro-channel FT reactor could be derived. The barrels-per-day scale pilot reactor has been fabricated, and is now prepared for the commissioning.

Based on the reactor model, an optimal steady-state GTL process was suggested. The steady state model utilizing the micro-channel FT reactor was developed by

implementing this reactor model onto the process model. The derivative-free optimization problem, minimizing the objective function of the overall cost, was formulated and solve by using Nelder-Mead algorithm. The total income for the optimal design increased by approximately 18% compared to that for the reference design, mainly due to the energy saving in CO₂ separation and improvement in wax production.

The dynamic modeling for the 3-D reactor was performed by solving the modified cell-coupling reactor model, where the temporal variation was taken into account. The model could simulate the response of the reactor in step change of some important manipulating variable, e.g., the coolant flow rate. It was also able to describe the situation in which the input variables are changed and recovered back by the user's control action. The dynamic simulation for the micro-channel FT reactor system was also performed. Optimal strategies for start-up and shut-down could be derived by analyzing several operating scenarios. The developed dynamic model and the suggested operating procedure further can be used in the control logic design and real plant operation.

Hopefully, the proposed modeling and design work in this thesis will be helpful to those who want to solve similar design problems.

5.6. Future works

In the future, the developed reactor model will be applied to demonstrating its validity with predicting the pilot-scale micro-channel FT reactor which is now prepared for the commissioning under various circumstances. The reactor was designed and fabricated for the purpose of achieving the production of 1 barrelper-day of wax. Temporal and spatial temperature profiles for the reactor will be measured, which will then be utilized for the demonstration and parameter-tuning of the developed reactor model.

Extension of the optimization methodologies in this thesis will be made to other GTL process alternatives such as tri-reformer, steam-methane-reformer, steam-CO₂-reformer, etc, in order to find the best process configuration. In addition, future work will continue to evaluate the effect of other design variables, such as reformer's outlet temperature, CO₂ recovery, and steam-to-carbon ratio.

For the dynamic model part, further analyses on the various variables that affect the reactor's performances will be conducted. Such variables include the reactant's inlet temperature, syngas flow rate, or catalyst deactivation. More detailed analysis will help us to understand the dynamics and transient behavior of the micro-channel reactors. Furthermore, the dynamic simulation will be extended to the whole GTL process by integrating the FT reaction subprocess with the syngas production process, which will allow us to develop more rigorous, robust, and realistic operating strategies and control logic for the entire process.

Nomenclature

T_P – Matrix of temperatures (K) of process channel cells for every element

T_C – Matrix of temperatures (K) of cooling channel cells for every element

U – Matrix of overall heat-transfer coefficients [$W/(m^2 K)$] between two paired cells for every element

Q – Matrix of heat generation values (kJ) from process channel cells for every element

$h_{process}$ – Convective heat-transfer coefficient [$W/(m^2 K)$] in process channel cell

$h_{coolant}$ – Convective heat-transfer coefficient [$W/(m^2 K)$] in coolant channel cell

$k_{channel}$ – Thermal conductivity [$W/(m K)$] of channel material

Δx – Gap (m) between two paired cells

m_c – Mass flow rate (kg/s) of coolant

\widehat{h}_c – Specific enthalpy (kJ/kg) of coolant

ΔH_r – Heat of reaction (kJ/mol)

r_{CO} – CO consumption rate [$mol/(g-cat s)$]

E_a – Activation energy (kJ/mol)

C_x – Concentration (mol/L) of component x

γ_s – Flow path s

γ_s^t – t -th segment of flow path s

\mathbb{R}^n – n -dimensional vector space

$c(j, i, h)$ – A coolant cell at the position of (j, i, h) in the cell coordinate

$p(j, i, h)$ – A process cell at the position of (j, i, h) in the cell coordinate

ρ – Fluid density (kg/m³)

\mathbf{u} – Velocity vector (m/s)

p – Pressure (bar)

\mathbf{I} – Identity matrix

τ – Viscous stress tensor (bar)

\mathbf{F} – Volume force (N/m³)

p_i – Partial pressure of component i (bar)

$X_{CO,measured}$ – Conversion of carbon monoxide measured (and calculated) from kinetic experiment

$X_{CO,estimated}$ – Conversion of carbon monoxide estimated from 1-D pseudo-homogeneous single channel model

ΔT_{max} – Difference between the maximum temperature of the process

channel cell and the inlet temperature of the syngas

C_B – Base cost

D – Diameter of the vessel

L – Length of the vessel

A – Area of the heat exchanger

C_V – Vessel cost

C_{PL} – Cost for platforms and ladders

D_i – Inner diameter

F_P – Effect of pressure when calculating capital cost

F_M – Effect of material when calculating capital cost

Q – Heat duty for a fired heater

W_{HP} – Brake horse power for a compressor

s_1 – Split ratio for purge stream

s_2 – Split ratio for the FT reactor

M – Centered point

R – Reflected point

W – Worst point

B – Best point

N_i – Mole of component i in a control volume

F_i – Flow rate of component i into/out from a control volume

r_i – Reaction rate of generation of component i in a control volume

\hat{E}_{sys} – Total energy of the system

H_i – Enthalpy of component i

\dot{Q} – Heat flowing into the control volume

\dot{W}_s – Shaft work done by the system

N_x^u – Mole of component x at a time u

Δt – Step change of time

r_{wx}^u – Reaction rate of generation of component x by reaction w at a time

u

C_{px} – Heat capacity of component x

ΔH_r – Heat of reaction

k_{w0} – Frequency factor for reaction w

E_w – Activation energy for reaction w

$C_{p,c}$ – Heat capacity of coolant

ρ_c – Density of coolant

Abbreviations

ANN – Artificial neural network

ASU – Air separation unit

ATR – Autothermal reformer

CAPEX – Capital cost

CFD – Computational fluid dynamics

FID – Flame ionization detector

FPSO – Floating, production, storage, and offloading

FT – Fischer–Tropsch

GHSV – Gas hourly space velocity

GTL – Gas to liquid

LHV – Low heating value

MEA – Monoethanolamine

NG – Natural gas

OPEX – Operating cost

PFD – Process flow diagram

SSE – Sum of square error

TCD – Thermal conductivity detector

Literature cited

- (1) Bao, B.; El-Halwagi, M. M.; Elbashir, N. O., Simulation, integration, and economic analysis of gas-to-liquid processes. *Fuel Processing Technology* **2010**, 91, (7), 703-713.
- (2) Cao, C.; Hu, J.; Li, S.; Wilcox, W.; Wang, Y., Intensified Fischer–Tropsch synthesis process with microchannel catalytic reactors. *Catalysis Today* **2009**, 140, (3), 149-156.
- (3) Deshmukh, S. R.; Tonkovich, A. L. Y.; Jarosch, K. T.; Schrader, L.; Fitzgerald, S. P.; Kilanowski, D. R.; Lerou, J. J.; Mazanec, T. J., Scale-up of microchannel reactors for Fischer– Tropsch synthesis. *Industrial & Engineering Chemistry Research* **2010**, 49, (21), 10883-10888.
- (4) Kim, Y. H.; Jun, K.-W.; Joo, H.; Han, C.; Song, I. K., A simulation study on gas-to-liquid (natural gas to Fischer–Tropsch synthetic fuel) process optimization. *Chemical Engineering Journal* **2009**, 155, (1), 427-432.
- (5) Knochen, J.; Güttel, R.; Knobloch, C.; Turek, T., Fischer–Tropsch synthesis in milli-structured fixed-bed reactors: Experimental study and scale-up considerations. *Chemical Engineering and Processing: Process Intensification* **2010**, 49, (9), 958-964.
- (6) Lee, C.-J.; Lim, Y.; Kim, H. S.; Han, C., Optimal gas-to-liquid product selection from natural gas under uncertain price scenarios. *Industrial & Engineering Chemistry Research* **2008**, 48, (2), 794-800.
- (7) Lee, Y. J.; Hong, S.-I.; Moon, D. J., Studies on the steam and CO₂ reforming of methane for GTL-FPSO applications. *Catalysis Today* **2011**,

174, (1), 31-36.

- (8) Park, D.; Moon, D. J.; Kim, T., Steam-CO₂ reforming of methane on Ni/ γ -Al₂O₃-deposited metallic foam catalyst for GTL-FPSO process. *Fuel Processing Technology* **2013**, 112, 28-34.
- (9) Cao, C.; Xia, G.; Holladay, J.; Jones, E.; Wang, Y., Kinetic studies of methanol steam reforming over Pd/ZnO catalyst using a microchannel reactor. *Applied Catalysis A: General* **2004**, 262, (1), 19-29.
- (10) Chin, Y.-h.; Hu, J.; Cao, C.; Gao, Y.; Wang, Y., Preparation of a novel structured catalyst based on aligned carbon nanotube arrays for a microchannel Fischer-Tropsch synthesis reactor. *Catalysis today* **2005**, 110, (1), 47-52.
- (11) Deshmukh, S.; Keyes, L. W.; Luzenski, R. J.; Marchiando, M. A.; Marco, J. L.; Marco, J. D.; Neagle, P. W.; Tonkovich, A. L.; Yuschak, T., Laminated, Leak-Resistant Chemical Processors; Methods of Making, and Methods of Operating. In United States Patent: 2011.
- (12) Arzamendi, G.; Diéguez, P.; Montes, M.; Odriozola, J.; Falabella Sousa-Aguiar, E.; Gandía, L., Computational fluid dynamics study of heat transfer in a microchannel reactor for low-temperature Fischer–Tropsch synthesis. *Chemical Engineering Journal* **2010**, 160, (3), 915-922.
- (13) Arzamendi, G.; Diéguez, P.; Montes, M.; Odriozola, J.; Sousa-Aguiar, E. F.; Gandía, L., Methane steam reforming in a microchannel reactor for GTL intensification: A computational fluid dynamics simulation study. *Chemical Engineering Journal* **2009**, 154, (1), 168-173.
- (14) Jeon, S. W.; Yoon, W. J.; Baek, C.; Kim, Y., Minimization of hot spot in a microchannel reactor for steam reforming of methane with the stripe combustion

catalyst layer. *International Journal of Hydrogen Energy* **2013**, 38, (32), 13982-13990.

(15) Mohammadi, M.; Jovanovic, G. N.; Sharp, K. V., Numerical study of flow uniformity and pressure characteristics within a microchannel array with triangular manifolds. *Computers & Chemical Engineering* **2013**, 52, 134-144.

(16) Shin, M.-S.; Park, N.; Park, M.-J.; Jun, K.-W.; Ha, K.-S., Computational fluid dynamics model of a modular multichannel reactor for Fischer–Tropsch synthesis: Maximum utilization of catalytic bed by microchannel heat exchangers. *Chemical Engineering Journal* **2013**, 234, (0), 23-32.

(17) Troshko, A. A.; Zdravistch, F., CFD modeling of slurry bubble column reactors for Fisher–Tropsch synthesis. *Chemical Engineering Science* **2009**, 64, (5), 892-903.

(18) Uriz, I.; Arzamendi, G.; López, E.; Llorca, J.; Gandía, L., Computational fluid dynamics simulation of ethanol steam reforming in catalytic wall microchannels. *Chemical Engineering Journal* **2011**, 167, (2), 603-609.

(19) Gumuslu, G.; Avci, A. K., Parametric analysis of Fischer-tropsch synthesis in a catalytic microchannel reactor. *AIChE Journal* **2012**, 58, (1), 227-235.

(20) Guettel, R.; Turek, T., Comparison of different reactor types for low temperature Fischer–Tropsch synthesis: a simulation study. *Chemical Engineering Science* **2009**, 64, (5), 955-964.

(21) Park, S.; Jung, I.; Lee, Y.; Kshetrimayum, K. S.; Na, J.; Park, S.; Shin, S.; Ha, D.; Lee, Y.; Chung, J.; Lee, C.-J.; Han, C., Design of Microchannel Fischer-Tropsch Reactor Using Cell-Coupling Method: Effect of Flow Configurations and Distribution. *Chemical Engineering Science* **accepted**.

- (22) Gabriel, K. J.; Linke, P.; Jiménez-Gutiérrez, A.; Martínez, D. Y.; Noureldin, M.; El-Halwagi, M. M., Targeting of the Water-Energy Nexus in Gas-to-Liquid Processes: A Comparison of Syngas Technologies. *Industrial & Engineering Chemistry Research* **2014**, *53*, (17), 7087-7102.
- (23) Hall, K. R., A new gas to liquids (GTL) or gas to ethylene (GTE) technology. *Catalysis Today* **2005**, *106*, (1–4), 243-246.
- (24) Lee, C.-J.; Lim, Y.; Kim, H. S.; Han, C., Optimal Gas-To-Liquid Product Selection from Natural Gas under Uncertain Price Scenarios. *Industrial & Engineering Chemistry Research* **2009**, *48*, (2), 794-800.
- (25) Castelo Branco, D. A.; Szklo, A. S.; Schaeffer, R., CO₂e emissions abatement costs of reducing natural gas flaring in Brazil by investing in offshore GTL plants producing premium diesel. *Energy* **2010**, *35*, (1), 158-167.
- (26) Dillerop, C.; van den Berg, H.; van der Ham, A. G. J., Novel Syngas Production Techniques for GTL-FT Synthesis of Gasoline Using Reverse Flow Catalytic Membrane Reactors. *Industrial & Engineering Chemistry Research* **2010**, *49*, (24), 12529-12537.
- (27) Deshmukh, S. R.; Tonkovich, A. L. Y.; Jarosch, K. T.; Schrader, L.; Fitzgerald, S. P.; Kilanowski, D. R.; Lerou, J. J.; Mazanec, T. J., Scale-Up of Microchannel Reactors For Fischer–Tropsch Synthesis. *Industrial & Engineering Chemistry Research* **2010**, *49*, (21), 10883-10888.
- (28) Mancaruso, E.; Sequino, L.; Vaglieco, B. M., GTL (Gas To Liquid) and RME (Rapeseed Methyl Ester) combustion analysis in a transparent CI (compression ignition) engine by means of IR (infrared) digital imaging. *Energy* **2013**, *58*, (0), 185-191.

- (29) Rahimpour, M. R.; Mirvakili, A.; Paymooni, K., A novel water perm-selective membrane dual-type reactor concept for Fischer–Tropsch synthesis of GTL (gas to liquid) technology. *Energy* **2011**, 36, (2), 1223-1235.
- (30) Sharma, A.; Philippe, R.; Luck, F.; Schweich, D., A simple and realistic fixed bed model for investigating Fischer–Tropsch catalyst activity at lab-scale and extrapolating to industrial conditions. *Chemical Engineering Science* **2011**, 66, (24), 6358-6366.
- (31) de Klerk, A.; Furimsky, E., Catalysis in the refining of Fischer–Tropsch syncrude. *A quarterly journal of research on the science and technology of the platinum group metals and developments in their application in industry* **2011**, 55, (4), 263-267.
- (32) Pratt, J. W., A Fischer-Tropsch synthesis reactor model framework for liquid biofuels production. *Sandia National Laboratories, California* **2012**.
- (33) Cao, C.; Palo, D. R.; Tonkovich, A. L. Y.; Wang, Y., Catalyst screening and kinetic studies using microchannel reactors. *Catalysis Today* **2007**, 125, (1–2), 29-33.
- (34) Butcher, H.; Quenzel, C. J. E.; Breziner, L.; Mettes, J.; Wilhite, B. A.; Bossard, P., Design of an annular microchannel reactor (AMR) for hydrogen and/or syngas production via methane steam reforming. *International Journal of Hydrogen Energy* **2014**, 39, (31), 18046-18057.
- (35) Irani, M., EXPERIMENTAL AND CFD MODELING OF A BENCH-SCALE GTL PACKED-BED REACTOR BASED ON FE/CU CATALYST. *Petroleum & Coal* **2014**, 56, (1), 62-73.
- (36) Deshmukh, S. R.; Vlachos, D. G., Effect of flow configuration on the

- operation of coupled combustor/reformer microdevices for hydrogen production. *Chemical Engineering Science* **2005**, 60, (21), 5718-5728.
- (37) Agrawal, G.; Kaisare, N. S.; Pushpavanam, S.; Ramanathan, K., Modeling the effect of flow mal-distribution on the performance of a catalytic converter. *Chemical Engineering Science* **2012**, 71, (0), 310-320.
- (38) Park, S.; Jung, I.; Lee, U.; Na, J.; Kshetrimayum, K. S.; Lee, Y.; Lee, C.-J.; Han, C., Design and modeling of large-scale cross-current multichannel Fischer–Tropsch reactor using channel decomposition and cell-coupling method. *Chemical Engineering Science* **2015**, 134, 448-456.
- (39) Yates, I. C.; Satterfield, C. N., Intrinsic kinetics of the Fischer-Tropsch synthesis on a cobalt catalyst. *Energy & Fuels* **1991**, 5, (1), 168-173.
- (40) Eliason, S.; Bartholomew, C., Reaction and deactivation kinetics for Fischer–Tropsch synthesis on unpromoted and potassium-promoted iron catalysts. *Applied Catalysis A: General* **1999**, 186, (1), 229-243.
- (41) Iglesia, E.; Reyes, S. C.; Madon, R. J.; Soled, S. L., Selectivity control and catalyst design in the Fischer-Tropsch synthesis: sites, pellets, and reactors. *Advances in Catalysis* **1993**, 39, 221-302.
- (42) Panahi, M.; Rafiee, A.; Skogestad, S.; Hillestad, M., A natural gas to liquids process model for optimal operation. *Industrial & Engineering Chemistry Research* **2011**, 51, (1), 425-433.
- (43) Baltrusaitis, J.; Luyben, W. L., Methane Conversion to Syngas for Gas-to-Liquids (GTL): Is Sustainable CO₂ Reuse via Dry Methane Reforming (DMR) Cost Competitive with SMR and ATR Processes? *ACS Sustainable Chemistry & Engineering* **2015**, 3, (9), 2100-2111.

- (44) Asteasuain, M.; Tonelli, S.; Brandolin, A.; Bandoni, J., Dynamic simulation and optimisation of tubular polymerisation reactors in gPROMS. *Computers & Chemical Engineering* **2001**, 25, (4), 509-515.
- (45) Sayer, C.; Lima, E.; Pinto, J., Dynamic modeling of SBR emulsion polymerization reactors refrigerated by thermosyphons. *Chemical engineering science* **1997**, 52, (3), 341-356.
- (46) Morud, J. C.; Skogestad, S., Analysis of instability in an industrial ammonia reactor. *AIChE Journal* **1998**, 44, (4), 888-895.
- (47) Arcuri, K. B., Process for the start-up of a Fischer-Tropsch reactor. In United States Patent: 1986.
- (48) Sumerford, S. D.; Moise, J. E.; Rouge, B.; La., Starting up procedure for the synthesis of hydrocarbons. In United States Patent: 1958.
- (49) Song, H.-S.; Ramkrishna, D.; Trinh, S.; Wright, H., Operating strategies for Fischer-Tropsch reactors: A model-directed study. *Korean Journal of Chemical Engineering* **2004**, 21, (2), 308-317.
- (50) Bezemer, G. L.; Mesters, C. M. A. M.; Remans, T. J.; Smits, J. T. M., High-speed stop in Fischer-Tropsch process. In United States Patent: 2015.

Abstract in Korean (요 약)

지난 수십년간 Gas-to-Liquid (GTL) 공정은 천연가스를 청정 합성연료로 전환할 수 있는 기술로 많은 주목을 받아왔다. GTL 공정에서 우선 개질기에서 천연가스가 수소와 일산화탄소로 구성된 합성가스로 전환된다. 이후 합성가스는 피셔-트롭쉬 (FT) 반응기에서 반응을 일으켜 탄소 사슬수가 긴 탄화수소로 전환된다. 탄소수가 1개부터 30개 이상인 탄화수소는 FT 합성 연료라고도 불리는데, 옥탄가와 세탄가가 높고 질소 성분과 황 성분이 거의 없어 고급 청정 연료로 활용된다.

FT 반응은 일산화탄소 1몰 반응당 약 165kJ만큼의 반응열이 나오는 고발열 반응이다. 이 반응열은 반응기의 thermal-runaway와 같은 비안정성과 직접적인 연관이 있기 때문에 반응기 내에서 효율적으로 제거되어야 한다. 이를 위해 많은 종류의 반응기, 이를테면 슬러리 버블 반응기, 고정층 반응기, 유동층 반응기들이 GTL 공정에 적용되어 왔으나, 해양 플랫폼 등 특수한 상황에서는 이보다 더 작고 생산 효율이 높은 반응기가 필요하다는 의견이 꾸준히 제기되어왔다.

이에 최근 마이크로채널 FT 반응기의 개념이 대두하였는데, 마이크로채널 반응기는 채널 사이즈가 매우 작기 때문에 단위부피당 열교환 면적이 커서 반응열을 빠르고 효율적으로 제거할 수 있다는 특징이 있다. 한 문헌에서는 일반적인 고정층 반응기보다 마이크로채널 반응기가 약 15배 가량 열 제거 속도가 빠르다고 나와있다. 또한 마이크로 채널 반응기는 모듈화가 가능하기 때문에 scale-up에서도 유리하다. 이러한 열교환

효율성과 모듈화 덕분에 스케일이 작은 단일 채널의 반응기와 파일럿 스케일의 반응기의 성능이 거의 동일하다고 알려져 있다.

본 논문에서는 마이크로채널 반응기를 기반으로 한 최적 GTL공정의 설계를 다룬다. 이를 위해 마이크로 채널 FT 반응기의 모델을 수립하였고, 그 반응기 모델을 바탕으로 한 GTL 공정의 모델을 만들어 최적화를 수행했으며, 마이크로 채널 FT 반응기의 동적 모사를 통한 최적 운전 절차를 제안하였다. 반응기 모델은 실제 반응기의 운전 데이터로부터 실증(validation) 하였다.

첫째로, 반응기에 대한 distributed-parameter 모델을 채널 분해와 셀 결합이라는 새로운 방식으로 구성했다. 셀 결합 모델에서는 인접한 반응 채널과 냉각채널간의 상호 작용, 즉 물질 수지와 열 수지, 열전달에 대한 방정식을 전체 셀 공간 내에서 세우고 해를 구한다. 그 모델 계산 결과와 실제 파일럿 스케일 반응기 데이터를 비교해보니 서로 경향성과 크기가 거의 일치함을 확인했다. 또한, 촉매의 충전량, 냉매의 유량, 그리고 채널의 사이즈에 대한 효과를 파악하기 위해 cross-current 반응기에 대해 민감도 분석을 수행했다.

나아가 유로의 구성과 흐름 분배 효과를 반영해 개선된 셀 결합 모델을 개발했다. 이를 위해 각각의 유로 구성에 대해 셀의 영역을 재정의하였고, 전산유체역학의 결과를 모델에 이식해 흐름 분배에 대한 효과를 반영했다. 개선된 모델을 통해 유로의 구성, 흐름 분배, 그리고 촉매의 충전 구간에 대한 민감도 분석을 수행하였다. 그 결과 cross-co-cross

current 구조가 다른 구조들에 비해 열 제거 측면에서 가장 성능이 좋았다.

다음으로 개발된 마이크로채널 반응기 모델을 이용해 최적 GTL 공정에 대한 연구를 수행했다. 우선 정상 상태의 GTL 공정을 모델링 했는데, 이 때 반응기 모델은 인공 신경망으로 모사하였다. 이후 순이익의 음수 값을 최소화하는 최적화 문제를 구성했다. 이 문제에서 설계 변수로는 FT 반응기의 온도, 압력, purge 비율, 그리고 FT반응기로 들어가는 비율을 사용했다. 본 최적화 문제를 풀기 위해 Nelder-Mead 알고리즘을 사용하였고, 그 결과 FT 반응기의 반응열을 이산화탄소 분리에 필요한 재기화기의 열량을 보충해줘서 효율이 증가했다. 얻어진 최적 해는 기존 공정보다 경제적으로 더 나은 성능을 보였다.

끝으로 FT 반응기의 동적 모델을 개발했다. 셀 결합 모델의 구조를 이용해 편미분방정식을 단순화하여 시간에 대한 반응기 내의 3차원적인 온도 프로파일을 구할 수 있었다. 이 모델을 이용해 마이크로채널 반응기의 동적 거동을 분석했다. 또한 별도로 FT 반응기 시스템에 대한 동적 모사를 수행하여 공정의 최적 start-up과 shut-down 절차를 제안했다.

본 연구는 마이크로채널 피셔-트롭쉬 반응기를 기반으로 한 최적 GTL 공정을 설계하는 데 기여할 수 있을 것이다. 개발된 반응기 모델, 정상 상태의 모델과 동적 모델, 실제 GTL 시스템을 설계하고 운전하는 데 이용하고 거기에서 발생하는 수많은 문제점을 해결하는 데 활용할

수 있을 것으로 기대한다.

주요어: 마이크로채널 반응기, 피셔-트롭쉬, 반응기 모델링, GTL 공정,
공정 최적화, 동적 모사

학번: 2011-21036

성명: 박 성 호